GL-TR-90-0080

# AD-A231 914

## Path Characterization Algorithms for FASCODE

R. G. Isaacs
S. A. Clough
R. D. Worsham
J. L. Moncet
B. L. Lindner
L. D. Kaplan



14 March 1990

Atmospheric and Environmental Research, Inc.
840 Memorial Drive
Cambridge, MA 02139

Final Report
17 July 1987 - 17 January 1990

**APPROVED FOR PUBLIC RELEASE; DISTRIBUTION UNLIMITED**

Geophysics Laboratory
Air Force Systems Command
United States Air Force
Hanscom AFB, MA 01731-5000

"This technical report has been reviewed and is approved for publication"

G. P. ANDERSON
Contract Manager
Atmospheric Effects Branch
Optical and Infrared Technology Division

ROBERT R. O'NEIL, Chief
Atmospheric Effects Branch
Optical and Infrared Technology Division

FOR THE COMMANDER

R. EARL GOOD, SES, Director
Optical and Infrared Technology Division

This report has been reviewed by the ESD Public Affairs Office (PA) and is releasable to the National Technical Information Service (NTIS).

Qualified requestors may obtain additional copies from the Defense Technical Information Center. All others should apply to the National Technical Information Service.

If your address has changed, or if you wish to be removed form the mailing list, or if the addressee is no longer employed by your organization, please notify GL/IMA, Hanscom AFB, MA 01731. This will assist us in maintaining a current mailing list.

Do not return copies of this report unless contractual obligations or notices on a specific document requires that it be returned.

Unclassified

SECURITY CLASSIFICATION OF THIS PAGE

# REPORT DOCUMENTATION PAGE

| | |
|---|---|
| 1a. REPORT SECURITY CLASSIFICATION<br>Unclassified | 1b. RESTRICTIVE MARKINGS |
| 2a. SECURITY CLASSIFICATION AUTHORITY | 3. DISTRIBUTION / AVAILABILITY OF REPORT<br>**Approved for public release; Distribution unlimited** |
| 2b. DECLASSIFICATION / DOWNGRADING SCHEDULE | |
| 4. PERFORMING ORGANIZATION REPORT NUMBER(S) | 5. MONITORING ORGANIZATION REPORT NUMBER(S)<br>GL-TR-90-0080 |
| 6a. NAME OF PERFORMING ORGANIZATION<br>Atmospheric and Environmental Research, Inc.<br>6b. OFFICE SYMBOL (*If applicable*) | 7a. NAME OF MONITORING ORGANIZATION<br>Geophysics Laboratory |
| 6c. ADDRESS (*City, State, and ZIP Code*)<br>840 Memorial Drive<br>Cambridge, MA 02139 | 7b. ADDRESS (*City, State, and ZIP Code*)<br>Hanscom AFB, MA 01731-5000 |
| 8a. NAME OF FUNDING / SPONSORING ORGANIZATION<br>Air Force Geophysics Laboratory<br>8b. OFFICE SYMBOL (*If applicable*)<br>AFGL/SULR | 9. PROCUREMENT INSTRUMENT IDENTIFICATION NUMBER<br>F19628-87-C-0129 |
| 8c. ADDRESS (*City, State, and ZIP Code*)<br>Hanscom AFB, MA 01731 | 10. SOURCE OF FUNDING NUMBERS<br>PROGRAM ELEMENT NO. 62101F; PROJECT NO. 7670; TASK NO. 09; WORK UNIT ACCESSION NO. BA |
| 11. TITLE (*Include Security Classification*)<br>Path Characterization Algorithms for FASCODE | |
| 12. PERSONAL AUTHOR(S)<br>R.G. Isaacs, S.A. Clough, R.D. Worsham, J.L. Moncet, B.L. Lindner, L.D. Kaplan | |
| 13a. TYPE OF REPORT<br>Final<br>13b. TIME COVERED<br>FROM 7/17/87 TO 1/17/90 | 14. DATE OF REPORT (*Year, Month, Day*)<br>14 March 1990<br>15. PAGE COUNT<br>206 |
| 16. SUPPLEMENTARY NOTATION | |

| 17. COSATI CODES | | | 18. SUBJECT TERMS (*Continue on reverse if necessary and identify by block number*) |
|---|---|---|---|
| FIELD | GROUP | SUB-GROUP | Inversions<br>Remote Sensing<br>Retrievals |
| | | | |
| | | | |

19. ABSTRACT (*Continue on reverse if necessary and identify by block number*)

This report has described the results of a study undertaken at AER to identify and implement a state-of-the-art nonlinear retrieval approach to characterize line of sight variability of atmospheric thermal and constituent environments. This path characterization capability was designed to interface with the existing Geophysics Laboratory (GL) line-by-line radiance/transmittance code, FASCODE.

Accomplishments of the study include: (a) a review of the relevant literature concerning potential path characterization retrieval algorithms, selection of a physical least squares (PLS) nonlinear retrieval approach for implementation based on criteria including flexibility within the context of FASCODE and a certain degree of robustness in application; (b) development of a stand alone, preprocessing screening procedure to identify potential channels for path characterization based on user requirements; (c) formulation and implementation of the path characterization retrieval algorithm including suitable interfaces with

(continued on reverse)

| | |
|---|---|
| 20. DISTRIBUTION / AVAILABILITY OF ABSTRACT<br>☐ UNCLASSIFIED/UNLIMITED ☐ SAME AS RPT ☐ DTIC USERS | 21. ABSTRACT SECURITY CLASSIFICATION<br>Unclassified |
| 22a. NAME OF RESPONSIBLE INDIVIDUAL<br>Gail Anderson | 22b. TELEPHONE (*Include Area Code*)<br>22c. OFFICE SYMBOL<br>GL/OPE |

**DD FORM 1473, 84 MAR** 83 APR edition may be used until exhausted. All other editions are obsolete.

SECURITY CLASSIFICATION OF THIS PAGE

Unclassified

19. Abstract (continued)
FASCODE; (d) inclusion of a comprehensive error analysis capability as an integral part of the retrieval procedure; (e) demonstration of the approach for the retrieval of temperature, water vapor and ozone; and (f) comprehensive documentation of the path characterization code implementations.

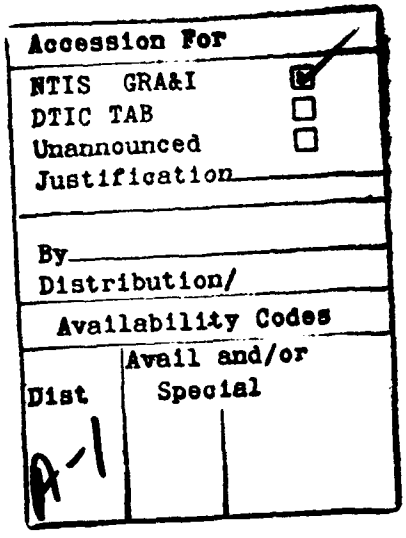


## TABLE OF CONTENTS

TABLE OF CONTENTS (continued)

## LIST OF FIGURES

## LIST OF FIGURES (Continued)

## LIST OF FIGURES (Continued)

## LIST OF TABLES

# 1. INTRODUCTION

## 1.1 Study Objectives

This report describes the results of study undertaken at AER to identify and implement a state-of-the-art nonlinear retrieval approach to characterize line of sight variability of atmospheric thermal and constituent environments. This path characterization capability is designed to interface with the existing Geophysics Laboratory (GL) line-by-line radiance/transmittance code, FASCODE.

Military and commercial endeavors have become increasingly reliant on sophisticated electro-optical communications and sensor systems operating in both active and passive modes throughout the electromagnetic spectrum. Such systems enhance the effectiveness of decision makers to obtain timely and accurate meteorological, environmental, ecological, and military data upon which to formulate and execute operational plans. Since the atmospheric path is an integral component of these electro-optical systems, adverse environmental effects can seriously degrade their reliability. Therefore, optimum design and deployment of such systems requires the capability to simulate and predict the impact of the intrinsic variability of factors affecting the line of sight propagation paths over which they operate. Fundamental among the factors affecting path characterization are those thermodynamic and compositional parameters which determine the optical properties of the path such as temperature, pressure (density), and the abundances of relevant absorbing gases and scattering aerosols. Furthermore, it is desired to systematically evaluate the degree of success potentially achievable in the characterization of relevant path parameters from acquired sensor data sets. Comprehensive error analysis provides the formalism necessary to accomplish this evaluation.

## 1.2 Implementation Approach

We have divided the path characterization procedure into a few definable steps (Isaacs, 1988). Sensor design first requires the ability to select channel sets which will provide data with the potential to measure changes in the desired path parameters. To provide a first-look opportunity to identify potentially fruitful spectral regions for sensor channel placement in the sensor design process, we have developed a simple screening algorithm. This

preprocessing step uses a simple model of atmospheric transmittance for model atmospheres to locate optically thick spectral regions for the species of concern to the user. Once candidate sensor channels are selected it is necessary to simulate representative data sets for the hypothetical instrument concept. This capability is called data simulation or the forward problem. The availability of state-of-the-art line-by-line data and radiative transfer codes (such as FASCODE) enables users to calculate high resolution, spectrally dependent transmittances and radiances over broad spectral ranges by defining the relevant thermodynamic and compositional properties of a specific line of sight path. In this manner, sensor operation can be simulated and synthetic data calculated for a variety of environmental scenarios. Thus, the capability exists to answer the question: "How will the sensor respond to a given variation in the character of the path?"

An equally valid and perhaps more challenging question constitutes the so-called inverse or retrieval problem. Given spectrally dependent transmittance or emittance (i.e., radiance) data obtained for a specified path (e.g. it could be obtained using a forward problem simulation or actual sensor data), what can be said about the variability of its thermodynamic and compositional properties? The mathematical formalisms applicable to treating this question are described by a variety of extant path characterization retrieval approaches. In particular, our study of potential nonlinear retrieval schemes with the mix of flexibility and robustness for implementation with the GL forward problem models has identified a simple physical least squares (PLS) approach.

Finally, there is the problem of providing statistically appropriate path characterization retrieval accuracy assessment indices. One must consider the problem of retrieval design, implementation, and evaluation from a systems perspective (Peckham and Flower, 1983). The retrieval code per se does not choose the optimum set of frequencies to obtain a sounding of a particular path, nor does it generally evaluate the accuracy of results, i.e., the retrieval algorithm is only one submodule of the overall inversion system. Recognizing these factors, error analysis assessment must be combined with the forward problem and retrieval capabilities to provide a complete path characterization system.

The path characterization approach is summarized in Figure 1-1. Identified are the major path characterization program elements described above including: (a) the spectral screening procedure for channel identification, (b) the data simulation to assess path sampling characteristics and provide the forward problem model generator for the PLS retrieval, (c) the PLS retrieval algorithm, and (d) the error analysis to diagnose retrieval accuracy.

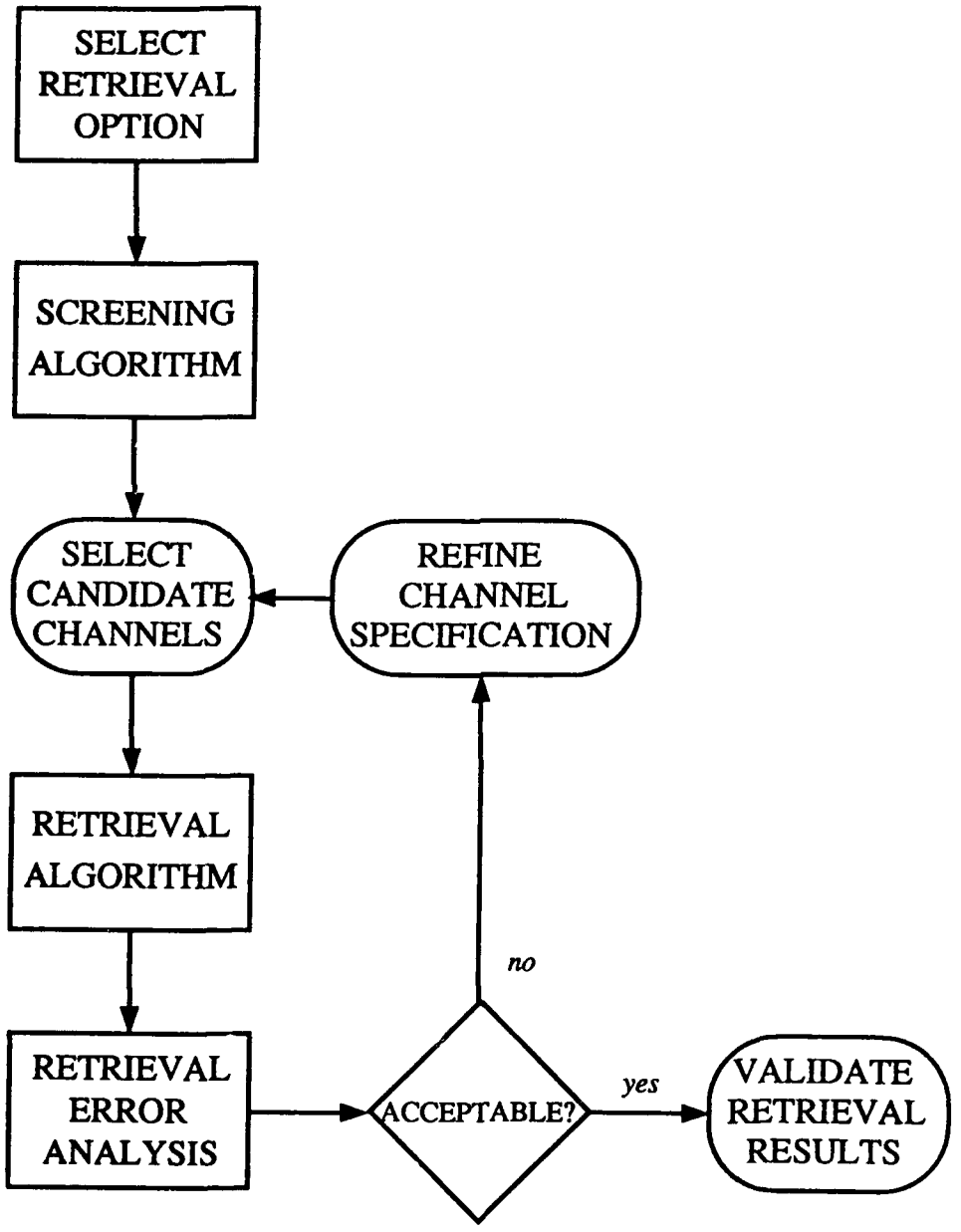


Figure 1-1. Path characterization concept.

## 1.3 Overview of Report

The report is divided into nine sections and five appendices. Following this introduction is a review of retrieval techniques relevant to the path characterization problem (Section 2). This review was undertaken to determine an appropriate approach for implementation with the FASCODE forward problem algorithm. Based on this review, we have selected a physical least squares (PLS) approach. Section 3 describes a preprocessing algorithm developed to aid the user in screening for spectral regions which should prove fruitful for further detailed analysis with the path characterization retrieval code. A comprehensive description of the theory employed in the implementation of the PLS retrieval code is described in Section 4. The retrieval error analysis capability is described in Section 5. In addition to the error analysis approach employed, examples are provided. Section 6 contains application of the path characterization retrieval to two test cases. A comprehensive program description including flow charts of the path characterization algorithm is provided in Section 7. Conclusions and recommendations are given in Section 8. Finally, references are provided in Section 9.

The main body of the text is supplemented by four related appendices. These include: (a) screening algorithm output, (b) user instructions, (c) test case input, and (d) test case output. This is followed an appendix (e) related to publications and presentations associated with this research.

# 2. PATH CHARACTERIZATION REVIEW

## 2.1 The Forward Problem

Given a set of data acquisition requirements (usually stated in terms of desired path characteristics), a procedure is required to identify instrumental spectral response regions with sufficient signal to discern variations in the desired parameters. We call this procedure spectral screening. Once channels are selected, one would like to be able to simulate sensor data in order to investigate its sensitivity to changes in the path parameters. Sensor data, i.e. the system measurements, are in reality complicated mathematical convolution integrals involving the desired path characterization parameters and the system instrumental response function. The form of these

relationships between data and desired parameters is expressed by the radiative transfer equation (RTE).

### 2.1.1 Spectral Screening

Practical sensor channel selection is intuitive and, perhaps, something of an art. One has to be aware of the possible spectral regions applicable to the retrieval of each desired parameter, of interferences from absorption features from other perhaps irrelevant species, and of the potential effects of continuum extinction due to aerosol scattering which may reduce or mask the desired signal. The process is most often iterative.

The basic tool for channel selection via spectral screening is one of the available spectral line parameter compilations. To insure that a particular path parameter significantly affects the path optical properties, we may require that the line strength is greater than a threshold value. Using the graphical line strength data catalog of Park et al. (1981), for example, this can be done visually, including an assessment of potential interferences from other absorbing species. In order to include the characteristics of the path including absorber concentrations and the temperature and pressure dependences of absorption line parameters in the screening procedure, however, a more detailed procedure is required. This can be implemented using a computerized algorithm which uses a data base of spectrally averaged line strengths and halfwidths (computed off-line using a suitable averaging increment, say 0.5 $cm^{-1}$) together with atmospheric model profiles of temperature and absorber amounts to provide the characteristics of selected paths. The spectral data are modified to account for line strength, temperature dependence, and pressure and temperature dependence of halfwidths. These data sets are then combined using an appropriate simple band model to calculate path optical depths which are then screened using a critical optical depth criterion to insure sufficient signal. The procedure is performed for all absorbers present to identify potential interferences. The result of the spectral screening is the identification of suitable wavenumber regions to measure the desired path parameters.

The screening procedure provides a zeroth order channel selection which is refined using sensitivity analyses performed with the forward problem simulator. Sensitivity analyses based on signal to noise criteria allow one

to optimally select the channels needed to infer the desired path parameters. In general, the ability to infer a change in a parameter of magnitude $\delta p$ will depend on the detection of a measurable change in the signal of magnitude $\delta d$ in one or more of the sensor channels. These changes are related through the forward problem described below.

### 2.1.2 The Exact Forward Problem

The dependence of remotely-sensed data on desired atmospheric parameters (i.e., the forward problem) can be stated rigorously in terms of an appropriate solution to the radiative transfer equation. Stated generally, the sensor incident radiance, $R_i(\theta,p_o)$, in the ith sensor channel (with characteristic wavenumber, $\nu_i$ for look angle $\theta$) is given by Goody (1964).

$$R_i(\theta,\ p_o) = R_i(\theta,\ p_b)\ \tau_i(\theta,p_b) + \int_{p_b}^{p_o} S(p)\ \frac{d}{dp}\ \tau_i(\theta,p)\ dp \qquad (2.1)$$

where $R_i(p_b)$ is the radiance emerging from a boundary at pressure $p_b$, $\tau_i(\theta,p)$ is the mean atmospheric transmittance evaluated from level p to $p_o$ along look angle $\theta$, and S(p) is the source function of emitted and/or scattered radiance at level p in the atmosphere. Here, $p_o$ is the pressure at the path starting point. Usually $p_b$ is a physical boundary such as the Earth's surface or the top of a cloud.

The atmospheric transmittance $\tau_i(\theta,p)$ consists of contributions by lines, $\tau_{i\ell}$, the continua, $\tau_{ic}$, and particulate extinction, $\tau_{ie}$:

$$\tau_i(\theta,p) = \tau_{i\ell}(\theta,p)\ \tau_{ic}(\theta,p)\ \tau_{ie}(\theta,p). \qquad (2.2)$$

The contribution due to n discrete absorption lines is

$$\tau_{i\ell}(\theta,p) = \int \phi_i(\nu)\ \exp\left\{\frac{-\sec\theta}{g}\ \sum_n\ \int_{p_o}^{p} k_n[\nu,p',T(p')]\ q_n(p')\ dp'\right\} d\nu \qquad (2.3)$$

where $\phi_i$ is the response (i.e., filter) function of the ith sensor channel, $k_n(\nu,p,T)$ is the absorption coefficient for the nth line, and $q_n(p)$ is the mixing ratio profile of the absorbing gas contributing to the nth line. The

absorption coefficient depends on an assumed spectral line shape (Goody, 1984) and an appropriate set of absorption line parameters such as the AFGL line parameter data set (Rothman et al., 1983; Rothman et al., 1987; Poynter and Pickett, 1980; Poynter and Pickett, 1984). Much of the inaccuracy in calculating the forward problem may be traced to uncertainties in the line shape and in determining some of these parameters. Existing line-by-line techniques to evaluate Eq. (2.3) include the NASA model and the AFGL FASCODE algorithm (Susskind et al., 1983; Clough et al., 1981; Clough et al., 1986).

Continua contributions to total transmittance, $\tau_{ic}$, include the collision-induced absorption by nitrogen and oxygen (Rinsland et al., 1989; Kneizys et al., 1980; Vodar and Vu, 1963) and water vapor continua throughout much of the spectrum (Clough et al., 1989; Clough et al., 1980; Clough et al., 1981; Burch and Gryvnak, 1980; Liebe, 1980).

Particulate transmittance, $\tau_{ie}$, includes the effect of Mie scattering (Van deHulst, 1957; Diermendjian, 1969) of aerosols and cloud in the visible and infrared (Shettle and Fenn, 1979), and of cloud and rain in the infrared and millimeter/microwave regions (Diermendjian, 1975; Falcone et al., 1979).

The specific forms of $R_i(p_b)$, $\tau_i(\theta,p)$, and $S(p)$ in Eq. (2.1) above will vary from one spectral region to another due to the wavelength dependence of atmospheric scattering and absorption processes. Consequently, the choice of observational wavelengths provides a means to focus selectively on particular meteorological parameters. Table 2-1 summarizes the features of boundary and atmospheric source functions, $R_i(p_b)$ and $S(p)$, respectively, in different wavelength regions (Isaacs et al., 1986).

In Eq. (2.1) the scattering source function contribution to the total source function (see Table 2-1) is given by the product of the single scattering albedo $\omega_i(p)$, i.e., the local ratio of total scattering to total extinction, and the scattering source function $J_i(p,\Omega)$ defined by

$$J_i(p,\Omega) = \frac{1}{4\pi} \int P_i(p,\Omega,\Omega') \, R_i(p,\Omega') \, d\Omega' \qquad (2.4)$$

where $P_i$ is the angular scattering function and $R_i(p,\Omega')$ is the value of the local radiance field (Chandrasekhar, 1960). Angular scattering (e.g., phase) functions have been evaluated for aerosol in the visible and infrared (Ridgway et al., 1982); cloud in the infrared (Yamamoto et al., 1971); and

Table 2-1 Radiative source functions. Forms of boundary, $R_i(P_b)$, and atmospheric, S(p), contributions to sensor-incident radiances, $R_i(\theta)$.

| Spectral Region | Boundary, $R_i(p_b)$ | Source Function, S(p) |
|---|---|---|
| [1] Ultraviolet/visible ($\lambda < 0.7$ $\mu$m) | $\pi F_i \rho_i(\Omega_o) \tau_i(\theta_o, p_b)$ | $\omega_i(p) J_i(p,\Omega)$ |
| [2] Near infrared $0.7 < \lambda < 4.0$) | $\pi F_i \rho_i(\Omega) \tau_i(\theta_o, p_b)$ + $\epsilon_i B_i[T(p_b)]$ | $[1-\omega_i(p)] B_i[T(p)]$ + $\omega_i(p) J_i(p,\Omega)$ + $(1-\epsilon_i) R_i\downarrow(p_b)$ (note 1) |
| [3] Infrared ($4.0 < \lambda < 100$ $\mu$m) | $\epsilon_i B_i[T(p_b)]$ + $(1-\epsilon_i) R_i\downarrow(p_b)$ | $B_i[T(p)]$ (note 2) |
| [4] Millimeter/microwave ($\lambda > 100$ $\mu$m) | $\epsilon_i B_i[T(p_b)]$ + $(1-\epsilon_i) R_i\downarrow(p_b)$ | $[1-\omega_i(p)] B[T(p)]$ + $\omega_i(p) J_i(p,\Omega)$ (note 3) |

Legend

| | |
|---|---|
| $F_i$ | solar irradiance |
| $\rho_i$ | bidirectional reflectance of boundary |
| $\Omega_o, \theta_o$ | sun/sensor reflection angle, solar zenith angle |
| $\epsilon_i$ | boundary emissivity |
| $\omega_i$ | single scattering albedo |
| $R_i\downarrow$ | downward atmospheric flux |
| $B_i$ | Planck function (thermal source function) |
| $J(p,\Omega)$ | scattering source function for scattering angle $\Omega$ |

Notes:
(1) Assumes scattering by aerosol or cloud.
(2) Assumes no scattering, if scattering, same as [2].
(3) Assumes scattering by precipitation; if no scattering, same as [3].

precipitation in the microwave (Savage, 1978; Isaacs et al., 1988). Since the scattering source function depends on the local radiance field a numerical solution is required (Lenoble, 1985).

Parameters determining the radiometric properties of the boundary (temperature, emissivity, albedo) and those related to these properties (e.g., surface wind over the ocean and soil moisture over land in the microwave region) may be inferred directly from the first term in Eq. (2.1) if the atmospheric contributions from the second term are negligible or can be subtracted away. Spectral regions satisfying these criteria are commonly referred to as atmospheric transmission "windows". Window spectral regions

are summarized in Table 2-2 (Fraser and Curran, 1976). In addition to surface related information, imaging wavelengths also provide a means to observe the influence of atmospheric scatterers such as aerosol, cloud, and precipitation (depending on spectral region) on sensor incident radiances. In this case contributions from the second term in the r.h.s. of Eq. (2.2) are no longer negligible. Parameters potentially observable in this manner include cloud optical depth at visible wavelengths and cloud liquid water content and rainfall rate in the millimeter/microwave regions.

In spectral regions where scattering can be ignored (i.e., $\omega_i = 0.0$), the wavelength dependence of transmissivity can be exploited as a means to sound the atmosphere's vertical structure (Kaplan, 1959). Assuming unit surface emissivity ($\epsilon_i = 1.0$) and choosing spectral regions with a single active absorber, Eqs. (2.1) and (2.3) may be combined using Table 2-1 to yield the following retrieval equation for nadir viewing:

Table 2-2 Transmission windows. Major atmospheric windows available for spacecraft remote sensing (Fraser and Curran, 1976).

| Spectral Region | Windows |
|---|---|
| Microwave | 20.0+ mm |
| | 7.5-11.5 |
| | 3.0-3.75 |
| | 2.06-2.22 |
| Thermal Infrared | 17.0-22.0 μm |
| | 10.2-12.4 |
| | 8.0-9.2 |
| Mid-Infrared | 4.5-5.0 |
| | 3.5-4.16 |
| Near-Infrared | 2.05-2.4 |
| | 1.55-1.75 |
| | 1.19-1.34 |
| | 1.0-1.12 |
| Ultraviolet and Visible | 0.77-0.91 |
| | 0.30-0.75 |

$$R_i(\theta,p_o) = B_i[T(p_b)]\ \tau_i(\theta,p_b) \qquad (2.5)$$

$$+ \frac{1}{g}\int_{p_b}^{p_o} B_i[T(p)]\ q(p)\ k(\nu_i,p)\ \exp[\frac{-1}{g}\int_{p_o}^{p} q(p')\ k(\nu_i,p')dp']dp$$

For uniformly mixed gases such as $CO_2$ or $O_2$, q(p) is assumed to be constant, and Eq. (2.5) may be used to obtain the temperature profile, T(p). Conversely, given the temperature profile, a mixing ratio profile (such as that of $H_2O$, for example) may be obtained. Applicable temperature sounding wavelengths and corresponding species are summarized in Table 2-3.

Table 2-3 Sounding wavelengths and species

| Band | Species | Wavelength |
|---|---|---|
| Visible | $O_3$ | 0.6 $\mu$m |
| Near IR | $H_2O$ | 0.94 |
| | | 1.16 |
| | | 1.38 |
| | | 1.89 |
| | $CO_2$-$H_2O$ | 2.51 |
| Middle IR | $CO_2$ | 4.30 |
| | $H_2O$ | 6.70 |
| Thermal IR | $O_3$ | 9.6 |
| | $CO_2$ | 15.0 |
| | $H_2O$ | 20 |
| Microwave | $H_2O$ | 0.16 cm (183 $GH_z$) |
| | | 1.35 cm (22.235 $GH_z$) |
| | $O_2$ | 0.25 cm (118 $GH_z$) |
| | | 0.5 cm (60 $GH_z$) |

### 2.1.3 Rapid Algorithms

Rapid transmittance algorithms are devices to reduce computer usage time when many retrieval scenarios are desired and the channel set and desired path are well defined (McMillin and Fleming, 1976; Fleming and McMillin, 1977; McMillin et al., 1979; Susskind et al., 1982; Eyre and Woolf, 1989). In circumstances when the user wishes to obtain many retrieval simulations obtained under a variety of environmental conditions, the use of a line-by-line code as the forward problem simulator may not be the most efficient approach. This would be the case, for example, when the sensor channel set has been selected, and it is desired to obtain statistics to evaluate the dependence of retrieval accuracy on regional or seasonal meteorology. Once sensor channels and particular paths are selected, line-by-line (LBL) calculations can be avoided by parameterizing layer transmittance as functions of path related temperature and constituent abundances. These parameterizations are derived based on and calibrated by the LBL transmittance calculations. The rapid algorithm reproduces the required channel transmittances, including their dependence on the important path variables such as temperature and constituent abundances to a desired accuracy. Given an analytical form of the approximate transmittance model, LBL calculations are used both to generate empirical coefficients and to verify the model.

For example, a rapid algorithm was developed at NASA Goddard Space Flight Center to provide accurate simulations of the radiances from the HIRS2 infrared temperature and moisture sounder (Susskind et al., 1982). The averaged discrete line transmittance, $\bar{\tau}_{i\ell}$, through the atmosphere from pressure p to pressure $p_\ell$ along a given atmospheric path, at a zenith $\theta$ as seen by channel i, is modeled as:

$$\bar{\tau}_{i\ell}(\theta,p) = \prod_{j=1}^{\ell} \bar{\tau}_{iF}(p_j,p_{j-1},\theta)\bar{\tau}_{iO}(p_j,p_{j-1},\theta)\,\bar{\tau}_{iW}(p_j,p_{j-1},\theta) \qquad (2.6)$$

where $\bar{\tau}_{iF}$, $\bar{\tau}_{iO}$, and $\bar{\tau}_{iW}$ represent models for effective layer transmittances from pressure $p_j$ to $p_{j-1}(p_j > p_{j-1})$ at zenith angle $\theta$. The term $\bar{\tau}_{iF}$

represents absorption by gases assumed to have a fixed mixing ratio, while $\bar{\tau}_{iO}$ and $\bar{\tau}_{iW}$ represent absorption due to ozone and water vapor, respectively.

Most of the absorption for the HIRS2 temperature sounding channels is due to the gases of fixed distribution, primarily $CO_2$ and $N_2O$. In these cases, transmittance at a given angle depends only on the temperature profile. The model for mean layer transmittance due to gases of fixed distribution for each reference angle is given by:

$$\tau_{iF}(p_j, p_{j-1}, \theta) = A_{ij}(\theta) + B_{ij}(\theta)\left[T_j - T_j^0\right] + C_{ij}(\theta)\left[T_{ij}(\theta) - T_{ij}^0(\theta)\right] \qquad (2.7)$$

where $T_j$ is the mean temperature in the layer j, between $p_j$ and $p_{j-1}$, for the temperature profile under consideration, $T_j^0$ is the mean temperature in layer j in a standard temperature profile, and $T_{ij}$ and $T_{ij}^0$ are effective mean temperatures for the entire profile from $p_j$ to the top of the atmosphere for the temperature profile under consideration and the standard temperature profile, respectively. The effective mean temperature above pressure p for channel i is defined as the average temperature above pressure p weighted by the weighting function for channel i. The effective temperature is then channel and angle dependent and is defined as:

$$T_{ij}(\theta) = \frac{1}{1-\tau_i^0(p_j,\theta)} \int_0^{p_j} T(p) \frac{d\tau_i}{dp}(\theta)\, dp \qquad (2.8)$$

where $\tau_i^0(p,\theta)$ is the transmittance of channel i for the standard temperature profile. The coefficients $A_{ij}(\theta)$, $B_{ij}(\theta)$, and $C_{ij}(\theta)$ are determined so as to give the best fit in the least squares sense to the values of $\tau_{iF}$ obtained from LBL calculations. Similar expressions are used to obtain layer transmittances due to water vapor and ozone.

A rapid algorithm generator has not been provided as part of the path characterization effort; however, any appropriate band model can be adopted for this purpose.

## 2.2 The Inverse Problem

The fundamental retrieval problem may be stated as follows: given a set of measurements of the radiation emitted, scattered, and/or reflected from the earth-atmosphere system what can be deduced about the physical state of this system? There are many individual retrieval methods. However, a recurrent theme of the many comprehensive reviews available (Westwater and Strand, 1972; Rodgers, 1976; Towmey, 1977; Fymat and Zuev, 1978) is the conceptual unity among apparently diverse approaches. This is due to the fact that these approaches all share the same general underlying mathematical problem.

Stated symbolically, we obtain radiance data $d_j$, $j = 1,...M$ which are the sum of an unknown error, $\epsilon_j$ and a contribution $F_j$ which depends on the thermodynamic and compositional parameters of interest, $p_i$, $i = 1,...N$. That is,

$$d_j = F_j(p_1, p_2,...p_N) + \epsilon_j \qquad j = 1,...M. \tag{2.9}$$

The $F_j$ are known as mapping functions. The retrieval problem is: given the $d_j$, determine the $p_i$. For the problem at hand the $F_j$ are determined by the wavelength dependent radiative transfer processes, including absorption, emission and scattering by the atmosphere, by clouds and by the surface. The desired parameters $p_i$ include atmospheric temperatures T(p), surface temperature $T_s$, surface pressure $p_s$, and relevant gaseous absorber amounts q(p). For the purpose of discussion consider a mapping function of the form

$$F = \int_{\ln p_o}^{\ln p_b} B(T(p))\, W(p,T(p))\, d\ln p \tag{2.10}$$

where B, the Planck function, and W, the weighting function, are known. The major contribution to the mapping functions for the retrieval of atmospheric temperature structure has this form. Since T(p) is a function of pressure but the number of available channels of data, M, is finite, such problems, even in the absence of measurement errors, do not have unique solutions and are thus not well-posed. To be well-posed a problem must have a solution which exists, which is unique and which depends continuously on the data of the problem. By data we mean the parameters, functions, etc., used to specify the particular

problem. In our example, the measurements $d_j$ and the functions B and W are the data. The retrieval problem may be rendered well-posed by adding some constraints on the physical parameters to be retrieved. For example, T(p) may be expressed as a finite sum of known empirical structure functions. With this formulation the coefficients of the structure functions become the unknowns and the problem reduces to a finite set of algebraic equations. Such systems of equations will not in general be well-posed, but if the number of (independent) channels is equal to the number of coefficients the problem will be well-posed. However, well-posedness and its implied continuous dependence on the data is not enough to insure that the solution to a problem will be useful when the data are uncertain.

In practice, the data always have some degree of uncertainty, and solutions of a well-posed problem can still be ill-conditioned, that is very sensitive to the data. When this is the case, small measurement errors may be translated into large errors in the retrieved parameters. Ill-conditioning occurs for example when variation of one of the geophysical parameters has only a small effect on the measured radiances. In our example, decreasing the number of coefficients used and minimizing the sum of squared $\epsilon_j$ will usually improve the conditioning of the problem.

Ultimately, all retrieval methods are constructed to address the problems of ill-posedness and ill-conditioning. One or both of these problems may cause a particular method to produce nonphysical results or fail to converge. Methods which are successful circumvent these potential pitfalls by introducing some (explicit or implicit) constraint on the solution based on a priori knowledge of the physical system. We will classify the constraints as one of the following: (1) a smoothness constraint, (2) a statistical constraint, or (3) a physical constraint. These classes of constraints correspond to three types of retrieval methods: smoothing (Phillips, 1962; Twomey, 1963; Tikhonov, 1963) as applied, for example, by Wark and Fleming (1966), statistical (Strand et al., 1970; Rodgers, 1971; Smith et al., 1970; Turchin et al., 1971; Smith and Woolf, 1976), and physical (Chahine, 1968; Chahine, 1972; Smith, 1970; Susskind et al., 1984; Smith et al., 1986).

A fourth approach (Backus and Gilbert, 1967; 1968; 1970) which is usually applied to the design and analysis of the instruments themselves rather than to the actual retrievals, recognizes that sufficient constraints may not exist

to render the problem well-posed and, furthermore, that it may not be possible to reduce noise levels in the data to a level which results in acceptable conditioning of the retrieval problem. Thus, there is a tradeoff between acceptable noise and sufficient resolution in retrieving the desired parameters. The approach of Backus and Gilbert provides criteria to select the set of retrieved parameters. This approach has been applied diagnostically to study the vertical resolution available from temperature retrievals (Conrath, 1972; Thompson, 1982).

Although all the techniques cited above are designed to solve the same mathematical problem, they may produce results which differ considerably in practice. This is a consequence of using different a priori data, adaptability to a particular problem, and computational details.

## 2.3 Path Characterization Approaches

There are a considerable number of potential algorithms available for implementation as path characterization approaches. Table 2-4 summarizes the path characterization retrieval related approaches to be discussed in this section and their applications.

Table 2-4 Candidate path characterization retrieval approaches discussed in this section

| Retrieval Method/ [Section] | Reference | Application |
|---|---|---|
| nonlinear, iterative [2.3.1] | Chahine, 1968; 1972; Smith, 1970 | Thermal and constituent retrievals; requires forward problem simulator; time consuming line-by-line simulation can be avoided by implementing a rapid transmittance algorithm. Implementation straightforward. |
| statistical [2.3.2] | Smith and Woolf, 1976; Westwater and Strand, 1968; Isaacs and Deblonde, 1987 | Requires statistics relating parameters and data; if concurrent data/parameter observations are available, no forward problem is necessary; alternatively, synthetic data can be simulated; statistical retrievals provide excellent first guess profiles for nonlinear, iterative method. Easy to implement. |
| simultaneous [2.3.3] | Smith et al., 1986; Isaacs, 1989 | Combines attributes of statistical and Chahine-type retrieval. Obtains thermal and constituent soundings simultaneously. |

### 2.3.1 Nonlinear, Iterative Retrievals

Chahine (1968; 1972) has developed a general nonlinear, relaxation method to invert the radiative transfer equation for all atmospheric parameters which appear in its integrand. The approach provides the capability to retrieve such desired parameters as temperature and species concentrations of active absorbers along a specified path using little a priori information. Chahine (1972) has discussed the necessity for a nonlinear approach to treat ill-conditioned problems such as those commonly encountered in path retrieval calculations. The method does require an accurate code to calculate the forward problem. In the present context, the forward problem generators discussed in Section 2.1 would be appropriate.

The solution is obtained iteratively, adjusting a first guess sounding of the desired parameter based on comparison of simulated with actual data. Adjustments are made to the trial parameter profiles by associating each sensor channel brightness temperature with that layer in the atmosphere which is most sensitive to a local change in the desired parameter. This association is made through the channel weighting functions. A solution is obtained when simulated data obtained using the iterative, trial sounding is consistent with the actual data. The iterations are terminated and the retrieval said to converge when the simulated and actual data differ by sensor channel noise equivalent radiances.

The forward problem simulation of path radiance is obtained from the radiative transfer equation. The radiances in each of the N selected sensor channels, $R(\nu_i)$, i=1,..N, will depend on the temperature and constituent profiles through the relation:

$$R(\nu_i) = B(\nu_i,T_s)\tau(\nu_i,p_1) + \int_{\ell np_1}^{\ell np_2} B[\nu_i,T(p)] \frac{\partial \tau}{\partial \ell np} \partial \ell np \qquad (2.11)$$

where $p_1$ and $p_2$ are the pressures at the specified path endpoints and a target with unit emissivity and temperature $T_s$ is placed at the path terminus. For general paths, this equation could have been written in terms of a range variable rather than pressure. For consistency with the retrieval literature, we have retained pressure as the independent variable. The temperature profile T(p) appears explicitly as an argument of the Planck function, B. However, the dependence of the radiance on the composition profile of the relevant absorbing gas, q(p), is implicit in the transmittance factor.

The retrieval is obtained by starting from an arbitrary initial guess for temperature or composition profile (i.e., $T_n(p)$, $q_n(p)$; n=0). If any subsequent trial profile is a retrieval solution, then the residuals for each channel defined as:

$$\Delta^n(\nu_i) = R(\nu_i) - R^n(\nu_i) \tag{2.12}$$

will approach the magnitude of the computational and instrumental noise for all channels. If this convergence criteria is not satisfied, the desired parameter profile is adjusted. The adjustments are applied within specific domains of the path determined by the sensitivity of each channel's response to path changes in the desired parameter. For simplicity, adjustments are made at N path positions using the N channels of dat The location of these positions is determined by the channel weighting functions. The adjustment for each channel is accomplished via a relaxation equation.

The form of the relaxation depends on whether temperature or composition is being treated. For temperature, it is easy to show that a new guess (i.e., the n+1th iteration) for the Planck function (and hence, temperature profile) at each of the N path domains associated with a channel can be calculated from the nth trial Planck function and its associated simulated radiance $R^n(\nu_i)$ and the radiance data for that channel, $R(\nu_i)$, by the expression:

$$B[\nu_i, T^{n+1}(p)] = \frac{R(\nu_i) \quad B[\nu_i, T^n(p)]}{R^n(\nu_i)} \tag{2.13}$$

This expression can be simplified to obtain the following form for the relaxation equation for temperature:

$$T^{n+1}(p_i) = a_i T^n(p_i) \tag{2.14}$$

To apply the approach for composition profiles, Eq. (2.11) above is integrated by parts to obtain:

$$I(\nu_i) = B(\nu_i, p_2) - \int_{\ell np_1}^{\ell np_2} \tau[\nu, q(p)] \frac{\partial B}{\partial \ell np} \, \partial \ell np. \tag{2.15}$$

From this form of the equation a similar relaxation equation for the composition profile is obtained:

$$q^{n+1}(p_i) = a_i q^n(p_i) \tag{2.16}$$

After each iteration and application of the relaxation equation, the adjusted profile is obtained by connecting the N path domains by a suitable interpolation formula. The relaxation is repeated until the relaxation parameters $a_i$ approach unity and the residual criteria are met.

The Chahine-type retrieval has been widely applied in the remote sensing community. Smith (1970) developed a similar approach to obtain temperature profiles from satellite borne radiometer data. Recently, Kaplan et al. (1986) used the Chahine retrieval approach to investigate the water vapor profile retrieval capabilities of a proposed next generation infrared sounder.

### 2.3.2 Statistical Estimation

Statistical retrievals are based on an approach to obtaining geophysical parameters from radiometric data discussed by Rodgers (1976), Westwater and Strand (1968), Smith and Woolf (1976), and Isaacs and Deblonde (1987). The essential element of the scheme is to choose, in a statistical sense, the most probable combination of atmospheric path properties which produces the set of measured radiometric data values. It is a general statistical regression technique which minimizes the mean square error between the estimated and observed values of the parameter of interest. As applied to the path characterization problem, the desired parameters, $p_i$, are the thermodynamic and compositional state of the path. The data, $d_j$, are measured radiances, brightness temperatures, or transmittances. Of course, the forward problem algorithm can be used to generate synthetic data sets from which to obtain statistics. The statistical estimation formalism provides two important capabilities: (1) use of statistical estimation can provide excellent first guesses for the Chahine-type retrieval (Kaplan et al., 1986), and (b) the eigensystem decomposition of the covariance matrices of parameter and data sets calculated as an intermediate step in the evaluation of the regression or "D" matrix (described below) provide insight into the information content of the retrieval.

An individual retrieval of a specified parameter vector (e.g. temperatures at r levels) is obtained from:

$$\bar{p} = D\bar{d} \tag{2.17}$$

with

$$D = (UT^t)(T^*\Lambda^{*-1}\hat{T}^{*t}) \tag{2.18}$$

where

$\bar{p}$ is the parameter vector, a vector giving a statistical estimate of the profile of the desired parameter in each of r layers

$\bar{d}$ is the data vector, a vector whose components are n brightness temperatures or radiances

$U_{rs}$ is the parameter profiles matrix at r levels for s atmospheric samples

$T_{ns}$ is the brightness temperature or radiance matrix for n channels for s samples

$\hat{T}^*$ are "selected" eigenvectors of $TT^t$

$\Lambda^*$ is the diagonal matrix whose elements are the corresponding eigenvalues

The eigenvectors having relatively small eigenvalues (compared with the largest eigenvalue) can be discarded since they represent noise. In the algorithm employed, only eigenvectors of the covariance matrix of the data set with itself have the potential to be discarded. The advantage of the method is that by truncating the sequence of eigenvalues, one reduces the condition number of the matrix, and therefore also the sensitivity to noise. In this method, if none of the eigenvectors are discarded, the problem reduces to that of solving the least squares fit problem, i.e.

$$D = UT^t(TT^t)^{-1} \tag{2.19}$$

From Eq. (2.17), it can be seen that the statistical retrieval reduces computationally to the multiplication of the "D" matrix with the data vector, $\bar{p}$. It is therefore qui e an efficient approach.

### 2.3.3 Smith's Simultaneous Approach

This approach employs a perturbation form of the radiative transfer equation which relates changes in atmospheric path parameters to changes in sensor channel brightness temperatures. These changes are defined with respect to a selected a priori first guess or climatological mean. By inverting this relationship in a least squares sense, residuals in channel brightness temperatures (defined as the difference between observed brightness temperatures and those evaluated assuming the first guess atmospheric profiles) can be used to evaluate the most likely atmospheric profile. This approach uses all channels and retrieves such path parameters as the temperature and water vapor profiles, surface temperature, and surface emissivity simultaneously. Therefore, Smith calls it a simultaneous retrieval method. Other approaches generally use "temperature" channels to retrieve temperature, "water vapor" channels to retrieve water vapor, etc.

Writing Eq. (2.5) in a perturbation form, the change in ith channel radiance is given by:

$$\delta R_i = \int_{p_s}^{0} \delta T \frac{\partial B}{\partial T} \frac{\partial \tau}{\partial p} dp - \int_{p_s}^{0} \delta q \frac{\partial \tau}{\partial q} \frac{\partial B}{\partial p} dp$$

$$+ \delta \epsilon_i B_i (T_s) \tau_i (p_s) \qquad (2.20)$$

$$+ \delta T_s \epsilon_i \tau_i (p_s) \frac{\partial B_i}{\partial T_s} (T_s)$$

where $\delta T(p)$, $\delta q(p)$, $\delta \epsilon$, and $\delta T_s$ are changes in the temperature and moisture profiles, surface emissivity, and surface temperature for an a priori value, e.g.,

$$\delta T(p) = T(p) - \bar{T}(p). \tag{2.21}$$

The a priori value can be a first guess or climatological value. The change in $i$th channel brightness temperature is given by

$$\delta T_{B_i} = \delta R_i / \left[\frac{\partial B}{\partial T}\right]_{T_{B_i}} \tag{2.22}$$

Focusing on the temperature profile alone, the perturbation profile $\delta T(p)$ can be expanded about a suitable set of functions $\phi_j$:

$$\delta T(p) = \sum_{j=1}^{M} \alpha_j \phi_j(p). \tag{2.23}$$

We have used empirical orthogonal functions (EOFs) of temperature and moisture in our work. (Smith uses the weighting functions.) This result is:

$$\delta T_{B_i} = \sum_{j=1}^{M} \alpha_j \Phi_{ij}.$$

or

$$\delta \bar{T}_B = \Phi \bar{\alpha} \tag{2.24}$$

where

$$\Phi_{ij} = \left[\frac{\partial B_i}{\partial T}\right]^{-1} \int_0^{p_s} \phi_j(p) \frac{\partial B_i}{\partial T} \frac{\partial \tau_i}{\partial p} \, dp. \tag{2.25}$$

In this equation, $\delta \bar{T}_B$ is a vector of residuals of observed brightness temperature from an a priori set based on the assumed first guess temperature and water vapor profiles. By linearizing the result above, it can be related to the physical temperature retrieval approach described by Susskind et al. (Susskind et al., 1984).

The inversion for the temperature profile is obtained by solving (2.24) above for the vector, $\bar{\alpha}$, of coefficients in the EOF expansion about the first guess. This is done using least squares:

$$\bar{\alpha} = (\Phi^T \Phi + \sigma I)^{-1} \Phi^T \delta\bar{T}_B \tag{2.26}$$

where the $\sigma I$ term stabilizes the matrix inversion. This type of least squares is often called ridge regression and $\sigma$ the ridge parameter. Once inverted:

$$T(p) = \bar{T}(p) + \delta T(p) \tag{2.27}$$

$$\text{where } \delta T(p) = \sum \alpha_i \phi_i(p). \tag{2.28}$$

Smith et al. (1986) have applied this technique to retrieve temperature and water vapor using HIRS2 data and to HIS interferometric data sets (Smith et al., 1987). The simultaneous approach has also been adopted to unify retrievals using DMSP microwave mission sensor (i.e., SSM/T, SSM/T-2, SSM/I) data (Isaacs, 1989).

## 2.4 Selection of Path Characterization Retrieval Algorithm

Based on our review of the computational attributes of these methods and the requirements imposed by interfaces with the FASCODE formalism, a variation of the simultaneous approach which we have called the physical least squares method has been selected as the viable methodology for the path characterization problem.

A number of considerations have contributed to this decision:

(a) Statistical: Implementation of the statistical retrieval approach is based on the availability of statistics relating sensor channel data (brightness temperatures, radiances, spectra) and the desired path characteristics (level temperatures, constituent abundances, etc.). In a sense, this is the most versatile approach since sensor data can easily be correlated with path dependent parameters of any kind. As a practical matter, however, such statistical data bases, even if available, can't readily be included with FASCODE. We require that the path characterization retrieval process should be independent of external data bases. The required statistics could be generated using FASCODE as the sensor simu-

lation model. However, in our judgment we feel that, in its current form, the production of simulated statistical data bases would be too costly for the average user. (These considerations depend to a certain extent on whether an efficient rapid algorithm is feasible for use with FASCODE). Another nontrivial disadvantage of the statistical approach is its inherent linearity which limits its applicability to the retrieval of constituent abundances. Finally, the approach proceeds somewhat independently of the essential physics of the radiative transfer process. This is not very satisfying to us.

(b) Chahine - The Chahine type retrieval avoids the requirement for statistical data bases required above. It also treats the nonlinearities of the problem and includes the essential physics of radiative transfer. We see a difficulty, however, in a straightforward, generic code implementation which will treat the broad range of user defined problems which will potentially be encountered. The most effective formulation of these retrievals are individually designed to specifically treat temperature, moisture, clouds, etc. This is an important consideration because the retrieval of constituent abundances will require a retrieved temperature profile. In the satellite retrieval problem, clouds are done first, followed by temperature, and then perhaps moisture (see Susskind et al., 1984). It is not clear that this hierarchy of retrieval calculation can easily be established for the generic path characterization problem. For example, assuming that two or more constituent abundances are required, and that it is always necessary to do the temperature retrieval first, how does one decide which species to retrieve first?

An additional consideration, often missed, is that the relaxation equation used in the Chahine type retrieval, must be carefully formulated to optimize the problem. The relaxation equation provides the relationship which adjusts the $n^{th}$ order trial solution to obtain the $n+1^{th}$ solution. Studies at AER have indicated that this must be carefully selected for the water vapor problem, bearing in mind the physics of the water vapor absorption process for the selected channel set. This is not possible in a generic formulation, and we suspect the relaxation can be suboptimal (i.e. over- or under-relaxed). This could lead to convergence problems. Finally, as with all iterative approaches, first guess values

for desired parameters are required. This is not an important restriction, however, since the inherent FASCODE model atmospheres can be used to provide the appropriate first guesses.

(c) Simultaneous - The simultaneous retrieval avoids most of the pitfalls discussed with respect to the approaches above. It has the following attributes: (a) no extensive supplementary data sets are required, (b) the method is self-contained, (c) nonlinearities and the physics are all treated, (d) there is no requirement to establish a hierarchy for the retrieval process since all path parameters are treated simultaneously, and (e) the analog of the relaxation equation, based on a perturbation approach applied to the forward problem, is intrinsic to the formulation and need not be individually formulated. A further appeal is its capability for generic application.

The discussion above is summarized in the attached Table 2-5. The FASCODE related attributes of each retrieval approach which were considered in the selection process are illustrated. The desirable attributes are indicated in italics. The choice of the simultaneous retrieval approach is most consistent with the desired attributes relative to a FASCODE implementation.

## 3. PREPROCESSING ALGORITHM

The purpose of the screening algorithm is to provide the user with potentially fruitful spectral regions for the retrieval of desired atmospheric properties. The spectral data for each molecule is taken from the HITRAN database, the background atmosphere is specified via FASCODE procedures, and the screening algorithm selects the ideal set of wavenumbers to cover the range in optical depth.

### 3.1 Spectral Screening

The objective of this code segment is to avoid the necessity to perform multiple FASCODE calculations at full spectral resolution to identify potentially useful spectral regions.

Table 2-5 FASCODE related attributes of candidate retrieval approaches

| Attribute | Approach/Reference Statistical (Gaut et al., 1975) | Iterative (Chahine, 1972) | Simultaneous (Smith et al., 1985) |
|---|---|---|---|
| External data bases required | yes | *no* | **minimal** |
| Nonlinear | no | *yes* | *yes* |
| Physics treated | no | *yes* | *yes* |
| Hierarchy required for multiple parameters | *no* | yes | *no* |
| Relaxation equation optimization | n/a | *no* | yes |
| First guess required | *no* | yes | yes |
| Generically applicable | *yes* | no | *yes* |

We have decided that a suitable band model would provide the essential information to accomplish this aspect of the preprocessing. The following discussion describes the development of this band model. The governing equation for the emitted flux reaching the top of a plane-parallel stratified atmosphere overlying a black surface at pressure $p_s$ is (Kaplan et al., 1977):

$$I_j = \int_{p_0}^{0} B_j[T(p)][d\tau_j(p,0)/d\ln p]d\ln p + B_j[T(p_s)]\tau_j(p_s,0), \quad (3.1)$$

where $B_j(T,\nu_j)$ is the blackbody radiance in a channel centered at frequency $\nu_j$.

If the channel has an effective bandpass $D_j$ and contains a random array of lines of individual equivalent widths $W_{ji}$, the average transmittance is (Kaplan, 1953):

$$\tau_j(p,0)_{lines} = \exp\left[-\sum_i W_{ji}(p,0)/D_j\right] \tag{3.2}$$

to the extent that the lines in $D_j$ are representative of those in a broader bandpass. If, further, the lines have a Lorentz shape and their intensities $S_{ji}$ and halfwidths $\alpha_{ji}$ are independent of temperature and the absorbing gas is uniformly mixed in the atmosphere with volume fraction q, the individual equivalent widths have the value (Pederson, 1942):

$$W_{ji}(p,0) = 2\sqrt{\pi(\alpha_{0_{ji}} p/p_0)}\Gamma(\eta_{ji} + 1/2)/\Gamma(\eta_{ji}), \tag{3.3}$$

where $\alpha_{0_{ji}}$ is the halfwidth at reference pressure $p_o$, and

$$\eta_{ji} = (qS_{ji}p_0)/(2\pi\alpha_{0_{ji}}\rho_o g) \tag{3.4}$$

is independent of height with $\rho_0$ being the reference density used to define $S_{ji}$ and g the acceleration of gravity.

With the substitution of Eq. (3.3), Eq. (3.2) becomes

$$\tau_j(p,0)_{lines} = \exp(-\alpha_j p), \tag{3.5}$$

where

$$\alpha_j = \frac{2\sqrt{\pi}}{p_0 D_j} \sum_i \alpha_{0_{ji}} \Gamma(\eta_{ji} + 1/2)\Gamma(\eta_{ji}) \tag{3.6}$$

is a constant, which approaches proportionality to

$$\sqrt{(q/\rho_0)} \sum_i (S_{ji}\alpha_{0_{ji}})^{1/2}$$

as the $\eta_{ji}$'s increase, and to $(q/\rho_0)\sum_i S_{ji}$ as the $\eta_{ji}$'s decrease.

In terms of absorber amount

$$m = \frac{q}{\rho_0 g} p_0 \tag{3.7}$$

the optical path in the vertical from $p_0$ to the top of the atmosphere is obtained from Eqs. (3.2) through (3.6):

$$-\ln\tau_j(p_0,0) = \frac{2\sqrt{\pi}}{D_{ji}} \sum_i \alpha_{0_{ji}} \frac{\Gamma(S_{ij}m/2\pi\alpha_0 + 1/2)}{\Gamma(S_{ij}m/2\pi\alpha_0)} \tag{3.8}$$

This asymptotically approaches, in the weak- and strong-line limit, respectively,

$$-\ln \tau_j(p_0,0)_{WL} = \lim_{Sm\to 0} (-\ln \tau_j(p_0,0) = \sum_i S_{ji}m/D_j \tag{3.9}$$

$$-\ln(\tau_j(p_0,0)_{SL} = \lim_{Sm/\alpha_0\to\infty} (-\ln \tau_j(p_0,0) = \sum_i \sqrt{2S_{ji}m\alpha_{0ji}}/D_j. \tag{3.10}$$

It can be represented by, and has the same asymptotic limits as, a computationally efficient approximation

$$-\ln \tau_j(p_0,0) = \sum_i \frac{S_{ji}m}{D_j} \left[1 + \frac{S_{ji}m}{2\alpha_{0_{ji}}}\right]^{-1/2}, \tag{3.11}$$

which agrees with (3.8) to better than one or two percent. It is similar in form to the Goody (1952) random exponential model, which, however, differs in the strong-line limit by a factor of $\sqrt{\pi}/2$.

The weak- and strong-line approximations (3.9) and (3.10), can be used for a preliminary spectral screening to eliminate parts of the spectra that would not be useful for remote sensing purposes. For example, spectral regions $D_j$ need not even be considered for temperature sounding in the nadir viewing mode if the equivalent optical path of the molecular species considered is less than say, 0.01.

To the extent that the assumption of constant temperature and composition hold, the integrated optical path from the top of the atmosphere to any pressure level can be obtained by a linear multiplication of $p/p_o$, as can be seen from Eq. (3.3). This is the quantity required to compute the weighting functions. Further screening and preliminary channel selection require taking

into account variation with height of temperature and composition, using various typical or standard distributions. The temperature and composition corrections can be accomplished, in first order, by Godson's (Rodgers and Walshaw, 1966) scaling approximations, with the use of precalculated tabulation of ratios of $\sum_i S_{ji}$ and of $\sum_i \sqrt{S_{ji}\alpha_{oji}}$ as functions of temperature.

We account for the temperature dependence of the line strengths by compiling the quantities, $\sum_i S_{ji}$ and of $\sum_i \sqrt{S_{ji}\alpha_{oji}}$ as a function of temperature using the values, 200K, 250K, 296K, 340K, and interpolating as required. An efficient and accurate parameterization which we have developed uses a mixing function, $\gamma = \tau_{WL}/(\tau_{WL} + \tau_{SL})$. To obtain a hybrid optical depth for the region intermediate between the two limits, the following criteria have been established:

If $\gamma \leq 0.5$,

$$\tau \tilde{=} A(\gamma)\, \tau_{WL} \tag{3.12}$$

$$\text{where} \quad A(\gamma) = \left[\frac{(1-\gamma)^2}{(1-\gamma)^2 + \gamma^2}\right]1/2$$

If $\gamma > 0.5$,

$$\tau = B(\gamma)\tau_{SL}$$

$$\text{where} \quad B(\gamma) = \left[\frac{\zeta^2}{(1-\gamma)^2 + \gamma^2}\right]1/2 \tag{3.13}$$

Equations (3.12) and (3.13) provide a good approximation to the optical depth while allowing for a simple Curtis-Godson path characterization and computational efficiency.

Figures 3-1 and 3-2 illustrate results of the optical depth calculation for water vapor and ozone, respectively, for the first 100 $cm^{-1}$ at 1 $cm^{-1}$ resolution. The choice of resolution should be guided by the trade-off between high resolution FASCODE run time and faster screening algorithm application. For example, 1 $cm^{-1}$ would not be appropriate to screen for $O_2$ in the microwave, but would be to look at $CO_2$ in the infrared. Plotted are the

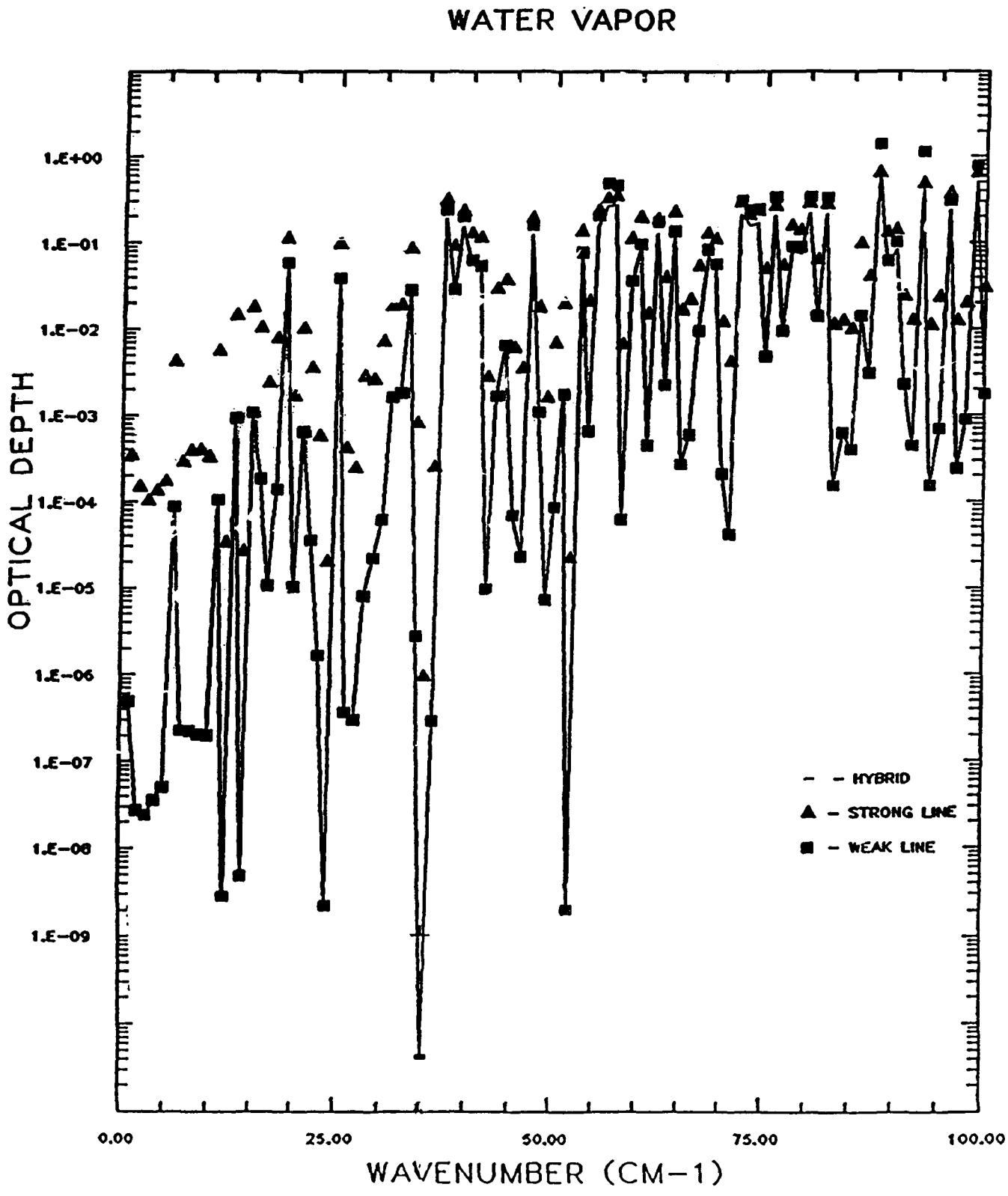


Figure 3-1. Screening algorithm calculation of water vapor optical depths for 0-100 $cm^{-1}$ region.

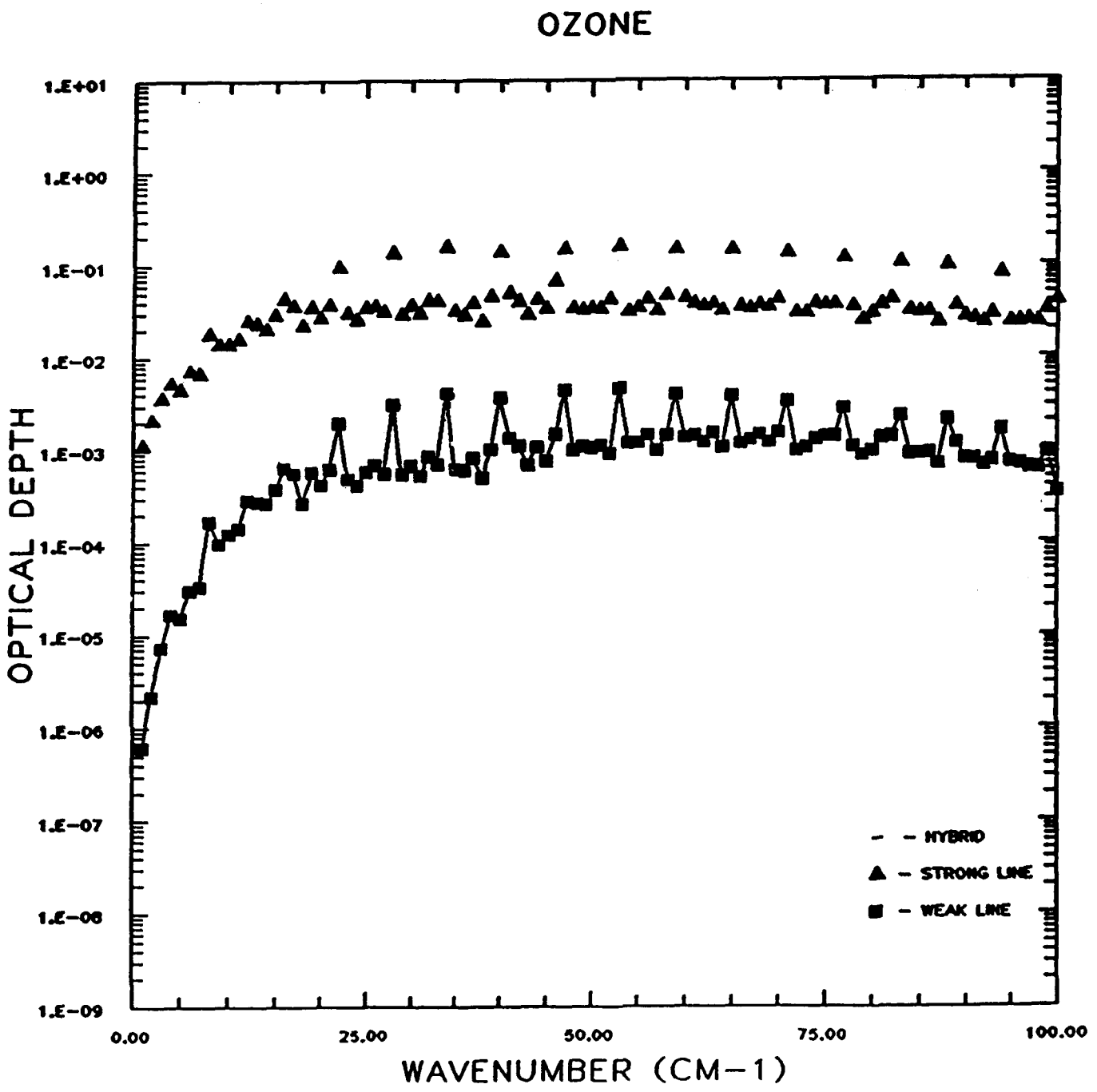


Figure 3-2. Screening algorithm calculation of ozone optical depths for 0-100 $cm^{-1}$ region.

weak-line, strong-line, and intermediate (see Eqs. (3.12) and (3.13)) optical thickness for each absorber assuming a path from space to an altitude of 40 km. These values scale with the Curtis-Godson modified absorber amounts. The rotational water vapor features at 22.235, 183.31, and 326 GHz are apparent as is the regular nature of the weak ozone absorption. Bear in mind that this data base is to be used for screening purposes only.

## 3.2 Screening Algorithm Implementation

The screening algorithm uses as inputs the object code FSCATMB (from FASCODE), input files Tape 5 (for FSCATM), and database files T200P1, T200P2, T200P3, T250P1, T250P2, T250P3, T296P1,T296P2, T29613, T340P1, T340P2, and T340P3. The database files store the molecular strong-line and weak-line optical depths for 4 temperatures and 28 molecules. The main output file is Tape 20, with a plotting file Tape 19.

The screening algorithm is shown schematically in Figure 3-3. To use the algorithm, the user specifies the atmosphere in normal FASCODE mode, specifies the wavenumber interval to be screened, and designates which molecules are of interest and which molecules constitute the background (usually all molecules are included). The algorithm echos back this information in the printout. It then reads the strong-line and weak-line molecular opacities off the database for the appropriate temperature, wavenumber, and molecules. A temperature and pressure interpolation is done. The strong-line and weak-line molecular opacities are scaled by column amounts and then are combined into a hybrid opacity. The optical depths are binned for the molecules of interest according to the number of channels selected by the user to specify his sounding.

The algorithm evaluates the optical depth for the molecules of interest versus the optical depth for the entire atmosphere as a function of wavenumber over the wavenumber interval. The algorithm prints out a histogram of the optical depths for the molecules of interest. Next it prints out a histogram of the number of wavenumber bins where the molecules of interest are easy to pick out from the background atmosphere. Then the algorithm selects and prints out the best wavenumber in each optical depth bin (channel) which has the best discrimination to do that sounding. The data can be plotted with standard FASCODE plotting routines using the plotting output file, Tape 19.

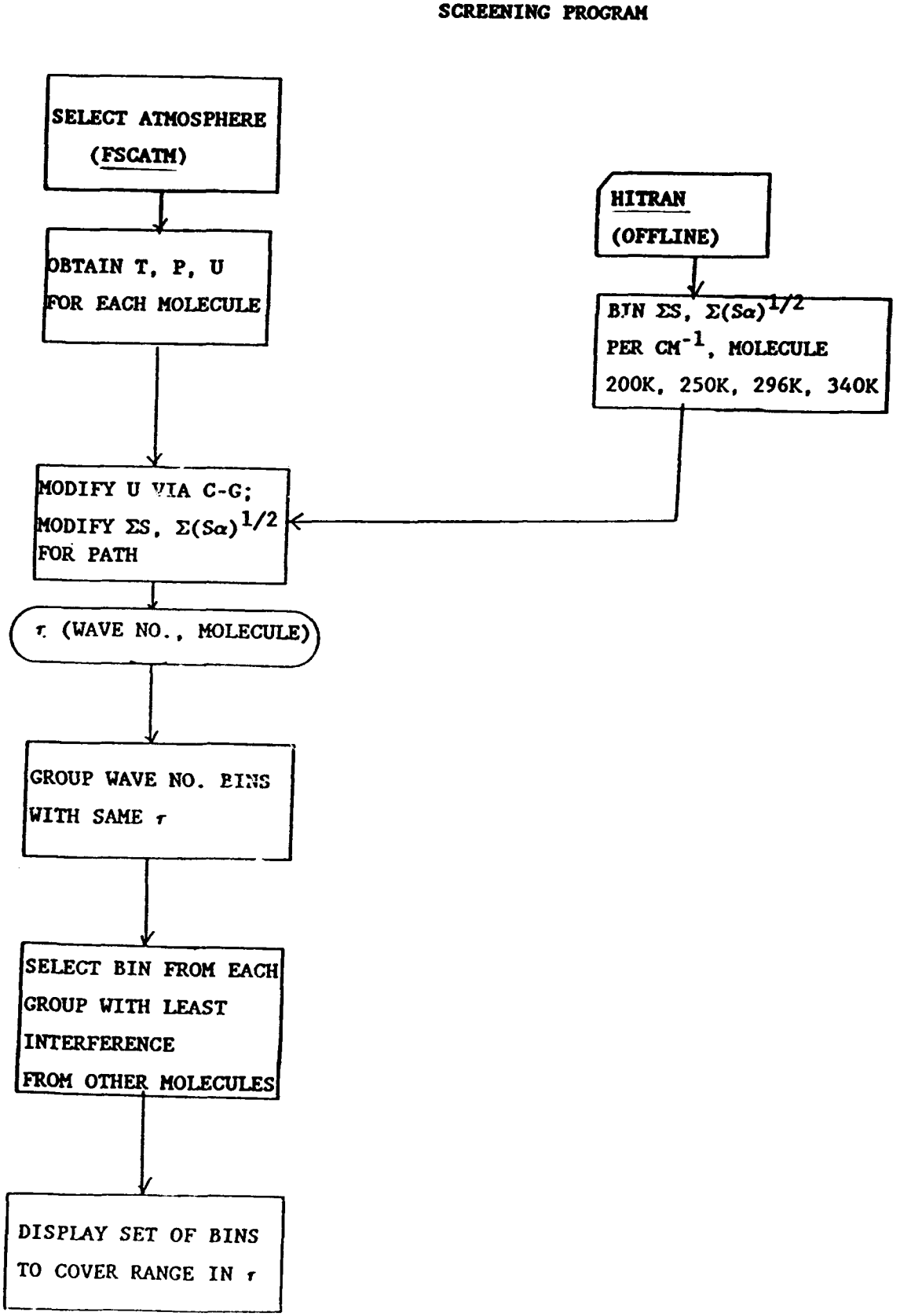


Figure 3-3. Schematic of retrieval screening algorithm.

### 3.3 Sample Output

Appendix A contains sample output from the screening algorithm. This case used a wavenumber interval of 1200 to 1950 $cm^{-1}$, a background atmosphere (FASCODE model 6) which used all 28 molecules, and the molecule of interest was water vapor.

## 4. RETRIEVAL CODE IMPLEMENTATION

### 4.1 Retrieval Approach

As the primary element of our path characterization model a general program has been developed to retrieve atmospheric state parameters including temperature, molecular species concentrations, path boundary parameters (emissivity/reflectivity) and the pressure at the boundary (or lowest limb layer) from path optical properties such as atmospheric path radiance and transmittance. The present retrieval approach assumes that an accurate forward model is available which, provided with the atmospheric state parameters, calculates accurate path optical properties. Since this retrieval method is directly dependent on the physics included in the forward model, the present approach represents a physical retrieval method. FASCODE has been used for the forward model in the current implementation because of its flexibility and accuracy. The model has a distinct advantage in terms of the spectral extent over which it is capable of performing atmospheric radiance and transmittance calculations from the microwave to UV. A principal liability of using an accurate line-by-line calculation such as FASCODE for the forward problem, is the computational cost of performing the forward calculation. While this model is currently not viable for operational retrievals, utilization of rapid algorithms (see Section 2.1.3), anticipated future improvement in computational power and more importantly the utilization of parallel computational methods may ultimately enable the use of line-by-line codes for operational retrievals. Another significant advantage of using FASCODE for the forward model is the ability to control the resolution of the model. The present method enables the study of the dependence of a retrieval measurement approach on resolution. Further, retrieval results may be studied for combined high resolution microwave measurements (AMSU) and lower resolution infrared measurements (AIRS).

The nonlinear method of physical least squares (PLS) has been utilized to retrieve the atmospheric state parameters from radiance measurements. For this method, derivatives with respect to the state parameters are required. These derivatives are obtained from discrete finite differences by perturbing the forward model. This operation constitutes the most computationally intensive aspect of the present method. In general, the least squares method in the absence of constraints requires that the number of measurement values exceed the number of parameters to be retrieved. This point will be considered in more detail in the context of the constrained least squares method.

Two options are provided by the current PLS model: the maximum likelihood method (MLM) and the ridge regression method. Included in the implementation is an option to perform an eigenanalysis of the system including parameter retrieval from the eigenvalues. An error analysis is provided given estimates of the measurement noise and the error covariance of the first guess if the maximum likelihood method is selected. Also, included in the program is the capability to add noise to the measurements either with a fixed seed or user supplied seed. The retrieval may be performed in a representation in which the measurements are linear in radiance or in a representation linear in equivalent brightness temperature.

It is desirable in a retrieval scheme of this type to constrain the retrieved state parameters to physically realizable values. An example of such a constraint relates to the retrieval of the mixing ratio of water vapor profiles for which the relative humidity at each level should be constrained to be greater than zero and less than 100%. Such linear and nonlinear constraints may readily be added to the present program. However, in the studies performed with the code thus far, violation of physical constraints has not been observed. This is attributable to the constrained least squares method we have adopted for which the state parameters that might not be well determined (thus possibly having non physical values) tend to be constrained toward physical values. Wherever possible, consideration has been given to developing the model in the context of physical constraints. For instance the hydrostatic equation is implicitly contained in the retrieval results for application to the terrestrial atmosphere. This is a consequence of the fact that changes in the retrievable layer parameters have minimal effect on the mass of the layer (variation of the water column in a layer may have a small effect on layer pressures).

## 4.2 Physical Least Squares Theory

The physical least squares (PLS) approach is advantageous for path characterization since it explicitly treats all variables affecting path electro-optical properties on an equivalent mathematical basis. For this problem of the estimation of state parameters from observations, the concept of two limiting spaces proves useful: measurement space and null space. A state parameter is considered to be in measurement space if the estimation of the parameter is strongly dependent on measurements from the observing system and in the null space if it is not dependent on the measurements. For atmospheric state parameters that are outside null space, there is no requirement for a priori climatological data on the desired path parameters. Such information is, however, useful in formulating the first guess and accelerating convergence. Our implementation of the PLS method is consistent with the approach of Rodgers (1976, 1990) and more recently Eyre (1989).

The problem of retrieving atmospheric state parameters, x, is posed in terms of minimizing the square of the differences between the observations and the forward model F(x) such that the variance, $\sigma^2$, given by

$$\sigma^2 = \sum_i W_i \left[R_i - F_i(x)\right]^2 \tag{4.1}$$

is a minimum. $W_i$ is the weight for the i'th observed radiance, $R_i$. This approach has two attractive attributes: (1) an extensive body of work exists on methods for solving the problem formulated in this way and (2) the final solution is in the linear regime enabling the implementation of a comprehensive error analysis. We follow the customary approach to the solution of this problem by adding a penalty function, $x^T \Gamma x$, to $\sigma^2$ obtaining

$$\sigma^2 = [R - F(x)]^T W [R - F(x)] + x^T \Gamma x \tag{4.2}$$

For the maximum likelihood method we have

$$\Gamma = S_x^{-1} \tag{4.3}$$

with $S_x$ the error covariance of the first guess and

$$W = S_R^{-1} \tag{4.4}$$

with $S_R$ the error covariance of the measurements. For the ridge regression approach, $\Gamma$ is given by

$$\Gamma_{ij} = \delta_{ij}\gamma_j \tag{4.5}$$

where $\gamma_j$ is a stability (damping) parameter. In this approach $\Gamma$ is viewed as constraining the direction and length of the step for the nonlinear problem (Levenberg, 1944; Marquardt, 1963) as well as providing a procedure to treat the ill-posedness.

The retrieval is obtained by iterative implementation of the relation (compare to 2.26-2.28)

$$x^{n+1} = x^n + (K^T W K + \Gamma)^{-1} K^T W\, r^n. \tag{4.6}$$

The radiance residuals, $r^n$, are given by

$$r^n = R - F(x^n) \tag{4.7}$$

with $x^0$ the first guess. The matrix K represents the Jacobian of the forward model with respect to the state parameters, obtained in our case from finite forward differences.

$$K = \frac{F(x^0 + \delta x) - F(x^0)}{\delta x} \tag{4.8}$$

The derivatives are updated as infrequently as possible as a consequence of the high cost of the forward calculation. In most of the cases we have studied, convergence has been achieved in two or three iterations without derivative updates. The quantity

$$H = K^T W K + \Gamma \tag{4.9}$$

from Eq. (4.6) represents the covariance matrix for the measurement vectors and $H^{-1}$ is the covariance matrix for the state vectors. The error analysis associated with this development for the PLS is provided in Section 5.

## 4.3 Role of the Penalty Function

The penalty function (see Eq. 4.2) serves two important but unrelated purposes in the PLS retrieval method. The first purpose relates to the fact that retrievals of the type we consider here are often associated with ill-posed or poorly posed problems (see Section 2.2). The source of the ill-posedness is related to the fact that some of the state parameters may be in null space or that a near linear relationship may exist among two or more of the state parameters. In the case of ill-posedness, the covariance matrix H, in the absence of the penalty function, $\Gamma$=0, is ill conditioned and the determinant is near zero, precluding the determination of a stable inverse. The penalty function serves to address this problem. In the case of the maximum likelihood method the quantity $\Gamma$ is given by the inverse of the error covariance matrix, Eq. (4.3), so the problem of ill-conditioning is addressed in a prescribed way. For ridge regression, the situation is less clear. For this case, $\Gamma_{ij}$ is often given by Eq. (4.5) so that a quadratic penalty function from Eq. (4.2), $P_q$, is given by

$$P_q = \sum_j \gamma_j \, x_j^2, \tag{4.10}$$

This definition effectively creates a parabolic well around the current value of the state parameters, the steepness of the well controlled by $\gamma_j$. The selection of $\gamma_j$ in dealing with ill-conditioning has traditionally been a difficult issue. In our experience a choice is made based on an estimate of the allowable increase in $\sigma^2$ as a consequence of a given change in $x_j$. In actuality this approach represents a crude approximation to using the diagonal elements of the inverse of the error covariance matrix in the maximum likelihood method.

The second purpose for the penalty function is to control the step size and direction in the implementation of the Levenberg (1944) - Marquardt (1963) approach to nonlinear least square problems. For this aspect of the application of the penalty function, $\gamma_j$ is chosen to be as small as possible

consistent with the solution space remaining in the same well. As the problem is iterated, the $\gamma_j$ are relaxed to zero to accelerate convergence. This topic has been discussed extensively in the literature, a particularly good reference is Dennis and Schnable (1983). For the present work, we have found that using the error covariance matrix with the maximum likelihood method has served to fulfill the role of controlling the step size and length for the iterative solution. As a consequence, the relaxation of the penalty function for the purposes of accelerating the solution has not been pursued.

It should be mentioned that the matrix $\Gamma$ in the penalty function need not be diagonal. In particular, $\Gamma$ is not diagonal for the maximum likelihood method for which it is given by the inverse of the error covariance matrix of the state parameters, although we have not had the full matrix available to study the effects of off diagonal terms. The matrix $\Gamma$ must be positive definite in order that the covariance matrix S be positive definite. One of the well known consequences of retrieving state vectors using the present method is a tendency toward alternating error in the retrieved state parameters, an effect sometimes described as jacknifing. Twomey (1977) has pointed out that a smoothness constraint may be imposed on the retrieved state parameters through the application of symmetric matrices with off diagonal elements. For instance the following form of $\Gamma$

$$\Gamma = \frac{1}{2} \begin{vmatrix} 1 & -1 & & \\ -1 & 2 & -1 & \\ & -1 & 2 & -1 \\ & & -1 & 1 \end{vmatrix} \tag{4.11}$$

will serve to minimize differences between adjacent state parameters providing a smoothness constraint. Second derivative smoothing can be particularly effective.

## 4.4 Retrieval System Eigenanalysis

In order to study the condition of the covariance matrix and to provide an alternate solution method for the state vectors, an eigenanalysis has been included in the program. Eq. (4.6), expressed as

$$\delta_x = (K^T W K + \Gamma)^{-1} (K^T W r), \tag{4.12}$$

$$K^T W r = (K^T W K + \Gamma)\, \delta x$$

may be written in matrix form as

$$Y = H\, x \tag{4.13}$$

where

$$X = \delta x, \tag{4.14}$$

$$Y = K^T\, W\, r \tag{4.15}$$

and H is the covariance matrix of the Jacobian for the problem. Performing a diagonalization and obtaining eigenvectors T and eigenvalues $\lambda I$ we have

$$\tilde{T} Y T = \tilde{T} H T\, \tilde{T} X T \tag{4.16a}$$

and

$$\tilde{T} Y T = \lambda I\, \tilde{T} X T. \tag{4.16b}$$

The spectrum of the eigenvalues with $\Gamma$=0 provides information on the number of parameters that may be retrieved for a given problem. The eigenvectors for a given eigenvalue provides information on the linear combination contributing to a given eigenvalue. If a linear relation exists between one or more state parameters, an eigenvalue is identically zero and the eigenvectors identify the linear relationship. The determinant may readily be obtained as the product of the eigenvalues. The solution vector for X is also available from the relation

$$X = T\, \lambda^{-1}\, I\, \tilde{T}\, Y \tag{4.17}$$

## 4.5 Initial Guess Dependence

One of the most important aspects of a regression approach of the type implemented here is the choice of the initial guess, $x^o$. In both the linear and nonlinear situation, the state parameters are constrained to the initial guess for the parameters which are in null space. In the linear problem, for parameters in measurement space, the choice of initial guess will not influ-

ence the result. In the nonlinear case, the choice of initial guess determines the well in which the retrieved parameters are finally obtained. For cases in which Eq. (4.2) has more than one local minimum the choice of the first guess is a particularly important issue. In general for the nonlinear problem we seek the solution that represents the global minimum. Finally, in the intermediate region between null space and measurement space, the initial guess will have an influence on the retrieved parameters. It is useful to define an equivalent parameter index (EPI, $\epsilon_j$), which is a measure of the degree to which a parameter is in measurement space ($\epsilon_j$=1) or null space ($\epsilon_j$=0). EPI is given by the relationship

$$\epsilon_j = \left\{ [K^T W K + \Gamma]^{-1} \; [K^T W K] \right\}_{jj} \tag{4.18}$$

or equivalently

$$\epsilon_j = \left\{ H^{-1} \; K^T W K \right\}_{jj} \tag{4.19}$$

The number of equivalent parameters ($N_{ep}$) for the problem is given by the trace, so that we have

$$N_{ep} = \text{tr} \left\{ H^{-1} K^T W K \right\} \tag{4.20}$$

or equivalently

$$N_{ep} = \sum_j \epsilon_j . \tag{4.21}$$

This quantity will be required for the error analysis. The values for $\epsilon$ range from 0 to 1 so that the $N_{ep}$ cannot exceed the number of state variables in the problem, $N_x$. As a consequence, it is possible to study a problem in which the number of state variables exceeds the effective number of measurements, as long as $N_{ep}$ does not approach the number of measurements. It is in this context that the assimilation of the AMSU A and AMSU B radiances into the British Meteorological Office NWP model is proposed (Eyre, 1989).

In general the performance of the retrieval procedure is improved in cases for which the first guess is close to the true solution. The effect of the transition region between measurement space and null space is reduced and the convergence to the true solution in the nonlinear case is facilitated. Operational applications of the PLS retrieval method have approached this problem in at least two interesting ways. For the British Meteorological Office NWP application, the first guess for temperature and water profiles are obtained from the prediction of the NWP model itself (Eyre, 1989). It is estimated that this will provide a guess temperature profile within 2K of the correct profile and water vapor to 50% at the NWP levels. For retrievals at NOAA/NESDIS, a classification scheme has been implemented to attain a guess profile close to the true solution, then the PLS method is applied (MacMillan, 1989).

Strategies for the solution of non-linear minimization problems are widely studied in optimization theory. An approach that facilitates the retrieval procedure is the solution of the problem in sub-spaces in advance of seeking a solution in the full space. The reason for this is that the smaller matrices are generally better conditioned than the larger matrices; the sub-problem is better posed than the full problem. This has implications for the question of sequential versus simultaneous retrievals and for retrieval of atmospheric profiles for the limb case. It is instructive to consider an example of this strategy for the retrieval of temperature and water vapor using microwave and infrared channels. First a temperature profile would be retrieved using microwave channels least affected by water vapor or other molecular absorption, since this is essentially a linear problem. Then the infrared radiances would be included and a refined atmospheric temperature profile obtained. Next, water radiance channels would be included and a water vapor profile obtained using the previously obtained temperature profile. Finally, the full problem would be treated retrieving simultaneously temperature and water vapor profiles. The current path characterization code has the capability to study such strategies in a relatively straightforward manner.

## 5. COMPREHENSIVE ERROR ANALYSIS

This section describes a comprehensive error analysis package that has been developed based on Rodgers' work (see Rodgers, 1990) and incorporated into the retrieval program. This algorithm provides an estimate of the covariance of the retrieval errors that includes the effect of the measurement noise and the uncertainty on the prior information which constrains the inversion. A measure of the performance of the retrieval is derived, whenever possible, from a comparison of the covariance of the state parameters before and after measurement. The important problem of the effects of errors in the forward model parameters, which have not been explicitly considered in the current version of the algorithm, will also be discussed in this section.

### 5.1 Theory

#### 5.1.1 Perfect Model Case

In the following it is assumed that the solution $x^n$ at the nth iteration lies sufficiently close to the target profile so the forward model in a linearized form,

$$r^n = K(x-x^n) - \epsilon_r, \tag{5.1}$$

where $\epsilon_r$ is the measurement noise, is valid. Using (5.1) in the general solution given in Eq. (4.6) leads to the following expression for the new estimate $x^{n+1}$ of x

$$x^{n+1} = x^n - H^{-1}K^TWK\,(x-x^n) + H^{-1}K^TW\,\epsilon_r, \tag{5.2}$$

or after rearranging the terms in Eq. (5.2) to give $x^{n+1}$ as a departure from x,

$$x^{n+1} - x = H^{-1}\Gamma(x^n-x) + H^{-1}K^TW\,\epsilon_r. \tag{5.3}$$

Equation (5.3) expresses the total error in the retrieved parameters as the sum of a "null-space" error, so-called because it corresponds to those parameters that cannot be measured by the observing system, and the contribution

of measurement errors. The total error covariance can be calculated from Eq. (5.3) as

$$S = S_N + S_M \tag{5.4}$$

where,

$$S_N = H^{-1}(\Gamma S_x \Gamma)\, H^{-1} \tag{5.4a}$$

and

$$S_M = H^{-1}\,(K^T S_r^{-1} K)\, H^{-1} \tag{5.4b}$$

are respectively the null-space and measurement error covariance matrices (it was assumed here that $W = S_r^{-1}$). For the maximum likelihood method, $\Gamma = S_x^{-1}$ and a much simpler form of (5.4) is obtained,

$$S = H^{-1}. \tag{5.5}$$

Note that it is the covariance of the first guess, $S_x$, that has been used in Eq. (5.4a) instead of the covariance of $x^n$, the solution parameters at the nth iteration. This approximation is valid since the values of parameters that belong to the null-space of the observing system remain close to the values of the initial guess. Outside the null-space, the total error is dominated by the measurement error and the impact of replacing $x^n$ by $x^o$, in Eq. (5.3), is generally minor.

### 5.1.2 Model Errors

Model error is an issue that has not been considered in the previous development. We are concerned here with the systematic bias in the estimate of the observed radiance residuals that arises from errors in the forward model such as spectral line data, continua, photometric calibration, radiance algorithms and atmospheric layering. In principle, these biases can be estimated based on a large number of independent measurements or can be removed by tuning of the forward model. When model tuning is not performed, it is possible to account for the systematic errors in the above error analysis by adding in Eq. (5.4) an extra term of the form,

$$S_s = H^{-1}\,[K^T W K_b S_b K_b^T W K]\, H^{-1} \tag{5.6}$$

where $K_b$ represents the sensitivity of the measurements to the model parameters and $S_b$ is the covariance of our knowledge of the model parameters. In this probabilistic approach, $S_s$ is the component of the total error covariance that is due to the uncertainties on the model parameters. The expression for $S_s$ given in Eq. (5.6) is similar to the one suggested by Rodgers (1990). Although this expression incorporates the effects of the model errors in a mathematically consistent way, it is difficult to apply as such when dealing with line-by-line models. In this case, the large number of parameters that are to be considered makes it cumbersome to attempt to evaluate $K_b$. As a possible shortcut, a rough estimate of $S'_b = K_b S_b K_b^T$ can be obtained from a comparison of radiance calculations that are performed using perturbed forward model parameters such as different spectral line parameters. When the model errors are taken into account in the solution, the general expression for the total error covariance becomes

$$S = H^{-1}[\Gamma S_x \Gamma + K^T (S_r + S'_b)^{-1} K] H^{-1}. \qquad (5.7)$$

It should be noted that the error due to effects such as aerosol and cloud contamination which would give rise to systematic errors if only molecular absorption is included in the forward model, can be included in the present treatment of model error.

### 5.1.3 Retrieval Performance

The matrix S as given by Eq. (5.7) can generally be taken as a good estimate of the covariance matrix of the retrieval in nonlinear problems, at least when K does not vary rapidly with x. One can therefore assess the performance of the retrieval by comparing S to the covariance of the a priori information. The simplest measure of the performance of the system involves the diagonal elements of these matrices which contain the variances of the state parameters. It is useful for instance to evaluate the reduction in the variance of each individual parameter as a consequence of the measurement. Similarly, it is common to use the rms error, obtained in this context as the trace of the covariance matrix, as a performance index for the whole profile. However these diagnostics may be sometimes misleading as they do not take into account the correlations between the errors at different levels. In that sense, the concept of "information content" (Rodgers, 1976) is more appropriate. The

information content of a measurement is defined as the change $\Delta H$ in the entropy of the probability density function of x due to the retrieval process.

Assuming that the error statistics are Gaussian, the information content of a measurement is given by

$$\Delta H = \frac{1}{2} \log_2 |S| - \frac{1}{2} \log_2 |S_x|, \qquad (5.8)$$

where $||$ designates the determinant of a matrix (see Rodgers, 1976).

## 5.2 Algorithm Description

The different actions taken by the error analysis algorithm depend on the nature of the information supplied by the user. These are summarized in a diagram of Figure 5-1.

A full error analysis can be carried out only if the a priori error covariance of the state parameters, $S_x$, and the channels weights, W, are provided. When $S_x$ is not available a solution profile can still be obtained with the ridge regression method. However, the algorithm will not perform the complete diagnosis of the retrieval and will provide only an estimate of the measurement errors.

As far as the channel weights are concerned, the matrix W is treated as a diagonal matrix. No provision has been made yet for dealing with inter-channel correlations. The user can input the elements $\{W_{ii}\}$ directly or choose to enter a set of standard deviations of the measurement noise either in radiance units or in equivalent brightness temperature. The weights are scaled internally by a factor $\alpha$ such that,

$$\alpha \sum_{i=1}^{N} W_{ii} = 1.$$

where N is the number of non-zero elements. The solution profile remains unchanged if both W and $\Gamma$ are multiplied by a constant. The purpose of the scaling is to fix the range of reasonable values of the damping factors, thereby facilitating the tuning of the solution whenever the conventional

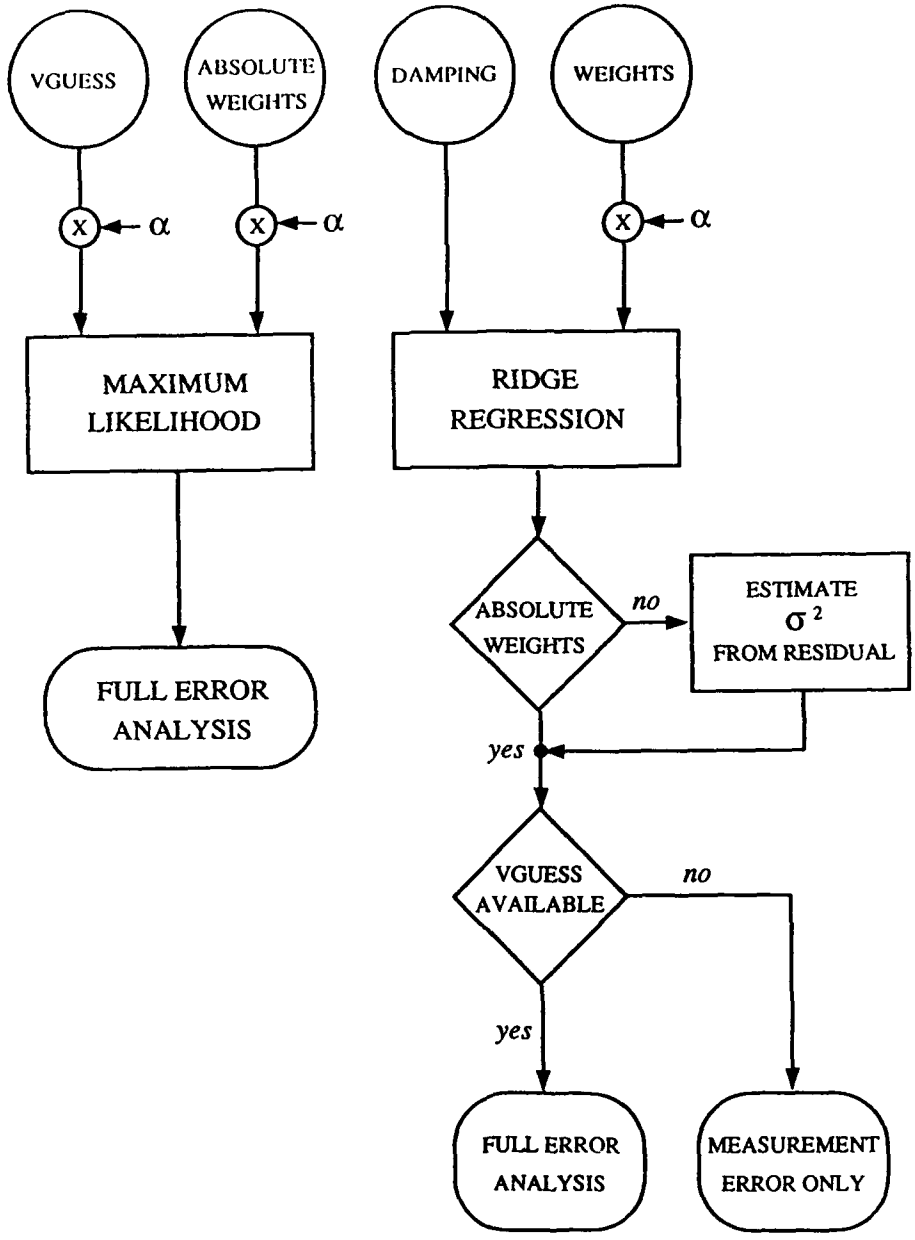


Figure 5-1. Flow diagram of the FASCODE retrieval error analysis for the maximum likelihood and ridge regression options. The circled names correspond to the user input data (here VGUESS is the error covariance matrix of the first guess). The quantity $\alpha$ is a scale factor applied to the input data (see text).

ridge regression method is used. It is easily shown that in this case, an appropriate expression for the covariance of the solution is,

$$S = (K^T W' K + \Gamma')^{-1} [\alpha K^T W' K + \Gamma' S_x^{-1} \Gamma'] (K^T W' K + \Gamma')^{-1}, \tag{5.9}$$

where, $W' = \alpha S_r^{-1}$ is the scaled channel weights matrix and $\Gamma'$ is the matrix that contains the input values of the damping parameters.

In order to facilitate the comparison with the ridge regression method, it was decided to treat the weights in the same way when the maximum likelihood option is selected. In this case, the scaling is applied to $S_x^{-1}$ also. The covariance of the solution can be obtained directly in terms of $S'^{-1}_x = \alpha S_x^{-1}$ and $S_r'^{-1} = \alpha S_r^{-1}$, as

$$S = \alpha(K^T S'^{-1}_r K + S'^{-1}_x)^{-1}. \tag{5.10}$$

One interesting feature of the program is its ability to carry out the error analysis in the absence of a complete characterization of the measurement noise when the ridge regression method is used. In this case, the program will supply the missing information by performing an analysis with the measurement residuals. In the simple situation considered so far, it is assumed that only the relative weighting of the channels is known to the user. In other words,

$$W' = \alpha S_r^{-1}$$

where $\alpha$ is now an unknown multiplicative constant. Noting that the variance $\sigma^2$ of the weighted measurement noise is precisely equal to $\alpha$,

$$\sigma^2 I = \underline{P} S_r \underline{P} = \alpha I, \tag{5.11}$$

where $\underline{P}$ is a symmetric matrix such that $\underline{P}^2 = W$, a convenient estimate of $\alpha$ is

$$\hat{\alpha} = \frac{\sum_{n=1}^{N} r_n^2}{tr[I-R(\Gamma')]} = \frac{\sum_{n=1}^{N} r_n^2}{N-tr[R(\Gamma')]}, \tag{5.12}$$

with $R(\Gamma') = \underline{P}KH^{-1}K\underline{P}$ (see Engle et al., 1986). By analogy with the standard linear regression formula, we can define the number of equivalent parameters by $tr[R(\Gamma')]$. It is important to point out that $\hat{\alpha}$ is a good estimate of $\alpha$ when the damping is not too strong. In fact, the damping of the solution introduces a bias in the calculated radiances. However, when correct values of $\Gamma$ are used, the constraints affect mainly the null-space of the observing system and this bias is only important in the transition region between null space and measurement space.

Finally, the output listing for the full error analysis includes the variances of the retrieved parameters, $S_{ii}$, as well as the a priori variances $S_{x_{ii}}$. Also listed are the fraction of unexplained variances (FUV) defined for the ith parameter as

$$FUV(i) = \frac{S_{ii}}{S_{x_{ii}}} . \tag{5.13}$$

## 6. PATH CHARACTERIZATION RESULTS

The path characterization method has been applied to a number of problems including the retrieval of temperature and water vapor profiles from SCRIBE (Stratospheric Cryogenic Interferometric Balloon Experiment) radiance spectra (Murcray et al., 1984; 1985). This has proven to be a particularly interesting retrieval because we have been able to identify errors in the intensities for some of the weaker carbon dioxide bands on the HITRAN data base. This has been accomplished following the adjustment of the state parameters using the present retrieval method. This retrieval application to the SCRIBE data will be described at greater length in the final report under contract 19628-86-C-0172. Here we describe the results for two cases. The first is a simulation case based on the microwave AMSU (Advanced Microwave Sounding Unit) channels. This case was chosen since the temperature retrieval in this spectral region is a linear problem and can be used to study the path characterization model from the point-of-view of Sections 4 and 5. We also performed retrieval for water vapor and a simultaneous retrieval for temperature and water vapor for this case. The second problem we have studied is the retrieval of ozone from an aircraft measurement with the U. of Wisconsin HIS (High resolution Interferometer Sounder), (Smith et al., 1983).

## 6.1 AMSU Test Case

The channels for the AMSU test case are provided in Table 6-1a. Channel numbers 4, 8, 11, 13, 15, and 17 were added in the expectation that the system might be underdetermined, the number of state parameters being determined by

Table 6-1a Specifications for the channels used in this analysis (includes AMSU/A and AMSU/B). The weights are based on the noise equivalent delta temperature (NEDT).

| CHANNEL NUMBER | FREQ (GHZ) | +/- (GHZ) | +/- (GHZ) | RADIANCE W CM-1 STER-1 | NEDT K | NER W CM-1 STER-1 | WEIGHT |
|---|---|---|---|---|---|---|---|
| 1 | 50.3000 | .00000 | .0000 | 4.595E-10 | .40 | 9.3216E-13 | .16467 |
| 2 | 52.8000 | .00000 | .0000 | 6.353E-10 | .25 | 6.4195E-13 | .34720 |
| 3 | 53.5957 | .00000 | .0000 | 6.545E-10 | .25 | 6.6145E-13 | .32704 |
| 4 | 53.8600 | .00000 | .0000 | 6.642E-10 | .25 | 6.6799E-13 | .32066 |
| 5 | 54.4000 | .00000 | .0000 | 6.516E-10 | .25 | 6.8145E-13 | .30812 |
| 6 | 54.9400 | .00000 | .0000 | 6.370E-10 | .25 | 6.9505E-13 | .29618 |
| 7 | 55.5000 | .00000 | .0000 | 6.283E-10 | .25 | 7.0929E-13 | .28441 |
| 8 | 56.4000 | .00000 | .0000 | 6.501E-10 | 25 | 7.3248E-13 | .26668 |
| 9 | 57.2904 | .00000 | .0000 | 6.543E-10 | .40 | 1.2093E-12 | .09785 |
| 10 | 57.2904 | .21700 | .0000 | 6.591E-10 | .40 | 1.2093E-12 | .09785 |
| 11 | 57.2904 | .32214 | .1000 | 6.597E-10 | .40 | 1.2093E-12 | .09785 |
| 12 | 57.2904 | .32214 | .0480 | 6.712E-10 | .40 | 1.2093E-12 | .09785 |
| 13 | 57.2904 | .32214 | .0310 | 6.814E-10 | .50 | 1.5116E-12 | .06262 |
| 14 | 57.2904 | .32214 | .0220 | 6.913E-10 | .60 | 1.8139E-12 | .04349 |
| 15 | 57.2904 | .32214 | .0140 | 7.077E-10 | .70 | 2.1162E-12 | .03195 |
| 16 | 57.2904 | .32214 | .0100 | 7.221E-10 | .80 | 2.4185E-12 | .02446 |
| 17 | 57.2904 | .32214 | .0065 | 7.423E-10 | 1.00 | 3.0231E-12 | .01566 |
| 18 | 57.2904 | .32214 | .0045 | 7.593E-10 | 1.20 | 3.6278E-12 | .01087 |
| 19 | 18.7000 | .00000 | .0000 | 4.064E-11 | .30 | 9.6628E-14 | 15.32445 |
| 20 | 31.4000 | .00000 | .0000 | 1.202E-10 | .30 | 2.7244E-13 | 1.92767 |
| 21 | 89.0000 | .00000 | .0000 | 1.295E-09 | .50 | 3.6479E-12 | .01075 |
| 22 | 23.8000 | .00000 | .0000 | 7.479E-11 | .30 | 1.5652E-13 | 5.84041 |
| 23 | 166.0000 | .00000 | .0000 | 6.312E-09 | .60 | 1.5229E-11 | .00062 |
| 24 | 183.3101 | 1.00000 | .0000 | 7.490E-09 | .80 | 2.4761E-11 | .00023 |
| 25 | 183.3101 | 3.00000 | .0000 | 7.888E-09 | .80 | 2.4761E-11 | .00023 |
| 26 | 183.3101 | 7.00000 | .0000 | 8.302E-09 | .80 | 2.4761E-11 | .00023 |

Table 6-1b The standard deviation (K) of the background temperature profile for the maximum likelihood method, Fig's. 6.4 - 6.7.

| PAR NUM | LAYER & PARAMETER | BACKGR. STD. DEV. |
|---|---|---|
| 1 | 17 TEMP | 15.789870 |
| 2 | 16 TEMP | 11.249889 |
| 3 | 15 TEMP | 5.140039 |
| 4 | 14 TEMP | 5.549775 |
| 5 | 13 TEMP | 5.870264 |
| 6 | 12 TEMP | 8.429709 |
| 7 | 11 TEMP | 10.080179 |
| 8 | 10 TEMP | 9.979980 |
| 9 | 9 TEMP | 9.590099 |
| 10 | 8 TEMP | 7.149825 |
| 11 | 7 TEMP | 7.071068 |
| 12 | 6 TEMP | 7.289719 |
| 13 | 5 TEMP | 6.920260 |
| 14 | 4 TEMP | 7.071068 |
| 15 | 3 TEMP | 10.969959 |
| 16 | 2 TEMP | 10.989995 |
| 17 | 1 TEMP | 13.019985 |
| 18 | SURF TEMP | 15.000000 |

the FASCODE layering, and that additional measurement channels would be helpful. The addition of these layers eventually proved to be unecessary as will be discussed. The central frequency and the associated frequency splittings are given in the next two columns. The simulated radiances were developed to be representative of a tropical model atmosphere. This was accomplished by replacing the U.S. Standard temperature profile in the calculation of simulated radiances with the tropical temperature profile for the temperature retrieval, the U.S. Standard water vapor profile with the tropical water profile for the water retrieval and replacing both for the simultaneous retrieval. The atmosphere has 17 layers; the geometry is nadir viewing from 100 km. The noise equivalent brightness temperature (NEDT) for each channel is provided together the the calculated noise equivalent radiance (NER) and the calculated relative weight. The standard deviations for the background temperature profile are indicated in Table 6-1b. These values of the standard deviation were estimates based on a climatological data set. The weighting functions for the AMSU A channels are provided in Figure 6-1 (Houghton et al., 1984).

The first guess for the temperature retrieval is the U.S. Standard temperature profile shown in Figure 6-2a together with the tropical temperature profile representative of the correct solution. Of particular note is the sharp temperature reversal and the low temperature at the tropopause for the atmosphere to be retrieved. In Figure 6-2b the weighting functions on the same log pressure scale as the temperature profiles are provided. The results of the PLS temperature retrieval using the maximum likelihood method are indicated in Figure 6-3a. The curve labelled TROPICAL-STD represents the error in the first guess. The temperature residual profile labelled TROPICAL-C1 is the result after one iteration and TROPICAL-C3 is the result of the third iteration. The radiances used for this retrieval set are without measurement noise.

The derivatives were computed in the reference representation, the U.S. Standard atmosphere. Of particular interest is the ability of the PLS algorithm to retrieve the cold and sharp tropopause of the tropical atmosphere as evidenced by the temperature residuals at 100 mb. In Figure 6-3b the $\pm 1\sigma$ errors for the temperature retrieval are provided. At lower pressures, the errors approach those of the estimated error covariances of the first guess. This is further evidenced by the retrieval results in which the error approaches that of the first guess below 0.4 mb. It may also be noted that above 500 mb the retrieval error is less than two degrees and is 0.34K at the

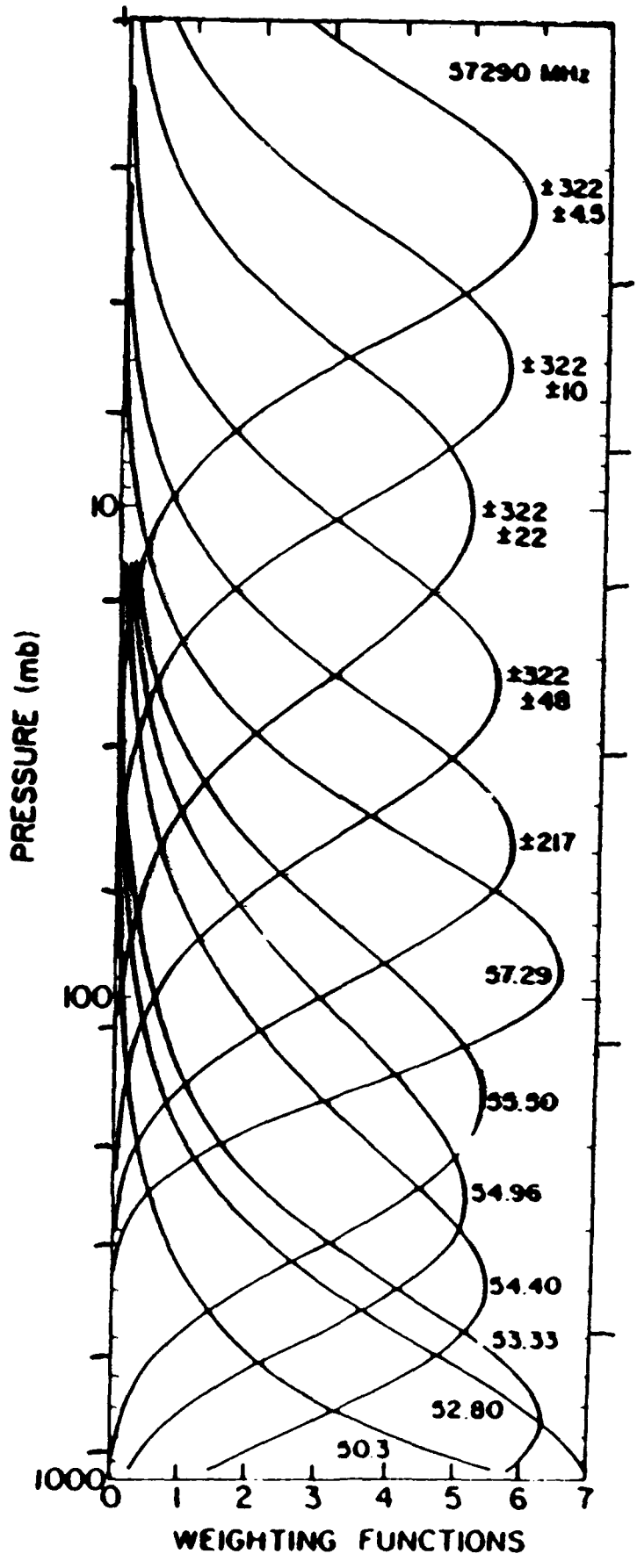


Figure 6-1. Weighting functions for the AMSU/A channels (from Hougton et al., 1984).

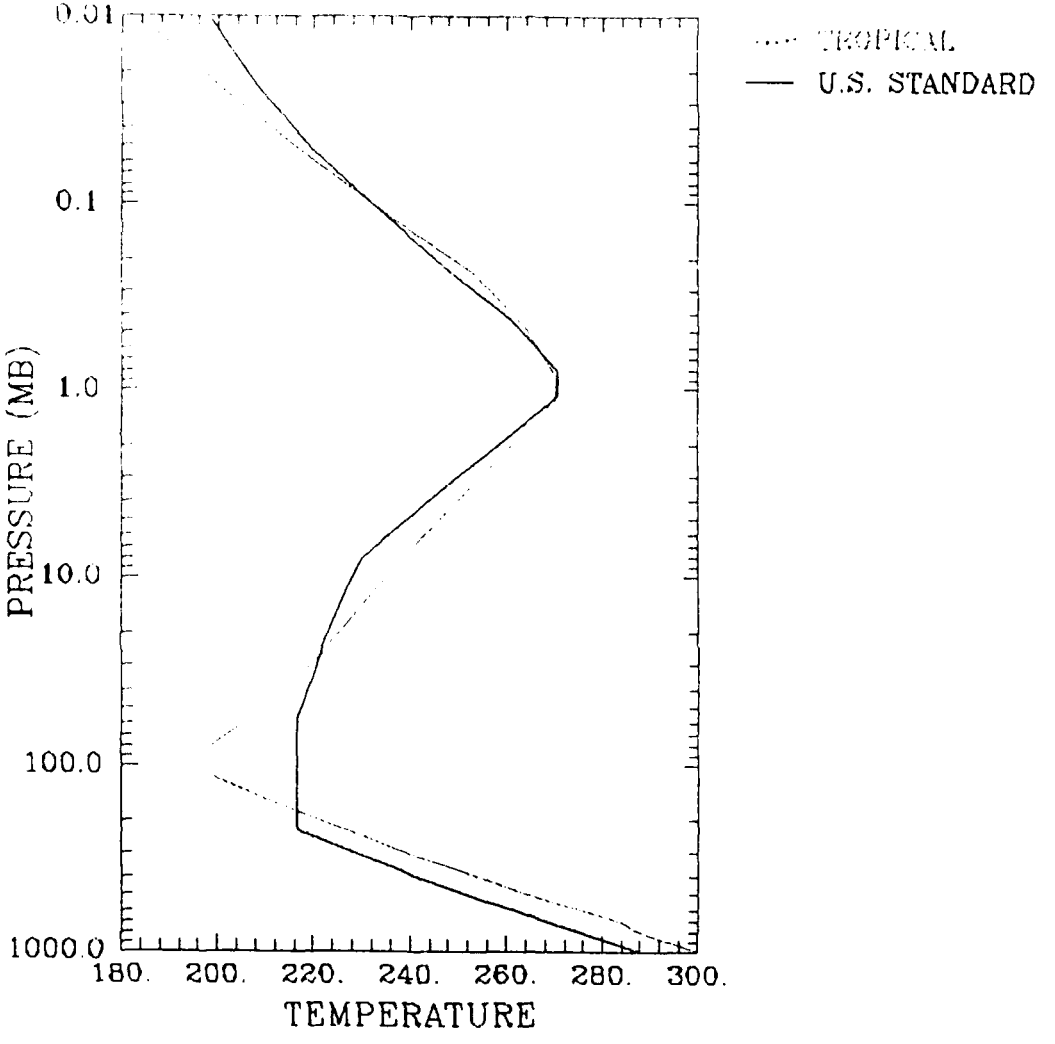


Figure 6-2a. Temperature profiles for the U.S. Standard and Tropical model atmospheres. Tropical (.....) atmosphere is used for simulated data; U.S. Standard (____) is the first guess.

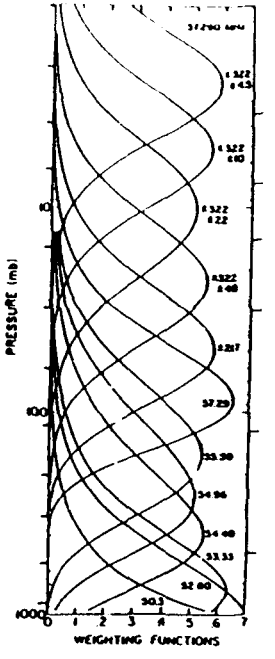


Figure 6-2b. The weighting functions of Fig. 6-1 for the same pressure scale as the model atmospheres.

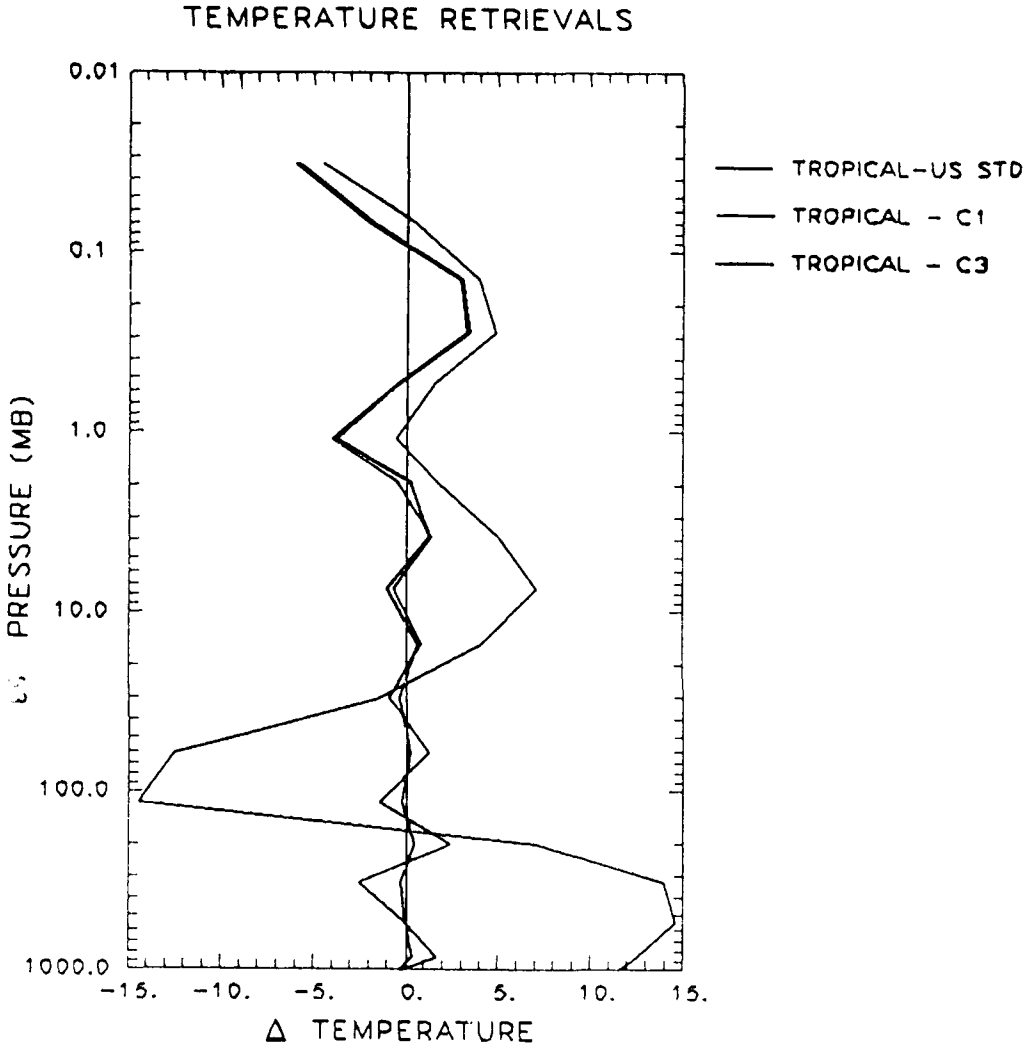


Figure 6-3a. Atmospheric temperature residuals as a function of iteration number:
_____ Tropical - $x^0$; (U.S. Standard)
__ __ Tropical - $x^1$;
__ _ __ Tropical - $x^2$
The simulated radiances do not include measurement noise.

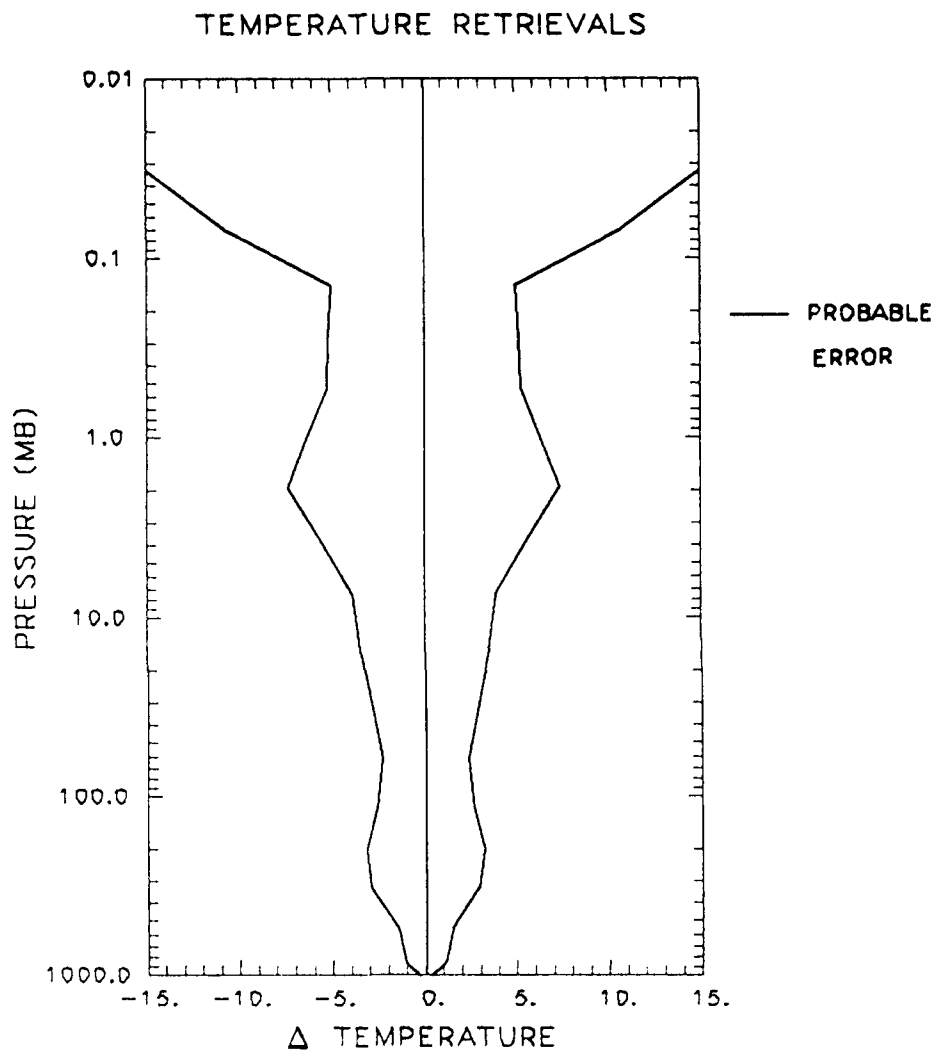


Figure 6-3b. Probable errors ($1\sigma$) for the retrieval temperatures using MLM.

surface. At lower pressures the error is less than 4K until the 10 mb level s reached.

### 6.1.1 Temperature Retrieval

Table 6-2 contains the results for this temperature retrieval. Column C2 gives the temperature used in the FASCODE forward model calculation for the third iteration. The linearly predicted constants are given by column C3 with the indicated probable error ($1\sigma$). Since the maximum likelihood method is used, the damping is achieved through the first guess error covariance so the damping factors including GAMMA are presented as zero. The equivalent parameter or fit index (EPI) is provided in the final column, zero indicating that the parameter is in null space and one in measurement space. The number of equivalent parameters is obtained from the sum of EPI which for this case gives 10.96, the possible number of state variables being 18 for the problem. Of interest is the estimated noise value obtained from the residuals associated with the retrieval compared with that based on the assumed standard derivation of the measurement noise. After three iterations the variance for this retrieval, which did not include noise in the simulated radiances, is 0.11576 of that based on the assumed measurement noise. The fact that it is not zero may be attributed to possible error contributions from the null space transition regions, lack of full convergence, and discrete numerical effects in the forward problem.

Table 6-3 provides explanatory information related to the retrieval including the reference state parameters, $x^o$, the change in state variable for the derivatives, the difference between the current state variable results (C3) and the reference values and the percentage changes. The latter quantity is especially relevant for the retrieval of column abundances. For cases in which simulated data is used, columns providing the state values for the simulated case, the difference between the simulated and reference case and the difference between simulated and the current result are provided. Note that it is these latter values that are plotted in Figure 6-3a.

Having established that the number of equivalent variables for the extended AMSU channels was substantially less than the number of measurement channels, the experiment for the original AMSU channel set was considered by setting the weights for the added channels to zero ($S_{R_{ii}}$ set large for channels 4, 8, 1, 13, 15 and 17). The results of this retrieval are provided

Table 6-2 Results from the second iteration for the temperature retrieval showing the constants C2($x^2$), the predicted change DELC3, the predicted temp C3($x^3$), and the probable error using MLM.

MICROWAVE RUN - AMSU CHANNELS - TROPICAL TEMPERATURE PROFILE INVRT 89/12/13 09.37.20

FASCODE PATH CHARACTERIZATION RETRIEVAL

GAMMA = 0.000E+00

| PAR NUM | LAYER & PARAMETER | C2 SV | DEL C3 | C3 SV | PROBABLE ERROR FOR C3 | PERCENT DEL C3/C2 | DAMPING FACTOR | FIT INDEX |
|---|---|---|---|---|---|---|---|---|
| 1 | 17 TEMP | 213.826521 | .065454 | 213.891975 | 15.670800 | .030611 | 0.000E+00 | .015025 |
| 2 | 16 TEMP | 226.831400 | .106175 | 226.937575 | 10.765889 | .046808 | 0.000E+00 | .084194 |
| 3 | 15 TEMP | 238.999616 | .039793 | 239.039409 | 4.985886 | .016650 | 0.000E+00 | .059082 |
| 4 | 14 TEMP | 253.272694 | .057969 | 253.330663 | 5.161775 | .022888 | 0.000E+00 | .134938 |
| 5 | 13 TEMP | 266.045472 | .050774 | 266.096246 | 5.248437 | .019085 | 0.000E+00 | .200636 |
| 6 | 12 TEMP | 273.037437 | -.082282 | 272.955155 | 6.459797 | -.030136 | 0.000E+00 | .412764 |
| 7 | 11 TEMP | 260.863089 | -.192242 | 260.670847 | 7.339175 | -.073695 | 0.000E+00 | .469900 |
| 8 | 10 TEMP | 248.663237 | .114151 | 248.777388 | 5.545287 | .045906 | 0.000E+00 | .691263 |
| 9 | 9 TEMP | 240.255829 | -.060427 | 240.195402 | 3.875051 | -.025151 | 0.000E+00 | .836729 |
| 10 | 8 TEMP | 228.282258 | .164168 | 228.446426 | 3.476311 | .071915 | 0.000E+00 | .763601 |
| 11 | 7 TEMP | 219.708495 | -.227969 | 219.480526 | 2.908806 | -.103760 | 0.000E+00 | .830777 |
| 12 | 6 TEMP | 203.956787 | .281039 | 204.237826 | 2.333386 | .137793 | 0.000E+00 | .897541 |
| 13 | 5 TEMP | 203.002734 | -.549828 | 202.452906 | 2.611045 | -.270847 | 0.000E+00 | .857641 |
| 14 | 4 TEMP | 222.822813 | .938184 | 223.760997 | 3.168437 | .421045 | 0.000E+00 | .799220 |
| 15 | 3 TEMP | 246.876506 | -.903354 | 245.973152 | 2.933627 | -.365913 | 0.000E+00 | .928485 |
| 16 | 2 TEMP | 270.418298 | .243394 | 270.661692 | 1.462842 | .090006 | 0.000E+00 | .982283 |
| 17 | 1 TEMP | 291.021090 | .047790 | 291.068880 | 1.076954 | .016422 | 0.000E+00 | .993158 |
| 18 | SURF TEMP | 299.955780 | .021038 | 299.976818 | .346188 | .007014 | 0.000E+00 | .999467 |

STM. WGHTED NOISE VAR.= 6.3707E-28 TRUE WGHTED NOISE VAR.= 5.5032E-27 RATIO= 1.1576E-01

Table 6-3. Retrieval results for a case with simulated data. REF indicates the constants for the first guess, DEL refers to the parameter increment for the derivatives and SIM indicates the constants for the simulated data.

MICROWAVE RUN - AMSU CHANNELS - TROPICAL TEMPERATURE PROFILE INVRT 89/12/13 09.37.20

REFERENCE AND SIMULATION DATA

| PAR NUM | LAYER & PARAMETER | REF DATA | DEL DERIV | DIF C3-REF | PERCENT (C3-REF)/REF | SIM DATA | DIF SIM-REF | DIF SIM-C3 |
|---|---|---|---|---|---|---|---|---|
| 1 | 17 TEMP | 212.430000 | 2.000000 | 1.461975 | .688215 | 207.890000 | -4.540000 | -6.001975 |
| 2 | 16 TEMP | 224.480000 | 2.000000 | 2.457575 | 1.094786 | 224.910000 | .430000 | -2.027575 |
| 3 | 15 TEMP | 238.100000 | 2.000000 | .939409 | .394544 | 241.950000 | 3.850000 | 2.910591 |
| 4 | 14 TEMP | 251.810000 | 2.000000 | 1.520663 | .603893 | 256.590000 | 4.780000 | 3.259337 |
| 5 | 13 TEMP | 264.180000 | 2.000000 | 1.916246 | .725356 | 265.720000 | 1.540000 | -.376246 |
| 6 | 12 TEMP | 269.750000 | 2.000000 | 3.205155 | 1.188195 | 269.180000 | -.570000 | -3.775155 |
| 7 | 11 TEMP | 259.240000 | 2.000000 | 1.430847 | .551939 | 260.920000 | 1.680000 | .249153 |
| 8 | 10 TEMP | 245.050000 | 2.000000 | 3.727388 | 1.521073 | 250.050000 | 5.000000 | 1.272612 |
| 9 | 9 TEMP | 232.150000 | 2.000000 | 8.045402 | 3.465605 | 239.190000 | 7.040000 | -1.005402 |
| 10 | 8 TEMP | 225.020000 | 2.000000 | 3.426426 | 1.522721 | 229.070000 | 4.050000 | .623574 |
| 11 | 7 TEMP | 220.580000 | 2.000000 | -1.099474 | -.498447 | 219.120000 | -1.460000 | -.360526 |
| 12 | 6 TEMP | 217.010000 | 2.000000 | -12.772174 | -5.885523 | 204.480000 | -12.530000 | .242174 |
| 13 | 5 TEMP | 216.700000 | 2.000000 | -14.247094 | -6.574570 | 202.240000 | -14.460000 | -.212906 |
| 14 | 4 TEMP | 217.210000 | 2.000000 | 6.550997 | 3.015974 | 224.210000 | 7.000000 | .449003 |
| 15 | 3 TEMP | 231.770000 | 2.000000 | 14.203152 | 6.128124 | 245.680000 | 13.910000 | -.293152 |
| 16 | 2 TEMP | 256.060000 | 2.000000 | 14.601692 | 5.702449 | 270.620000 | 14.560000 | -.041692 |
| 17 | 1 TEMP | 278.890000 | 2.000000 | 12.178880 | 4.366912 | 291.400000 | 12.510000 | .331120 |
| 18 | SURF TEMP | 288.200000 | 2.000000 | 11.776818 | 4.086335 | 299.700000 | 11.500000 | -.276818 |

REGION = 1 V1 = 1.678 V2 = 1.678 DV = 8.584E-07 NLIM = 26

TIMING FOR INVRT

| READ | AMAT | EIGN | INVT | MULT | STAT | OUTP |
|---|---|---|---|---|---|---|
| .7900 | .5280 | .0000 | .2640 | .5980 | .0590 | .1550 |

TIME LEAVING INVRT 10.2830 TOTAL 2.5650

in Figure 6-4a and the $\pm 1\sigma$ error in Figure 6-4b. It may be noted that at the third iteration, the retrieval residuals for the temperature profile are slightly greater than those for the extended channel set. The retrieval errors are only slightly greater than those for the extended channel set and the probable errors are only slightly larger, with the biggest difference being somewhat over 1K at 10 mb.

For this near linear case, the retrieval of the temperature profile in the microwave, the PLS algorithm performs extremely well. A nearly correct solution is obtained at the third iteration even though the initial guess is far from the correct solution. The oscillating character of the temperature residuals, referred to previously as jacknifing, is apparent in the early stages of the retrieval. By the third iteration this effect has diminished to a level small compared with the probable retrieval error. In Figure 6-5a and 6-5b we indicate the effect of decreasing the variance of the measurement error by a factor of two. The retrieval error ($\pm 1\sigma$) decreases by a factor of two for parameters in measurement space and is unchanged for parameters in null space as expected. The transition regime from measurement space to null space extends over a rather large pressure range, roughly 80 mb to 1 mb.

A final test of the retrieval procedure consists of invoking the option to add noise to the simulated data and is shown in Figure 6-6. The level of the measurement noise is determined by the equivalent brightness temperature noise specified for the channel. This test was performed after the first iteration; consequently, the temperature profile residuals are slightly different from those of the previous examples. The temperature retrieval residuals with noise are entirely consistent with the probable error as given in Figure 6-4b.

### 6.1.2 Pulse Retrieval

An interesting question arises as to the ability of a retrieval algorithm of this type to treat discontinuities in the atmospheric profile. To demonstrate the response of the PLS algorithm, we have performed two retrievals containing discontinuities in the atmospheric temperature profile: one in which the temperature of the 550 mb layer is increased by 3K and one in which the temperature of the 61 mb layer is increased by 3K. For these tests, no measurement noise has been added to the simulated radiances. The retrievals for these cases are shown in Figures 6-7a and 6-7b, respectively. In the

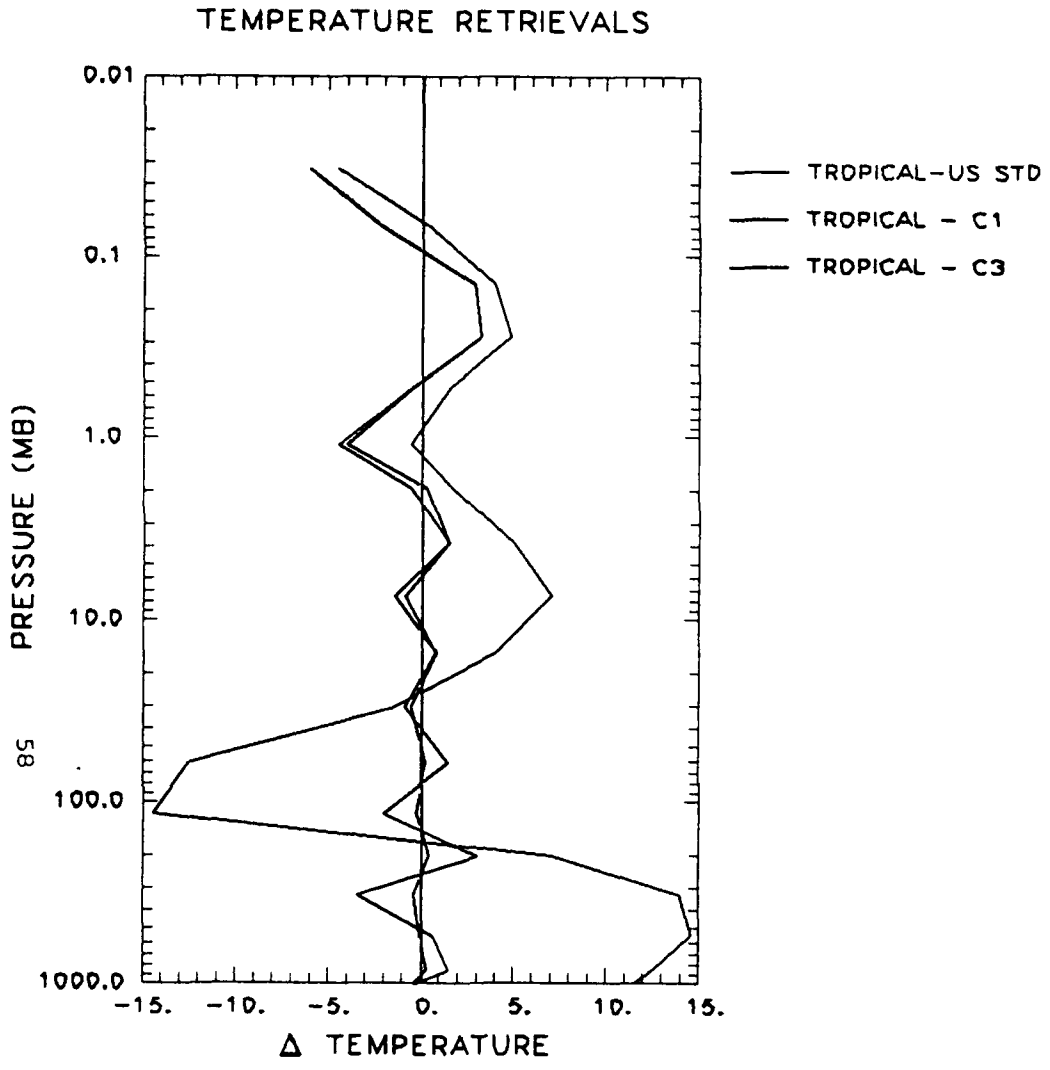




Figure 6-4a. Temperature retrieval results using MLM with the AMSU channels only. **The simulated radiances do not include measurement noise.**

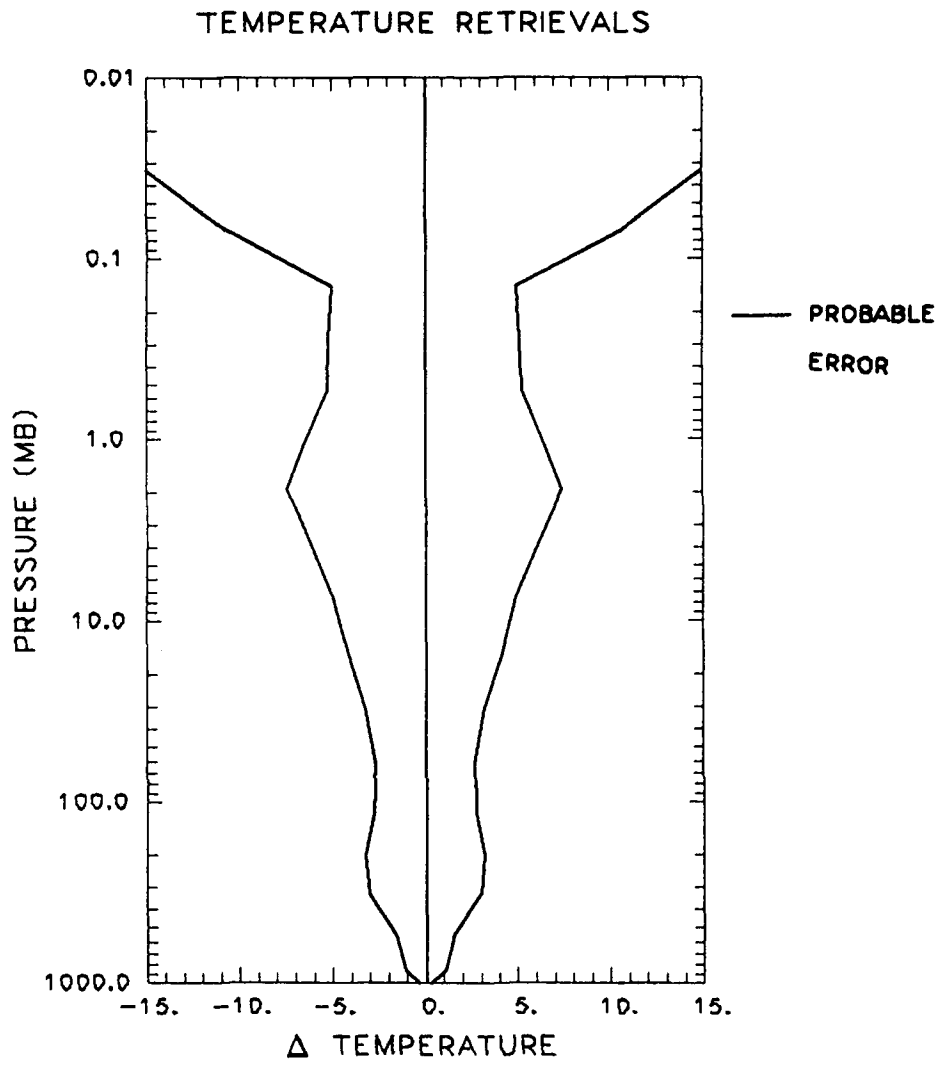


Figure 6-4b. Probable error ($1\sigma$) of the temperature profile using MLM with the AMSU channels only.

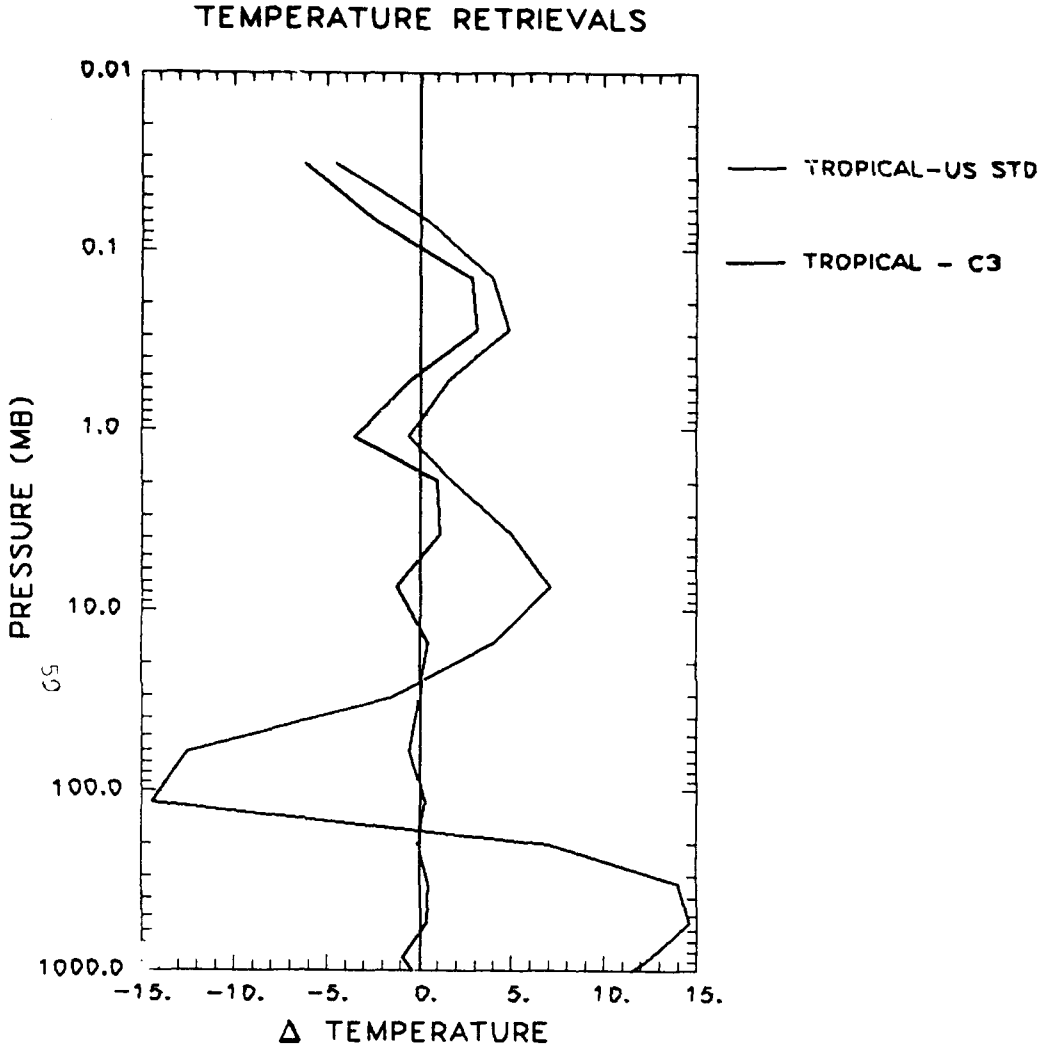


Figure 6-5a. Temperature residuals using extended AMSU channels but with the noise equivalent delta temperature for each channel reduced by the factor 0.5. The simulated radiances do not include measurement noise.

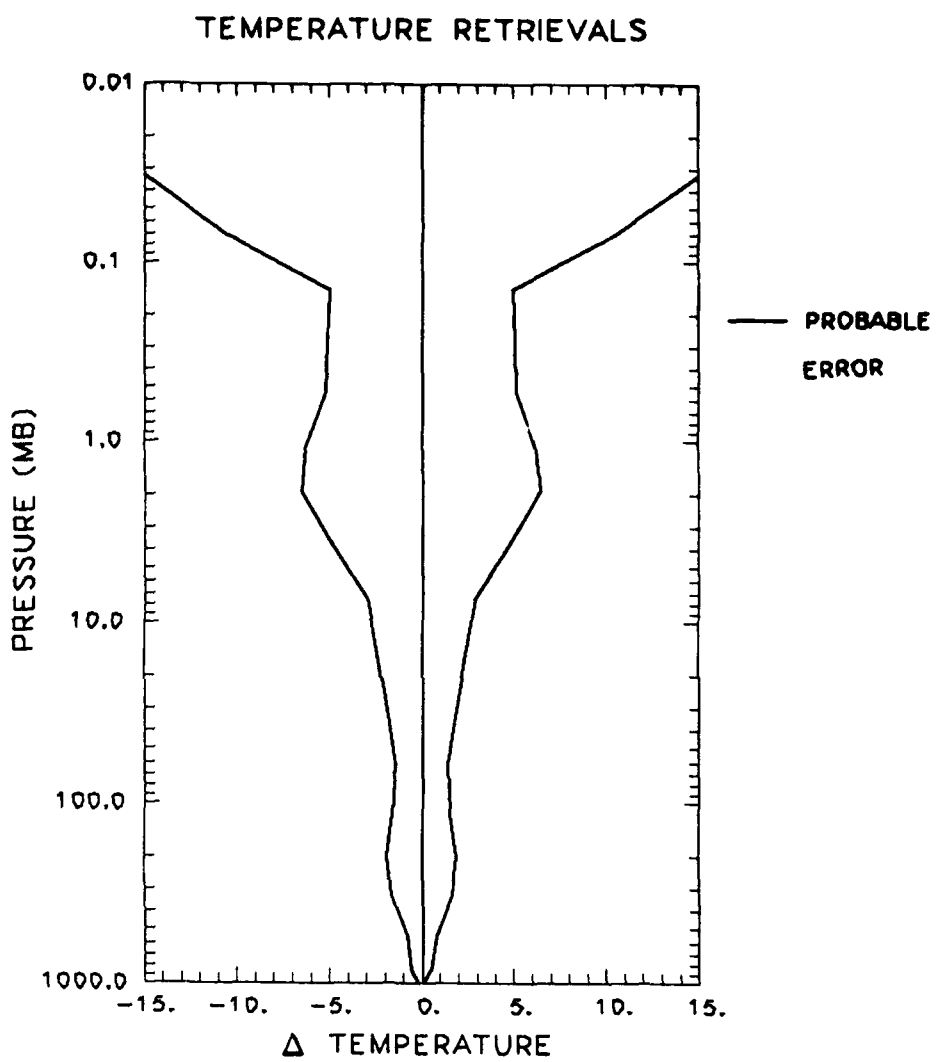


Figure 6-5b. The probable error ($1\sigma$) of the retrieval temperature profile with reduced noise.

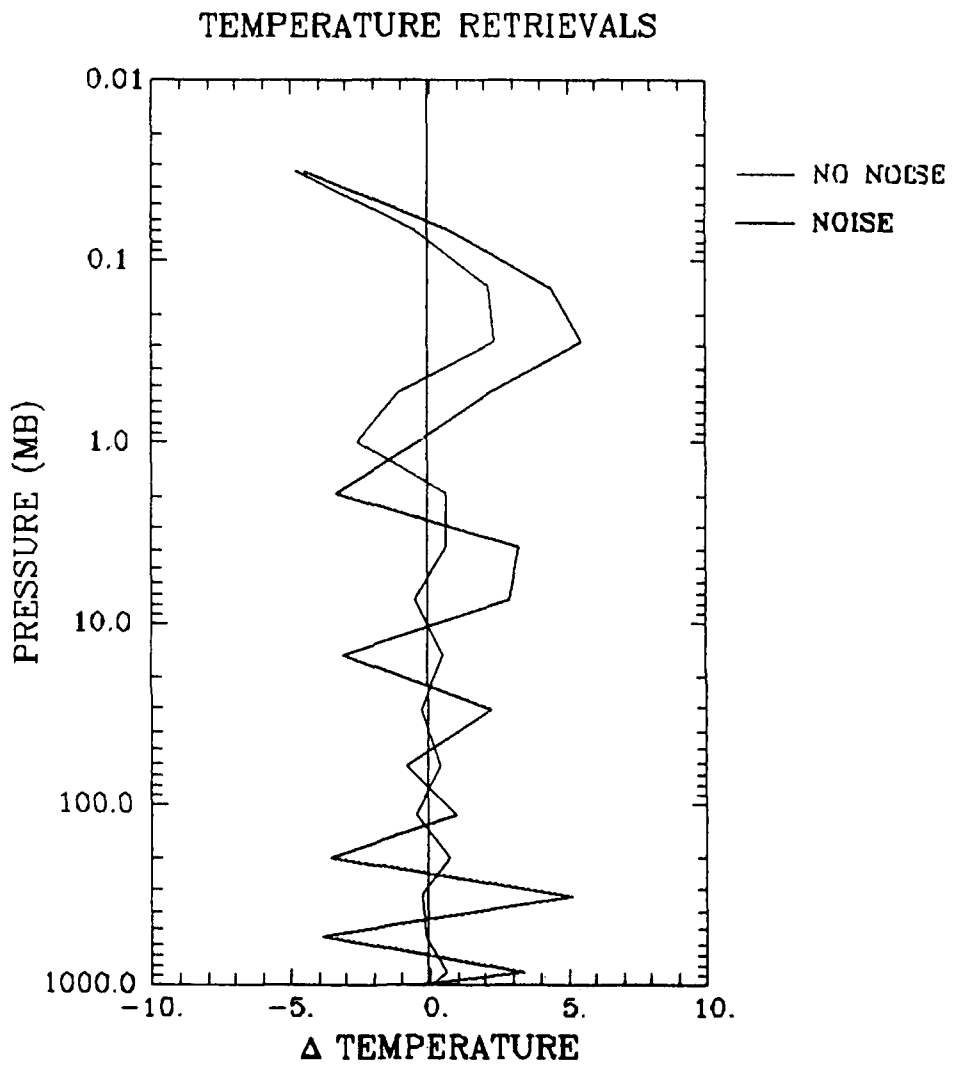


Figure 6-6. Temperature profile residuals as a function of iteration number for the case in which random noise has been added to each channel.

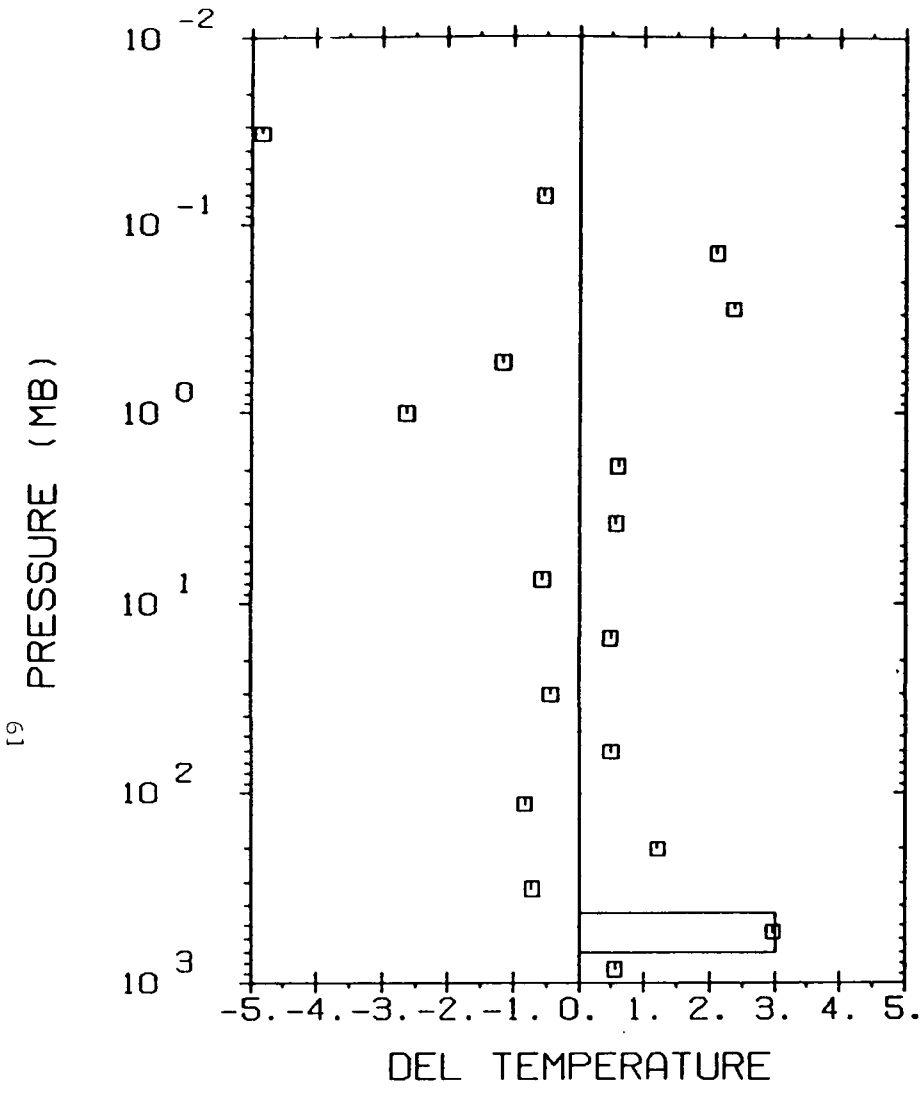


Figure 6-7a. Temperature profile residuals for a case in which a +3K temperature pulse is added to the 550 mb layer. No iterations have been performed.

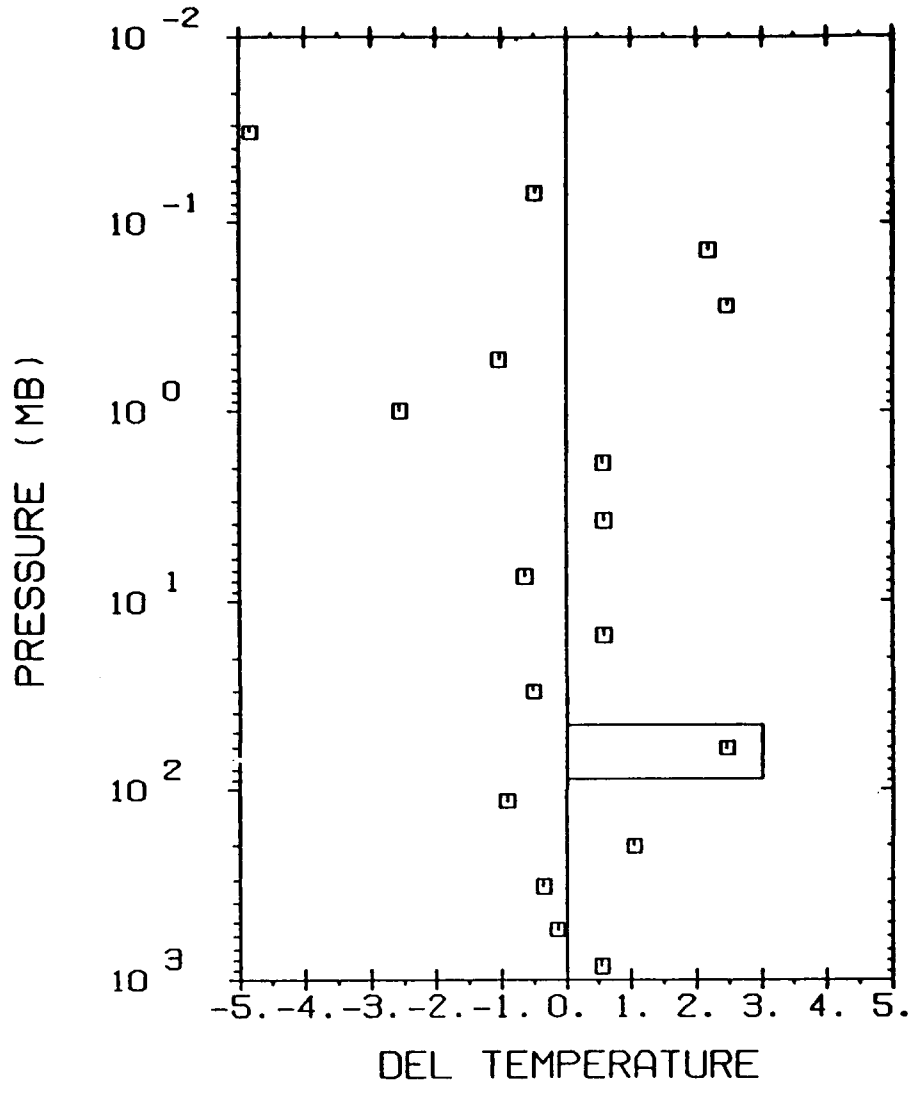


Figure 6-7b. Temperature profile residuals for a case in which a +3K temperature pulse is added to the 61 mb layer. No iterations have been performed.

550 mb case the temperature is retrieved very accurately, but the oscillatory behavior at the other levels has increased significantly. This ringing effect would be reduced by performing additional iterations; the results we show are for a single iteration. For the 61 mb case, in which the pulse is added to a layer close to the tropopause, the pulse temperature is not as well retrieved. The ringing effect is also apparent for this case. Again, if the problem were iterated the solution would converge on the atmospheric profile including the discontinuity. Although this capability of reproducing a discontinuity may be regarded as an advantage of the present method, it is the same property of the algorithm that allows it to follow the noise. So, while a more statistical approach may have the advantage of being less influenced by measurement noise, it has limited capability for retrieving discontinuities. In a more extended sense, the statistical approach has less capability to describe unusual or extreme situations, but may be expected to perform better on "average".

### 6.1.3 Water Vapor Retrieval

The next aspect of the AMSU measurement set that we have considered is the retrieval of water vapor. In this case the simulated data were obtained by replacing the water vapor column abundances for the reference atmosphere (U.S. Standard) by the column abundances for the tropical atmosphere and running the forward model. The mixing ratio profiles for the two atmospheres are given in Figure 6-8. Of particular interest is the much higher water vapor mixing ratio at the higher atmospheric pressure levels for the tropical atmosphere, approximately a factor of three times greater than for the U.S. Standard. The weighting functions for both the tropical and the U.S. Standard atmospheres for the AMSU water vapor channels related are provided in Figures 6-9a and 6-9b. Of particular note here are the significant vertical shifts in the peaks of the weighting functions for the two atmospheres which is consistent with the differences in the mixing ratio profiles. Since this is a nonlinear retrieval, this altitude shift has the potential to cause difficulty in the retrieval. In Figure 6-10a we show the residuals expressed as a percentage change from the correct solution from the first guess, TROPICAL-US STD; for the first iteration, TROPICAL-C1; and after the second iteration, TROPICAL-C3. The variable chosen in the algorithm for the retrieval of column abundances is percentage change. This variable may

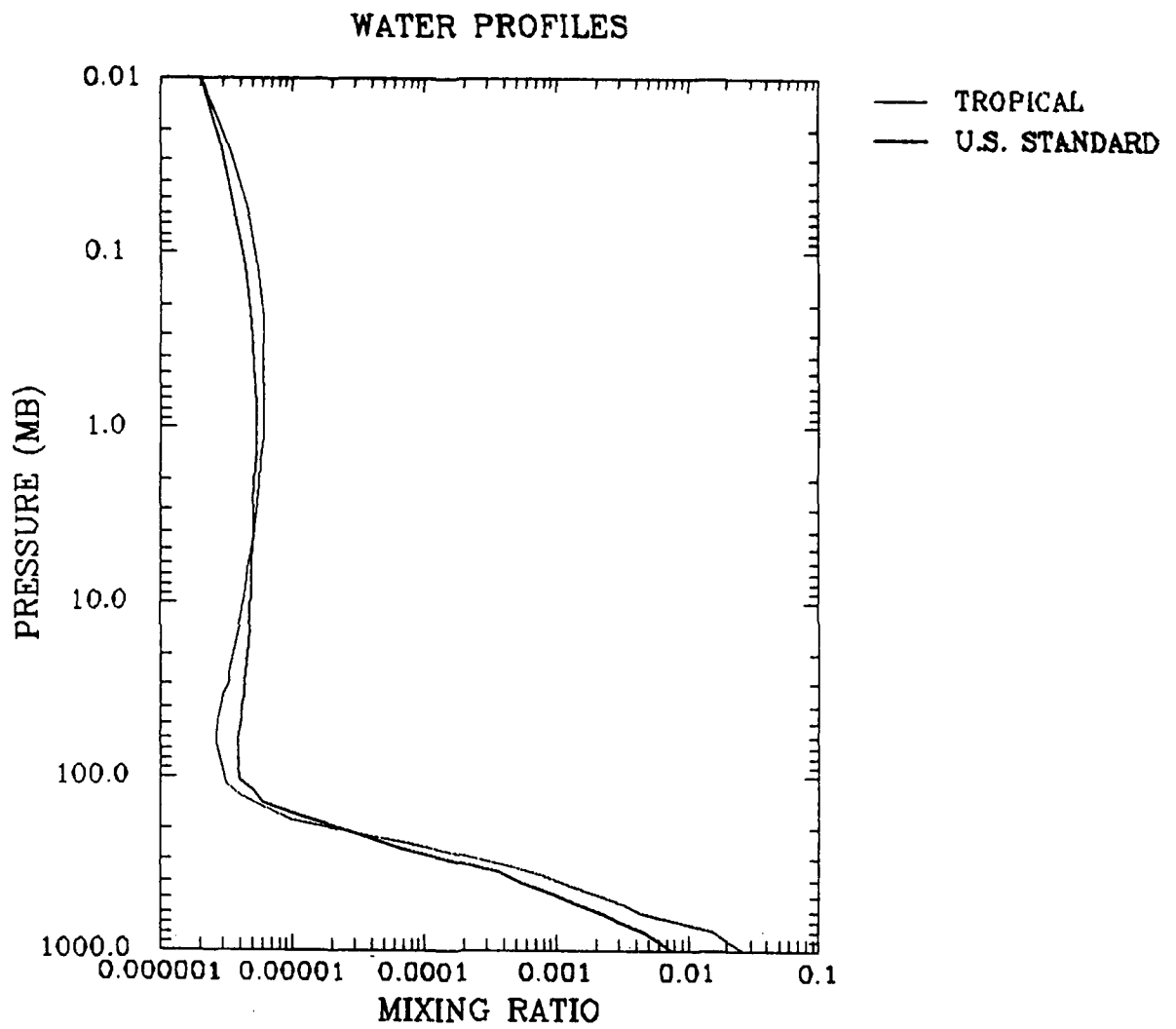


Figure 6-8. Water vapor mixing ratio profiles for the U.S. Standard (_____) and the Tropical (..... ) model atmospheres. The Tropical profile is used for the simulated data and the U.S. Standard is the first guess.

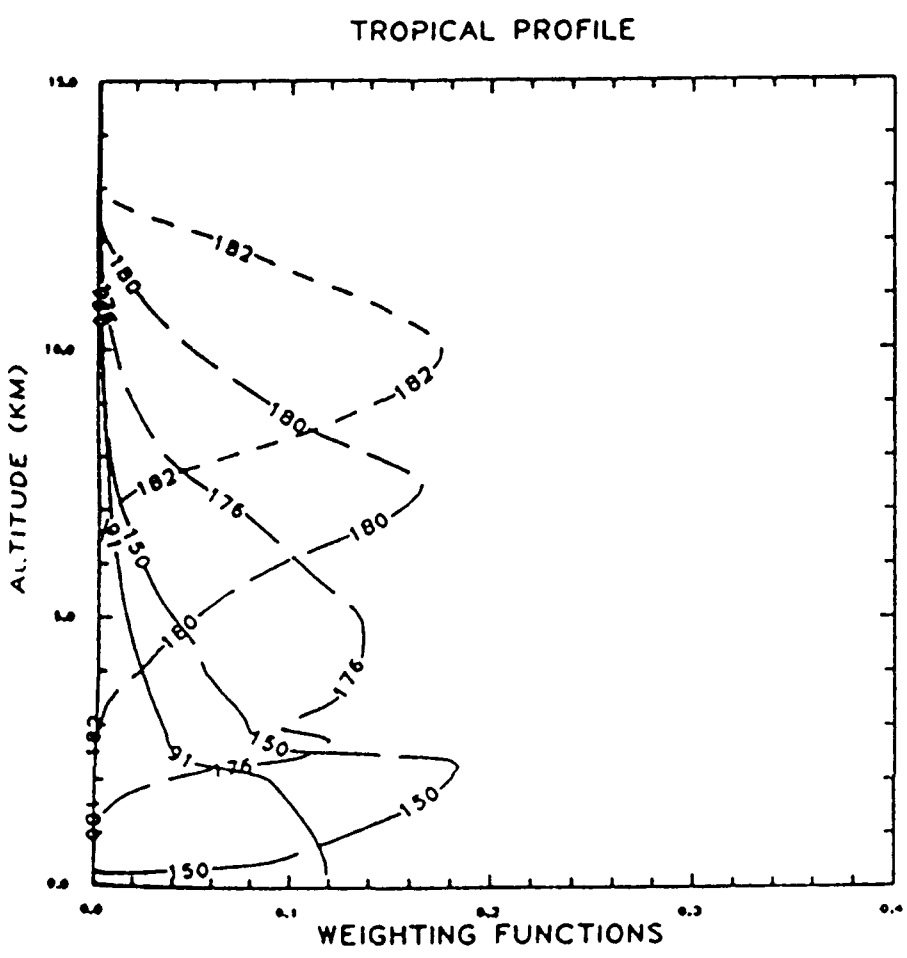


Figure 6-9a. Weighting functions for the AMSU water vapor channels for the Tropical model atmospheres.

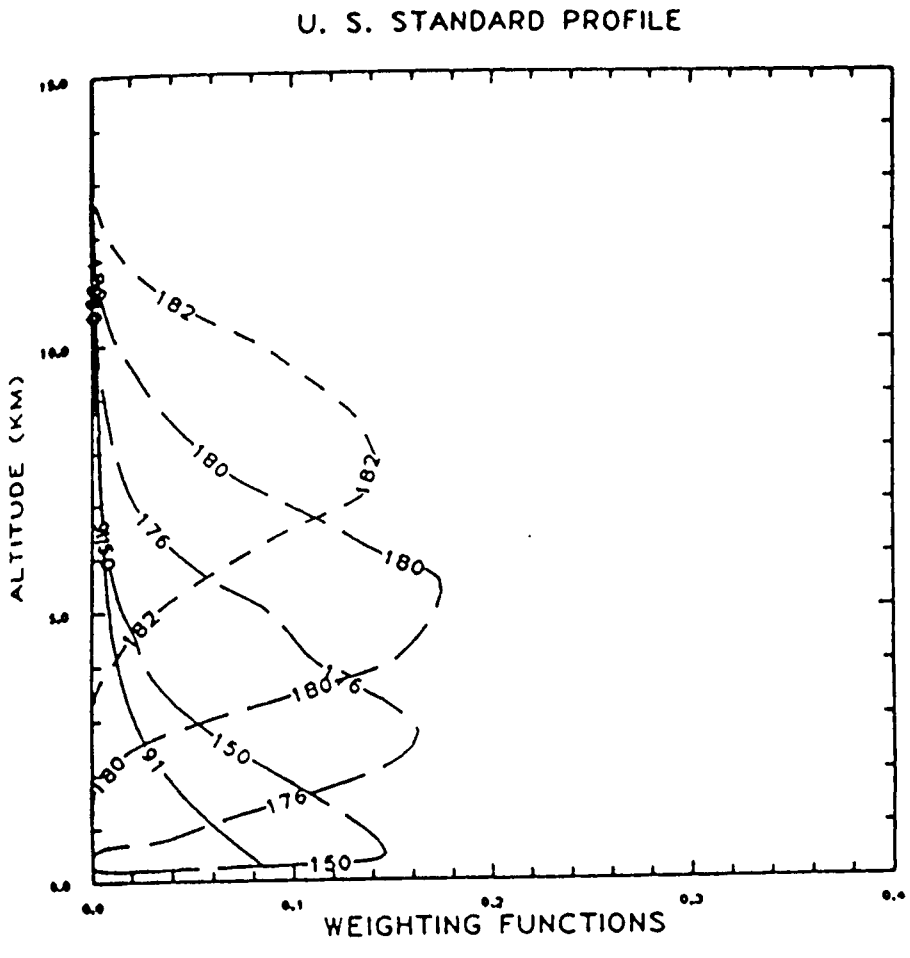


Figure 6-9b. Weighting functions for the AMSU water vapor channels for the U.S. Standard model atmospheres.

equally well be considered as applied to the layer column amounts or to the layer mixing ratios, since these two variables are linearly related. The water vapor profile is well retrieved, ~±10%, for pressures above 300 mb as evidenced by Figure 6-10a. At lower pressure levels, the water vapor state parameters are essentially in null space. This is partially due to the location of the weighting function peaks as indicated in Figure 6-10b but more importantly due to the rapid decrease in the column abundances of water vapor as a function of altitude. The transition region from measurement space to null space occurs rapidly from 300 mb to 200 mb as indicated in the ± 1$\sigma$ error result of Figure 6-11. Only three of the 17 layer levels are outside of null space for this case and the effective number of parameters is approximately one.

Finally, the results for the simultaneous retrieval are provided in Figure 6-10a with parameter error provided in Figure 6-10b. There is some increased instability in the temperature retrieval for this case. Although the temperature part of this retrieval may be considered linear, the entire problem is nonlinear due to the simultaneous treatment of water vapor. Had the initial guess been taken from the results of the previous two retrievals, then the simultaneous retrieval would likely have converged in the first iteration to a very accurate result. The retrieved water vapor profile for the simultaneous retrieval is somewhat improved over the previous retrieval for water vapor alone.

## 6.2 HIS Ozone Retrieval Test Case

The PLS method has also been applied to the retrieval of an ozone profile from data taken with the University of Wisconsin High Resolution Interferometer Sounder (HIS) (Smith et al., 1983). The data were taken with the NASA ER2 at 19.6 km with a nadir view.

The initial validation of FASCODE with these measurements has been described by Clough et al. (1989). The measured unappodized radiance spectrum in equivalent brightness temperature from 600-1100 $cm^{-1}$ is shown in Figure 6-12. The difference between the measured spectrum of Figure 6-12 and a forward model calculation with FASCOD2 using radiosonde defined atmospheric parameters is shown in Figure 6-13a. The strong spectral residuals at

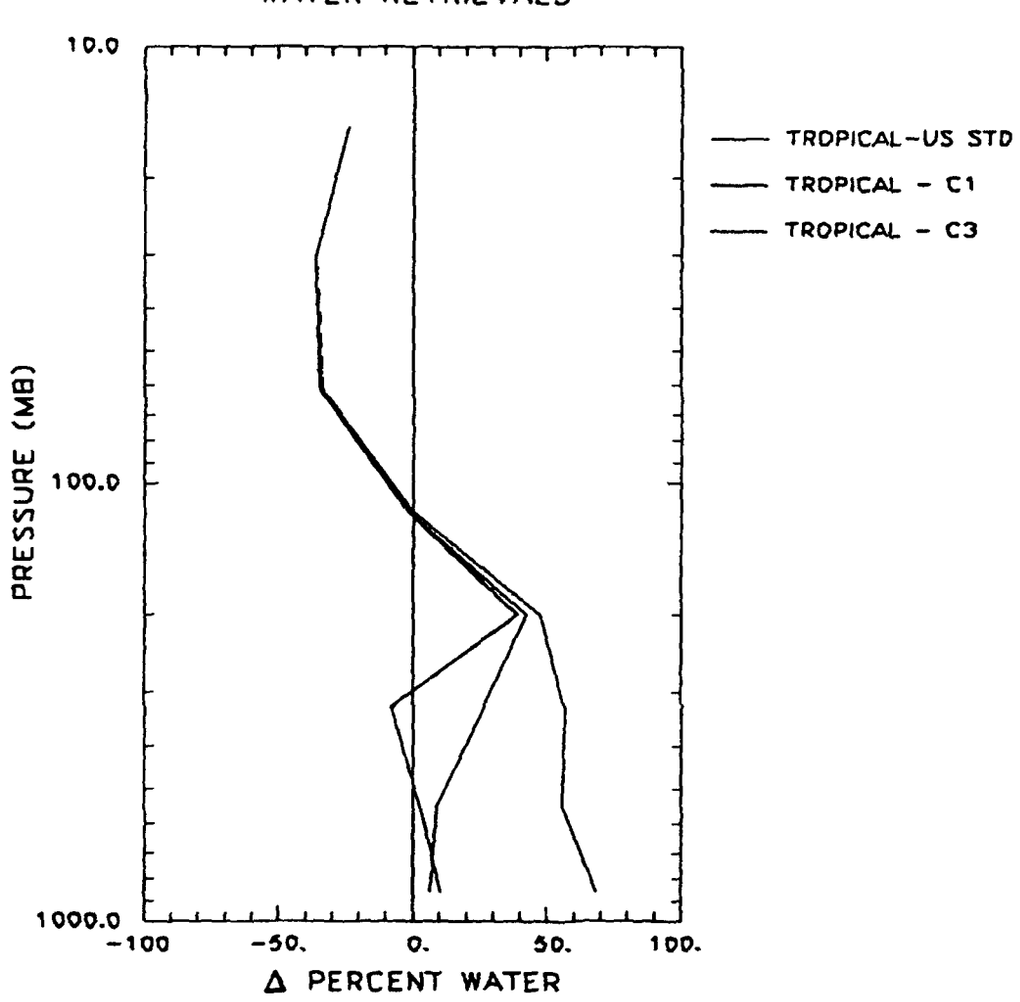


Figure 6-10a. Water vapor retrieval results using MLM as a function of iteration number:
_____ Tropical - $x^o$ (U.S. Standard);
__ __ Tropical - $x^1$;
__ _ __ Tropical - $x^2$.

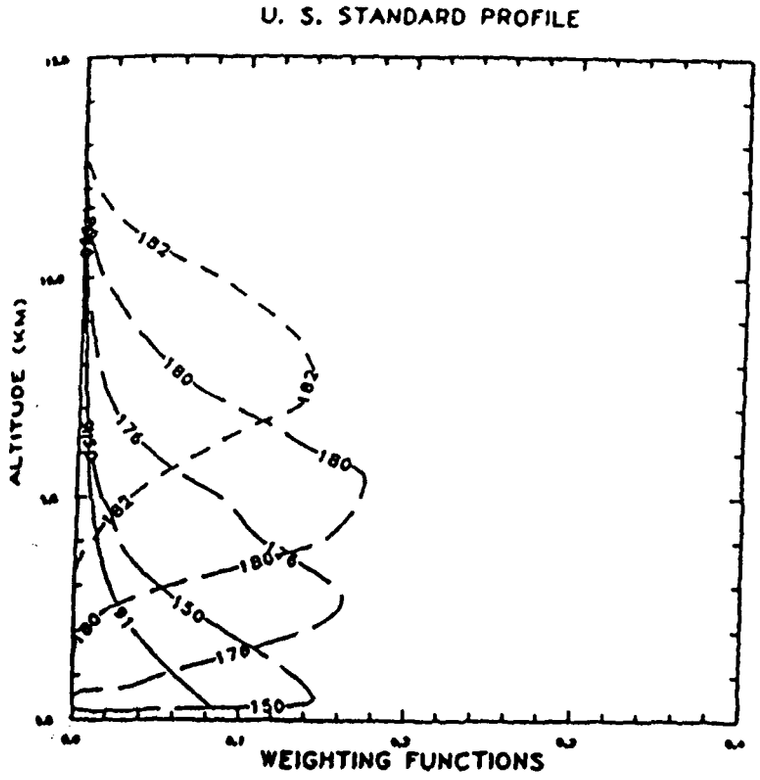


Figure 6-10b. Weighting functions for the AMSU channels on the same pressure scale as 6-10a for U.S. Standard atmosphere.

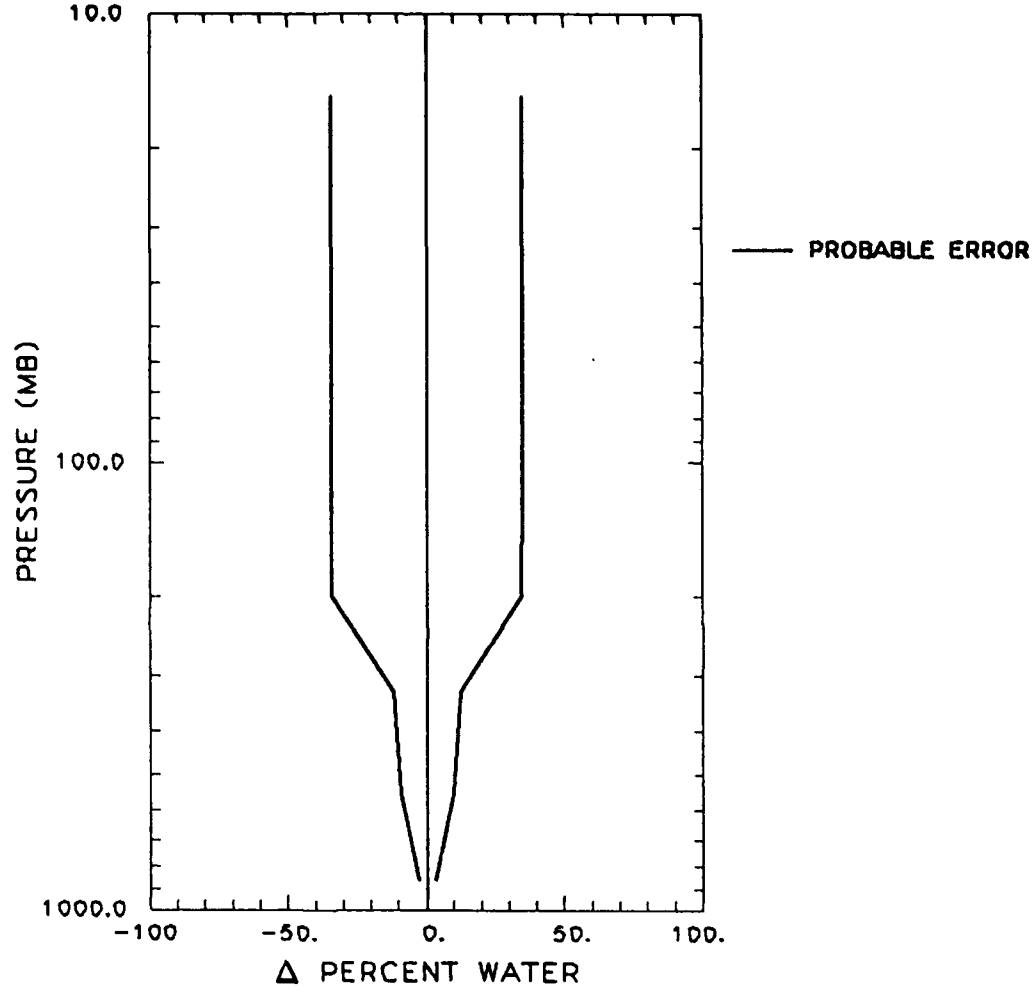


Figure 6-11. Retrieval error ($1\sigma$) for water vapor.

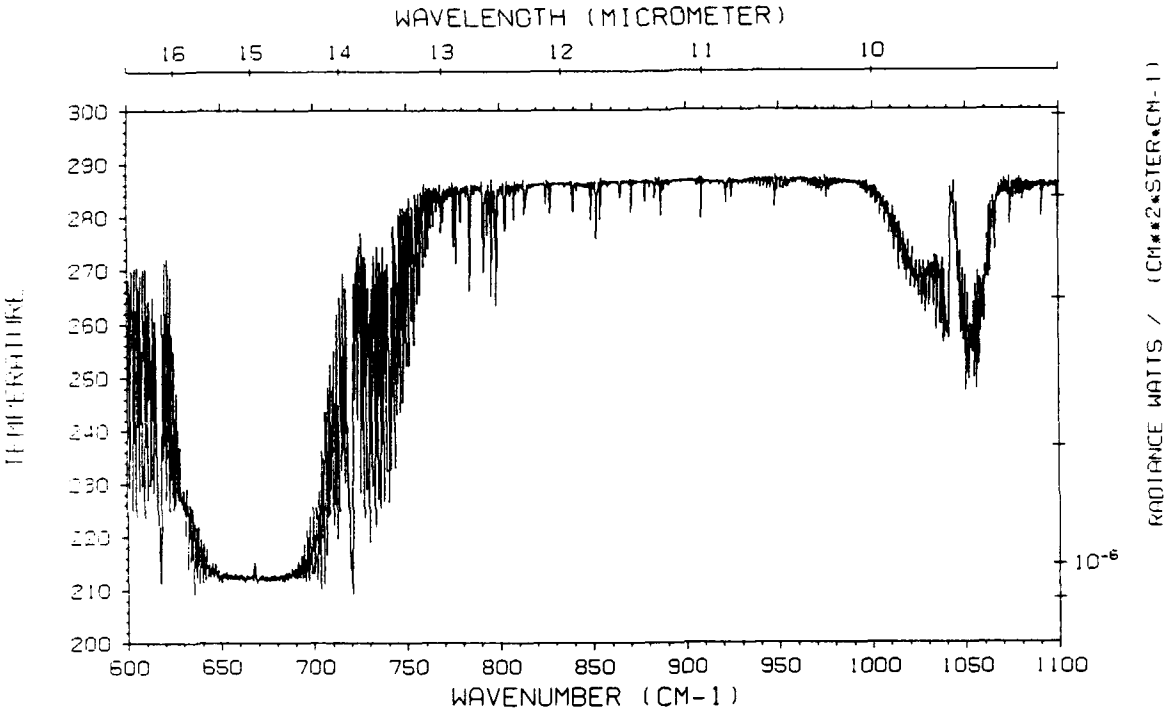


Figure 6-12. HIS measured radiance spectrum (equivalent brightness temperature) taken over the ocean on 14 April 1986 from 19.6 km.

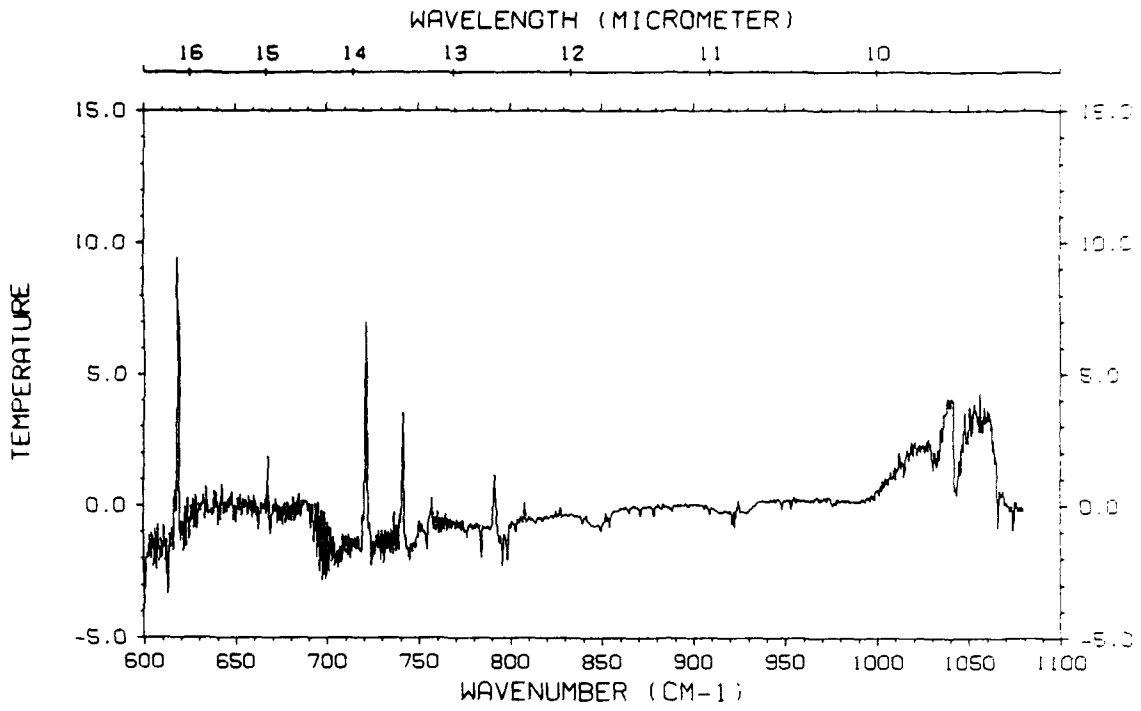


**Figure 6-13a.** Difference between the HIS measured spectrum and a FASCOD2 calculated spectrum using a radiosonde specified atmosphere with U.S. Standard ozone.

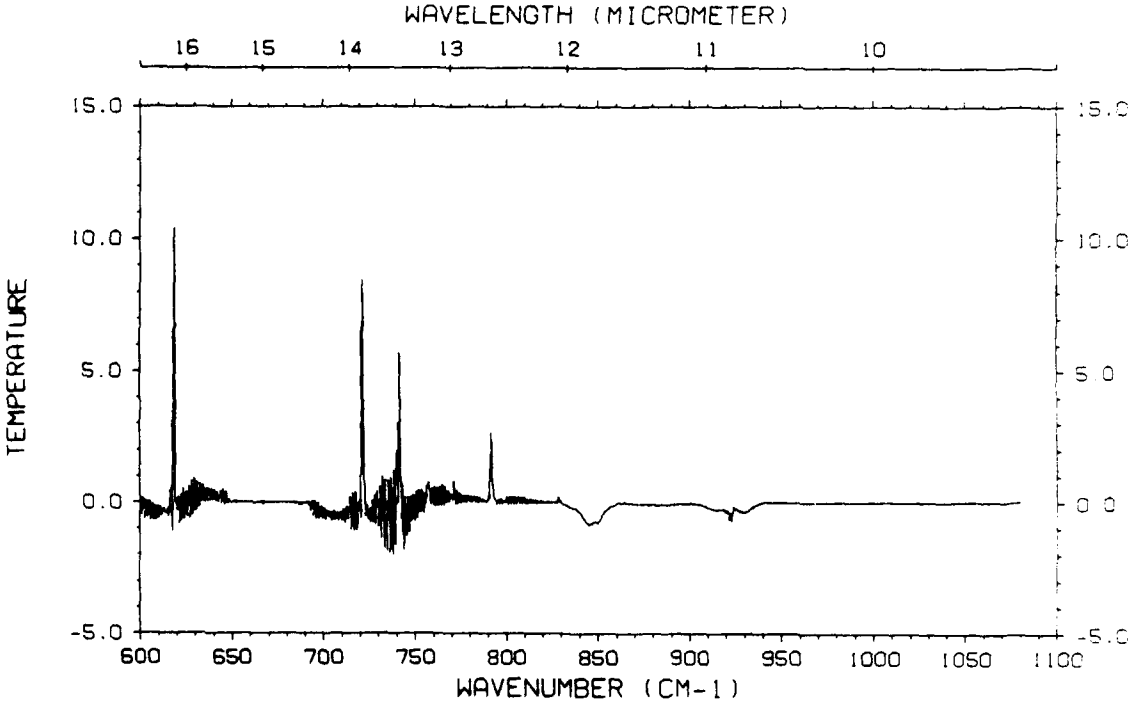


**Figure 6-13b.** Difference between an enhanced version of FASCODE including line coupling effects, improved carbon dioxide intensities, and treatment of CFC11 and CFC12 absorption and the previous FASCOD2 calculated spectrum. Note that most differences are accounted for with the exception of the ozone absorption region, 980 - 1100 $cm^{-1}$.

618 $cm^{-1}$, 720 $cm^{-1}$, 741 $cm^{-1}$, and 791 $cm^{-1}$ are due to line coupling and the broader absorption features at 850 $cm^{-1}$ and 925 $cm^{-1}$ are due to CFC11 and CFC12 respectively. Some of the spectral differences at 729 $cm^{-1}$ are due to $CCl_4$. In Figure 6-13b we show the difference between a spectrum from an improved FASCODE model which includes line coupling and CFC11 and CFC12 effects and the FASCOD2 model used for Figure 6-13a. For this improved model a modified set of carbon dioxide intensities was required (Rothman, 1988). The similarity of Figure 6-13a and 6-13b represents the current state of our validation for FASCODE and the line data base for this problem. Notably, however, the ozone region from 1000 $cm^{-1}$ to 1100 $cm^{-1}$ does not show agreement and this is primarily a consequence of an incorrect atmospheric profile for ozone. The other possible issue is the adequacy of the ozone lines on the 1986 HITRAN data base (Rothman et al., 1987). For the present study we have applied the PLS retrieval procedure to retrieve an improved ozone profile.

The initial guess for the retrieval is the U.S. Standard ozone profile. Figure 6-14 shows the HIS spectrum of Figure 6-12 for the ozone region on an expanded scale. In Figure 6-15a we show the difference between the measurement and a FASCODE calculation using the U.S. Standard ozone profile, Figure 6-13a for the ozone region. Applying the PLS retrieval we obtain after the second iteration the spectral residuals indicated in Figure 6-13b. It should be emphasized that the rms deviation of these spectral residuals is approximately five times the measurement noise. Possible explanations for this situation include our failure to properly account for the instrument function of the HIS instrument, a small frequency calibration error in the data, and problems associated with the HITRAN database. Current efforts to deal with the first two points have realized a factor of two improvement in the residuals. Of interest in this difference spectrum are the reasonably strong spectral residuals at 1009 $cm^{-1}$, 1014 $cm^{-1}$, 1028 $cm^{-1}$ and 1066 $cm^{-1}$. These residuals are due to intensity errors in the weak water vapor lines in this spectral region. With the possible exception of the feature at 1066 $cm^{-1}$, it would have been unlikely that this problem would have been noticed using the spectral residuals of Figure 6-15a.

The maximum likelihood method has been used to obtain the retrieved result. The error covariance was quite arbitrarily set to a value corresponding to an 8% probable error for the first guess. The retrieved ozone

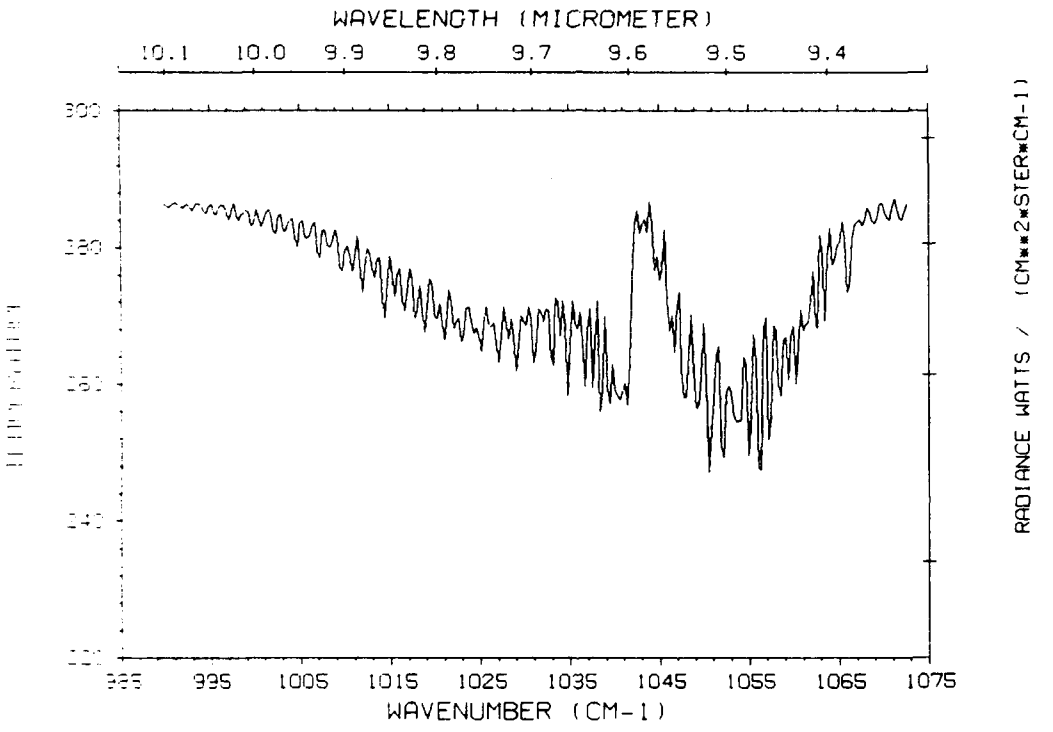


Figure 6-14. An expanded representation of the measured equivalent brightness spectrum in the ozone region.

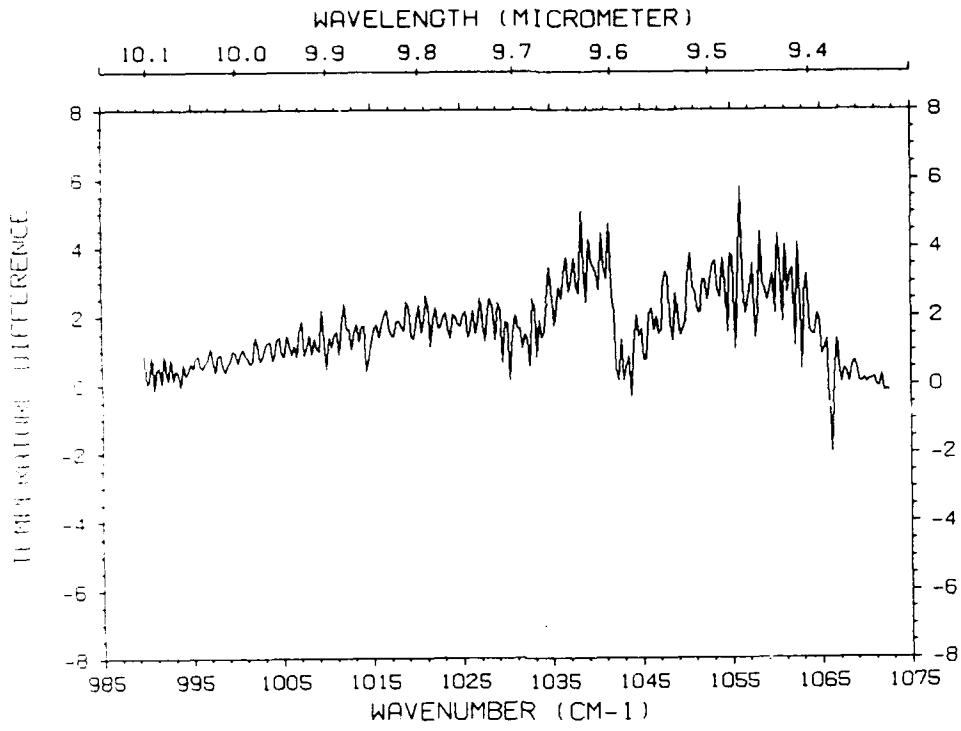


Figure 6-15a. The spectral difference in brightness temperature between the measurement and the calculation in the ozone region.

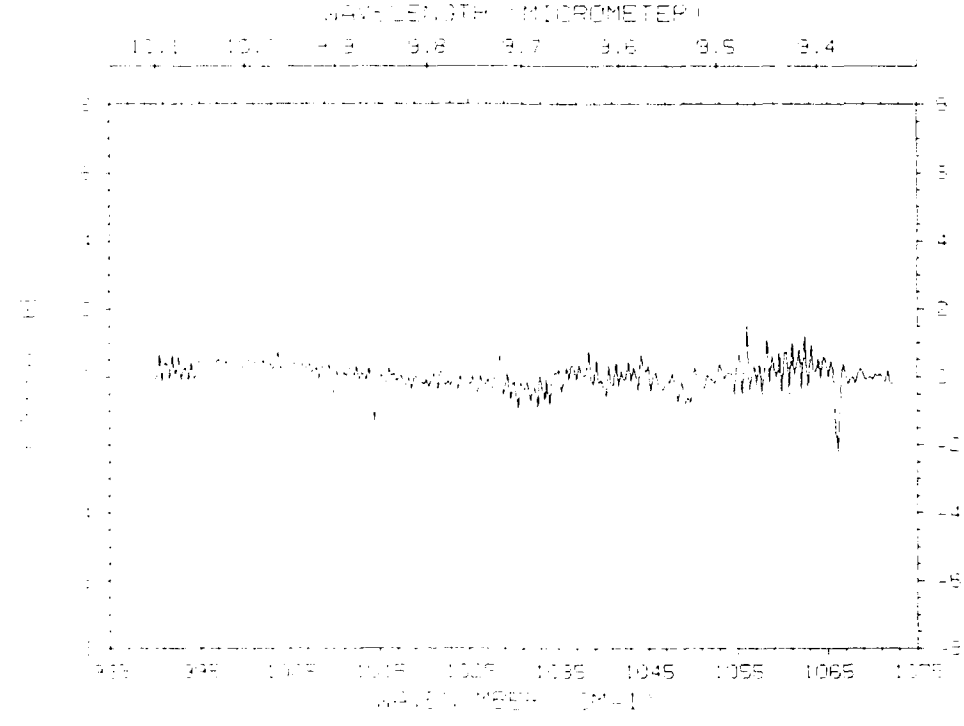

Figure 6-15b. Residuals in equivalent brightness temperature as a consequence of performing a retrieval for the ozone profile.

profile is provided in Figure 6-16a. The vertical line at 0 corresponds to no change from the first guess U.S. Standard ozone profile. The retrieval residuals marked C1-U.S. STANDARD are after the second iteration. The derivatives are for the reference profile. These results appear quite reasonable with the possible exception of the mixing ratio change for the first layer. An abrupt change of this magnitude in the atmospheric profile is possible but bears further analysis. A possible explanation of this result is that the measurement is being made in the atmosphere in a region of high ozone concentration and that the forward model does not adequately model the radiance from a strongly absorbing layer directly in front of the measurement. A new algorithm for the computation of radiance has been implemented in a recent version of FASCODE and it will be of interest to ascertain if this will have an effect on this apparent anomaly.

## 6.3 Pressure Retrieval of Lowest Level

For the examples of the path characterization algorithms presented here, retrievals for the lowest atmospheric pressure level or alternatively the pressure of the lowest layer, have not been included. The implementation of this capability was accomplished after the present studies were accomplished. Some general comments about the retrieval of pressure are warranted. For the terrestrial atmosphere the change in the mass of a layer is essentially independent of the state parameters being retrieved. Changes in layer temperature have an effect on the density of a layer, but not on the mass. The molecules for which the concentrations may be retrieved do not include nitrogen, oxygen and argon which are principally responsible for the mass of the atmospheric layer, so that the mass distribution by layer is unaffected by the retrieval. The minor exception to this is water vapor for which changes in the concentration profile may have a small effect on pressure; these small changes in pressure are negligible in terms of affecting the pressure broadening for the layer. They can be important, however, in terms of the association of the layers with altitudes as is relevant for numerical weather prediction applications. For the path characterization algorithm as applied to the earth's atmosphere, if the hydrostatic equation is satisfied for the reference atmosphere, then to good approximation it will be satisfied for the retrieved atmosphere. For applications to more general inhomogeneous atmospheres, the retrieval of molecular concentrations may sufficiently alter the mass of the

layers so as to have a non-negligible effect on the layer pressure. In this case the interaction of the retrieved concentration and the pressure must be included as part of the non-linear problem.

In the context of the path characterization algorithm, the pressure at the lowest atmospheric level is the state parameter which characterizes the mass, layer pressure and mass path of the lowest layer. For nadir problems this pressure is associated with the pressure at the surface and for limb cases it is associated with the pressure at the tangent height. For the present implementation, the finite difference with respect to this parameter is attained by perturbing the lowest altitude in the path by a specified amount, resulting in a perturbation at the lowest path boundary. The actual variable for the problem is the fractional change in the lowest level pressure, consistent with the approach used for the molecular concentrations.

# 7. PROGRAM DESCRIPTION AND IMPLEMENTATION

## 7.1 Program Overview and Description of User Instructions

### 7.1.1 Program RETRVL

RETRVL is the driver for the Path Characterization subroutines. Several features have been built into the program. These include:

- FASCOD3
  - FASCOD3 is a subroutine to RETRVL and is called within the derivative loop

- Radiance and Brightness Temperature derivatives
  - the user can optionally select either radiance or brightness temperature derivatives to be calculated

- Retrievable constituents currently include layer temperature, water and ozone, plus surface temperature and pressure

- An extensive error analysis scheme is available

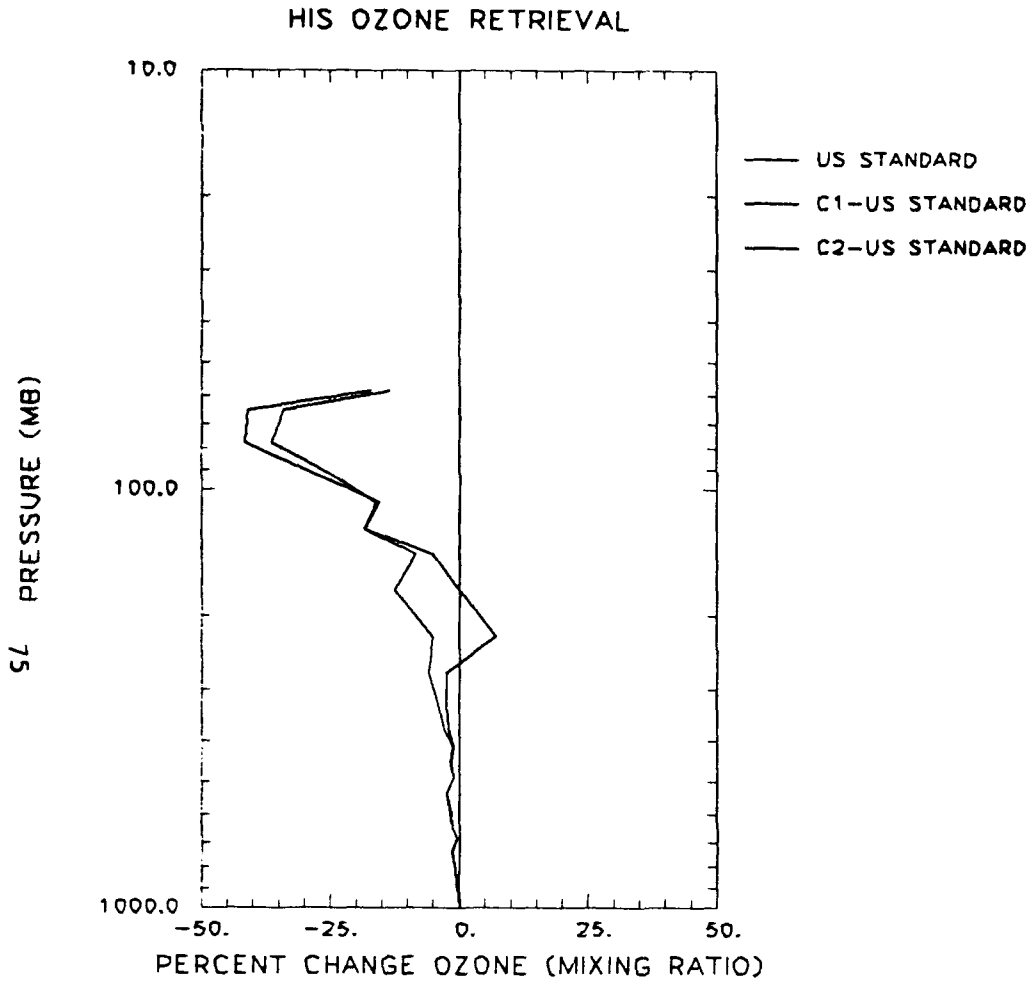


Figure 6-16a. Ozone profile retrieval as a function of iteration.

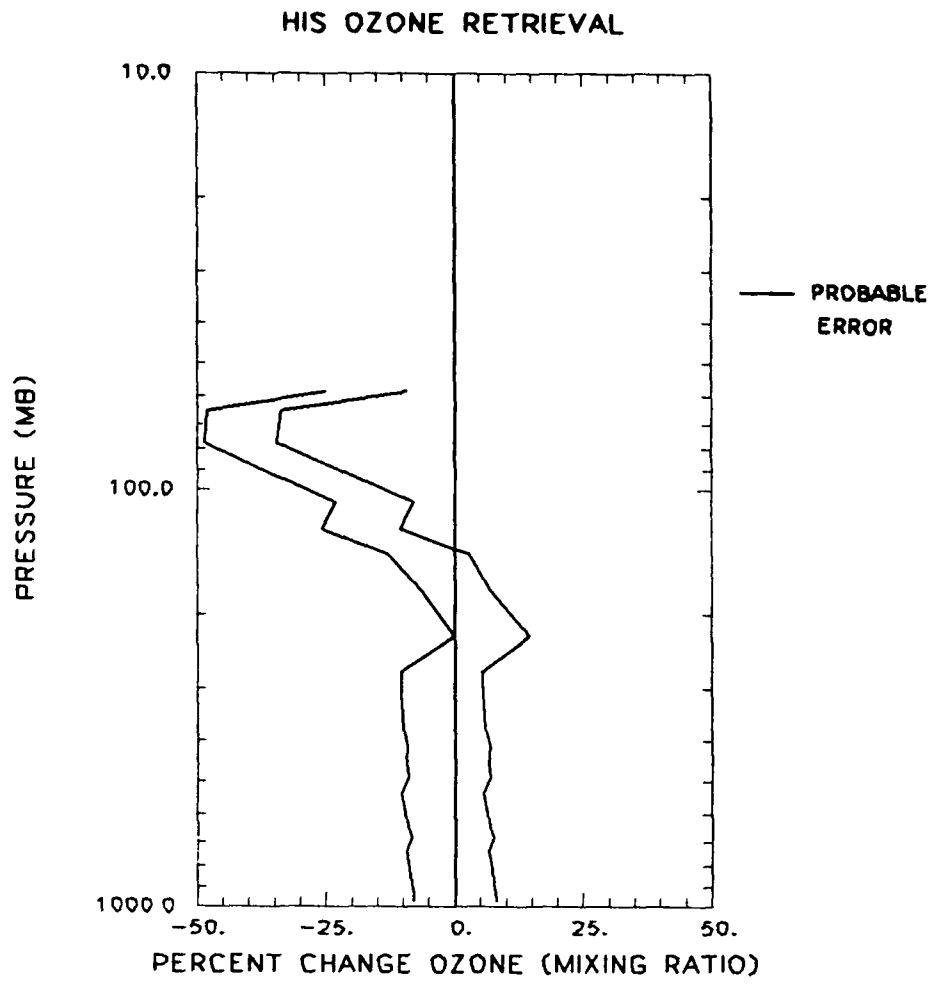


Figure 6-16b. Probable error ($1\sigma$) for the profile of Fig. 6-16a.

### 7.1.2 RETRVL Program Overview

The structure of the Program RETRVL will be discussed in Section 7.3, but the following provides an overview of the program's operation. The first thing that is required in order to run RETRVL is an idea of the atmosphere to be retrieved. Once an appropriate problem is selected, the user should run FASCOD3 using the IPUNCH option to produce a TAPE7 which can be used as input for the retrieval run. Once the user has selected the constituent(s) to be retrieved, a run may be accomplished.

In order to do a retrieval the user must first select an appropriate TAPE3 (FASCOD3 Line File) and get the initial TAPE5 as T5REF. The input file RETVCTL contains the control cards which select or deselect the appropriate options. We will assume for the sake of discussion that all of the options, excluding IFASC3 have been selected. For this case we require for input the following files:

| | | |
|---|---|---|
| TAPE3 | - | FASCOD3 Line File |
| T5REF | - | Reference TAPE5 |
| T5SIM | - | Simulated Radiances TAPE5 |
| RETVCTL | - | Input control file for RETRVL |

Upon entering RETRVL the first operation that is performed is the calculation of the Reference Case. This is the FASCOD3 run to which all subsequent FASCOD3 calculations will be compared. The reference case is calculated by copying T5REF to TAPE5 and running FASCOD3. The scanned output file is then copied to T11SEQ which will form the basis for the derivatives.

The next option is to calculated T11SEQ itself. This requires the user to have selected constituent(s) on which the derivatives will be based. We will assume that layer temperature and surface temperature were selected. The first step is to call ATMOD and have it modify the temperature of the first layer by the quantity DELSV. This will produce a 'new' TAPE5 which will contain the modification. FASCOD3 is then run and the resulting scanned file is copied directly after the reference case onto T11SEQ. We then continue around the loop and modify the next layer temperature. The resulting FASCOD3 output is then copied to T11SEQ. We continue in this fashion through all of the desired layers and then for the last run, we do the surface temperature. Once

this FASCOD3 output file has been copied to T11SEQ this step has been completed. We now have a file (T11SEQ) which contains our reference run and all of the resulting outputs which were obtain from perturbing the atmosphere.

We are now ready to calculate derivatives. We can either chose radiance or brightness temperature derivatives. For this case we will call RADBT and calculate brightness temperature derivatives. RADBT takes T11SEQ as input and converts all the radiances to brightness temperatures and stores them on T11BT. DERIV is then called and each of the FASCOD3 runs is compared to the reference case and a derivative is calculated. The resulting file is stored in RADERV0.

The next step is to calculate T11SIM. This can be real data, or a FASCOD3 simulation on which the retrieval is being tested. For this case we will use the file T5SIM to calculate a set of simulated radiances. The file T5SIM is copied to TAPE5 and a subsequent FASCOD3 run produces our simulated radiances.

We now need to produce a difference file which the retrieval can use in order to attempt to retrieve our simulation. Since the derivatives have been calculated in brightness temperature, we must calculate the differences in brightness temperature also. So we first call RADBT and it produces a file T11SBT which contains the simulated brightness temperature. This file is then compared with the reference case on T11BT and the resulting difference is written to the file RADDIF0. We now have the required input necessary for the retrieval.

INVERT is now called and a matrix inversion is performed. This produces a vector which contains the changes to the reference case in order to retrieve the simulation. These results are written to the files RETVOUT and PARAMOT. RETVOUT is the full output listing, PARAMOT is used for the next iteration and plotting.

In order to facilitate the next iteration we also call ATMDT5 which reads the files PARAMOT and T5REF and produces a new 'TAPE5' called T5ITR which has the 'required' changes to the reference case. This TAPE5 then becomes the reference for the next iteration, or set of derivatives.

### 7.1.3 RETRVL User Instructions

Appendix B contains the user instructions for RETRVL. These instructions will be explained in further detail below. The user instructions for FASCOD3 will not be discussed here, but we refer the user to the FASCOD3 documentation for a complete input description. Record 1 of the user instructions for RETRVL is the HEADER which is used for file RADDIF0. This record is required for all runs not just IFDIF > 0.

Record 2 contains the main control flags for RETRVL. IRCASE selects the calculation of the reference case or not. IFSEQ flags the calculation of the file T11SEQ which contains the reference case and the perturbed FASCOD3 runs. IDERIV selects the derivative calculation and allows the choice of radiance or brightness temperature derivatives. ISIMUL selects the calculation of simulated radiances as the 'data' to be retrieved. IFDIF selects the difference calculation and allows the choice of radiance or brightness temperature differences. JINVRT selects the matrix inversion or retrieval which uses the derivatives and differences to produce a retrieved solution. IATMT5 allows the user to modify the reference case by the retrieved solution to produce a new TAPE5 for the next iteration. IFASC3 allows the user to run FASCOD3 using RETVCTL as the input file. This allows the user to utilize the FASCOD3 plotting routines in order to plot the retrieval results.

Record 3.1 contains the five possible constituents to be retrieved. ICNST is defined as one of the following:

a) 0,-1 ends read of parameters
b) 1-28 corresponds to the molecules as used by FASCODE i.e. 1=$H_2O$, 2=$CO_2$, 3=$O_3$, ... etc.
c) 29 corresponds to the layer temperature
d) 30 corresponds to the surface temperature
e) 31 corresponds to the surface emissivity (not currently implemented)
f) 32 corresponds to the lowest boundary pressure

LAYB is the beginning layer for retrieving parameter ICNST. LAYE is the ending layer for retrieving parameter ICNST. DELSV is the change that is applied to the state parameter which is used in calculating the derivatives.

Record 3.2 contains the control flag NZFLG which is the total number of layer boundaries which are to be read in to determine to layers to be used.

Record 3.3 contains the layer boundaries which are determined by NZFLG on Record 3.2. ZLEVP must be a subset of the boundaries which are found on T5REF.

Record 4.1 contains the header which is used by INVERT. JHEADR is used for labeling the files RETVOUT and PARAMOT.

Record 4.2 contains the main control flags for INVERT. NUMFIL selects the total number of frequency regions (files) which will be used by the retrieval. NUMFIL = 2 would require the files RADERV0, RADERV1, RADDIF0 and RADDIF1 in addition to any other required files. NREF selects the index for the reference constants. NPAR is the total number of parameters to be retrieved. NPRT is the number of parameters to be output per page. NEIG is the flag which selects running the Eigen solution, which is provided for informational purposes only. IREFD flags the reference data input. This allows the user to use the quantities on file PARAMIN instead of those present on the derivative file header. This is useful for analysis in cases of multiple derivatives. NSIM is the flag for reading in simulated atmosphere data from PARAMIN.

Record 4.3 contains IOUT which selects the parameters and order for the retrieval. This allows the user to tailor the input and output of the parameters.

Record 4.4 contains the control flags used for retrieval output. IKMAT selects the printing of the KMATRIX. IHMAT selects the printing of the H matrix. IHCOR selects the printing of the correlation H matrix. IHINV selects the printing of the H inverse matrix. IHICR selects the printing of the correlation H inverse matrix. IHHIN selects the printing of the H matrix times H inverse matrix. IHHIN selects the printing of the H matrix times H inverse matrix. IYVEC selects the printing of the Y vector. IDRDI selects the printing of the residual vectors (RD-Rn), (Rn+1-Rn) and (RD-Rn+1).

Record 4.5 contains control flags for additional retrieval options. IGUESS determines whether or not a error covariance matrix is read in and used. MXLKHD selects the retrieval method, either ridge regression or maximum likelihood. PEIG selects the printing of the eigenvalues and eigenvectors for NEIG = 1.

Record 4.6 contains the control parameters for the damping, weighting and noise factors. GAMMA is the damping factor which is applied to all of the parameters. NDAMP is the number of individual damping factors to be read in on Records 4.6.1 and 4.6.2. IWGHT is the flag for measurement weights to be input on Record 4.6.3. NOISE flags the addition of noise to the retrieval. DSEED is the seed which is used by the random number generator in calculating the noise.

Record 4.6.1 contains the list of parameters to which damping is to be applied. IDAMP is the desired parameter to be damped.

Record 4.6.2 contains the damping factors which are applied to each parameter. DAMP corresponds to the parameter defined by IDAMP in Record 4.6.1.

Record 4.6.3 contains the weights to be applied to particular points in the retrieval. IWFLG selects how the weight is to be used. IFWGHT is the input file to which the weights will be applied. IBWGHT is the beginning point on file IFWGHT which will be used. IEWGHT is the ending point of file IFWGHT which will be used. WGTFAC is the weighting factor to be applied. FREQ is the wavenumber value used in converting the brightness temperature noise to radiance noise. CHTMP is the average temperature for the spectral interval. CHTMP is used to convert the brightness temperature noise to radiance noise. For microwave runs, CHTMP should be zero.

Records 5.1-5.XX contain the FASCOD3 input file which is selected by IFASC3 = 1. See the FASCOD3 user instructions for a description.

### 7.1.4 RETRVL File Utilization

RETRVL used three types of file structures: a) formatted I/O files, i.e. RETVCTL, RETVOUT, PARAMIN, PARAMOT, RADDIF0, ERCOVCG, T5REF, T5SIM and T5ITR, b) unformatted binary file, i.e. KMATRIX, and c) unformatted FASCODE files, i.e. T11SEQ, T11BT, T11SIM, T11SBT, RADERV0 and RESIDFS.

These files and their use are outlined below:

1) ERCOVCG - is the error covariance matrix input file used for the first guess. This file is used by INVERT.

2) KMATRIX - contains the derivatives which are used by INVERT. The derivatives are ordered by the parameter IOUT and were created by DERIV.

3) PARAMIN - contains the retrieval results from the previous iteration which are to be used by the current iteration. PARAMIN also contains the simulated atmosphere when used. PARAMIN and PARAMOT share a common structure which we will now describe. The files consist of 9 columns of data. The first column is simply an integer index of the parameter. The second column contains the layer number and constituent which is being retrieved. The third column contains the reference data used for the retrieval. The forth column contains the results of the retrieval which is the change which is to be applied to the reference case to produce the retrieved results. The fifth column contains the retrieved results. The sixth column contains the reference data that was used in calculating the derivatives. The seventh column contains the simulation data when needed. The eighth and ninth columns contain the lower and upper boundary altitudes for the associated layer.

4) PARAMOT - is the results from the current retrieval. PARAMOT becomes PARAMIN for the next iteration. PARAMOT is also used by ATMDT5 to created the new TAPE5 (T5ITR) from T5REF.

5) RADDIF0 - contains the differences between the simulated radiances or data and the current reference case. RADDIF0 is created by FSCDIF and used by INVERT.

6) RADERV0 - contains the derivatives which were calculated by perturbing the input file to FASCOD3. RADERV0 is created by DERIV and used by INVERT.

7) RESIDFS - contains the three vector results of the retrieval which are stored in FASCODE format for plotting. These vectors are $(RD-R_n)$, $(R_{n+1}-R_n)$ and $(RD-R_n)$. RESIDFS is created by INVERT.

8) RETVCTL - is the input control file for RETRVL.

9) RETVOUT - is the print output file resulting from a run of INVERT.

10) T5ITR - is the TAPE5 for the next iteration. T5ITR is created by ATMDT5 by using the retrieval results from PARAMOT and modifying T5REF to produce T5ITR.

11) T5REF - is the TAPE5 for the reference case. T5REF is used as the basis for the derivative calculation.

12) T5SIM - is the TAPE5 for the simulated radiances. T5SIM is used when simulated radiances are desired instead of data.

13) T6REF - is the TAPE6 resulting from the reference case. T6REF is output from FASCOD3.

14) T6SIM - is the TAPE6 resulting from the simulation run. T6SIM is output from FASCOD3.

15) T11BT - is the result of converting T11SEQ to brightness temperature. T11BT is the output from RADBT.

16) T11SBT - is the result of converting T11SIM to brightness temperature. T11SBT is the output from RADBT.

17) T11SEQ - contains the result of the reference case, and the perturbed FASCOD3 runs. T11SEQ is used by RADBT and DERIV.

18) T11SIM - contains the result of the simulated radiance run. T11SIM is used by RADBT and FSCDIF.

## 7.2 Implementation of RETRVL

### 7.2.1 Compiling and Linking RETRVL Modules

RETRVL is made up of seven modules. These are outlined below:

a) RETRVL - contains main driver program and all modules excluding INVERT and FASCD3 subroutines
b) INVERT - contains the matrix inversion driver routine
c) IMSL - contains the IMSL routines used by INVERT
d) FASCD3 - contains the main FASCOD3 subroutines
e) FSCATM - contains the FASCOD3 atmosphere subroutines
f) FASLOW - contains the LOWTRN aerosol subroutines
g) FSCMS - contains the multiple scattering subroutines

For compiling and linking these routines on the AFGL Cyber, a segload file is provided in Table 7-1. Once these routines are compiled and linked together we can run the test cases.

### 7.2.2 Test Cases for RETRVL

Two test cases were selected for RETRVL. They were selected in order to demonstrate the retrieval code without a significant amount of computation. Each test case requires approximately 35 seconds on the AFGL Cyber.

#### 7.2.2.1 Input Description

Appendix C contains the input files used for the two test cases. Test Case 1 is designed to test all of the primary RETRVL options excluding IFASC3. The first record contains a header which will be written to RADDIFO. The next record selects the calculation of the reference case, T11SEQ, the derivatives in brightness temperature, the simulated radiances, the differences in brightness temperature, a retrieval, and the creation of T5ITR containing the TAPE5 for the next iteration. The next record contains the constituents to be retrieved, the beginning and ending layers, and the perturbation which is to be applied. For the first constituent, layer temperature will be perturbed for layers 1-3 by 0.5 degrees. For the second constituent, surface temperature will be perturbed by 0.5 degrees. The next

Table 7-1. Segmentation directives for path characterization model

```
DRIVER   TREE      RETRVL-(FSCD3,ATMOD,RADBT,DERIV,INVERT,ATMDT5)
RETRVL   GLOBAL    MAIN,LAMCHN,CONSTS,IFIL,BNDPRP,FILHDR,MSACCT,TIMIN,
,IFILAT,CHDATA,CONTRL,VSTOR
RETRVL   INCLUDE   RETRVL,BUFIN,BUFOUT,COPYFL,ENDFIL,T5COPY,FSCFIL
*
ATMOD    INCLUDE   ATMOD,OPNFLA,ZCNST
*
RADBT    INCLUDE   RADBT,OPNFLB,BT
*
DERIV    INCLUDE   DERIV,OPNFLD,RHEAD
*
INVERT   INCLUDE   INVERT,OPNFIL,MATINV,MULTIP,OUTCOR,OUTMAT,
,VECXMT,VECYMT,VREAD,VWRITE,ADNOIS,DPLNCK,GGNQF,MDNRIS,MERFI,
,UERTST,UGETIO,USPKD,EBALAF,EBBCKF,EHBCKF,EHESSF,EHOBKS,EHOUSS,
,EIGRF,EIGRS,EQRH3F,EORT2S,LEQT1F,LEQT2F,LGINF,LGING,LINV1F,
,LINV1P,LINV2F,LINV2P,LSVDB,LSVG1,LSVG2,LUDATF,LUDATN,LUDECP,
,LUELMF,LUELMN,LUELMP,LUREFF,LUREFN,LUREFP,UERSET,VHS12
*
ATMDT5   INCLUDE   ATMDT5,OPNFLT
*
FSCD3    TREE      FASCD3-(LAYRS,LASER,SCANFN,INTRPL,PLOTT,
,FLTRFN,TESTMM,PRLNHD)
FASCD3   GLOBAL    LASIV,ADRIVE,MSCONS,LINHDR
FASCD3   INCLUDE   FASCD3
*
PRLNHD   INCLUDE PRLNHD
*
LAYRS    TREE      XLAYER-(OPPATHS,OPDPTHS,XMERGES,XMERGIS,
,XLAYMSS)
XLAYER   GLOBAL    XMMS,ABSORA,SCATTA,ASYMMA,RMRG
XLAYER   INCLUDE   XLAYER,XLAYMS,SCANRD,SCNINT,SCNMRG,
,FLTRRD,FLTMRG,FLTPRT

OPPATHS  TREE      OPPATH-(FSCATMA,LOWT,PATH)
OPPATH   GLOBAL    CNTRL,PATHD,ZOUTP-SAVE
OPPATH   INCLUDE   OPPATH
*
FSCATMA  TREE      FSCATM-(FSCGEO,MDLATM)
FSCATM   INCLUDE   FSCATM,ATMPTH,ATMCON,PACK,WATVAP
FSCATM   GLOBAL    CONSTN,HMOLS,PARMTR,DEAMT,BNDRY-SAVE
FSCGEO   INCLUDE   RFPATH,ALAYER,AUTLAY,EXPINT,FINDSH,SCALHT,ANDEX,
,RADREF,HALFWD,FSCGEO,FDBETA,FNDHMN,REDUCE,AMERGE
MDLATM   INCLUDE   MDLATM,NSMDL,MLATMB,CONVRT,RDUNIT,DEFALT
MDLATM   GLOBAL    MLATM,TRAC-SAVE
*
LOWT     TREE      LOWTRN-(GEO,TRANS,AERNS,VSA,CIRRUS,NEWMDL)
LOWTRN   INCLUDE   TITLE
LOWTRN   GLOBAL    LCRD1,LCRD2,LCRD2D,LCRD3,LCRD4,MODEL,CNSTNS,
,MDLZ,ZVSALY,MART,USRDTA,TITL,RAIN-SAVE
GEO      INCLUDE   GEO,GEOINL,REDUCL,EXPINT,RADREF,SCALHT,ANDEX,
,RFPATL,FDBETL,FNDHML,FINDSL,FILL,LOLAYR
GEO      GLOBAL    PARMLT,RFRPTH-SAVE
TRANS    INCLUDE   TRANS,AEREXT,TNRAIN,DEBYE,DOP,INDX,AB,
,GAMFOG,AITK,GMRAIN,EXABIN,EXTDTA,GAMFOG,
,AITK,GMRAIN
TRANS    GLOBAL    EXTD
AERNS    TREE      AERNSM
AERNSM   INCLUDE   AERNSM,AERPRF,PRFDTA,MARINE,MARDTA,STDMDL,MDTA
AERNSM   GLOBAL    MDATA-SAVE
*
PATH     INCLUDE   PATH
*
XMERGES  TREE      XMERGE-(SABINIT,ABSMRG,SEMINIT,RADMRG)
XMERGE   GLOBAL    XME
XMERGE   INCLUDE   RADFN,XMERGE,GETEXT,ADARSL,AERF
*
XMERGIS  TREE      XMERGI-(TABINIT,ABSINT,TEMINIT,RADINT)
XMERGI   GLOBAL    XMI
XMERGI   INCLUDE   RADFN,XMERGI,GETEXT,ADARSL,AERF
*
SEMINIT  INCLUDE   EMINIT,EMIN,EMOUT,BBFN,AERF
*
TEMINIT  INCLUDE   EMINIT,EMIN,EMOUT,BBFN,AERF
*
SABINIT  INCLUDE   ABINIT,ABSOUT
*
TABINIT  INCLUDE   ABINIT,ABSOUT
*
OPDPTHS  TREE      OPDPTH-(HIRAC1,LINF4,CONTNM,NLTE)
OPDPTH   GLOBAL    LBLF,ABSORB,SCATTR
*
HIRAC1   INCLUDE   HIRAC1,SHAPEL,SHAPEG,VOICON,RDLIN,CNVFNV,PANEL,MOLEC
,QV,ABSOUT,VERFN,R1PRNT,XINT,BMOLEC,BHIRAC,BSHAPL,YDIH1,
,LBLF4,RDLIN4,CONVF4
HIRAC1   GLOBAL    FNSH-SAVE
*
LINF4    INCLUDE   LINF4,RDLNFL,MOLEC,QV,SHRINK,VOICON,BMOLEC
*
CONTNM   TREE      CONTNM-(SL296,SL260,FRN296,FRNCO2,
,N2CONT,XO3CHP,O3HHTO,O3HHT1,O3HHT2,O3HHUV,O2CONT)
CONTNM   INCLUDE   CONTNM,XINT
XO3CHP   INCLUDE   XO3CHP,O3CH
O3HHTO   INCLUDE   O3HHTO,BO3HHO
O3HHT1   INCLUDE   O3HHT1,BO3HH1
O3HHT2   INCLUDE   O3HHT2,BO3HH2
O3HHUV   INCLUDE   O3HHUV,BO3HUV
O2CONT   INCLUDE   O2CONT,BO2C
SL296    INCLUDE   SL296,BS296
SL260    INCLUDE   SL260,BS260
FRN296   INCLUDE   FRN296,BFH2O
FRNCO2   INCLUDE   FRNCO2,BFCO2
N2CONT   INCLUDE   N2CONT,BN2
*
NLTE     TREE      NONLTE-(HIRACQ,VIBTMP,VIBPOP)
NONLTE   GLOBAL    VBNLTE
HIRACQ   INCLUDE   HIRACQ,SHAPEL,SHAPEG,VOICON,RDLIN,CNVFNQ,PANELQ,
,MOLEC,QV,ABSOUT,VERFN,R1PRNT,XINT,BMOLEC,BHIRAQ,BSHAPL,YDIH1,
,LBLF4,RDLIN4,CONVF4
HIRACQ   GLOBAL    FNSQ-SAVE
*
ABSMRG   INCLUDE   ABSMRG,ABSOUT
ABSINT   INCLUDE   ABSINT,ABSOUT
*
RADMRG   INCLUDE   RADMRG,EMIN,EMOUT,BBFN,AERF,EMBND
*
RADINT   INCLUDE   RADINT,EMIN,EMOUT,BBFN,AERF,EMBND
*
SCANFN   INCLUDE   SCANFN,SHAPEG,RDSCAN,SHRKSC,SHAPET,CONVSC,PANLSC,
,CNVREC,SINCSQ
*
INTRPL   INCLUDE   INTRPL,RDPANL,INTERP,OTPANL
*
FLTRFN   INCLUDE   FLTRFN,RDSCAN,CNVFLT
*
TESTMM   INCLUDE   TESTMM,BTEST
*
PLOTT    TREE      PLTFAS-(BBSCLE,HEADER,AXEST,FPLINE)
PLTFAS   GLOBAL    PLTHDR,AXISXY,YCOM,POINTS,TITLOC,NAME
PLTFAS   INCLUDE   PLTFAS,LINT,EXPT,XNTLOG,TEMPFN,TENLOG,MNMX,FSCLIN,
,ENDPLT
*
AXEST    TREF      AXES-(AXISL,AXLOG,AX2)
*
XLAYMSS  TREE      XMRGMS-(EMITMS,RMRGMS,FLUXLP,FLUXES,YLAYMS)
XMRGMS   INCLUDE   XMRGMS,RADFN,GETEXT,ADARSL,AERF,MSCOPY
XMRGMS   GLOBAL    MLTSCT,OLDMS,MSFLUX
*
EMITMS   INCLUDE   EMITMS,EMINMS,EMOUT,MSIN,MSOUT,BBFN,AERF,FLXADD,E3,
,EMMSFN
*
RMRGMS   INCLUDE   RMRGMS,EMINMS,EMOUT,MSIN,MSOUT,BBFN,AERF,FLXADD,E3,
,EMMSFN
*
FLUXES   TREE      FLXDWN-(SRCFCN)
FLXDWN   INCLUDE   FLXDWN,RADFN,GETEXT,FLXADD,MSIN,MSOUT,E3,AERF,
,BBFN,EMMSFN
*
SRCFCN   INCLUDE   SRCFCN,BETABS,MSEMIS
*
YLAYMS   INCLUDE   YLAYMS,GETEXT,RADFN,FLUXLP,MSIN,MSOUT,EMINMS,EMOUT,
,FLXADD,BBFN,AERF,E3,EMMSFN
*
FLUXLP   INCLUDE FLUXLP,FLXADD,MSIN,MSOUT,BBFN,AERF,EMINMS,E3,EMMSFN
*
         END
```

record indicates that the parameter input is concluded. The next record contains the number of layer boundaries to be read in, and for this case, we choose zero. The next record contains the header which is used by INVERT. This is followed by a record containing the main control cards for INVERT. For this case we are using 1 file, this is the initial run so NREF = 0, there are 4 parameters (3 layer temperature, 1 surface temperature), no eigenvalues nor eigenvectors are calculates, NPRT = 12 for the print output, IREFD is set to zero to use the reference data from the derivative file header and NSIM = 1 since simulation data is available on PARAMIN. The next record contains the variables of IOUT which selects the parameters and their order. For this case we have selected the parameters in order of altitude, with the highest at the top, and the surface at the bottom. The next two records control some of the I/O from INVERT. We have selected a sample print from each of the matrices and vectors, and will use ridge regression for the retrieval. The next record contains the damping factor and the weight and noise control flags. For this case, the damping is 0.0, and no additional weights or noise is desired.

Test Case 2 is basically the same as case 1 except that we want to make 2 layers out of the three layers on T5REF. This requires a change to Record 3.2 and the layer temperatures become parameters 1 and 2, and the surface temperature becomes parameter 3. In order to facilitate combining the three layers into two, we set NZFLG = 3 so that we can read in three layer boundaries to produce two layers. The next record contains the layer boundaries. Note, that the boundaries that are chosen consist of a subset of the layer boundaries that are on T5REF. The only additional change that is required is to set NPAR = 3 on Record 4.2 for the inversion.

Both Test Cases also require a TAPE3 (FASCOD3 Line File), T5REF which contains a FASCOD3 TAPE5 which doesn't use the atmosphere, and T5SIM which contains the TAPE5 which will be used for the simulated radiances. A note should be made concerning the T5REF file. It is a standard FASCOD3 input file with IATM = 0. We have added a parameter ITYL to Record 1.5.1 to ensure that the sampling interval, DV, is the same for every layer as the temperature parameter is perturbed in the calculation of the derivatives using discrete differences. This has been found necessary to decrease the effects of discretization effects in the FASCODE calculation.

7.2.2.2 Output Description

The output files for the Test Cases are found in Appendix D. The output file which will be described is the file RETVOUT which is the result of the INVERT module. The first page consists of the banner containing the header and the date and time entering INVERT, followed by a print out of the K matrix which shows a panel of the first and last five points for each parameter. The user should note that the K matrix parameters are also ordered by IOUT. Page 2 shows the H matrix, which is followed on page 3 by the correlation H matrix. The bottom of page 3 also has a print from the IMSL inversion routine which shows a value of IER = 0, implying the inversion was accomplished with no errors. Page 4 shows a print out of the inverted H matrix. Page 5 shows the correlation H inverse matrix, and page 6 shows the result of H matrix times H inverse matrix. Page 7 shows the results of the inversion. The first block shows the layer and the constituent retrieved, followed by the value for each constituent before the retrieval. For this case, since NREF = 0, we see the reference case values. This is followed by the change which will be applied to the reference case in order to produce the retrieved quantities which are printed in the following column. The user should note that the retrieval is trying to place a 0.5 degree pulse in layer 2, which is precisely what was done to generate the simulation. The next column shows the probable error for the retrieved parameter. The next column contains the percent change between the retrieved parameter and the reference value. The following columns provide the individual damping factor which was used, and the fit index for the parameter. The next panel shows a printout of the Y vector, which is followed by a panel containing the residuals: (RD-R0), (R1-R0) and (RD-R1). The final panel on page 7 contains the statistics generated in order to evaluate the retrieval. Page 8 shows the comparison of the retrieved parameter with the original simulated values. The last column shows the simulated minus the retrieved, which indicates a good retrieval. The final two panels on page 8 show the spectral region which was used, and the time required by INVERT.

The output from Test Case 2 is basically the same as for Test Case 1 except we have chosen one less layer for the parameters. If we look at the results on page 7, we again see that the retrieval is trying to place a 0.5 degree pulse on layer 1. This is consistent with the simulation which placed

a 0.5 degree pulse on layers 1 and 2 of the reference case which were combined to form the retrieved layer 1.

## 7.3 Description of Program

Program RETRVL is the driver for the retrieval package. A block diagram of the program is shown in Figures 7-1 and 7-2. A discussion of each routine follows:

Subroutine ADNOIS adds random noise to the K matrix as per instructions from the input file. ADNOIS is called from MATINV.

Subroutine ATMDT5 processes the results from the inversion run to produce a new 'TAPE5' for use by FASCODE. The results are inputed from PARAMOT and written to the file 'T5ITR'. ATMDT5 is called from RETRVL.

Subroutine ATMOD is used within the derivative loop to modify 'TAPE5' to reflect the constituent for which a derivative is being calculated. ATMOD reads from T5REF and changes the desired constituent producing a new TAPE5. ATMOD is called from RETRVL.

Function BT calculates the brightness temperature corresponding to the inputed radiance and frequency. BT is called from RADBT.

Subroutine DERIV calculates the derivative for the given constituent based upon the adjustment which was applied. DERIV is called from RETRVL.

Subroutine DPLNCK computes the inverse planck function, calculating the radiance which corresponds to the inputed temperature and frequency. DPLNCK is called from RETRVL.

Subroutine EIGRS is the IMSL driver for the calculation of eigenvalues and eigenvectors of a real symmetric matrix. EIGRS is called from MATINV.

Subroutine FASCD3 is the subroutine driver for FASCOD3. FASCD3 is called from RETRVL.

Subroutine FSCDIF differences two unformatted FASCODE files producing a formatted result. FSCDIF is called from RETRVL.

Subroutine FSCFIL checks to see if a particular unit is open, and closes any units which are open. FSCFIL is called from RETRVL.

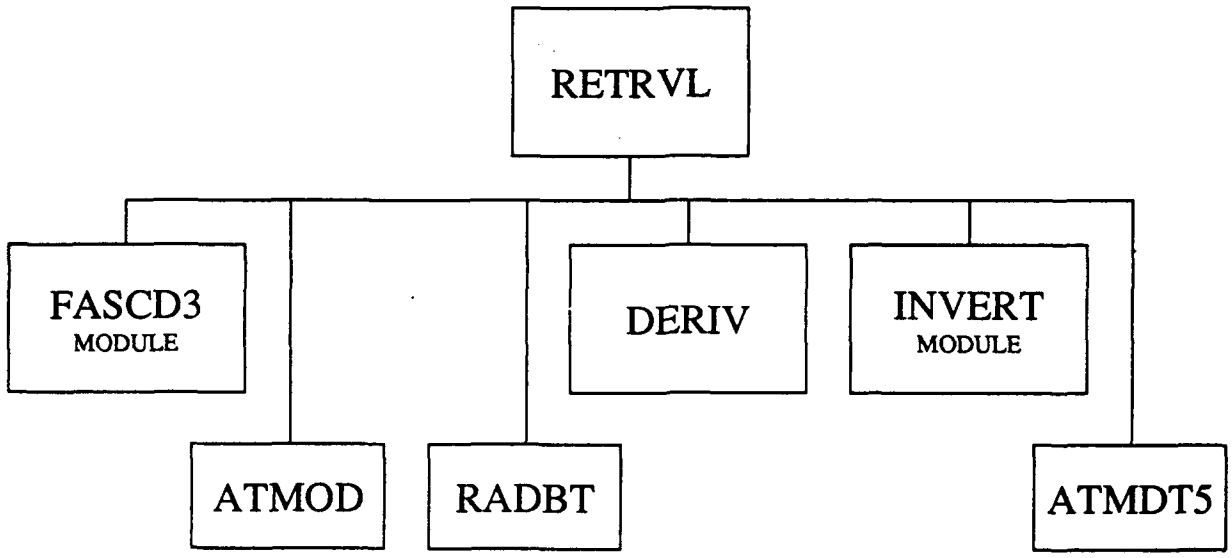


Figure 7-1. Program Retrvl

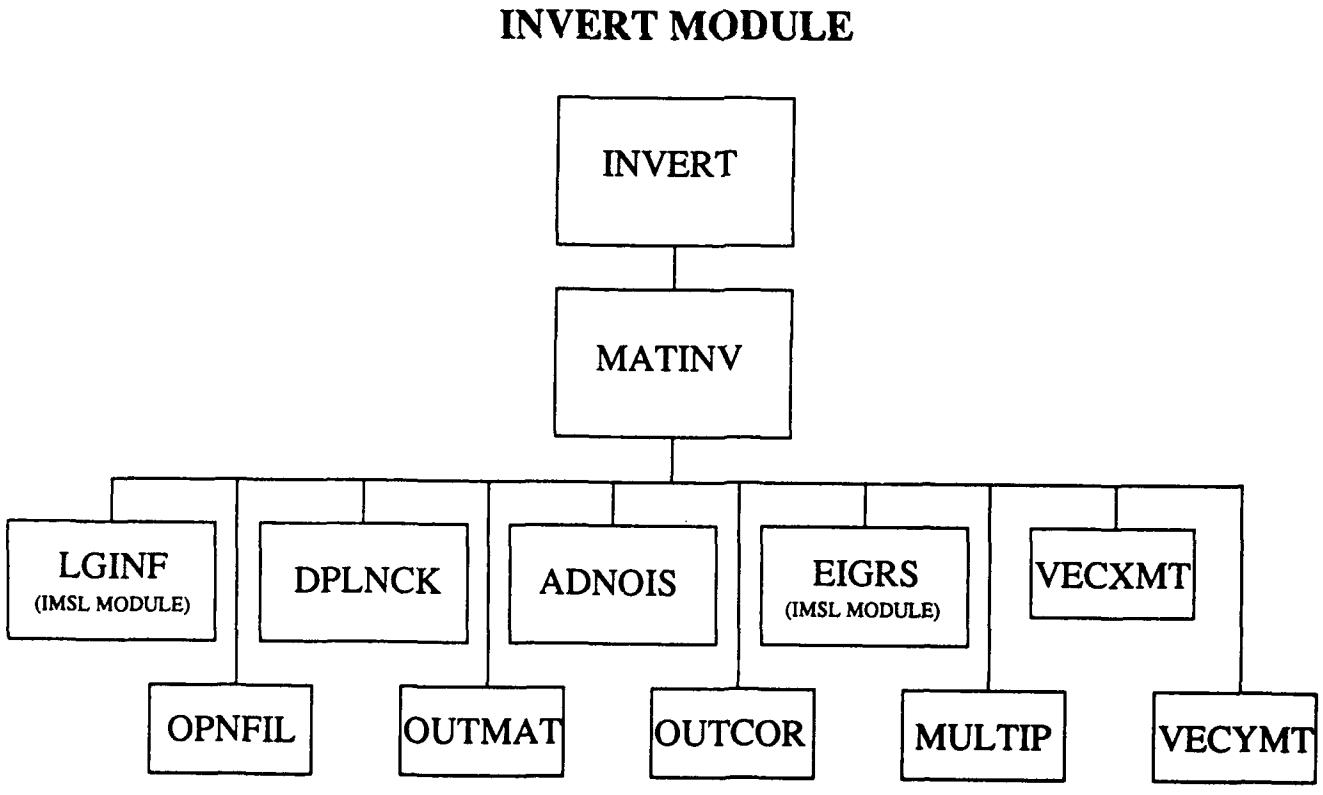


Figure 7-2. Invert Module

Function GGNQF is an IMSL routine which provides gaussian random numbers. GGNQF is used by ADNOIS.

Subroutine INVERT is the driver for the matrix inversion and retrieval subroutine MATINV. INVERT is called from RETRVL.

Subroutine LGINF is the IMSL driver for the calculation of the generalized inverse of a real matrix. LGINF is called from MATINV.

Subroutine MATINV is the driver for the matrix inversion and calculates the retrieved parameters. MATINV is called from INVERT.

Subroutine MULTIP performs a matrix multiplication. MULTIP is called from MATINV.

Subroutine OPNFIL opens all the files used by INVERT and its subroutines. OPNFIL is called from INVERT and MATINV.

Subroutine OPNFLA opens all the files used by ATMOD and its subroutines. OPNFLA is called from ATMOD.

Subroutine OPNFLB opens all the files used by RADBT and its subroutines. OPNFLB is called from RADBT.

Subroutine OPNFLD opens all the files used by DERIV and its subroutines. OPNFLD is called from DERIV.

Subroutine OPNFLF opens all the files used by FSCDIF and its subroutines. OPNFLF is called from FSCDIF.

Subroutine OPNFLT opens all the files used by ATMDT5. OPNFLT is called from ATMDT5.

Subroutine OUTCOR prints a correlation matrix to a file. OUTCOR is called from MATINV.

Subroutine OUTMAT prints a matrix to a file. OUTMAT is called from MATINV.

Subroutine RADBT converts an unformatted FASCODE file from radiance to brightness temperature. RADBT is called from RETRVL.

Program RETRVL is the main driver for the path characterization subroutine package.

Subroutine RHEAD reads the FASCODE file header to extract the necessary retrieval parameters. RHEAD is called from DERIV.

Subroutine T5COPY copies one formatted file to another. T5COPY is called from RETRVL.

Subroutine VECXMT multiples a vector times a matrix and returns the resulting vector. VECXMT is called from MATINV.

Subroutine VECYMT multiples a vector times K transpose matrix and returns the resulting vector. VECYMT is called from MATINV.

Subroutine VREAD reads in a vector of the K matrix from the file KMATRIX. VREAD is called from MATINV, OUTMAT, VECXMT and VECYMT.

Subroutine VWRITE writes out a vector of the K matrix to the file KMATRIX. VWRITE is called from MATINV.

Subroutine ZCNST determines the constituent to be modified, and the layers to which the modification will be applied for the calculation of derivatives. ZCNST is called from ATMOD.

# 8. CONCLUSIONS

## 8.1 Program Summary

This report has described the results of study undertaken at AER to identify and implement a state-of-the-art nonlinear retrieval approach to characterize line of sight variability of atmospheric thermal and constituent environments. This path characterization capability was designed to interface with the existing Geophysics Laboratory (GL) line-by-line radiance/transmittance code, FASCODE.

Accomplishments of the study include: (a) a review of the relevant literature concerning potential path characterization retrieval algorithms, selection of a physical least squares (PLS) nonlinear retrieval approach for implementation based on criteria including flexibility within the context of FASCODE and a certain degree of robustness in application; (b) development of a stand alone, preprocessing screening procedure to identify potential channels for path characterization based on user requirements; (c) formulation and implementation of the path characterization retrieval algorithm including

suitable interfaces with FASCODE; (d) inclusion of a comprehensive error analysis capability as an integral part of the retrieval procedure; (e) demonstration of the approach for the retrieval of temperature, water vapor and ozone; and (f) comprehensive documentation of the path characterization code implementations.

We believe that the path characterization capability developed in this study represents a significant enhancement to the existing FASCODE capabilities for applications to sensor design and analysis of experimental data sets consistent with current state-of-the-art retrieval theory.

## 8.2 Recommendations

In the course of our research we have identified a number of issues related to the implementation of the path characterization retrieval which require further elucidation. While we feel that the approach as implemented is quite useful, we recommend that these additional aspects of the method require further study.

The effects of nonlinearities in the parameter-data relationship has not been fully explored. To some degree our discussion of the role of the penalty function in Section 4.3. and the work with compositional retrievals of water vapor and ozone described in Section 6 have addressed this issue. However, it would be misleading to assert that all aspects of the impact of nonlinearities have been investigated. A viable advanced approach to treating the non-linear problem is available from optimization theory and could be implemented at a later date.

The mathematical formalism which we have adopted for the retrieval calculation is based on exploitation of the FASCODE layering capability. It is straightforward to implement the approach to retrieve profile properties rather than layer properties. An advantage is the ability to perturb profile rather than layer quantities in the evaluation of the required derivatives consistent with the updated radiance algorithm in FASCODE.

With respect to the evaluation of the derivatives, the retrieval is sensitive to systemmatic noise. This manifests itself in a number of ways, one being the numerical noise introduced in calculating derivatives. FASCODE is a numerical model. While forward problem discretization errors are small

with respect to radiance output, they may not be negligible with respect to the performance of the retrieval algorithm..

The potential importance of physical constraints on the retrieval procedure has also been discussed (Section 4.1). Although our test cases have not required invoking such constraints it is possible that they may be required in some problems.

While we have attempted to be as complete as possible in the implementation of the path characterization approach, we have put our testing and evaluation effort described here into the investigation of nadir retrieval. We believe the approach should be applicable to more general paths. These include downward looking paths at arbitrary viewing angles, upward looking paths, and limb paths. In the latter case a straightforward application of the PLS approach should be possible via an onion peeling method; however, we have not tested this hypothesis.

The use of the line-by-line algorithm as a forward problem model results in the use of considerable computational effort both in the iterations required and the generation of the K matrix coefficients (see Sections 4.1 and 4.2). It has been remarked that the use of rapid algorithms is one solution to this problem, and indeed plans for operational applications of physical retrievals resort to this approach. Although we have not included a rapid algorithm generation capability as part of the path characterization code, this is a relatively simple matter which can be accomplished using one of the approaches which has been cited in Section 2.1.3. The computational effort required to generate the band model coefficient for the selected channel set is considerably less than that required for any reasonable sensor design scenario, even in light of the necessity to generate the coefficients for new channels.

Sensitivity to systemmatic errors in the forward problem is also an issue with respect to use of so called "rapid" algorithms. While these may be the only practical means to treat low resolution channels (say on the order of a few wavenumbers in the middle infrared), they must be accurate enough to provide the required derivative functions. This is easily determined by assessing the accuracy of the rapid algorithm.

The last issue is application of the approach to path parameters other than temperature and composition. Conceptually, any variable which enters into the forward problem can be treated within the general framework of this approach. Such additional parameters include cloud and aerosol properties, properties of the surface such as surface reflectivity and emissivity, and non-local thermodynamic equilibrium (NLTE) properties in the upper atmosphere. A recently completed feasibility study (Isaacs et al., 1990) has addressed these applications; however, further work is needed.

## 9. REFERENCES


Backus, G.E., and J.F. Gilbert, 1967: Numerical applications of a formalism for geophysical inverse problems. Geophys. J. R. Astron. Soc., 13, 247-276.

Backus, G.E., and J.F. Gilbert, 1968: The resolving power of gross earth data. Geophys. J. R. Astron. Soc., 16, 169-205.

Backus, G.E., and J.F. Gilbert, 1970: Uniqueness in the inversion of inaccurate gross earth data. Phil. Trans. R. Soc. London, A266, 123-192.

Burch, D.A., and D.A. Gryvnak, 1980: Continuum absorption by $H_2O$ vapor in the infrared and millimeter regimes. In Atmospheric Water Vapor, edited by A. Deepak, T.D. Wilkenson, and L.H. Ruhnke, Academic Press, New York, pp. 47-76.

Chahine, M.T., 1968: Determination of the temperature profile in an atmosphere from its outgoing radiance. J. Opt. Soc. Am., 58, 1634-1637.

Chahine, M.T., 1972: A general relaxation method for inverse solution of the full radiative transfer equation. J. Atmos. Sci., 29, 741-747.

Chandrasekhar, S., 1960: Radiative Transfer. Dover, New York, 393 pp.

Clough, S.A., F.X. Kneizys, R. Davies, R. Gamache, and R. Tipping, 1980: Theoretical line shape for $H_2O$ vapor: Application to the continuum. In Atmospheric Water Vapor, edited by A. Deepak, T.D. Wilkenson, and L.H. Ruhnke, Academic Press, New York, pp. 25-46, 1980.

Clough, S.A., F.X. Kneizys, L.S. Rothman, and W.O. Gallery, 1981: Atmospheric spectral transmittance and radiance - FASCOD1Y. Atmospheric Transmission, Proc. SPIE, 277, 152 pp.

Clough, S.A., R.X. Kneizys, E.P. Shettle, and G.P. Anderson, 1986: Atmospheric Radiance and Transmittance: FASCOD2, Proceedings of the Sixth Conference on Atmospheric Radiance, Williamsburg, VA.

Clough, S.A., F.X. Kneizys, and R.W. Davies, 1989: Line Shape and the Water Vapor Continuum. Atmos. Res., 23, 229-241.

Clough, S.A., R.D. Worsham, W.L. Smith, H.E. Revercomb, R.O. Knuteson, G.P. Anderson, M.L. Hoke, and F.X. Kneizys, 1989: Validation of FASCODE Calculations with HIS Spectral Radiance Measurements. IRS '88. A. Deepak Publishing.

Conrath, B.J., 1972: Vertical resolution of temperature profiles obtained from remote radiation measurements. J. Atmos. Sci., 29, 1262-1272.

Deirmendjian, D., 1969: Electromagnetic Scattering on Spherical Polydispersion. Elsevier, New York.

Deirmendjian, D., 1975: Far-infrared and submillimeter wave attenuation by clouds and rain. J. Appl. Meteorol., 14, 1584-1593.

Dennis, J.E., Jr., and R.B. Schnabel, 1983: Numerical Methods for Unconstrained Optimization and Nonlinear Equations. Printice-Hall, Inc., Englewood Cliffs, NJ.

Eyre, J.R., 1989: Inversion of cloudy satellite sounding radiances by nonlinear optimal estimation: Theory and simulation for TOVS. Qtrly. Journal of the Royal Met. Soc., 115, 1001-1026.

Eyre, J.R. and H.M. Woolf, 1989: Transmittance of atmospheric gases in the microwave region: a fast model. Appl. Opt., 27, 15, 3244-3249.

Falcone, V.J., L.W. Abreu, and E.P. Shettle, 1979: Atmospheric attenuation of millimeter and submillimeter waves: Models and computer code. AFGL-TR-79-0253. ADA084485.

Fleming, H.E., and L.M. McMillin, 1977: Atmospheric transmittance of an absorbing gas 2: A computationally fast and accurate transmittance model for slant paths at different zenith angles. Appl. Opt., 16, 1366-1370.

Fraser, R.S., and R.J. Curran, 1976: Effects of the atmosphere on remote sensing, in Remote Sensing of Environment, edited by J. Lintz, Jr., and D.S. Simonett, Addison-Wesley, Reading, MA, pp. 34-84.

Fymat, A.L., and V.E. Zuev (Eds.), 1978: Remote Sensing of the Atmosphere: Inversion Methods and Applications. Elsevier, New York.

Gaut, N.E., M.G. Fowler, R.G. Isaacs, D.T. Chang, and E.C. Reifenstein, III, 1975: Studies of microwave remote sensing of atmospheric parameters. AFCRL-75-0007, Air Force Cambridge Research Laboratory. [NTIS ADA008042].

Goody, R.M., 1964: Atmospheric radiation. Oxford University Press, New York, 426 pp.

Hoke, M.L., S.A. Clough, W.J. Lafferty, and B.W. Olson, 1988: Line Coupling in Oxygen and Carbon Dioxide, IRS '88, A. Deepak Publishing.

Houghton, J.T., F.W. Taylor, and C.D. Rodgers, 1984: Remote Sensing of Atmospheres. Cambridge University Press.

Isaacs, R.G., 1988: Retrieval techniques for atmospheric path characterization. SPIE, 928, Modeling of the Atmosphere, 136-164.

Isaacs, R.G., 1989: A Unified Retrieval Methodology for the DMSP Meteorological Sensors. In Advances in Remote Sensing Retrieval Methods, A. Deepak, (ed.), pp. 203-214.

Isaacs, R.G. and G. Deblonde, 1987: Millimeter wave moisture sounding: the effect of clouds. Radio Science, 22, 3, 367-377.

Isaacs, R.G., R.N. Hoffman, and L.D. Kaplan, 1986: Satellite remote sensing of meteorological parameters for global numerical weather prediction. Rev. Geophys. Space Phys., 24, 701-743.

Isaacs, R.G., M. Livshits, and R.D. Worsham, 1988: Scattering properties of precipitation for the AFGL RADTRAN model. Appl. Opt., 27, 1, 14-16.

Isaacs, R.G., S.A. Clough, J.L. Moncet, and R.D. Worsham, 1990: Development of a Remote Sensing Algorithm for Non Thermodynamic Path Variables from Remote Sensing Data. GL-TR-89-0300 . Hanscom AFB, MA.

Kaplan, L.D., 1959: Inference of atmospheric structure from remote radiation measurements. J. Opt. Soc. Am., 49, 1004-1007.

Kaplan, L.D., M.T. Chahine, J. Susskind, and J.E. Searl, 1977: Spectral band passes for a high precision satellite sounder. Applied Optics, 16, 322-325.

Kaplan, L.D., R.G. Isaacs, and R.D. Worsham, 1986: A physical retrieval algorithm for obtaining improved remotely sensed humidity profiles. In Advances in Remote Sensing Retrieval Methods. A. Deepak, H.E. Fleming, and M.T. Chahine (eds.), pp. 269-284.

Kneizys, F.X., E.P. Shettle, W.O. Gallery, J.H. Chetwynd, Jr., L.W. Abreau, J.E.A. Selby, R.W. Fenn, and R.A. McClatchey, Atmospheric transmittance/radiance: Computer code LOWTRAN5, AFGL-TR-80-0067, 233 pp., 1980. [NTIS AD A088215]

Lenoble, J. (ed.), 1985: Radiative Transfer in Scattering and Absorbing Atmospheres: Standard Computational Procedures. A. Deepak Publishing, 300 pp.

Lenoble, J. and J.-F. Geleyn, 1989: IRS'88: Current Problems in Atmospheric Radiation, Proceedings of the International Radiation Symposium, Lille, France, 18-24 August 1988, A. Deepak Publishing, Hampton, VA.

Levenberg, K., 1944: A method for the solution of certain problems in least squares, Quart. Appl. Math, 2, pp. 164-168.

Liebe, H.J., 1980: Atmospheric water vapor: A nemesis for millimeter wave propagation. In Atmospheric Water Vapor, edited by A. Deepak, T.D. Wilkenson, and L.H. Ruhnke, Academic Press, New York, pp. 143-202.

Marquardt, D., 1963: An algorithm for least-squares estimation of nonlinear parameters, SIAM J. Appl. Math., 11, pp. 431-441.

McMillan, L.M., 1989: Evaluation of a classification retrieval method. National Oceanic and Atmospheric Administration, National Environmental Satellite, Data, and Information Service, Satellite Research Laboraytory, Washington, D.C., 20233.

McMillin, L.M., and H.E. Fleming, 1976: Atmospheric transmittance of an absorbing gas: A computationally fast and accurate transmittance model for absorbing gases with constant mixing ratios in inhomogeneous atmospheres. Appl. Opt., 15, 358-363.

McMillin, L.M., H.E. Fleming, and M.L. Hill, 1979: Atmospheric transmittance of an absorbing gas 3: A computationally fast and accurate transmittance model for absorbing gases with variable mixing ratios. Appl. Opt., 18, 1600-1606.

Murcray, F.H., F.J. Murcray, D.G. Murcray, J. Pritchard, G. Vanasse, and H. Sakai, 1984: Liquid nitrogen-cooled Fourier transform spectrometer system for measuring atmospheric emission at high altitudes. J. Atmos. Ocean. Technology, 1, 351-357.

Murcray, D.G., F.H. Murcray, F.J. Murcray, and G. Vanasse, 1985: Measurements of atmospheric emission at high spectral resolution. J. Meteorol. Soc. Japan, 63, 320-324.

Park, J.H., L.S. Rothman, C.P. Rinsland, M.A.H. Smith, D.J. Richardson, 2nd, J.C. Larsen, 1981: Atlas of absorption from 0 to 17,900 $cm^{-1}$. NASA.

Peckham, G.E., and D.A. Flower, 1983: The design of optimum remote-sensing instruments. Int. J. Remote Sensing, 4, 457-463.

Pederson, F., 1942: Meteor. Ann., 1, 115.

Phillips, D.L., 1962: A technique for the numerical solution of certain integral equations of the first kind. J. Assoc. Comput. Mach., 9, 84-97.

Poynter, R.L., and H.M. Pickett, 1980: Submillimeter, millimeter, and microwave spectral line catalogue, JPL Publication 80-23.

Poynter, R.L., and H.M. Pickett, 1984: Submillimeter, millimeter, and microwave spectral line catalogue, JPL Publication 80-23, Revision 2, 171 pp. Jet Propulsion Laboratory, California Institute of Technology, Pasadena, CA.

Ridgway, W.L., R.A. Moose, and A.C. Cogley, 1982: Single and multiple scattered solar radiation, AFGL-TR-82-0299, 196 pp. [NTIS AD A126323]

Rinsland, C.P., R. Zander, J.S. Namkung, C.B. Farmer, and R.H. Norton, 1989: Stratospheric Infrared Continuum Absorptions Observed by the Atmos Instrument. J. Geo. Res., 94, 16303-16322.

Rodgers, C.D., 1971: Some theoretical aspects of remote sounding in the Earth's atmosphere. J. Quant. Spectrosc. Radiat. Transfer, 11, 767-777.

Rodgers, C.D., 1976: Retrieval of atmospheric temperature and composition from remote measurements of thermal radiation. Rev. Geophys. Space Phys., 14, 609-624.

Rodgers, C.D., 1990: Characterization and Error Analysis of Profiles Retrieved from Remote Sounding Measurements. J. Geophys. Res., 95, D5, 5587-5595.

Rodgers, C.D. and C.D. Walshaw, 1966: The computation of infrared cooling rate in planetary atmospheres. Qtrly. J. of the Royal Met. Soc., 92, 67-92.

Rothman, L.S., R.R. Gamache, A. Barbe, A. Goldman, J.R. Gillis, L.R. Brown, R. A. Toth, J.-M. Flaud, and C. Camy-Peyret, 1983: AFGL atmospheric line parameters compilation. Appl. Opt., 22, 2247-2256.

Rothman, L.S., R.R. Gamache, A. Goldman, L.R. Brown, R.A. Toth, H.M. Pickett, J.-M. Flaud, C. Camy-Peyret, A. Barbe, N. Husson, C.P. Rinsland, and M.A.H. Smith, 1987: The HITRAN database: 1986 edition. Appl. Opt., 26, 19,4058-4097.

Savage, C.S., 1978: Radiative properties of hydrometeors at microwave frequencies. J. Appl. Meteorol., 17, 904-911.

Shettle, E.P., and R.W. Fenn, 1979: Models for the aerosols of the lower atmosphere and the effects of humidity variations on their optical properties. AFGL-TR-79-0214, 94 pp. [NTIS AD A085951]

Smith, W.L., 1970: Iterative solution of the radiative transfer equation for the temperature and absorbing gas profile of an atmosphere. Appl. Opt., 9, 1993-1999.

Smith, W.L., and H.M. Woolf, 1976: The use of eigenvectors of statistical covariance matrices for interpreting satellite sounding radiometer observations, J. Atmos. Sci., 33, 1127-1140.

Smith, W.L., H.M. Woolf, and W.J. Jacob, 1970: A regression method for obtaining real time temperature and geopotential height profiles from satellite spectrometer measurements and its application to NIMBUS 3 "SIRS" observations. Mon. Weather Rev., 98, 582-603.

Smith, W.L., H.E. Revercomb, H.B. Howell, and H.M. Woolf, 1983: HIS - A Satellite Instrument to Observe Temperature and Moisture Profiles with High Vertical Resolution, Proc. of the Sixth Conference on Atmospheric Radiation, AMS, Boston, MA.

Smith, W.L., H.M. Woolf, and A.J. Schreiner, 1985: Simultaneous retrieval of surface and atmospheric parameters. A physical and analytically-direct approach. In. A. Deepak, H.E. Fleming, and M.T. Chahine, eds., Advances in Remote Sensing Retrieval Methods, pp. 221-232. A. Deepak Publishing, Hampton, VA.

Smith, W.L., H.M. Woolf, and A.J. Schreiner, 1986: Simultaneous retrieval of surface and atmospheric parameters, a physical and analytically-direct approach. Advances in Remote Sensing Retrieval Methods. A. Deepak, Publishing, pp. 221-230.

Smith, W.L., H.M. Woolf, H.B. Howell, H.-L. Huang, and H.E. Revercomb, 1987: The simultaneous retrieval of atmospheric temperature and water vapor profiles - application to measurements with HIS. Proceedings, Workshop on Remote Sensing Retrieval Methods. A. Deepak Publishing (in press).

Strand, O.N., and E.R. Westwater, 1968: Statistical estimation of the numerical solution of a Fredholm integral equation of the first kind. J. Assoc. Comput. Mach., 15, 100-114.

Susskind, J., J. Rosenfield, D. Reuter, and M.T. Chahine, 1982: The GLAS Physical Inversion Method for Analysis of HIRS2/MSU Sounding Data. NASA-TM-84936, 101 pp.

Susskind, J., J. Rosenfield, and D. Reuter, 1983: An accurate radiative transfer model for use in the direct physical inversion of HIRS2 and MSU temperature sounding data. J. Geophys. Res., 88(C13), 8550-8568.

Susskind, J., J. Rosenfield, D. Reuter, and M.T. Chahine, 1984: Remote sensing of weather and climate parameters from the HIRS/MSU on TIROS-N. J. Geophys. Res., 89(D3), 4677-4697.

Thompson, O.E., 1982: HIRS-AMTS satellite soundings test - theoretical and empirical vertical resolving power. J. Appl. Meteorol., 21, 1550-1561.

Tikhonov, A.N., 1963: On the solution of incorrectly stated problems and a method of regularization. Dokl. Acad. Nauk. SSSR, 151.

Turchin, V.F., V.P. Kozlov, and M.S. Malkevich, 1971: The use of mathematical-statistics methods in the solution of incorrectly posed problems. Am. Inst. Phys., 13, 681-702.

Twomey, S., 1963: On the numerical solution of Fredholm integral equations of the first kind by the inversion of the linear system produced by quadrature. J. Assoc. Comput. Mach., 10, 97-101.

Twomey, S., 1977: Introduction to the Mathematics of Inversion in Remote Sensing and Indirect Measurements. Elsevier, New York.

Van de Hulst, H.C., 1957: Light Scattering by Small Particles. Wiley, New York.

Vodar, B., and H. Vu, 1963: Intensities absolves des transitions induites par la pression. J. Quant. Spectrosc. Radiat. Transfer., 3, 397-433.

Wark, D.Q., and H.E. Fleming, 1966: Indirect measurements of atmospheric temperature profiles from satellites: I, Introduction. Mon. Weather Rev., 94, 351-362.

Westwater, E.R., and O.N. Strand, 1968: Statistical information content of radiation measurements used in indirect sensing. J. Atmos. Sci., 25, 750.

Westwater, E.R., and O.N. Strand, 1972: Inversion techniques. In Remote Sensing of the Troposphere, edited by V.E. Derr, GPO, pp. 16-1-16-13.

Yamamoto, G., M. Tanaka, and S. Asano, 1971: Table of scattering function of infrared radiation from water clouds. NOAA-TR-NESS-57, 9 pp.

# APPENDIX A - SCREENING ALGORITHM OUTPUT

SCREENING ALGORITHM

YOU HAVE SELECTED THE FOLLOWING MOLECULES AS THOSE YOU WANT TO PROBE
 H2O

YOU HAVE SELECTED THE FOLLOWING MOLECULES AS CONSTITUTING THE BACKGROUND ATMOSPHERE
 H2O
 CO2
  O3
 N2O
  CO
 CH4
  O2
  NO
 SO2
 NO2
 NH3
HNO3
  OH
  HF
 HCL
 HBR
  HI
 CLO
 OCS
H2CO
HOCL
  N2
 HCN
CH3CL

H2O2
C2H2
C2H6
 PH3

/AVENUMBER INTERVAL IS   1201.000 TO   1950.000

CONTROL CARD 2.1: MODEL AND OPTIONS

| | | |
|---|---|---|
| MODEL | = | 6 |
| ITYPE | = | 2 |
| IBMAX | = | 0 |
| NOZERO | = | 0 |
| NOPRNT | = | 0 |
| NMOL | = | 0 |
| IPUNCH | = | 0 |
| RE | = | .000 KM |
| HSPACE | = | .000 KM |
| VBAR | = | .000 CM-1 |

CONTROL CARD 2.1 PARAMETERS WITH DEFAULTS:

| | | |
|---|---|---|
| MODEL | = | 6 |
| ITYPE | = | 2 |
| IBMAX | = | 0 |
| NOZERO | = | 0 |
| NOPRNT | = | 0 |
| NMOL | = | 7 |
| IPUNCH | = | 0 |
| RE | = | 6371.230 KM |
| HSPACE | = | 100.000 KM |
| VBAR | = | 1575.500 CM-1 |

SLANT PATH SELECTED, ITYPE = 2

CONTROL CARD 2.2: SLANT PATH PARAMETERS

| | | |
|---|---|---|
| H1 | = | 100.0000 KM |
| H2 | = | .0000 KM |
| ANGLE | = | 180.0000 DEG |
| RANGE | = | .0000 KM |
| BETA | = | .0000 DEG |
| LEN | = | 0 |

AUTOLAYERING SELECTED

| | | |
|---|---|---|
| AVTRAT | = | 2.00 |
| TDIFF1 | = | 8.00 |
| TDIFF2 | = | 12.00 |
| ALTD1 | = | .00 |
| ALTD2 | = | 100.00 |

ATMOSPHERIC PROFILE SELECTED IS: M = 6 U. S. STANDARD, 1976

| I | Z (KM) | P (MB) | T (K) | REFRACT INDEX-1 *1.ØE6 | DENSITY (MOLS CM-3) AIR | H2O | CO2 | O3 | N2O | CO | CH4 | O2 |
|---|---|---|---|---|---|---|---|---|---|---|---|---|
| 1 | .ØØØ | 1Ø13.ØØØØØ | 288.2Ø | 271.97 | 2.55E+19 | 1.97E+17 | 8.41E+15 | 6.78E+11 | 8.15E+12 | 3.82E+12 | 4.33E+13 | 5.33E+18 |
| 2 | 1.ØØØ | 898.8ØØØØ | 281.7Ø | 246.95 | 2.31E+19 | 1.4ØE+17 | 7.63E+15 | 6.78E+11 | 7.4ØE+12 | 3.35E+12 | 3.93E+13 | 4.83E+18 |
| 3 | 2.ØØØ | 795.ØØØØØ | 275.2Ø | 223.64 | 2.Ø9E+19 | 9.7ØE+16 | 6.91E+15 | 6.78E+11 | 6.7ØE+12 | 2.93E+12 | 3.56E+13 | 4.38E+18 |
| 4 | 3.ØØØ | 7Ø1.2ØØØØ | 268.7Ø | 2Ø2.Ø7 | 1.89E+19 | 6.Ø2E+16 | 6.24E+15 | 6.27E+11 | 6.Ø5E+12 | 2.55E+12 | 3.21E+13 | 3.95E+18 |
| 5 | 4.ØØØ | 616.6ØØØØ | 262.2Ø | 182.13 | 1.7ØE+19 | 3.68E+16 | 5.62E+15 | 5.77E+11 | 5.45E+12 | 2.24E+12 | 2.9ØE+13 | 3.56E+18 |
| 6 | 5.ØØØ | 54Ø.5ØØØØ | 255.7Ø | 163.73 | 1.53E+19 | 2.14E+16 | 5.Ø6E+15 | 5.77E+11 | 4.9ØE+12 | 2.ØØE+12 | 2.6ØE+13 | 3.2ØE+18 |
| 7 | 6.ØØØ | 472.2ØØØØ | 249.2Ø | 146.78 | 1.37E+19 | 1.27E+16 | 4.53E+15 | 5.65E+11 | 4.39E+12 | 1.77E+12 | 2.33E+13 | 2.87E+18 |
| 8 | 7.ØØØ | 411.1ØØØØ | 242.7Ø | 131.22 | 1.23E+19 | 7.Ø2E+15 | 4.Ø5E+15 | 6.15E+11 | 3.93E+12 | 1.53E+12 | 2.Ø9E+13 | 2.57E+18 |
| 9 | 8.ØØØ | 356.5ØØØØ | 236.2Ø | 116.92 | 1.Ø9E+19 | 4.Ø1E+15 | 3.61E+15 | 6.53E+11 | 3.5ØE+12 | 1.3ØE+12 | 1.86E+13 | 2.29E+18 |
| 1Ø | 9.ØØØ | 3Ø8.ØØØØØ | 229.7Ø | 1Ø3.88 | 9.71E+18 | 1.54E+15 | 3.21E+15 | 8.91E+11 | 3.11E+12 | 1.Ø6E+12 | 1.65E+13 | 2.Ø3E+18 |
| 11 | 1Ø.ØØØ | 265.ØØØØØ | 223.3Ø | 91.94 | 8.6ØE+18 | 6.Ø2E+14 | 2.84E+15 | 1.13E+12 | 2.73E+12 | 8.57E+11 | 1.45E+13 | 1.8ØE+18 |
| 12 | 11.ØØØ | 227.ØØØØØ | 216.8Ø | 81.12 | 7.58E+18 | 2.74E+14 | 2.5ØE+15 | 1.63E+12 | 2.38E+12 | 6.8ØE+11 | 1.27E+13 | 1.59E+18 |
| 13 | 12.ØØØ | 194.ØØØØØ | 216.7Ø | 69.36 | 6.48E+18 | 1.24E+14 | 2.14E+15 | 2.Ø1E+12 | 2.Ø1E+12 | 5.Ø7E+11 | 1.Ø8E+13 | 1.36E+18 |
| 14 | 13.ØØØ | 165.8ØØØØ | 216.7Ø | 59.27 | 5.54E+18 | 6.Ø2E+13 | 1.83E+15 | 2.13E+12 | 1.69E+12 | 3.54E+11 | 9.12E+12 | 1.16E+18 |
| 15 | 14.ØØØ | 141.7ØØØØ | 216.7Ø | 5Ø.66 | 4.74E+18 | 2.81E+13 | 1.56E+15 | 2.38E+12 | 1.42E+12 | 2.38E+11 | 7.71E+12 | 9.9ØE+17 |
| 16 | 15.ØØØ | 121.1ØØØØ | 216.7Ø | 43.29 | 4.Ø5E+18 | 2.Ø3E+13 | 1.34E+15 | 2.63E+12 | 1.19E+12 | 1.6ØE+11 | 6.5ØE+12 | 8.46E+17 |
| 17 | 16.ØØØ | 1Ø3.5ØØØØ | 216.7Ø | 37.ØØ | 3.46E+18 | 1.37E+13 | 1.14E+15 | 3.Ø1E+12 | 9.96E+11 | 1.Ø6E+11 | 5.48E+12 | 7.24E+17 |
| 18 | 17.ØØØ | 88.5ØØØØ | 216.7Ø | 31.64 | 2.96E+18 | 1.14E+13 | 9.77E+14 | 3.51E+12 | 8.24E+11 | 7.37E+1Ø | 4.6ØE+12 | 6.19E+17 |
| 19 | 18.ØØØ | 75.65ØØØ | 216.7Ø | 27.Ø5 | 2.53E+18 | 9.68E+12 | 8.35E+14 | 4.Ø2E+12 | 6.76E+11 | 4.97E+1Ø | 3.85E+12 | 5.29E+17 |
| 2Ø | 19.ØØØ | 64.67ØØØ | 216.7Ø | 23.12 | 2.16E+18 | 8.33E+12 | 7.14E+14 | 4.39E+12 | 5.47E+11 | 3.35E+1Ø | 3.2ØE+12 | 4.52E+17 |
| 21 | 2Ø.ØØØ | 55.29ØØØ | 216.7Ø | 19.77 | 1.85E+18 | 7.21E+12 | 6.1ØE+14 | 4.77E+12 | 4.37E+11 | 2.46E+1Ø | 2.63E+12 | 3.86E+17 |
| 22 | 21.ØØØ | 47.29ØØØ | 217.6Ø | 16.84 | 1.57E+18 | 6.26E+12 | 5.2ØE+14 | 4.77E+12 | 3.46E+11 | 1.94E+1Ø | 2.13E+12 | 3.29E+17 |
| 23 | 22.ØØØ | 4Ø.47ØØØ | 218.6Ø | 14.34 | 1.34E+18 | 5.46E+12 | 4.43E+14 | 4.89E+12 | 2.75E+11 | 1.65E+1Ø | 1.71E+12 | 2.8ØE+17 |
| 24 | 23.ØØØ | 34.67ØØØ | 219.6Ø | 12.23 | 1.14E+18 | 4.8ØE+12 | 3.78E+14 | 4.77E+12 | 2.25E+11 | 1.5ØE+1Ø | 1.36E+12 | 2.39E+17 |
| 25 | 24.ØØØ | 29.72ØØØ | 22Ø.6Ø | 1Ø.44 | 9.76E+17 | 4.2ØE+12 | 3.22E+14 | 4.52E+12 | 1.83E+11 | 1.37E+1Ø | 1.Ø9E+12 | 2.Ø4E+17 |
| 26 | 25.ØØØ | 25.49ØØØ | 221.6Ø | 8.91 | 8.33E+17 | 3.69E+12 | 2.75E+14 | 4.27E+12 | 1.46E+11 | 1.25E+1Ø | 8.8ØE+11 | 1.74E+17 |
| 27 | 27.5ØØ | 17.43ØØØ | 224.ØØ | 6.Ø3 | 5.64E+17 | 2.58E+12 | 1.86E+14 | 3.27E+12 | 8.96E+1Ø | 9.Ø1E+Ø9 | 5.57E+11 | 1.18E+17 |
| 28 | 3Ø.ØØØ | 11.97ØØØ | 226.5Ø | 4.Ø9 | 3.83E+17 | 1.81E+12 | 1.26E+14 | 2.51E+12 | 5.42E+1Ø | 6.55E+Ø9 | 3.5ØE+11 | 8.ØØE+16 |
| 29 | 32.5ØØ | 8.Ø1ØØØ | 23Ø.ØØ | 2.7Ø | 2.52E+17 | 1.22E+12 | 8.33E+13 | 1.86E+12 | 2.94E+1Ø | 4.67E+Ø9 | 2.Ø9E+11 | 5.28E+16 |
| 3Ø | 35.ØØØ | 5.746ØØ | 236.5Ø | 1.88 | 1.76E+17 | 8.63E+11 | 5.81E+13 | 1.38E+12 | 1.63E+1Ø | 3.54E+Ø9 | 1.31E+11 | 3.68E+16 |
| 31 | 37.5ØØ | 4.15ØØØ | 242.9Ø | 1.32 | 1.24E+17 | 6.13E+11 | 4.Ø9E+13 | 9.66E+11 | 8.29E+Ø9 | 2.75E+Ø9 | 8.19E+1Ø | 2.59E+16 |
| 32 | 4Ø.ØØØ | 2.871ØØ | 25Ø.4Ø | .89 | 8.3ØE+16 | 4.18E+11 | 2.74E+13 | 6.Ø7E+11 | 3.75E+Ø9 | 2.Ø8E+Ø9 | 4.69E+1Ø | 1.74E+16 |
| 33 | 42.5ØØ | 2.Ø6ØØØ | 257.3Ø | .62 | 5.8ØE+16 | 2.99E+11 | 1.91E+13 | 3.6ØE+11 | 1.6ØE+Ø9 | 1.64E+Ø9 | 2.68E+1Ø | 1.21E+16 |
| 34 | 45.ØØØ | 1.491ØØ | 264.2Ø | .44 | 4.Ø9E+16 | 2.14E+11 | 1.35E+13 | 2.15E+11 | 6.51E+Ø8 | 1.33E+Ø9 | 1.49E+1Ø | 8.55E+15 |
| 35 | 47.5ØØ | 1.Ø9ØØØ | 27Ø.6Ø | .31 | 2.92E+16 | 1.53E+11 | 9.64E+12 | 1.2ØE+11 | 2.74E+Ø8 | 1.Ø9E+Ø9 | 8.1ØE+Ø9 | 6.1ØE+15 |
| 36 | 5Ø.ØØØ | .7978Ø | 27Ø.7Ø | .23 | 2.13E+16 | 1.12E+11 | 7.Ø5E+12 | 6.62E+1Ø | 1.Ø2E+Ø8 | 9.82E+Ø8 | 4.49E+Ø9 | 4.46E+15 |
| 37 | 55.ØØØ | .425ØØ | 26Ø.8Ø | .13 | 1.18E+16 | 6.Ø2E+1Ø | 3.9ØE+12 | 2.13E+1Ø | 3.54E+Ø7 | 7.84E+Ø8 | 1.95E+Ø9 | 2.47E+15 |
| 38 | 6Ø.ØØØ | .219ØØ | 247.ØØ | .Ø7 | 6.42E+15 | 3.Ø5E+1Ø | 2.12E+12 | 7.Ø7E+Ø9 | 1.33E+Ø7 | 6.9ØE+Ø8 | 9.64E+Ø8 | 1.34E+15 |
| 39 | 65.ØØØ | .1Ø9ØØ | 233.3Ø | .Ø4 | 3.38E+15 | 1.42E+1Ø | 1.12E+12 | 2.37E+Ø9 | 5.1ØE+Ø6 | 6.3ØE+Ø8 | 5.ØØE+Ø8 | 7.ØØE+14 |
| 4Ø | 7Ø.ØØØ | .Ø522Ø | 219.6Ø | .Ø2 | 1.72E+15 | 6.Ø3E+Ø9 | 5.69E+11 | 5.17E+Ø8 | 1.98E+Ø6 | 5.27E+Ø8 | 2.58E+Ø8 | 3.6ØE+14 |
| 41 | 75.ØØØ | .Ø24ØØ | 2Ø8.4Ø | .Ø1 | 8.34E+14 | 2.36E+Ø9 | 2.75E+11 | 2.Ø9E+Ø8 | 7.42E+Ø5 | 5.32E+Ø8 | 1.25E+Ø8 | 1.74E+14 |
| 42 | 8Ø.ØØØ | .Ø1Ø5Ø | 198.6Ø | .ØØ | 3.83E+14 | 7.86E+Ø8 | 1.26E+11 | 1.15E+Ø8 | 2.7ØE+Ø5 | 5.74E+Ø8 | 5.75E+Ø7 | 8.Ø1E+13 |
| 43 | 85.ØØØ | .ØØ446 | 188.9Ø | .ØØ | 1.71E+14 | 2.28E+Ø8 | 5.48E+1Ø | 8.56E+Ø7 | 9.78E+Ø4 | 5.54E+Ø8 | 2.57E+Ø7 | 3.42E+13 |
| 44 | 9Ø.ØØØ | .ØØ184 | 186.9Ø | .ØØ | 7.13E+13 | 6.Ø7E+Ø7 | 2.21E+1Ø | 5.ØØE+Ø7 | 3.36E+Ø4 | 4.17E+Ø8 | 9.99E+Ø6 | 1.36E+13 |
| 45 | 95.ØØØ | .ØØØ76 | 188.4Ø | .ØØ | 2.92E+13 | 1.58E+Ø7 | 7.89E+Ø9 | 2.Ø5E+Ø7 | 1.15E+Ø4 | 2.96E+Ø8 | 3.8ØE+Ø6 | 5.26E+12 |
| 46 | 1ØØ.ØØØ | .ØØØ32 | 195.1Ø | .ØØ | 1.19E+13 | 4.76E+Ø6 | 2.32E+Ø9 | 4.76E+Ø6 | 3.95E+Ø3 | 2.Ø1E+Ø8 | 1.43E+Ø6 | 1.9ØE+12 |

CASE 2A: GIVEN H1, H2, ANGLE

EITHER A SHORT PATH (LEN=Ø) OR A LONG PATH THROUGH A TANGENT HEIGHT (LEN=1) IS POSSIBLE: LEN = Ø

SLANT PATH PARAMETERS IN STANDARD FORM

| | | |
|---|---|---|
| H1 | = | 100.000 KM |
| H2 | = | .000 KM |
| ANGLE | = | 180.000 DEG |
| PHI | = | .000 DEG |
| HMIN | = | .000 KM |
| LEN | = | 0 |

FASCODE LAYER BOUNDARIES PRODUCED BY THE AUTOMATIC LAYERING ROUTINE AUTLAY
THE USER SHOULD EXAMINE THESE BOUNDARIES AND MODIFY THEM IF APPROPRIATE
THE FOLLOWING PARAMETERS ARE USED:

| | | | |
|---|---|---|---|
| AVTRAT | = | 2.00 | = MAX RATIO OF VOIGT WIDTHS |
| TDIFF1 | = | 8.00 | = MAX TEMP DIFF AT 0. KM |
| TDIFF2 | = | 12.00 | = MAX TEMP DIFF AT 100. KM |
| ALZERO | = | .100 CM-1 | = AVERAGE LORENTZ WIDTH AT STP |
| AVMWT | = | 36.00 | = AVERAGE MOLECULAR WEIGHT |
| VBAR | = | 1575.50 CM-1 | = AVERAGE WAVENUMBER |

| I | Z (KM) | P (MB) | T (K) | LORENTZ (CM-1) | DOPPLER (CM-1) | ZETA | VOIGT (CM-1) | VOIGT RATIO | TEMP DIFF (K) |
|---|---|---|---|---|---|---|---|---|---|
| 1 | .000 | 1013.00000 | 288.20 | .10132 | .00160 | .984 | .10134 | 1.14 | 7.8 |
| 2 | 1.200 | 877.00865 | 280.40 | .08893 | .00157 | .983 | .08896 | 1.14 | 7.8 |
| 3 | 2.400 | 756.06135 | 272.60 | .07775 | .00155 | .980 | .07779 | 1.15 | 7.8 |
| 4 | 3.600 | 649.14075 | 264.80 | .06773 | .00153 | .978 | .06777 | 1.15 | 7.8 |
| 5 | 4.800 | 554.92880 | 257.00 | .05878 | .00151 | .975 | .05881 | 1.16 | 7.8 |
| 6 | 6.000 | 472.20000 | 249.20 | .05079 | .00148 | .972 | .05083 | 1.16 | 7.8 |
| 7 | 7.200 | 399.54885 | 241.40 | .04366 | .00146 | .968 | .04371 | 1.17 | 7.8 |
| 8 | 8.400 | 336.24513 | 233.60 | .03736 | .00144 | .963 | .03741 | 1.17 | 7.7 |
| 9 | 9.600 | 281.42833 | 225.86 | .03180 | .00141 | .957 | .03186 | 1.18 | 7.8 |
| 10 | 10.800 | 234.13690 | 218.10 | .02692 | .00139 | .951 | .02699 | 1.97 | 1.4 |
| 11 | 15.200 | 117.35548 | 216.70 | .01354 | .00138 | .907 | .01368 | 1.99 | .0 |
| 12 | 19.800 | 57.05029 | 216.70 | .00658 | .00138 | .826 | .00686 | 2.00 | 5.0 |
| 13 | 25.100 | 25.10539 | 221.70 | .00286 | .00140 | .672 | .00343 | 1.78 | 8.8 |
| 14 | 32.700 | 7.79994 | 230.52 | .00087 | .00143 | .379 | .00193 | 1.10 | 9.1 |
| 15 | 36.200 | 4.91511 | 239.57 | .00054 | .00146 | .270 | .00175 | 1.05 | 9.0 |
| 16 | 39.400 | 3.13644 | 248.60 | .00034 | .00148 | .186 | .00166 | 1.03 | 9.3 |
| 17 | 42.700 | 2.00741 | 257.85 | .00021 | .00151 | .123 | .00162 | 1.01 | 9.4 |
| 18 | 46.200 | 1.28284 | 267.27 | .00013 | .00154 | .080 | .00161 | 1.04 | 6.1 |
| 19 | 54.800 | .43584 | 261.20 | .00005 | .00152 | .029 | .00154 | 1.02 | 9.8 |
| 20 | 58.400 | .27076 | 251.42 | .00003 | .00149 | .019 | .00151 | 1.02 | 9.9 |
| 21 | 62.000 | .16567 | 241.52 | .00002 | .00146 | .012 | .00147 | 1.02 | 10.1 |
| 22 | 65.700 | .09832 | 231.38 | .00001 | .00143 | .008 | .00144 | 1.02 | 10.4 |
| 23 | 69.500 | .05619 | 220.97 | .00001 | .00140 | .005 | .00140 | 1.03 | 10.6 |
| 24 | 74.100 | .02760 | 210.42 | .00000 | .00136 | .002 | .00137 | 1.03 | 10.6 |
| 25 | 79.400 | .01160 | 199.78 | .00000 | .00133 | .001 | .00133 | 1.03 | 11.0 |
| 26 | 85.400 | .00416 | 188.74 | .00000 | .00129 | .000 | .00129 | .98 | 6.4 |
| 27 | 100.000 | .00032 | 195.10 | .00000 | .00131 | .000 | .00131 | .00 | .0 |

CALCULATION OF THE REFRACTED PATH THROUGH THE ATMOSPHERE

| I | ALTITUDE FROM (KM) | TO (KM) | THETA (DEG) | DRANGE (KM) | RANGE (KM) | DBETA (DEG) | BETA (DEG) | PHI (DEG) | DBEND (DEG) | BENDING (DEG) | PBAR (MB) | TBAR (K) | RHOBAR (MOL CM-3 |
|---|---|---|---|---|---|---|---|---|---|---|---|---|---|
| | H2 TO H1 | | | | | | | | | | | | |
| 1 | .000 | 1.000 | .000 | 1.000 | 1.000 | .000 | .000 | 180.000 | .000 | .000 | 955.683 | 284.990 | 2.43E+19 |
| 2 | 1.000 | 1.200 | .000 | .200 | 1.200 | .000 | .000 | 180.000 | .000 | .000 | 887.896 | 281.052 | 2.29E+19 |
| 3 | 1.200 | 2.000 | .000 | .800 | 2.000 | .000 | .000 | 180.000 | .000 | .000 | 835.876 | 277.826 | 2.18E+19 |
| 4 | 2.000 | 2.400 | .000 | .400 | 2.400 | .000 | .000 | 180.000 | .000 | .000 | 775.500 | 273.907 | 2.05E+19 |
| 5 | 2.400 | 3.000 | .000 | .600 | 3.000 | .000 | .000 | 180.000 | .000 | .000 | 728.565 | 270.665 | 1.95E+19 |
| 6 | 3.000 | 3.600 | .000 | .600 | 3.600 | .000 | .000 | 180.000 | .000 | .000 | 675.107 | 266.766 | 1.83E+19 |
| 7 | 3.600 | 4.000 | .000 | .400 | 4.000 | .000 | .000 | 180.000 | .000 | .000 | 632.844 | 263.507 | 1.74E+19 |
| 8 | 4.000 | 4.800 | .000 | .800 | 4.800 | .000 | .000 | 180.000 | .000 | .000 | 585.661 | 259.628 | 1.63E+19 |
| 9 | 4.800 | 5.000 | .000 | .200 | 5.000 | .000 | .000 | 180.000 | .000 | .000 | 547.708 | 256.352 | 1.55E+19 |
| 10 | 5.000 | 6.000 | .000 | 1.000 | 6.000 | .000 | .000 | 180.000 | .000 | .000 | 506.204 | 252.495 | 1.45E+19 |
| 11 | 6.000 | 7.000 | .000 | 1.000 | 7.000 | .000 | .000 | 180.000 | .000 | .000 | 441 .16 | 245.996 | 1.30E+19 |
| 12 | 7.000 | 7.200 | .000 | .200 | 7.200 | .000 | .000 | 180.000 | .000 | .000 | 405.319 | 242.052 | 1.21E+19 |
| 13 | 7.200 | 8.000 | .000 | .800 | 8.000 | .000 | .000 | 180.000 | .000 | .000 | 377.946 | 238.831 | 1.15E+19 |
| 14 | 8.000 | 8.400 | .000 | .400 | 8.400 | .000 | .000 | 180.000 | .000 | .000 | 346.354 | 234.908 | 1.07E+19 |
| 15 | 8.400 | 9.000 | .000 | .600 | 9.000 | .000 | .000 | 180.000 | .000 | .000 | 322.083 | 231.668 | 1.01E+19 |
| 16 | 9.000 | 9.600 | .000 | .600 | 9.600 | .000 | .000 | 180.000 | .000 | .000 | 294.677 | 227.798 | 9.36E+18 |
| 17 | 9.600 | 10.000 | .000 | .400 | 10.000 | .000 | .000 | 180.000 | .000 | .000 | 273.199 | 224.588 | 8.81E+18 |
| 18 | 10.000 | 10.800 | .000 | .800 | 10.800 | .000 | .000 | 180.000 | .000 | .000 | 249.508 | 220.733 | 8.18E+18 |
| 19 | 10.800 | 11.000 | .000 | .200 | 11.000 | .000 | .000 | 180.000 | .000 | .000 | 230.565 | 217.452 | 7.68E+18 |
| 20 | 11.000 | 12.000 | .000 | 1.000 | 12.000 | .000 | .000 | 180.000 | .000 | .000 | 210.499 | 216.751 | 7.02E+18 |
| 21 | 12.000 | 13.000 | .000 | 1.000 | 13.000 | .000 | .000 | 180.000 | .000 | .000 | 179.900 | 216.700 | 6.00E+18 |
| 22 | 13.000 | 14.000 | .000 | 1.000 | 14.000 | .000 | .000 | 180.000 | .000 | .000 | 153.750 | 216.700 | 5.13E+18 |
| 23 | 14.000 | 15.000 | .000 | 1.000 | 15.000 | .000 | .000 | 180.000 | .000 | .000 | 131.400 | 216.700 | 4.38E+18 |
| 24 | 15.000 | 15.200 | .000 | .200 | 15.200 | .000 | .000 | 180.000 | .000 | .000 | 119.228 | 216.700 | 3.98E+18 |
| 25 | 15.200 | 16.000 | .000 | .800 | 16.000 | .000 | .000 | 180.000 | .000 | .000 | 110.428 | 216.700 | 3.69E+18 |
| 26 | 16.000 | 17.000 | .000 | 1.000 | 17.000 | .000 | .000 | 180.000 | .000 | .000 | 96.000 | 216.700 | 3.20E+18 |
| 27 | 17.000 | 18.000 | .000 | 1.000 | 18.000 | .000 | .000 | 180.000 | .000 | .000 | 82.075 | 216.700 | 2.74E+18 |
| 28 | 18.000 | 19.000 | .000 | 1.000 | 19.000 | .000 | .000 | 180.000 | .000 | .000 | 70.160 | 216.700 | 2.34E+18 |
| 29 | 19.000 | 19.800 | .000 | .800 | 19.800 | .000 | .000 | 180.000 | .000 | .000 | 60.860 | 216.700 | 2.03E+18 |
| 30 | 19.800 | 20.000 | .000 | .200 | 20.000 | .000 | .000 | 180.000 | .000 | .000 | 56.170 | 216.700 | 1.88E+18 |
| 31 | 20.000 | 21.000 | .000 | 1.000 | 21.000 | .000 | .000 | 180.000 | .000 | .000 | 51.293 | 217.138 | 1.71E+18 |
| 32 | 21.000 | 22.000 | .000 | 1.000 | 22.000 | .000 | .000 | 180.000 | .000 | .000 | 43.883 | 218.086 | 1.45E+18 |
| 33 | 22.000 | 23.000 | .000 | 1.000 | 23.000 | .000 | .000 | 180.000 | .000 | .000 | 37.572 | 219.086 | 1.24E+18 |
| 34 | 23.000 | 24.000 | .000 | 1.000 | 24.000 | .000 | .000 | 180.000 | .000 | .000 | 32.197 | 220.086 | 1.06E+18 |
| 35 | 24.000 | 25.000 | .000 | 1.000 | 25.000 | .000 | .000 | 180.000 | .000 | .000 | 27.607 | 221.086 | 9.03E+17 |
| 36 | 25.000 | 25.100 | .000 | .100 | 25.100 | .000 | .000 | 180.000 | .000 | .000 | 25.298 | 221.648 | 8.27E+17 |
| 37 | 25.100 | 27.500 | .000 | 2.400 | 27.500 | .000 | .000 | 180.000 | .000 | .000 | 21.274 | 222.774 | 6.84E+17 |
| 38 | 27.500 | 30.000 | .000 | 2.500 | 30.000 | .000 | .000 | 180.000 | .000 | .000 | 14.705 | 225.167 | 4.67E+17 |
| 39 | 30.000 | 32.500 | .000 | 2.500 | 32.500 | .000 | .000 | 180.000 | .000 | .000 | 9.995 | 228.124 | 3.13E+17 |
| 40 | 32.500 | 32.700 | .000 | .200 | 32.700 | .000 | .000 | 180.000 | .000 | .000 | 7.905 | 230.259 | 2.49E+17 |
| 41 | 32.700 | 35.000 | .000 | 2.300 | 35.000 | .000 | .000 | 180.000 | .000 | .000 | 6.777 | 233.333 | 2.09E+17 |
| 42 | 35.000 | 36.200 | .000 | 1.200 | 36.200 | .000 | .000 | 180.000 | .000 | .000 | 5.331 | 237.989 | 1.62E+17 |
| 43 | 36.200 | 37.500 | .000 | 1.300 | 37.500 | .000 | .000 | 180.000 | .000 | .000 | 4.533 | 241.181 | 1.36E+17 |
| 44 | 37.500 | 39.400 | .000 | 1.900 | 39.400 | .000 | .000 | 180.000 | .000 | .000 | 3.645 | 245.595 | 1.07E+17 |
| 45 | 39.400 | 40.000 | .000 | .600 | 40.000 | .000 | .000 | 180.000 | .000 | .000 | 3.004 | 249.485 | 8.71E+16 |
| 46 | 40.000 | 42.500 | .000 | 2.500 | 42.500 | .000 | .000 | 180.000 | .000 | .000 | 2.467 | 253.628 | 6.98E+16 |
| 47 | 42.500 | 42.700 | .000 | .200 | 42.700 | .000 | .000 | 180.000 | .000 | .000 | 2.034 | 257.575 | 5.72E+16 |
| 48 | 42.700 | 45.000 | .000 | 2.300 | 45.000 | .000 | .000 | 180.000 | .000 | .000 | 1.750 | 260.843 | 4.82E+16 |
| 49 | 45.000 | 46.200 | .000 | 1.200 | 46.200 | .000 | .000 | 180.000 | .000 | .000 | 1.387 | 265.69 | 3.77E+16 |
| 50 | 46.200 | 47.500 | .000 | 1.300 | 47.500 | .000 | .000 | 180.000 | .000 | .000 | 1.187 | 268.884 | 3.19E+16 |
| 51 | 47.500 | 50.000 | .000 | 2.500 | 50.000 | .000 | .000 | 180.000 | .000 | .000 | .944 | 270.647 | 2.51E+16 |
| 52 | 50.000 | 54.800 | .000 | 4.800 | 54.800 | .000 | .000 | 180.000 | .000 | .000 | .616 | 266.368 | 1.63E+16 |
| 53 | 54.800 | 55.000 | .000 | .200 | 55.000 | .000 | .000 | 180.000 | .000 | .000 | .430 | 260.999 | 1.19E+16 |
| 54 | 55.000 | 58.400 | .000 | 3.400 | 58.400 | .000 | .000 | 180.000 | .000 | .000 | .347 | 256.402 | 9.66E+15 |
| 55 | 58.400 | 60.000 | .000 | 1.600 | 60.000 | .000 | .000 | 180.000 | .000 | .000 | .245 | 249.273 | 7.09E+15 |

| | | | | | | | | | | | | | |
|---|---|---|---|---|---|---|---|---|---|---|---|---|---|
| 56 | 60.000 | 62.000 | .000 | 2.000 | 62.000 | .000 | .000 | 180.000 | .000 | .000 | .192 | 244.367 | 5.66E+15 |
| 57 | 62.000 | 65.000 | .000 | 3.000 | 65.000 | .000 | .000 | 180.000 | .000 | .000 | .137 | 237.649 | 4.13E+15 |
| 58 | 65.000 | 65.700 | .000 | .700 | 65.700 | .000 | .000 | 180.000 | .000 | .000 | .10- | 232.355 | 3.23E+15 |
| 59 | 65.700 | 69.500 | .000 | 3.800 | 69.500 | .000 | .000 | 180.000 | .000 | .000 | .077 | 226.580 | 2.41E+15 |
| 60 | 69.500 | 70.000 | .000 | .500 | 70.000 | .000 | .000 | 180.000 | .000 | .000 | .054 | 220.292 | 1.78E+15 |
| 61 | 70.000 | 74.100 | .000 | 4.100 | 74.100 | .000 | .000 | 180.000 | .000 | .000 | .040 | 215.428 | 1.30E+15 |
| 62 | 74.100 | 75.000 | .000 | .900 | 75.000 | .000 | .000 | 180.000 | .000 | .000 | .026 | 209.428 | 8.91E+14 |
| 63 | 75.000 | 79.400 | .000 | 4.400 | 79.400 | .000 | .000 | 180.000 | .000 | .000 | .018 | 204.546 | 6.04E+14 |
| 64 | 79.400 | 80.000 | .000 | .600 | 80.000 | .000 | .000 | 180.000 | .000 | .000 | .011 | 199.197 | 4.01E+14 |
| 65 | 80.000 | 85.000 | .000 | 5.000 | 85.000 | .000 | .000 | 180.000 | .000 | .000 | .007 | 194.355 | 2.63E+14 |
| 66 | 85.000 | 85.400 | .000 | .400 | 85.400 | .000 | .000 | 180.000 | .000 | .000 | .004 | 188.821 | 1.65E+14 |
| 67 | 85.400 | 90.000 | .000 | 4.600 | 90.000 | .000 | .000 | 180.000 | .000 | .000 | .003 | 187.941 | 1.10E+14 |
| 68 | 90.000 | 95.000 | .000 | 5.000 | 95.000 | .000 | .000 | 180.000 | .000 | .000 | .001 | 187.539 | 4.72E+13 |
| 69 | 95.000 | 100.000 | .000 | 5.000 | 100.000 | .000 | .000 | 180.000 | .000 | .000 | .001 | 191.235 | 1.93E+13 |

INTEGRATED ABSORBER AMOUNTS BY LAYER

| I | LAYER BOUNDARIES | | INTEGRATED AMOUNTS (MOL CM-2) | | | | | | | |
|---|---|---|---|---|---|---|---|---|---|---|
| | FROM | TO | AIR | H2O | CO2 | O3 | N2O | CO | CH4 | O2 |
| 1 | .000 | 1.000 | 2.426E+24 | 1.673E+22 | 8.014E+20 | 6.779E+16 | 7.772E+17 | 3.583E+17 | 4.129E+18 | 5.076E+23 |
| 2 | 1.000 | 1.200 | 4.576E+23 | 2.707E+21 | 1.511E+20 | 1.356E+16 | 1.466E+17 | 6.618E+16 | 7.786E+17 | 9.573E+22 |
| 3 | 1.200 | 2.000 | 1.742E+24 | 9.029E+21 | 5.754E+20 | 5.423E+16 | 5.580E+17 | 2.475E+17 | 2.964E+18 | 3.644E+23 |
| 4 | 2.000 | 2.400 | 8.201E+23 | 3.531E+21 | 2.708E+20 | 2.670E+16 | 2.626E+17 | 1.140E+17 | 1.395E+18 | 1.715E+23 |
| 5 | 2.400 | 3.000 | 1.169E+24 | 4.180E+21 | 3.861E+20 | 3.853E+16 | 3.744E+17 | 1.596E+17 | 1.989E+18 | 2.445E+23 |
| 6 | 3.000 | 3.600 | 1.099E+24 | 3.126E+21 | 3.630E+20 | 3.672E+16 | 3.520E+17 | 1.472E+17 | 1.870E+18 | 2.299E+23 |
| 7 | 3.600 | 4.000 | 6.957E+23 | 1.626E+21 | 2.297E+20 | 2.348E+16 | 2.227E+17 | 9.183E+16 | 1.183E+18 | 1.455E+23 |
| 8 | 4.000 | 4.800 | 1.306E+24 | 2.388E+21 | 4.312E+20 | 4.618E+16 | 4.182E+17 | 1.710E+17 | 2.222E+18 | 2.731E+23 |
| 9 | 4.800 | 5.000 | 3.095E+23 | 4.521E+20 | 1.022E+20 | 1.154E+16 | 9.910E+16 | 4.038E+16 | 5.265E+17 | 6.472E+22 |
| 10 | 5.000 | 6.000 | 1.450E+24 | 1.668E+21 | 4.788E+20 | 5.709E+16 | 4.643E+17 | 1.880E+17 | 2.467E+18 | 3.033E+23 |
| 11 | 6.000 | 7.000 | 1.298E+24 | 9.586E+20 | 4.287E+20 | 5.895E+16 | 4.157E+17 | 1.647E+17 | 2.208E+18 | 2.715E+23 |
| 12 | 7.000 | 7.200 | 2.426E+23 | 1.329E+20 | 8.012E+19 | 1.238E+16 | 7.769E+16 | 3.012E+16 | 4.124E+17 | 5.074E+22 |
| 13 | 7.200 | 8.000 | 9.161E+23 | 4.049E+20 | 3.026E+20 | 5.100E+16 | 2.934E+17 | 1.109E+17 | 1.557E+18 | 1.916E+23 |
| 14 | 8.000 | 8.400 | 4.271E+23 | 1.333E+20 | 1.410E+20 | 2.780E+16 | 1.367E+17 | 4.985E+16 | 7.250E+17 | 8.933E+22 |
| 15 | 8.400 | 9.000 | 6.039E+23 | 1.248E+20 | 1.994E+20 | 4.877E+16 | 1.932E+17 | 5.774E+16 | 1.024E+18 | 1.263E+23 |
| 16 | 9.000 | 9.600 | 5.618E+23 | 7.058E+19 | 1.856E+20 | 5.745E+16 | 1.794E+17 | 5.984E+16 | 9.606E+17 | 1.175E+23 |
| 17 | 9.600 | 10.000 | 3.523E+23 | 2.921E+19 | 1.164E+20 | 4.310E+16 | 1.122E+17 | 3.580E+16 | 5.947E+17 | 7.370E+22 |
| 18 | 10.000 | 10.800 | 6.543E+23 | 3.574E+19 | 2.161E+20 | 1.050E+17 | 2.072E+17 | 6.260E+16 | 1.101E+18 | 1.369E+23 |
| 19 | 10.800 | 11.000 | 1.536E+23 | 5.938E+18 | 5.072E+19 | 3.145E+16 | 4.832E+16 | 1.392E+16 | 2.576E+17 | 3.212E+22 |
| 20 | 11.000 | 12.000 | 7.020E+23 | 1.891E+19 | 2.318E+20 | 1.813E+17 | 2.190E+17 | 5.894E+16 | 1.172E+18 | 1.468E+23 |
| 21 | 12.000 | 13.000 | 6.001E+23 | 8.815E+18 | 1.982E+20 | 2.070E+17 | 1.845E+17 | 4.257E+16 | 9.931E+17 | 1.255E+23 |
| 22 | 13.000 | 14.000 | 5.128E+23 | 4.211E+18 | 1.694E+20 | 2.256E+17 | 1.552E+17 | 2.920E+16 | 8.394E+17 | 1.073E+23 |
| 23 | 14.000 | 15.000 | 4.383E+23 | 2.396E+18 | 1.447E+20 | 2.507E+17 | 1.303E+17 | 1.963E+16 | 7.086E+17 | 9.166E+22 |
| 24 | 15.000 | 15.200 | 7.969E+22 | 3.895E+17 | 2.632E+19 | 5.340E+16 | 2.342E+16 | 3.066E+15 | 1.278E+17 | 1.667E+22 |
| 25 | 15.200 | 16.000 | 2.949E+23 | 1.285E+18 | 9.738E+19 | 2.285E+17 | 8.570E+16 | 1.005E+16 | 4.696E+17 | 6.167E+22 |
| 26 | 16.000 | 17.000 | 3.202E+23 | 1.250E+18 | 1.057E+20 | 3.256E+17 | 9.072E+16 | 8.897E+15 | 5.024E+17 | 6.697E+22 |
| 27 | 17.000 | 18.000 | 2.738E+23 | 1.051E+18 | 9.040E+19 | 3.759E+17 | 7.473E+16 | 6.093E+15 | 4.211E+17 | 5.725E+22 |
| 28 | 18.000 | 19.000 | 2.340E+23 | 8.986E+17 | 7.728E+19 | 4.200E+17 | 6.089E+16 | 4.109E+15 | 3.515E+17 | 4.894E+22 |
| 29 | 19.000 | 19.800 | 1.625E+23 | 6.293E+17 | 5.367E+19 | 3.631E+17 | 4.005E+16 | 2.375E+15 | 2.371E+17 | 3.399E+22 |
| 30 | 19.800 | 20.000 | 3.755E+22 | 1.463E+17 | 1.240E+19 | 9.459E+16 | 8.944E+15 | 5.077E+14 | 5.370E+16 | 7.851E+21 |
| 31 | 20.000 | 21.000 | 1.707E+23 | 6.725E+17 | 5.638E+19 | 4.769E+17 | 3.896E+16 | 2.190E+15 | 2.375E+17 | 3.570E+22 |
| 32 | 21.000 | 22.000 | 1.454E+23 | 5.849E+17 | 4.803E+19 | 4.831E+17 | 3.091E+16 | 1.793E+15 | 1.913E+17 | 3.042E+22 |
| 33 | 22.000 | 23.000 | 1.240E+23 | 5.123E+17 | 4.093E+19 | 4.831E+17 | 2.493E+16 | 1.573E+15 | 1.528E+17 | 2.592E+22 |
| 34 | 23.000 | 24.000 | 1.057E+23 | 4.495E+17 | 3.492E+19 | 4.642E+17 | 2.033E+16 | 1.430E+15 | 1.222E+17 | 2.211E+22 |
| 35 | 24.000 | 25.000 | 9.026E+22 | 3.939E+17 | 2.981E+19 | 4.391E+17 | 1.641E+16 | 1.307E+15 | 9.818E+16 | 1.888E+22 |
| 36 | 25.000 | 25.100 | 8.266E+21 | 3.663E+16 | 2.730E+18 | 4.244E+16 | 1.450E+15 | 1.241E+14 | 8.716E+15 | 1.729E+21 |
| 37 | 25.100 | 27.500 | 1.641E+23 | 7.388E+17 | 5.420E+19 | 8.945E+17 | 2.747E+16 | 2.540E+15 | 1.677E+17 | 3.433E+22 |
| 38 | 27.500 | 30.000 | 1.168E+23 | 5.431E+17 | 3.858E+19 | 7.186E+17 | 1.761E+16 | 1.929E+15 | 1.113E+17 | 2.444E+22 |
| 39 | 30.000 | 32.500 | 7.825E+22 | 3.736E+17 | 2.584E+19 | 5.423E+17 | 1.014E+16 | 1.389E+15 | 6.843E+16 | 1.636E+22 |
| 40 | 32.500 | 32.700 | 4.973E+21 | 2.402E+16 | 1.642E+18 | 3.678E+16 | 5.745E+14 | 9.236E+13 | 4.113E+15 | 1.040E+21 |
| 41 | 32.700 | 35.000 | 4.798E+22 | 2.335E+17 | 1.585E+19 | 3.654E+17 | 4.984E+15 | 9.270E+14 | 3.774E+16 | 1.004E+22 |
| 42 | 35.000 | 36.200 | 1.943E+22 | 9.549E+16 | 6.416E+18 | 1.522E+17 | 1.673E+15 | 3.998E+14 | 1.411E+16 | 4.063E+21 |
| 43 | 36.200 | 37.500 | 1.765E+22 | 8.719E+16 | 5.829E+18 | 1.379E+17 | 1.292E+15 | 3.818E+14 | 1.207E+16 | 3.692E+21 |
| 44 | 37.500 | 39.400 | 2.028E+22 | 1.010E+17 | 6.697E+18 | 1.546E+17 | 1.183E+15 | 4.702E+14 | 1.268E+16 | 4.241E+21 |
| 45 | 39.400 | 40.000 | 5.229E+21 | 2.624E+16 | 1.727E+18 | 3.851E+16 | 2.478E+14 | 1.288E+14 | 3.008E+15 | 1.094E+21 |
| 46 | 40.000 | 42.500 | 1.744E+22 | 8.873E+16 | 5.760E+18 | 1.181E+17 | 6.305E+14 | 4.621E+14 | 8.971E+15 | 3.648E+21 |
| 47 | 42.500 | 42.700 | 1.144E+21 | 5.898E+15 | 3.777E+17 | 7.049E+15 | 3.081E+13 | 3.250E+13 | 5.231E+14 | 2.392E+20 |
| 48 | 42.700 | 45.000 | 1.109E+22 | 5.758E+16 | 3.662E+18 | 6.321E+16 | 2.326E+14 | 3.367E+14 | 4.535E+15 | 2.319E+21 |
| 49 | 45.000 | 46.200 | 4.528E+21 | 2.370E+16 | 1.495E+18 | 2.247E+16 | 6.390E+13 | 1.517E+14 | 1.546E+15 | 9.471E+20 |
| 50 | 46.200 | 47.500 | 4.145E+21 | 2.175E+16 | 1.369E+18 | 1.819E+16 | 4.496E+13 | 1.487E+14 | 1.238E+15 | 8.671E+20 |
| 51 | 47.500 | 50.000 | 6.264E+21 | 3.204E+16 | 2.069E+18 | 2.259E+16 | 4.341E+13 | 2.582E+14 | 1.529E+15 | 1.310E+21 |
| 52 | 50.000 | 54.800 | 7.814E+21 | 4.043E+16 | 2.580E+18 | 1.935E+16 | 3.066E+13 | 4.239E+14 | 1.482E+15 | 1.634E+21 |
| 53 | 54.800 | 55.000 | 2.389E+20 | 1.220E+15 | 7.888E+16 | 4.350E+14 | 7.237E+11 | 1.575E+13 | 3.963E+13 | 4.996E+19 |
| 54 | 55.000 | 58.400 | 3.286E+21 | 1.640E+16 | 1.085E+18 | 5.588E+15 | 8.788E+12 | 2.553E+14 | 5.265E+14 | 6.872E+20 |
| 55 | 58.400 | 60.000 | 1.134E+21 | 5.456E+15 | 3.746E+17 | 1.356E+15 | 2.495E+12 | 1.126E+14 | 1.730E+14 | 2.372E+20 |
| 56 | 60.000 | 62.000 | 1.133E+21 | 5.260E+15 | 3.741E+17 | 1.145E+15 | 2.206E+12 | 1.355E+14 | 1.701E+14 | 2.369E+20 |
| 57 | 62.000 | 65.000 | 1.238E+21 | 5.412E+15 | 4.088E+17 | 1.005E+15 | 2.067E+12 | 1.943E+14 | 1.858E+14 | 2.589E+20 |
| 58 | 65.000 | 65.700 | 2.260E+20 | 9.380E+14 | 7.463E+16 | 1.494E+14 | 3.345E+11 | 4.358E+13 | 3.392E+13 | 4.727E+19 |
| 59 | 65.700 | 69.500 | 9.147E+20 | 3.521E+15 | 3.021E+17 | 4.311E+14 | 1.211E+12 | 2.184E+14 | 1.373E+14 | 1.913E+20 |

| | | | | | | | | | | |
|---|---|---|---|---|---|---|---|---|---|---|
| 60 | 69.500 | 70.000 | 8.905E+19 | 3.148E+14 | 2.941E+16 | 2.792E+13 | 1.038E+11 | 2.659E+13 | 1.337E+13 | 1.863E+19 |
| 61 | 70.000 | 74.100 | 5.321E+20 | 1.724E+15 | 1.758E+17 | 1.495E+14 | 5.576E+11 | 2.169E+14 | 7.989E+13 | 1.113E+20 |
| 62 | 74.100 | 75.000 | 8.018E+19 | 2.312E+14 | 2.648E+16 | 2.040E+13 | 7.305E+10 | 4.785E+13 | 1.204E+13 | 1.677E+19 |
| 63 | 75.000 | 79.400 | 2.657E+20 | 6.649E+14 | 8.753E+16 | 7.144E+13 | 2.164E+11 | 2.420E+14 | 3.988E+13 | 5.557E+19 |
| 64 | 79.400 | 80.000 | 2.408E+19 | 5.038E+13 | 7.908E+15 | 7.150E+12 | 1.725E+10 | 3.426E+13 | 3.615E+12 | 5.037E+18 |
| 65 | 80.000 | 85.000 | 1.314E+20 | 2.252E+14 | 4.268E+16 | 4.977E+13 | 8.486E+10 | 2.819E+14 | 1.973E+13 | 2.697E+19 |
| 66 | 85.000 | 85.400 | 6.606E+18 | 8.638E+12 | 2.113E+15 | 3.349E+12 | 3.749E+09 | 2.192E+13 | 9.888E+11 | 1.319E+18 |
| 67 | 85.400 | 90.000 | 5.038E+19 | 5.448E+13 | 1.589E+16 | 2.973E+13 | 2.629E+10 | 2.192E+14 | 7.318E+12 | 9.839E+18 |
| 68 | 90.000 | 95.000 | 2.359E+19 | 1.667E+13 | 6.904E+15 | 1.652E+13 | 1.030E+10 | 1.766E+14 | 3.202E+12 | 4.383E+18 |
| 69 | 95.000 | 100.000 | 9.633E+18 | 4.598E+12 | 2.276E+15 | 5.383E+12 | 3.532E+09 | 1.228E+14 | 1.212E+12 | 1.651E+18 |
| TOTAL | 100.000 | .000 | 2.152E+25 | 4.737E+22 | 7.108E+21 | 9.248E+18 | 6.612E+18 | 2.386E+18 | 3.549E+19 | 4.502E+24 |

SUMMARY OF THE GEOMETRY CALCULATION

| | | |
|---|---|---|
| MODEL | = | U. S. STANDARD, 1976 |
| H1 | = | 100.000 KM |
| H2 | = | .000 KM |
| ANGLE | = | 180.000 DEG |
| RANGE | = | 100.000 KM |
| BETA | = | .000 DEG |
| PHI | = | .000 DEG |
| HMIN | = | .000 KM |
| BENDING | = | .000 DEG |
| LEN | = | 0 |
| AIRMAS | = | 1.00 RELATIVE TO A VERTICAL PATH , GROUND TO SPACE |

FINAL SET OF LAYERS FOR INPUT TO FASCODE
A LAYER AMOUNT MAY BE SET TO ZERO IF THE CUMULATIVE AMOUNT FOR THAT LAYER AND ABOVE IS LESS THAN 0.1 PERCENT
OF THE TOTAL AMOUNT. THIS IS DONE ONLY FOR THE FOLLOWING CASES
1. IEMIT = 0 (TRANSMITTANCE)
2. IEMIT = 1 (RADIANCE) AND IPATH = 3 (PATH LOOKING UP)
O2 IS NOT INCLUDED
IF THE AMOUNTS FOR ALL THE MOLECULES BUT O2 ARE ZEROED, THE REMAINING LAYERS ARE ELIMINATED

| L | LAYER BOUNDARIES FROM (KM) | TO (KM) | IPATH | PBAR (MB) | TBAR (K) | INTEGRATED AMOUNTS (MOLS CM-2) AIR | H2O | CO2 | O3 | N2O | CO | CH4 | O2 | OTHER |
|---|---|---|---|---|---|---|---|---|---|---|---|---|---|---|
| 1 | .000 | 1.200 | 1 | 944.92733 | 284.37 | 2.88E+24 | 1.94E+22 | 9.53E+20 | 8.13E+16 | 9.24E+17 | 4.24E+17 | 4.91E+18 | 6.03E+23 | 2.26E+24 |
| 2 | 1.200 | 2.400 | 1 | 816.55148 | 276.57 | 2.56E+24 | 1.26E+22 | 8.46E+20 | 8.09E+16 | 8.21E+17 | 3.62E+17 | 4.36E+18 | 5.36E+23 | 2.01E+24 |
| 3 | 2.400 | 3.600 | 1 | 702.66038 | 268.78 | 2.27E+24 | 7.31E+21 | 7.49E+20 | 7.53E+16 | 7.26E+17 | 3.07E+17 | 3.86E+18 | 4.74E+23 | 1.79E+24 |
| 4 | 3.600 | 4.800 | 1 | 602.05860 | 260.98 | 2.00E+24 | 4.01E+21 | 6.61E+20 | 6.97E+16 | 6.41E+17 | 2.63E+17 | 3.40E+18 | 4.19E+23 | 1.58E+24 |
| 5 | 4.800 | 6.000 | 1 | 513.50281 | 253.17 | 1.76E+24 | 2.12E+21 | 5.81E+20 | 6.86E+16 | 5.63E+17 | 2.28E+17 | 2.99E+18 | 3.68E+23 | 1.39E+24 |
| 6 | 6.000 | 7.200 | 1 | 435.81759 | 245.38 | 1.54E+24 | 1.09E+21 | 5.09E+20 | 7.13E+16 | 4.93E+17 | 1.95E+17 | 2.62E+18 | 3.22E+23 | 1.22E+24 |
| 7 | 7.200 | 8.400 | 1 | 367.90168 | 237.58 | 1.34E+24 | 5.38E+20 | 4.44E+20 | 7.88E+16 | 4.30E+17 | 1.61E+17 | 2.28E+18 | 2.81E+23 | 1.06E+24 |
| 8 | 8.400 | 9.600 | 1 | 308.87381 | 229.80 | 1.17E+24 | 1.95E+20 | 3.85E+20 | 1.06E+17 | 3.73E+17 | 1.28E+17 | 1.97E+18 | 2.44E+23 | 9.21E+23 |
| 9 | 9.600 | 10.800 | 1 | 257.80003 | 222.08 | 1.01E+24 | 6.50E+19 | 3.32E+20 | 1.48E+17 | 3.19E+17 | 9.84E+16 | 1.70E+18 | 2.11E+23 | 7.96E+23 |
| 10 | 10.800 | 15.200 | 1 | 175.78066 | 216.76 | 2.49E+24 | 4.07E+19 | 8.21E+20 | 9.49E+17 | 7.61E+17 | 1.67E+17 | 4.10E+18 | 5.20E+23 | 1.97E+24 |
| 11 | 15.200 | 19.800 | 1 | 87.19677 | 216.70 | 1.29E+24 | 0.00E+00 | 4.24E+20 | 1.71E+18 | 3.52E+17 | 3.15E+16 | 1.98E+18 | 2.69E+23 | 1.02E+24 |
| 12 | 19.800 | 25.100 | 1 | 41.07584 | 218.70 | 6.82E+23 | 0.00E+00 | 2.25E+20 | 2.48E+18 | 1.42E+17 | 8.93E+15 | 8.64E+17 | 1.43E+23 | 5.39E+23 |
| 13 | 25.100 | 32.700 | 1 | 16.56086 | 224.79 | 3.64E+23 | 0.00E+00 | 1.20E+20 | 2.19E+18 | 5.58E+16 | 5.95E+15 | 3.52E+17 | 7.62E+22 | 2.88E+23 |
| 14 | 32.700 | 36.200 | 1 | 6.36063 | 234.67 | 6.74E+22 | 0.00E+00 | 2.23E+19 | 5.18E+17 | 6.66E+15 | 1.33E+15 | 5.18E+16 | 1.41E+22 | 5.33E+22 |
| 15 | 36.200 | 39.400 | 1 | 4.05853 | 243.54 | 3.79E+22 | 0.00E+00 | 1.25E+19 | 2.93E+17 | 0.00E+00 | 8.52E+14 | 2.48E+16 | 7.93E+21 | 3.00E+22 |
| 16 | 39.400 | 42.700 | 1 | 2.56431 | 252.91 | 2.38E+22 | 0.00E+00 | 7.86E+18 | 1.64E+17 | 0.00E+00 | 6.23E+14 | 0.00E+00 | 4.98E+21 | 1.88E+22 |
| 17 | 42.700 | 46.200 | 1 | 1.64496 | 262.25 | 1.56E+22 | 0.00E+00 | 5.16E+18 | 8.57E+16 | 0.00E+00 | 4.88E+14 | 0.00E+00 | 3.27E+21 | 1.23E+22 |
| 18 | 46.200 | 54.800 | 1 | .85841 | 268.41 | 1.82E+22 | 0.00E+00 | 6.02E+18 | 6.01E+16 | 0.00E+00 | 8.31E+14 | 0.00E+00 | 3.81E+21 | 1.44E+22 |

| | | | | | | | | | | | | | | |
|---|---|---|---|---|---|---|---|---|---|---|---|---|---|---|
| 19 | 54.800 | 58.400 | 1 | .35304 | 256.71 | 3.52E+21 | 0.00E+00 | 0.00E+00 | 5.52E+15 | 0.00E+00 | 0.00E+00 | 0.00E+00 | 7.37E+20 | 2.79E+21 |

| L | PATH BOUNDARIES FROM (KM) | TO (KM) | PBAR (MB) | TBAR (K) | ACCUMULATED MOLECULAR AMOUNTS FOR TOTAL PATH AIR | H2O | CO2 | O3 | N2O | CO | CH4 | O2 | OTHER |
|---|---|---|---|---|---|---|---|---|---|---|---|---|---|
| 19 | .000 | 58.400 | 506.08084 | 250.24 | 2.15E+25 | 4.74E+22 | 7.10E+21 | 9.24E+18 | 6.61E+18 | 2.38E+18 | 3.55E+19 | 4.50E+24 | 1.70E+25 |
| | CURTIS GODSON MOLECULAR PRESSURE (MB) | | | | | 802.637 | 506.173 | 93.443 | 525.203 | 599.490 | 520.419 | 506.090 | |
| | CURTIS GODSON MOLECULAR TEMPERATURE (K) | | | | | 274.717 | 250.244 | 225.228 | 251.360 | 257.677 | 251.044 | 250.245 | |

THE FOLLOWING IS A LIST OF THE TOTAL OPTICAL DEPTH OF THE SPECIES OF INTEREST AND OF THE BACKGROUND ATMOSPHERE AS A WHOLE AS A FUNCTION OF WAVENUMBER. ALSO LISTED IS THE RATIO OF THE OPTICAL DEPTH OF THE SPECIES OF INTEREST TO THE TOTAL BACKGROUND OPTICAL DEPTH. THIS DATA HAS ALSO BEEN STORED IN PLOTTING FORMAT.

| WAVENUMBER | O.D.(SPECIES) | O.D.(ALL) | O.D.(SPECIES)/O.D.(ALL) |
|---|---|---|---|
| 1200.000 | 6.18617E-04 | 5.04363E-02 | 1.22653E-02 |
| 1201.000 | 1.10235E-02 | 4.05902E-02 | 2.71582E-01 |
| 1202.000 | 1.13110E-03 | 1.16845E-02 | 9.68038E-02 |
| 1203.000 | 1.81212E-03 | 1.10444E-02 | 1.64075E-01 |
| 1204.000 | 2.09834E-03 | 7.90397E-03 | 2.65480E-01 |
| 1205.000 | 5.18004E-03 | 1.12084E-02 | 4.62157E-01 |
| 1206.000 | 4.69723E-01 | 4.76775E-01 | 9.85209E-01 |
| 1207.000 | 9.99116E-03 | 1.32531E-02 | 7.53871E-01 |
| 1208.000 | 5.20114E-03 | 1.91780E-02 | 2.71204E-01 |
| 1209.000 | 2.47911E-02 | 2.69553E-02 | 9.19712E-01 |
| 1210.000 | 9.81285E-03 | 1.15184E-02 | 8.51926E-01 |
| 1211.000 | 8.18931E-01 | 8.20691E-01 | 9.97856E-01 |
| 1212.000 | 1.86956E-02 | 1.99476E-02 | 9.37237E-01 |
| 1213.000 | 5.31601E-01 | 5.32811E-01 | 9.97729E-01 |
| 1214.000 | 7.17234E-04 | 1.85734E-03 | 3.86162E-01 |
| 1215.000 | 1.02157E+00 | 1.02284E+00 | 9.98766E-01 |
| 1216.000 | 3.98668E-01 | 4.59545E-01 | 8.67528E-01 |
| 1217.000 | 4.90938E-02 | 5.05061E-02 | 9.72038E-01 |
| 1218.000 | 1.12754E-01 | 1.13770E-01 | 9.91063E-01 |
| 1219.000 | 4.92892E+00 | 4.92997E+00 | 9.99787E-01 |
| 1220.000 | 1.24746E-01 | 1.25873E-01 | 9.91051E-01 |
| 1221.000 | 8.15256E-01 | 8.16468E-01 | 9.98516E-01 |
| 1222.000 | 3.00520E-01 | 3.01861E-01 | 9.95558E-01 |
| 1223.000 | 8.63445E-02 | 1.72737E-01 | 4.99860E-01 |
| 1224.000 | 1.03679E-03 | 2.75088E-03 | 3.76895E-01 |
| 1225.000 | 5.75350E+00 | 5.75679E+00 | 9.99429E-01 |
| 1226.000 | 8.26016E-02 | 8.42805E-02 | 9.80080E-01 |
| 1227.000 | 3.57535E-02 | 3.82363E-02 | 9.35067E-01 |
| 1228.000 | 4.66614E-02 | 4.96359E-02 | 9.40073E-01 |
| 1229.000 | 2.38411E-01 | 2.41646E-01 | 9.86609E-01 |
| 1230.000 | 1.45277E-01 | 1.48996E-01 | 9.75038E-01 |
| 1231.000 | 0.00000E+00 | 1.06027E-02 | 0.00000E+00 |
| 1232.000 | 1.54480E-01 | 1.59629E-01 | 9.67748E-01 |
| 1233.000 | 1.72737E+00 | 1.73348E+00 | 9.96472E-01 |
| 1234.000 | 3.77628E-03 | 1.07035E-02 | 3.52807E-01 |
| 1235.000 | 1.54042E-05 | 8.16014E-03 | 1.88773E-03 |
| 1236.000 | 3.64687E-02 | 4.81121E-02 | 7.57994E-01 |
| 1237.000 | 6.20050E+00 | 6.21186E+00 | 9.98171E-01 |
| 1238.000 | 1.19956E+00 | 1.21326E+00 | 9.88702E-01 |
| 1239.000 | 4.28864E+00 | 4.41801E+00 | 9.70717E-01 |
| 1240.000 | 3.22018E+00 | 3.24070E+00 | 9.93669E-01 |
| 1241.000 | 2.50635E+00 | 2.52881E+00 | 9.91117E-01 |
| 1242.000 | 1.06771E-01 | 1.34583E-01 | 7.93350E-01 |
| 1243.000 | 1.56308E+00 | 1.59573E+00 | 9.79539E-01 |
| 1244.000 | 3.45723E+00 | 3.49518E+00 | 9.89141E-01 |
| 1245.000 | 3.82341E-01 | 4.26755E-01 | 8.95926E-01 |
| 1246.000 | 1.35100E-02 | 2.93615E-01 | 4.60125E-02 |
| 1247.000 | 2.40613E+00 | 2.41833E+00 | 9.94957E-01 |
| 1248.000 | 8.97649E-01 | 8.97649E-01 | 1.00000E+00 |
| 1249.000 | 1.73354E-01 | 1.73355E-01 | 9.99998E-01 |
| 1250.000 | 2.16302E-01 | 2.16302E-01 | 9.99999E-01 |
| 1251.000 | 1.29911E+00 | 1.29911E+00 | 1.00000E+00 |
| 1252.000 | 5.82332E-03 | 5.82350E-03 | 9.99968E-01 |
| 1253.000 | 2.94208E+00 | 2.94208E+00 | 1.00000E+00 |
| 1254.000 | 1.22666E+00 | 1.69532E+00 | 7.23555E-01 |

| | | | |
|---|---|---|---|
| 1255.000 | 4.02352E+00 | 4.02352E+00 | 1.00000E+00 |
| 1256.000 | 2.98746E+00 | 2.98746E+00 | 1.00000E+00 |
| 1257.000 | 6.00722E+00 | 6.00722E+00 | 1.00000E+00 |
| 1258.000 | 2.36190E-01 | 2.36190E-01 | 1.00000E+00 |
| 1259.000 | 4.11012E+00 | 4.11012E+00 | 1.00000E+00 |
| 1260.000 | 1.17125E+01 | 1.17125E+01 | 1.00000E+00 |
| 1261.000 | 3.09590E-02 | 3.09590E-02 | 9.99999E-01 |
| 1262.000 | 3.27692E+00 | 3.69964E+00 | 8.85741E-01 |
| 1263.000 | 4.49412E-01 | 4.49412E-01 | 1.00000E+00 |
| 1264.000 | 5.09302E+00 | 5.09302E+00 | 1.00000E+00 |
| 1265.000 | 1.63978E+00 | 1.63978E+00 | 1.00000E+00 |
| 1266.000 | 1.71577E+00 | 1.71577E+00 | 1.00000E+00 |
| 1267.000 | 3.15622E+00 | 3.15622E+00 | 1.00000E+00 |
| 1268.000 | 7.62525E+00 | 7.62525E+00 | 1.00000E+00 |
| 1269.000 | 1.99599E+00 | 1.99599E+00 | 1.00000E+00 |
| 1270.000 | 1.90531E+00 | 1.92058E+00 | 9.92049E-01 |
| 1271.000 | 2.01285E-01 | 2.01285E-01 | 1.00000E+00 |
| 1272.000 | 1.52661E+01 | 1.52661E+01 | 1.00000E+00 |
| 1273.000 | 5.54788E+00 | 5.54788E+00 | 1.00000E+00 |
| 1274.000 | 5.08194E+00 | 5.08194E+00 | 1.00000E+00 |
| 1275.000 | 2.16100E-01 | 2.16100E-01 | 1.00000E+00 |
| 1276.000 | 2.80419E+00 | 2.80419E+00 | 1.00000E+00 |
| 1277.000 | 1.37954E+00 | 1.95190E+00 | 7.06765E-01 |
| 1278.000 | 1.55959E+00 | 1.55959E+00 | 1.00000E+00 |
| 1279.000 | 1.31510E+00 | 1.31510E+00 | 1.00000E+00 |
| 1280.000 | 8.33428E+00 | 8.33428E+00 | 1.00000E+00 |
| 1281.000 | 3.68318E+00 | 3.68318E+00 | 1.00000E+00 |
| 1282.000 | 4.16003E+00 | 4.16003E+00 | 1.00000E+00 |
| 1283.000 | 4.51806E-01 | 4.51806E-01 | 1.00000E+00 |
| 1284.000 | 1.69864E+00 | 1.69864E+00 | 1.00000E+00 |
| 1285.000 | 7.51009E-01 | 7.62544E-01 | 9.84873E-01 |
| 1286.000 | 3.21161E+00 | 3.21161E+00 | 1.00000E+00 |
| 1287.000 | 4.08444E+00 | 4.08444E+00 | 1.00000E+00 |
| 1288.000 | 1.84911E+01 | 1.84911E+01 | 1.00000E+00 |
| 1289.000 | 4.71109E+00 | 4.71109E+00 | 1.00000E+00 |
| 1290.000 | 1.51338E+00 | 1.51338E+00 | 1.00000E+00 |
| 1291.000 | 2.36314E+00 | 2.36314E+00 | 1.00000E+00 |
| 1292.000 | 7.28208E-01 | 7.50092E-01 | 9.70826E-01 |
| 1293.000 | 9.27151E+00 | 9.68814E+00 | 9.56996E-01 |
| 1294.000 | 7.75716E-01 | 7.75716E-01 | 1.00000E+00 |
| 1295.000 | 1.20029E+00 | 1.20029E+00 | 1.00000E+00 |
| 1296.000 | 1.01090E+01 | 1.01090E+01 | 1.00000E+00 |
| 1297.000 | 1.85152E+00 | 1.85152E+00 | 1.00000E+00 |
| 1298.000 | 7.94999E-01 | 7.94999E-01 | 1.00000E+00 |
| 1299.000 | 6.19827E+00 | 6.19827E+00 | 1.00000E+00 |
| 1300.000 | 2.61542E+00 | 2.89376E+00 | 9.03815E-01 |
| 1301.000 | 6.23724E+00 | 6.23724E+00 | 1.00000E+00 |
| 1302.000 | 2.56911E+00 | 2.56911E+00 | 1.00000E+00 |
| 1303.000 | 5.93782E-01 | 5.93782E-01 | 1.00000E+00 |
| 1304.000 | 1.83618E+00 | 1.83618E+00 | 1.00000E+00 |
| 1305.000 | 7.15253E+00 | 7.15253E+00 | 1.00000E+00 |
| 1306.000 | 1.12160E+01 | 1.12160E+01 | 1.00000E+00 |
| 1307.000 | 3.36416E+00 | 3.36416E+00 | 1.00000E+00 |
| 1308.000 | 8.99697E+00 | 8.99697E+00 | 1.00000E+00 |
| 1309.000 | 6.58115E-01 | 6.58115E-01 | 1.00000E+00 |
| 1310.000 | 1.69172E+00 | 1.69172E+00 | 1.00000E+00 |
| 1311.000 | 7.29587E+00 | 7.29587E+00 | 1.00000E+00 |
| 1312.000 | 6.16370E-01 | 6.16370E-01 | 1.00000E+00 |
| 1313.000 | 1.26576E+00 | 1.26576E+00 | 1.00000E+00 |
| 1314.000 | 4.67887E-01 | 4.67887E-01 | 1.00000E+00 |
| 1315.000 | 1.28740E+00 | 1.28740E+00 | 1.00000E+00 |
| 1316.000 | 6.62392E-01 | 6.62392E-01 | 1.00000E+00 |
| 1317.000 | 9.88471E+00 | 9.88471E+00 | 1.00000E+00 |
| 1318.000 | 4.72154E+00 | 4.72154E+00 | 1.00000E+00 |

| | | | |
|---|---|---|---|
| 1319.000 | 4.01208E+00 | 4.01208E+00 | 1.00000E+00 |
| 1320.000 | 1.48391E+01 | 1.48391E+01 | 1.00000E+00 |
| 1321.000 | 6.60501E+00 | 6.60501E+00 | 1.00000E+00 |
| 1322.000 | 7.35565E+00 | 7.35565E+00 | 1.00000E+00 |
| 1323.000 | 7.01874E+00 | 7.01874E+00 | 1.00000E+00 |
| 1324.000 | 2.37368E+00 | 2.37368E+00 | 1.00000E+00 |
| 1325.000 | 1.77024E+00 | 1.77024E+00 | 1.00000E+00 |
| 1326.000 | 2.96916E+00 | 2.96916E+00 | 1.00000E+00 |
| 1327.000 | 7.29788E+00 | 7.29788E+00 | 1.00000E+00 |
| 1328.000 | 8.14145E-01 | 8.14145E-01 | 1.00000E+00 |
| 1329.000 | 3.51810E+00 | 3.51810E+00 | 1.00000E+00 |
| 1330.000 | 1.87085E+00 | 1.87085E+00 | 1.00000E+00 |
| 1331.000 | 6.57438E-01 | 6.57438E-01 | 1.00000E+00 |
| 1332.000 | 9.70105E+00 | 9.70105E+00 | 1.00000E+00 |
| 1333.000 | 1.45153E+01 | 1.45153E+01 | 1.00000E+00 |
| 1334.000 | 2.20215E+00 | 2.20215E+00 | 1.00000E+00 |
| 1335.000 | 2.71233E+00 | 2.71233E+00 | 1.00000E+00 |
| 1336.000 | 3.27409E+00 | 3.27409E+00 | 1.00000E+00 |
| 1337.000 | 5.38850E+00 | 5.38850E+00 | 1.00000E+00 |
| 1338.000 | 3.04188E+00 | 3.04188E+00 | 1.00000E+00 |
| 1339.000 | 3.07946E+01 | 3.07946E+01 | 1.00000E+00 |
| 1340.000 | 2.53977E+01 | 2.53977E+01 | 1.00000E+00 |
| 1341.000 | 8.55664E+00 | 8.55664E+00 | 1.00000E+00 |
| 1342.000 | 9.34890E-01 | 9.34890E-01 | 1.00000E+00 |
| 1343.000 | 6.84101E-01 | 6.84101E-01 | 1.00000E+00 |
| 1344.000 | 3.26952E-01 | 3.26952E-01 | 1.00000E+00 |
| 1345.000 | 1.95763E+00 | 1.95763E+00 | 1.00000E+00 |
| 1346.000 | 9.70247E-01 | 9.70247E-01 | 1.00000E+00 |
| 1347.000 | 2.05262E+00 | 2.05262E+00 | 1.00000E+00 |
| 1348.000 | 5.88903E-01 | 5.88903E-01 | 1.00000E+00 |
| 1349.000 | 2.35481E+01 | 2.35481E+01 | 1.00000E+00 |
| 1350.000 | 1.69575E+00 | 1.69575E+00 | 1.00000E+00 |
| 1351.000 | 7.97381E+00 | 7.97381E+00 | 1.00000E+00 |
| 1352.000 | 3.12664E+00 | 3.12664E+00 | 1.00000E+00 |
| 1353.000 | 4.26673E+00 | 4.26673E+00 | 1.00000E+00 |
| 1354.000 | 5.92094E-01 | 5.92094E-01 | 1.00000E+00 |
| 1355.000 | 2.50965E+00 | 2.50965E+00 | 1.00000E+00 |
| 1356.000 | 6.45944E+00 | 6.45944E+00 | 1.00000E+00 |
| 1357.000 | 4.00391E+00 | 4.00391E+00 | 1.00000E+00 |
| 1358.000 | 1.29509E+01 | 1.29509E+01 | 1.00000E+00 |
| 1359.000 | 4.82699E+00 | 4.82699E+00 | 1.00000E+00 |
| 1360.000 | 1.91546E+00 | 1.91546E+00 | 1.00000F+00 |
| 1361.000 | 1.15904E+00 | 1.15904E+00 | 1.00000E+00 |
| 1362.000 | 1.92787E+00 | 1.92787E+00 | 1.00000E+00 |
| 1363.000 | 4.93263E+00 | 4.93263E+00 | 1.00000E+00 |
| 1364.000 | 1.17756E+00 | 1.17756E+00 | 1.00000E+00 |
| 1365.000 | 1.36485E+00 | 1.36485E+00 | 1.00000E+00 |
| 1366.000 | 3.64972E+00 | 3.64972E+00 | 1.00000E+00 |
| 1367.000 | 1.36558E+00 | 1.36558E+00 | 1.00000E+00 |
| 1368.000 | 2.37217E+00 | 2.37217E+00 | 1.00000E+00 |
| 1369.000 | 3.92971E+00 | 3.92971E+00 | 1.00000E+00 |
| 1370.000 | 1.09467E+01 | 1.09467E+01 | 1.00000E+00 |
| 1371.000 | 7.48758E-01 | 7.48758E-01 | 1.00000E+00 |
| 1372.000 | 1.94691E+00 | 1.94691E+00 | 1.00000E+00 |
| 1373.000 | 4.28018E+00 | 4.28018E+00 | 1.00000E+00 |
| 1374.000 | 2.38211E+01 | 2.38211E+01 | 1.00000E+00 |
| 1375.000 | 6.93759E+00 | 6.93759E+00 | 1.00000E+00 |
| 1376.000 | 3.10910E+00 | 3.10910E+00 | 1.00000E+00 |
| 1377.000 | 1.00045E+00 | 1.00045E+00 | 1.00000E+00 |
| 1378.000 | 1.87983E+01 | 1.87983E+01 | 1.00000E+00 |
| 1379.000 | 4.80974E+00 | 4.80974E+00 | 1.00000E+00 |
| 1380.000 | 4.75483E+00 | 4.75483E+00 | 1.00000E+00 |
| 1381.000 | 2.23721E+00 | 2.23721E+00 | 1.00000E+00 |
| 1382.000 | 9.05183E-01 | 9.05183E-01 | 1.00000E+00 |

| | | | |
|---|---|---|---|
| 1383.000 | 4.50860E+00 | 4.50860E+00 | 1.000000E+00 |
| 1384.000 | 5.54623E-01 | 5.54623E-01 | 1.000000E+00 |
| 1385.000 | 1.34371E+00 | 1.34371E+00 | 1.000000E+00 |
| 1386.000 | 4.16357E+00 | 4.16357E+00 | 1.000000E+00 |
| 1387.000 | 1.36458E+00 | 1.36458E+00 | 1.000000E+00 |
| 1388.000 | 3.62125E+01 | 3.62125E+01 | 1.000000E+00 |
| 1389.000 | 5.72267E-01 | 5.72267E-01 | 1.000000E+00 |
| 1390.000 | 1.79653E-01 | 1.79653E-01 | 1.000000E+00 |
| 1391.000 | 2.59142E-01 | 2.59142E-01 | 1.000000E+00 |
| 1392.000 | 1.07243E+00 | 1.07243E+00 | 1.000000E+00 |
| 1393.000 | 3.69383E+00 | 3.69383E+00 | 1.000000E+00 |
| 1394.000 | 3.08501E+01 | 3.08501E+01 | 1.000000E+00 |
| 1395.000 | 3.62771E-01 | 3.62771E-01 | 1.000000E+00 |
| 1396.000 | 1.58172E+01 | 1.58172E+01 | 1.000000E+00 |
| 1397.000 | 3.05903E+00 | 3.05903E+00 | 1.000000E+00 |
| 1398.000 | 6.88549E+00 | 6.88549E+00 | 1.000000E+00 |
| 1399.000 | 6.80172E+00 | 6.80172E+00 | 1.000000E+00 |
| 1400.000 | 0.00000E+00 | 0.00000E+00 | 0.000000E+00 |
| 1401.000 | 9.48532E-01 | 9.48532E-01 | 1.000000E+00 |
| 1402.000 | 5.95644E+00 | 5.95644E+00 | 1.000000E+00 |
| 1403.000 | 1.87639E+01 | 1.87639E+01 | 1.000000E+00 |
| 1404.000 | 9.07179E-01 | 9.07179E-01 | 1.000000E+00 |
| 1405.000 | 3.50098E+00 | 3.50098E+00 | 1.000000E+00 |
| 1406.000 | 6.73114E-01 | 6.73114E-01 | 1.000000E+00 |
| 1407.000 | 1.65800E+00 | 1.65800E+00 | 1.000000E+00 |
| 1408.000 | 8.74078E+00 | 8.74078E+00 | 1.000000E+00 |
| 1409.000 | 3.49122E-01 | 3.49122E-01 | 1.000000E+00 |
| 1410.000 | 9.63469E-01 | 9.63469E-01 | 1.000000E+00 |
| 1411.000 | 3.17645E+00 | 3.17645E+00 | 1.000000E+00 |
| 1412.000 | 4.99567E+00 | 4.99567E+00 | 1.000000E+00 |
| 1413.000 | 4.13811E+00 | 4.13811E+00 | 1.000000E+00 |
| 1414.000 | 8.45761E+00 | 8.45761E+00 | 1.000000E+00 |
| 1415.000 | 9.30865E+00 | 9.30865E+00 | 1.000000E+00 |
| 1416.000 | 2.54099E+00 | 2.54099E+00 | 1.000000E+00 |
| 1417.000 | 4.04784E+00 | 4.04784E+00 | 1.000000E+00 |
| 1418.000 | 3.46084E+00 | 3.46084E+00 | 1.000000E+00 |
| 1419.000 | 2.98809E+00 | 2.98809E+00 | 1.000000E+00 |
| 1420.000 | 4.94160E+00 | 4.94166E+00 | 9.99987E-01 |
| 1421.000 | 2.60295E+00 | 2.60295E+00 | 1.000000E+00 |
| 1422.000 | 1.08224E+01 | 1.08224E+01 | 1.000000E+00 |
| 1423.000 | 5.47053E-01 | 5.47053E-01 | 1.000000E+00 |
| 1424.000 | 2.89356E+01 | 2.89356E+01 | 1.000000E+00 |
| 1425.000 | 1.06869E+00 | 1.06869E+00 | 1.000000E+00 |
| 1426.000 | 9.10098E+00 | 9.10098E+00 | 1.000000E+00 |
| 1427.000 | 3.69490E+00 | 3.69490E+00 | 1.000000E+00 |
| 1428.000 | 1.79583E+01 | 1.79583E+01 | 1.000000E+00 |
| 1429.000 | 6.54150E-01 | 6.54150E-01 | 1.000000E+00 |
| 1430.000 | 4.38541E+00 | 4.38541E+00 | 1.000000E+00 |
| 1431.000 | 6.00209E+00 | 6.00209E+00 | 1.000000E+00 |
| 1432.000 | 7.38474E+00 | 7.38474E+00 | 1.000000E+00 |
| 1433.000 | 7.13336E+00 | 7.13348E+00 | 9.99983E-01 |
| 1434.000 | 1.20316E+00 | 1.20316E+00 | 1.000000E+00 |
| 1435.000 | 5.41976E-01 | 5.41976E-01 | 1.000000E+00 |
| 1436.000 | 4.44542E+00 | 4.44542E+00 | 1.000000E+00 |
| 1437.000 | 1.12698E+00 | 1.12698E+00 | 1.000000E+00 |
| 1438.000 | 3.28615E-01 | 3.28615E-01 | 1.000000E+00 |
| 1439.000 | 4.22170E-03 | 4.22170E-03 | 1.000000E+00 |
| 1440.000 | 4.62808E-02 | 4.62808E-02 | 1.000000E+00 |
| 1441.000 | 5.94327E-01 | 5.94327E-01 | 1.000000E+00 |
| 1442.000 | 6.76779E-01 | 6.76779E-01 | 1.000000E+00 |
| 1443.000 | 1.35578E+00 | 1.35578E+00 | 1.000000E+00 |
| 1444.000 | 2.40511E+00 | 2.40511E+00 | 1.000000E+00 |
| 1445.000 | 1.06470E+01 | 1.06470E+01 | 1.000000E+00 |
| 1446.000 | 1.06088E+01 | 1.06088E+01 | 1.000000E+00 |

| | | | |
|---|---|---|---|
| 1447.000 | 1.54071E+00 | 1.54071E+00 | 1.00000E+00 |
| 1448.000 | 4.07958E+01 | 4.07958E+01 | 1.00000E+00 |
| 1449.000 | 3.58721E+00 | 3.58721E+00 | 1.00000E+00 |
| 1450.000 | 2.82147E+00 | 2.82147E+00 | 1.00000E+00 |
| 1451.000 | 3.77744E+00 | 3.77744E+00 | 1.00000E+00 |
| 1452.000 | 5.77831E+00 | 5.77831E+00 | 1.00000E+00 |
| 1453.000 | 1.32389E+00 | 1.32389E+00 | 1.00000E+00 |
| 1454.000 | 2.54518E+01 | 2.54518E+01 | 1.00000E+00 |
| 1455.000 | 1.60480E+00 | 1.60480E+00 | 1.00000E+00 |
| 1456.000 | 2.56757E+00 | 2.56757E+00 | 1.00000E+00 |
| 1457.000 | 1.75982E+01 | 1.75982E+01 | 1.00000E+00 |
| 1458.000 | 6.09049E+00 | 6.09049E+00 | 1.00000E+00 |
| 1459.000 | 1.96553E+00 | 1.96553E+00 | 1.00000E+00 |
| 1460.000 | 6.45026E-02 | 6.45026E-02 | 1.00000E+00 |
| 1461.000 | 1.80718E-01 | 1.80718E-01 | 1.00000E+00 |
| 1462.000 | 1.21200E-01 | 1.21200E-01 | 1.00000E+00 |
| 1463.000 | 2.92059E+00 | 2.92059E+00 | 1.00000E+00 |
| 1464.000 | 2.68986E-01 | 2.68986E-01 | 1.00000E+00 |
| 1465.000 | 9.75954E+00 | 9.75954E+00 | 1.00000E+00 |
| 1466.000 | 3.61836E+00 | 3.61836E+00 | 1.00000E+00 |
| 1467.000 | 3.24312E+00 | 3.24312E+00 | 1.00000E+00 |
| 1468.000 | 4.27152E+00 | 4.27152E+00 | 1.00000E+00 |
| 1469.000 | 1.42947E-02 | 1.42947E-02 | 1.00000E+00 |
| 1470.000 | 9.88889E-01 | 9.88889E-01 | 1.00000E+00 |
| 1471.000 | 1.29440E+00 | 1.29440E+00 | 1.00000E+00 |
| 1472.000 | 1.20587E+01 | 1.20587E+01 | 1.00000E+00 |
| 1473.000 | 1.97620E+00 | 1.97620E+00 | 1.00000E+00 |
| 1474.000 | 1.31765E+00 | 1.31765E+00 | 1.00000E+00 |
| 1475.000 | 1.26137E+00 | 1.26137E+00 | 1.00000E+00 |
| 1476.000 | 2.62423E+01 | 2.62423E+01 | 1.00000E+00 |
| 1477.000 | 3.52443E+00 | 3.52443E+00 | 1.00000E+00 |
| 1478.000 | 7.80326E+00 | 7.80326E+00 | 1.00000E+00 |
| 1479.000 | 4.15649E+00 | 4.15649E+00 | 1.00000E+00 |
| 1480.000 | 9.04355E+00 | 9.04355E+00 | 1.00000E+00 |
| 1481.000 | 7.16121E+00 | 7.16121E+00 | 1.00000E+00 |
| 1482.000 | 1.75162E+01 | 1.75162E+01 | 1.00000E+00 |
| 1483.000 | 1.41860E+00 | 1.41860E+00 | 1.00000E+00 |
| 1484.000 | 2.35132E+00 | 2.35132E+00 | 1.00000E+00 |
| 1485.000 | 2.18559E+00 | 2.18559E+00 | 1.00000E+00 |
| 1486.000 | 4.50721E+00 | 4.50721E+00 | 1.00000E+00 |
| 1487.000 | 7.21558E+00 | 7.21558E+00 | 1.00000E+00 |
| 1488.000 | 1.65617E+00 | 1.65617E+00 | 1.00000E+00 |
| 1489.000 | 2.64352E+01 | 2.64352E+01 | 1.00000E+00 |
| 1490.000 | 5.02408E+00 | 5.02408E+00 | 1.00000E+00 |
| 1491.000 | 1.80474E+01 | 1.80474E+01 | 1.00000E+00 |
| 1492.000 | 1.33490E-01 | 1.33490E-01 | 1.00000E+00 |
| 1493.000 | 2.60522E-01 | 2.60522E-01 | 1.00000E+00 |
| 1494.000 | 1.10535E-01 | 1.10535E-01 | 1.00000E+00 |
| 1495.000 | 6.34348E-01 | 6.34348E-01 | 1.00000E+00 |
| 1496.000 | 9.13422E+00 | 9.13422E+00 | 1.00000E+00 |
| 1497.000 | 1.77171E-02 | 1.77171E-02 | 1.00000E+00 |
| 1498.000 | 5.05080E+00 | 5.05080E+00 | 1.00000E+00 |
| 1499.000 | 6.30840E+00 | 6.30840E+00 | 1.00000E+00 |
| 1500.000 | 0.00000E+00 | 0.00000E+00 | 0.00000E+00 |
| 1501.000 | 1.96024E+00 | 1.96024E+00 | 1.00000E+00 |
| 1502.000 | 1.69792E+01 | 1.69792E+01 | 1.00000E+00 |
| 1503.000 | 1.48350E+01 | 1.48350E+01 | 1.00000E+00 |
| 1504.000 | 2.76680E-01 | 2.76680E-01 | 1.00000E+00 |
| 1505.000 | 3.43283E+00 | 3.43283E+00 | 1.00000E+00 |
| 1506.000 | 1.04108E+01 | 1.04108E+01 | 1.00000E+00 |
| 1507.000 | 2.05311E+00 | 2.05311E+00 | 1.00000E+00 |
| 1508.000 | 4.13009E+00 | 4.13009E+00 | 1.00000E+00 |
| 1509.000 | 8.85851E+00 | 8.85851E+00 | 1.00000E+00 |
| 1510.000 | 3.34810E+00 | 3.34810E+00 | 1.00000E+00 |

| | | | |
|---|---|---|---|
| 1511.000 | 0.000000E+00 | 0.000000E+00 | 0.000000E+00 |
| 1512.000 | 1.02618E+01 | 1.02618E+01 | 1.000000E+00 |
| 1513.000 | 1.25720E+00 | 1.25720E+00 | 1.000000E+00 |
| 1514.000 | 1.18545E+00 | 1.18545E+00 | 1.000000E+00 |
| 1515.000 | 2.20735E+01 | 2.20735E+01 | 1.000000E+00 |
| 1516.000 | 9.25865E-01 | 9.25865E-01 | 1.000000E+00 |
| 1517.000 | 1.53467E+00 | 1.53467E+00 | 1.000000E+00 |
| 1518.000 | 0.000000E+00 | 0.000000E+00 | 0.000000E+00 |
| 1519.000 | 3.06211E-01 | 3.06211E-01 | 1.000000E+00 |
| 1520.000 | 7.51975E+00 | 7.51975E+00 | 1.000000E+00 |
| 1521.000 | 1.45518E+01 | 1.45518E+01 | 1.000000E+00 |
| 1522.000 | 6.42215E-01 | 6.42215E-01 | 1.000000E+00 |
| 1523.000 | 5.79745E+00 | 5.79745E+00 | 1.000000E+00 |
| 1524.000 | 2.01413E+01 | 2.01413E+01 | 1.000000E+00 |
| 1525.000 | 3.23220E+00 | 3.23220E+00 | 1.000000E+00 |
| 1526.000 | 9.17587E+00 | 9.17587E+00 | 1.000000E+00 |
| 1527.000 | 2.08177E+00 | 2.08177E+00 | 1.000000E+00 |
| 1528.000 | 1.36934E+01 | 1.36934E+01 | 1.000000E+00 |
| 1529.000 | 1.04868E+00 | 1.04868E+00 | 1.000000E+00 |
| 1530.000 | 4.93155E-01 | 4.93155E-01 | 1.000000E+00 |
| 1531.000 | 1.67523E+00 | 1.67523E+00 | 1.000000E+00 |
| 1532.000 | 3.04752E+00 | 3.04752E+00 | 1.000000E+00 |
| 1533.000 | 1.67675E+00 | 1.67675E+00 | 1.000000E+00 |
| 1534.000 | 2.92006E+00 | 2.92006E+00 | 1.000000E+00 |
| 1535.000 | 1.71745E+01 | 1.71745E+01 | 1.000000E+00 |
| 1536.000 | 2.66543E+00 | 2.66543E+00 | 1.000000E+00 |
| 1537.000 | 1.59738E+00 | 1.59738E+00 | 1.000000E+00 |
| 1538.000 | 2.66971E+00 | 2.66971E+00 | 1.000000E+00 |
| 1539.000 | 6.00030E+00 | 6.00030E+00 | 1.000000E+00 |
| 1540.000 | 5.89000E+00 | 5.89000E+00 | 1.000000E+00 |
| 1541.000 | 3.75970E+00 | 3.75970E+00 | 1.000000E+00 |
| 1542.000 | 3.12019E+00 | 3.12019E+00 | 1.000000E+00 |
| 1543.000 | 1.36135E+01 | 1.36135E+01 | 1.000000E+00 |
| 1544.000 | 1.25826E+00 | 1.25826E+00 | 1.000000E+00 |
| 1545.000 | 9.76077E-02 | 9.76077E-02 | 1.000000E+00 |
| 1546.000 | 5.53428E+00 | 5.53428E+00 | 1.000000E+00 |
| 1547.000 | 7.41938E-01 | 7.41938E-01 | 1.000000E+00 |
| 1548.000 | 3.06606E+00 | 3.06606E+00 | 1.000000E+00 |
| 1549.000 | 6.78463E-02 | 6.78463E-02 | 1.000000E+00 |
| 1550.000 | 3.36072E+01 | 3.36072E+01 | 1.000000E+00 |
| 1551.000 | 8.44249E-01 | 8.44249E-01 | 1.000000E+00 |
| 1552.000 | 1.55554E+01 | 1.55554E+01 | 1.000000E+00 |
| 1553.000 | 2.40540E+00 | 2.40540E+00 | 1.000000E+00 |
| 1554.000 | 2.89700E+01 | 2.89700E+01 | 1.000000E+00 |
| 1555.000 | 1.14147E+01 | 1.14147E+01 | 1.000000E+00 |
| 1556.000 | 1.38326E+00 | 1.38326E+00 | 1.000000E+00 |
| 1557.000 | 2.29237E+01 | 2.29237E+01 | 1.000000E+00 |
| 1558.000 | 2.16967E+01 | 2.16967E+01 | 1.000000E+00 |
| 1559.000 | 2.60815E+00 | 2.60815E+00 | 1.000000E+00 |
| 1560.000 | 1.45779E+00 | 1.45779E+00 | 1.000000E+00 |
| 1561.000 | 1.10744E+00 | 1.10744E+00 | 1.000000E+00 |
| 1562.000 | 1.56897E-01 | 1.56897E-01 | 1.000000E+00 |
| 1563.000 | 1.24055E+00 | 1.24055E+00 | 1.000000E+00 |
| 1564.000 | 5.39045E-01 | 5.39045E-01 | 1.000000E+00 |
| 1565.000 | 2.03364E+00 | 2.03364E+00 | 1.000000E+00 |
| 1566.000 | 1.66858E-01 | 1.66858E-01 | 1.000000E+00 |
| 1567.000 | 8.25882E-02 | 8.25882E-02 | 1.000000E+00 |
| 1568.000 | 5.89928E-02 | 5.89928E-02 | 1.000000E+00 |
| 1569.000 | 8.59381E+00 | 8.59381E+00 | 1.000000E+00 |
| 1570.000 | 2.35111E+01 | 2.35111E+01 | 1.000000E+00 |
| 1571.000 | 7.33943E-01 | 7.33943E-01 | 1.000000E+00 |
| 1572.000 | 5.96770E-02 | 5.96770E-02 | 1.000000E+00 |
| 1573.000 | 1.89036E+00 | 1.89036E+00 | 1.000000E+00 |
| 1574.000 | 4.32200E+00 | 4.32200E+00 | 1.000000E+00 |

| | | | |
|---|---|---|---|
| 1575.000 | 1.62977E+00 | 1.62977E+00 | 1.00000E+00 |
| 1576.000 | 3.58765E+01 | 3.58765E+01 | 1.00000E+00 |
| 1577.000 | 1.13359E+00 | 1.13359E+00 | 1.00000E+00 |
| 1578.000 | 5.63042E-01 | 5.63042E-01 | 1.00000E+00 |
| 1579.000 | 1.42818E+00 | 1.42818E+00 | 1.00000E+00 |
| 1580.000 | 6.93692E-03 | 6.93692E-03 | 1.00000E+00 |
| 1581.000 | 6.04183E-01 | 6.04183E-01 | 1.00000E+00 |
| 1582.000 | 9.67389E-01 | 9.67389E-01 | 1.00000E+00 |
| 1583.000 | 6.95920E-01 | 6.95920E-01 | 1.00000E+00 |
| 1584.000 | 1.33052E+00 | 1.33052E+00 | 1.00000E+00 |
| 1585.000 | 2.19100E+00 | 2.19100E+00 | 1.00000E+00 |
| 1586.000 | 2.36583E+00 | 2.36583E+00 | 1.00000E+00 |
| 1587.000 | 2.52772E-02 | 2.52772E-02 | 1.00000E+00 |
| 1588.000 | 2.56486E-02 | 2.56486E-02 | 1.00000E+00 |
| 1589.000 | 1.98087E-01 | 1.98087E-01 | 1.00000E+00 |
| 1590.000 | 2.44470E+00 | 2.44470E+00 | 1.00000E+00 |
| 1591.000 | 1.20109E-01 | 1.20109E-01 | 1.00000E+00 |
| 1592.000 | 1.38977E+00 | 1.38977E+00 | 1.00000E+00 |
| 1593.000 | 5.66975E-02 | 5.66975E-02 | 1.00000E+00 |
| 1594.000 | 1.36945E+01 | 1.36945E+01 | 1.00000E+00 |
| 1595.000 | 3.25157E-01 | 3.25157E-01 | 1.00000E+00 |
| 1596.000 | 1.03167E+01 | 1.03167E+01 | 1.00000E+00 |
| 1597.000 | 3.53996E+00 | 3.53996E+00 | 1.00000E+00 |
| 1598.000 | 2.65836E+00 | 2.65836E+00 | 1.00000E+00 |
| 1599.000 | 3.13754E+00 | 3.13754E+00 | 1.00000E+00 |
| 1600.000 | 0.00000E+00 | 0.00000E+00 | 0.00000E+00 |
| 1601.000 | 0.00000E+00 | 0.00000E+00 | 0.00000E+00 |
| 1602.000 | 0.00000E+00 | 0.00000E+00 | 0.00000E+00 |
| 1603.000 | 0.00000E+00 | 0.00000E+00 | 0.00000E+00 |
| 1604.000 | 0.00000E+00 | 0.00000E+00 | 0.00000E+00 |
| 1605.000 | 0.00000E+00 | 0.00000E+00 | 0.00000E+00 |
| 1606.000 | 3.65400E-02 | 3.65400E-02 | 1.00000E+00 |
| 1607.000 | 1.19082E+00 | 1.19082E+00 | 1.00000E+00 |
| 1608.000 | 1.98817E-02 | 1.98817E-02 | 1.00000E+00 |
| 1609.000 | 3.49140E-01 | 3.49140E-01 | 1.00000E+00 |
| 1610.000 | 9.92137E-01 | 9.92137E-01 | 1.00000E+00 |
| 1611.000 | 5.68216E-02 | 5.68216E-02 | 1.00000E+00 |
| 1612.000 | 3.33059E-01 | 3.33059E-01 | 1.00000E+00 |
| 1613.000 | 5.58445E-02 | 5.58445E-02 | 1.00000E+00 |
| 1614.000 | 4.63323E-02 | 4.63323E-02 | 1.00000E+00 |
| 1615.000 | 3.24835E-01 | 3.24835E-01 | 1.00000E+00 |
| 1616.000 | 2.22102E-01 | 2.22102E-01 | 1.00000E+00 |
| 1617.000 | 7.70902E+00 | 7.70902E+00 | 1.00000E+00 |
| 1618.000 | 8.76572E-01 | 8.76572E-01 | 1.00000E+00 |
| 1619.000 | 4.03113E+00 | 4.03113E+00 | 1.00000E+00 |
| 1620.000 | 6.54550E+00 | 6.54550E+00 | 1.00000E+00 |
| 1621.000 | 2.10217E+00 | 2.10217E+00 | 1.00000E+00 |
| 1622.000 | 8.50472E-01 | 8.50472E-01 | 1.00000E+00 |
| 1623.000 | 1.09675E+01 | 1.09675E+01 | 1.00000E+00 |
| 1624.000 | 5.06665E+00 | 5.06665E+00 | 1.00000E+00 |
| 1625.000 | 4.21380E+00 | 4.21380E+00 | 1.00000E+00 |
| 1626.000 | 2.65934E+00 | 2.65934E+00 | 1.00000E+00 |
| 1627.000 | 9.13476E-02 | 9.13476E-02 | 1.00000E+00 |
| 1628.000 | 5.06546E-01 | 5.06546E-01 | 1.00000E+00 |
| 1629.000 | 1.27911E+00 | 1.27911E+00 | 1.00000E+00 |
| 1630.000 | 5.08249E-02 | 5.08249E-02 | 1.00000E+00 |
| 1631.000 | 1.96072E+00 | 1.96072E+00 | 1.00000E+00 |
| 1632.000 | 8.18773E-01 | 8.18773E-01 | 1.00000E+00 |
| 1633.000 | 1.15823E-01 | 1.15823E-01 | 1.00000E+00 |
| 1634.000 | 4.09511E-02 | 4.09511E-02 | 1.00000E+00 |
| 1635.000 | 1.00955E+01 | 1.00955E+01 | 1.00000E+00 |
| 1636.000 | 1.77971E+01 | 1.77971E+01 | 1.00000E+00 |
| 1637.000 | 2.22788E-03 | 2.22788E-03 | 1.00000E+00 |
| 1638.000 | 3.53122E+00 | 3.53122E+00 | 1.00000E+00 |

| | | | |
|---|---|---|---|
| 1639.000 | 4.50410E-01 | 4.50410E-01 | 1.00000E+00 |
| 1640.000 | 5.67229E-02 | 5.67229E-02 | 1.00000E+00 |
| 1641.000 | 3.81022E-01 | 3.81022E-01 | 1.00000E+00 |
| 1642.000 | 8.63784E+00 | 8.63784E+00 | 1.00000E+00 |
| 1643.000 | 9.00631E-02 | 9.00631E-02 | 1.00000E+00 |
| 1644.000 | 2.89668E+00 | 2.89668E+00 | 1.00000E+00 |
| 1645.000 | 2.17202E-01 | 2.17202E-01 | 1.00000E+00 |
| 1646.000 | 1.03688E+01 | 1.03688E+01 | 1.00000E+00 |
| 1647.000 | 1.04847E+01 | 1.04847E+01 | 1.00000E+00 |
| 1648.000 | 2.30637E+00 | 2.30637E+00 | 1.00000E+00 |
| 1649.000 | 4.26605E-01 | 4.26605E-01 | 1.00000E+00 |
| 1650.000 | 2.06061E+00 | 2.06061E+00 | 1.00000E+00 |
| 1651.000 | 4.16387E-02 | 4.16387E-02 | 1.00000E+00 |
| 1652.000 | 9.00263E+00 | 9.00263E+00 | 1.00000E+00 |
| 1653.000 | 2.16524E+01 | 2.16524E+01 | 1.00000E+00 |
| 1654.000 | 1.27681E-01 | 1.27681E-01 | 1.00000E+00 |
| 1655.000 | 5.75599E+00 | 5.75599E+00 | 1.00000E+00 |
| 1656.000 | 4.79665E-01 | 4.79665E-01 | 1.00000E+00 |
| 1657.000 | 5.62157E+00 | 5.62157E+00 | 1.00000E+00 |
| 1658.000 | 3.19291E+00 | 3.19291E+00 | 1.00000E+00 |
| 1659.000 | 5.52861E-01 | 5.52861E-01 | 1.00000E+00 |
| 1660.000 | 2.70267E-01 | 2.70267E-01 | 1.00000E+00 |
| 1661.000 | 5.15974E+00 | 5.15974E+00 | 1.00000E+00 |
| 1662.000 | 4.19084E-01 | 4.19084E-01 | 1.00000E+00 |
| 1663.000 | 3.76729E+00 | 3.76729E+00 | 1.00000E+00 |
| 1664.000 | 9.95511E-01 | 9.95511E-01 | 1.00000E+00 |
| 1665.000 | 1.38187E-01 | 1.38187E-01 | 1.00000E+00 |
| 1666.000 | 8.27381E-01 | 8.27381E-01 | 1.00000E+00 |
| 1667.000 | 7.84357E-01 | 7.84357E-01 | 1.00000E+00 |
| 1668.000 | 7.59574E+00 | 7.59574E+00 | 1.00000E+00 |
| 1669.000 | 1.05861E+01 | 1.05861E+01 | 1.00000E+00 |
| 1670.000 | 1.78014E-01 | 1.78014E-01 | 1.00000E+00 |
| 1671.000 | 4.66478E+00 | 4.66478E+00 | 1.00000E+00 |
| 1672.000 | 1.43350E+01 | 1.43350E+01 | 1.00000E+00 |
| 1673.000 | 2.58640E+00 | 2.58640E+00 | 1.00000E+00 |
| 1674.000 | 8.03286E-01 | 8.03286E-01 | 1.00000E+00 |
| 1675.000 | 7.82914E-01 | 7.82914E-01 | 1.00000E+00 |
| 1676.000 | 7.85682E+00 | 7.85682E+00 | 1.00000E+00 |
| 1677.000 | 0.00000E+00 | 0.00000E+00 | 0.00000E+00 |
| 1678.000 | 1.41491E-01 | 1.41491E-01 | 1.00000E+00 |
| 1679.000 | 8.10181E-01 | 8.10181E-01 | 1.00000E+00 |
| 1680.000 | 2.31972E+00 | 2.31972E+00 | 1.00000E+00 |
| 1681.000 | 2.63736E+00 | 2.63736E+00 | 1.00000E+00 |
| 1682.000 | 6.11068E-01 | 6.11068E-01 | 1.00000E+00 |
| 1683.000 | 8.81888E-01 | 8.81888E-01 | 1.00000E+00 |
| 1684.000 | 1.21525E+01 | 1.21525E+01 | 1.00000E+00 |
| 1685.000 | 1.01917E+00 | 1.01917E+00 | 1.00000E+00 |
| 1686.000 | 1.67269E+00 | 1.67269E+00 | 1.00000E+00 |
| 1687.000 | 3.89244E-01 | 3.89244E-01 | 1.00000E+00 |
| 1688.000 | 1.49269E+00 | 1.49269E+00 | 1.00000E+00 |
| 1689.000 | 6.49629E-01 | 6.49629E-01 | 1.00000E+00 |
| 1690.000 | 2.80490E+00 | 2.80490E+00 | 1.00000E+00 |
| 1691.000 | 2.84069E-01 | 2.84069E-01 | 1.00000E+00 |
| 1692.000 | 4.99000E+00 | 4.99000E+00 | 1.00000E+00 |
| 1693.000 | 3.52738E-01 | 3.52738E-01 | 1.00000E+00 |
| 1694.000 | 1.61494E+00 | 1.61494E+00 | 1.00000E+00 |
| 1695.000 | 1.06330E+00 | 1.06330E+00 | 1.00000E+00 |
| 1696.000 | 2.06273E+00 | 2.06273E+00 | 1.00000E+00 |
| 1697.000 | 9.85276E-02 | 9.85276E-02 | 1.00000E+00 |
| 1698.000 | 8.42575E-01 | 8.42575E-01 | 1.00000E+00 |
| 1699.000 | 8.57080E-01 | 8.57080E-01 | 1.00000E+00 |
| 1700.000 | 1.49106E+00 | 1.49106E+00 | 1.00000E+00 |
| 1701.000 | 6.23452E+00 | 6.23452E+00 | 1.00000E+00 |
| 1702.000 | 4.07713E+00 | 4.07713E+00 | 1.00000E+00 |

| | | | |
|---|---|---|---|
| 1703.000 | 3.85405E-01 | 3.85405E-01 | 1.000000E+00 |
| 1704.000 | 6.06892E+00 | 6.06892E+00 | 1.000000E+00 |
| 1705.000 | 3.81847E-01 | 3.81847E-01 | 1.000000E+00 |
| 1706.000 | 1.42447E+00 | 1.42447E+00 | 1.000000E+00 |
| 1707.000 | 6.86775E+00 | 6.86775E+00 | 1.000000E+00 |
| 1708.000 | 7.67855E-01 | 7.67855E-01 | 1.000000E+00 |
| 1709.000 | 1.09808E-01 | 1.09808E-01 | 1.000000E+00 |
| 1710.000 | 4.53589E+00 | 4.53589E+00 | 1.000000E+00 |
| 1711.000 | 2.01047E+00 | 2.01047E+00 | 1.000000E+00 |
| 1712.000 | 1.44643E+00 | 1.44643E+00 | 1.000000E+00 |
| 1713.000 | 7.13732E-01 | 7.13732E-01 | 1.000000E+00 |
| 1714.000 | 3.46723E+00 | 3.46723E+00 | 1.000000E+00 |
| 1715.000 | 5.71607E+00 | 5.71607E+00 | 1.000000E+00 |
| 1716.000 | 8.95696E-01 | 8.95696E-01 | 1.000000E+00 |
| 1717.000 | 1.50305E+01 | 1.50305E+01 | 1.000000E+00 |
| 1718.000 | 1.39943E+00 | 1.39943E+00 | 1.000000E+00 |
| 1719.000 | 1.02967E+00 | 1.02967E+00 | 1.000000E+00 |
| 1720.000 | 1.97404E+00 | 1.97404E+00 | 1.000000E+00 |
| 1721.000 | 8.86567E-03 | 8.86567E-03 | 1.000000E+00 |
| 1722.000 | 8.02066E-02 | 8.02066E-02 | 1.000000E+00 |
| 1723.000 | 1.41066E+00 | 1.41073E+00 | 9.99950E-01 |
| 1724.000 | 6.45098E-01 | 6.45236E-01 | 9.99788E-01 |
| 1725.000 | 1.80751E-01 | 1.80845E-01 | 9.99481E-01 |
| 1726.000 | 3.52833E+00 | 3.52843E+00 | 9.99971E-01 |
| 1727.000 | 8.47069E-01 | 8.47180E-01 | 9.99869E-01 |
| 1728.000 | 6.65369E-02 | 6.67604E-02 | 9.96652E-01 |
| 1729.000 | 5.97959E-01 | 5.98098E-01 | 9.99767E-01 |
| 1730.000 | 1.43268E+00 | 1.43282E+00 | 9.99898E-01 |
| 1731.000 | 0.00000E+00 | 1.48463E-04 | 0.00000E+00 |
| 1732.000 | 5.70358E-01 | 5.70519E-01 | 9.99718E-01 |
| 1733.000 | 3.49571E+00 | 3.49603E+00 | 9.99909E-01 |
| 1734.000 | 3.74150E+00 | 3.74200E+00 | 9.99867E-01 |
| 1735.000 | 1.77404E+00 | 1.77422E+00 | 9.99901E-01 |
| 1736.000 | 1.74831E+00 | 1.74849E+00 | 9.99898E-01 |
| 1737.000 | 3.01893E-01 | 3.02243E-01 | 9.98843E-01 |
| 1738.000 | 1.29533E+00 | 1.29550E+00 | 9.99063E-01 |
| 1739.000 | 1.89936E-01 | 1.90106E-01 | 9.99106E-01 |
| 1740.000 | 3.81590E+00 | 3.81606E+00 | 9.99957E-01 |
| 1741.000 | 1.48843E+00 | 1.48859E+00 | 9.99892E-01 |
| 1742.000 | 1.79144E-01 | 1.79552E-01 | 9.97728E-01 |
| 1743.000 | 1.32713E+00 | 1.32759E+00 | 9.99659E-01 |
| 1744.000 | 2.11283E+00 | 2.11300E+00 | 9.99923E-01 |
| 1745.000 | 3.40542E+00 | 3.40553E+00 | 9.99969E-01 |
| 1746.000 | 5.11279E+00 | 5.11287E+00 | 9.99985E-01 |
| 1747.000 | 5.78581E-01 | 5.78674E-01 | 9.99838E-01 |
| 1748.000 | 3.92174E+00 | 3.92177E+00 | 9.99993E-01 |
| 1749.000 | 8.87877E-01 | 8.91162E-01 | 9.96314E-01 |
| 1750.000 | 2.04800E+00 | 2.05121E+00 | 9.98432E-01 |
| 1751.000 | 3.47251E+00 | 3.47354E+00 | 9.99703E-01 |
| 1752.000 | 4.39229E-01 | 4.39695E-01 | 9.98939E-01 |
| 1753.000 | 4.52602E-01 | 4.52839E-01 | 9.99476E-01 |
| 1754.000 | 1.56739E-02 | 1.58575E-02 | 9.88423E-01 |
| 1755.000 | 2.10643E-01 | 2.10811E-01 | 9.99201E-01 |
| 1756.000 | 1.28857E-01 | 1.29039E-01 | 9.98594E-01 |
| 1757.000 | 3.53104E+00 | 3.53122E+00 | 9.99949E-01 |
| 1758.000 | 6.61471E-01 | 6.61827E-01 | 9.99463E-01 |
| 1759.000 | 7.83923E-01 | 7.84121E-01 | 9.99747E-01 |
| 1760.000 | 8.34429E-03 | 8.54158E-03 | 9.76902E-01 |
| 1761.000 | 5.37302E-01 | 5.51454E-01 | 9.74336E-01 |
| 1762.000 | 4.06350E-01 | 4.36468E-01 | 9.30995E-01 |
| 1763.000 | 1.52069E+00 | 1.56131E+00 | 9.73978E-01 |
| 1764.000 | 8.18457E-01 | 8.24397E-01 | 9.92795E-01 |
| 1765.000 | 2.70621E-01 | 2.73823E-01 | 9.88307E-01 |
| 1766.000 | 3.63971E-03 | 7.03741E-03 | 5.17194E-01 |

| | | | |
|---|---|---|---|
| 1767.000 | 2.36387E+00 | 2.37544E+00 | 9.95129E-01 |
| 1768.000 | 3.12219E-01 | 3.47990E-01 | 8.97205E-01 |
| 1769.000 | 7.11829E-01 | 7.32295E-01 | 9.72052E-01 |
| 1770.000 | 4.81842E-02 | 5.15336E-02 | 9.35006E-01 |
| 1771.000 | 5.84502E+00 | 5.84921E+00 | 9.99284E-01 |
| 1772.000 | 1.10088E-01 | 1.13832E-01 | 9.67114E-01 |
| 1773.000 | 1.76433E+00 | 1.77104E+00 | 9.96211E-01 |
| 1774.000 | 0.00000E+00 | 3.23555E-02 | 0.00000E+00 |
| 1775.000 | 3.26191E-01 | 3.46207E-01 | 9.42184E-01 |
| 1776.000 | 6.34503E+00 | 6.34813E+00 | 9.99511E-01 |
| 1777.000 | 1.14224E-01 | 1.19896E-01 | 9.52687E-01 |
| 1778.000 | 3.55445E-01 | 3.59757E-01 | 9.88015E-01 |
| 1779.000 | 3.78915E-01 | 3.84812E-01 | 9.84677E-01 |
| 1780.000 | 5.93729E-02 | 6.65046E-02 | 8.92764E-01 |
| 1781.000 | 1.09182E+01 | 1.09429E+01 | 9.97740E-01 |
| 1782.000 | 6.37737E-01 | 6.46028E-01 | 9.87166E-01 |
| 1783.000 | 3.19332E-01 | 3.23588E-01 | 9.86847E-01 |
| 1784.000 | 6.12795E-01 | 6.16470E-01 | 9.94038E-01 |
| 1785.000 | 4.15211E+00 | 4.15654E+00 | 9.98934E-01 |
| 1786.000 | 1.82267E-02 | 2.42775E-02 | 7.50765E-01 |
| 1787.000 | 3.00468E-01 | 3.08357E-01 | 9.74415E-01 |
| 1788.000 | 2.30814E-02 | 3.29562E-02 | 7.00365E-01 |
| 1789.000 | 3.07053E-01 | 3.09535E-01 | 9.91982E-01 |
| 1790.000 | 2.60637E-01 | 2.62363E-01 | 9.93424E-01 |
| 1791.000 | 1.12933E+00 | 1.13302E+00 | 9.96738E-01 |
| 1792.000 | 1.60189E+00 | 1.60441E+00 | 9.98435E-01 |
| 1793.000 | 0.00000E+00 | 2.39287E-03 | 0.00000E+00 |
| 1794.000 | 1.26756E-01 | 1.28178E-01 | 9.88911E-01 |
| 1795.000 | 2.47246E+00 | 2.47437E+00 | 9.99230E-01 |
| 1796.000 | 1.51992E+00 | 1.52137E+00 | 9.99048E-01 |
| 1797.000 | 0.00000E+00 | 8.33170E-04 | 0.00000E+00 |
| 1798.000 | 2.95031E-01 | 2.96095E-01 | 9.96408E-01 |
| 1799.000 | 2.27006E-01 | 2.27378E-01 | 9.98364E-01 |
| 1800.000 | 1.05009E-01 | 1.05063E-01 | 9.99480E-01 |
| 1801.000 | 5.50507E-01 | 5.52103E-01 | 9.97108E-01 |
| 1802.000 | 9.07571E-01 | 9.08468E-01 | 9.99013E-01 |
| 1803.000 | 4.41250E-02 | 4.65849E-02 | 9.47195E-01 |
| 1804.000 | 4.02199E-01 | 4.05436E-01 | 9.92017E-01 |
| 1805.000 | 5.57743E-02 | 5.81874E-02 | 9.58530E-01 |
| 1806.000 | 1.06030E-01 | 1.09948E-01 | 9.64362E-01 |
| 1807.000 | 6.54641E-02 | 6.77143E-02 | 9.66769E-01 |
| 1808.000 | 9.39334E-01 | 9.43148E-01 | 9.95956E-01 |
| 1809.000 | 3.53548E-01 | 3.57132E-01 | 9.89966E-01 |
| 1810.000 | 1.81256E-01 | 1.82578E-01 | 9.92756E-01 |
| 1811.000 | 2.88085E-01 | 2.91123E-01 | 9.89566E-01 |
| 1812.000 | 5.28765E-01 | 5.33615E-01 | 9.90913E-01 |
| 1813.000 | 5.38344E-01 | 5.42767E-01 | 9.91851E-01 |
| 1814.000 | 6.96320E-02 | 7.21576E-02 | 9.64998E-01 |
| 1815.000 | 3.60905E-01 | 3.62154E-01 | 9.96552E-01 |
| 1816.000 | 1.74420E+00 | 1.74700E+00 | 9.98396E-01 |
| 1817.000 | 5.95463E-01 | 5.99069E-01 | 9.93981E-01 |
| 1818.000 | 1.06555E-01 | 1.10905E-01 | 9.60775E-01 |
| 1819.000 | 8.11432E-02 | 8.41727E-02 | 9.64009E-01 |
| 1820.000 | 1.22200E-01 | 1.24074E-01 | 9.84894E-01 |
| 1821.000 | 1.22204E+00 | 1.22433E+00 | 9.98128E-01 |
| 1822.000 | 0.00000E+00 | 1.49178E-03 | 0.00000E+00 |
| 1823.000 | 3.30423E-01 | 3.31475E-01 | 9.96824E-01 |
| 1824.000 | 0.00000E+00 | 1.53244E-03 | 0.00000E+00 |
| 1825.000 | 7.34788E+00 | 7.34983E+00 | 9.99734E-01 |
| 1826.000 | 5.59237E-01 | 5.60698E-01 | 9.97393E-01 |
| 1827.000 | 2.06592E-03 | 2.76170E-03 | 7.48060E-01 |
| 1828.000 | 1.25790E-01 | 1.27011E-01 | 9.90383E-01 |
| 1829.000 | 0.00000E+00 | 9.65938E-04 | 0.00000E+00 |
| 1830.000 | 9.79816E-01 | 9.80492E-01 | 9.99311E-01 |

| | | | |
|---|---|---|---|
| 1831.000 | 1.81998E-02 | 1.87233E-02 | 9.72040E-01 |
| 1832.000 | 4.72489E-02 | 4.89475E-02 | 9.65297E-01 |
| 1833.000 | 1.44211E+00 | 1.44249E+00 | 9.99732E-01 |
| 1834.000 | 1.25836E-01 | 1.26195E-01 | 9.97155E-01 |
| 1835.000 | 2.14471E+00 | 2.14511E+00 | 9.99809E-01 |
| 1836.000 | 1.24009E-01 | 1.24594E-01 | 9.95303E-01 |
| 1837.000 | 2.27391E+00 | 2.27424E+00 | 9.99855E-01 |
| 1838.000 | 7.30006E-01 | 7.30851E-01 | 9.98844E-01 |
| 1839.000 | 2.37449E-01 | 2.38753E-01 | 9.94539E-01 |
| 1840.000 | 7.88324E-01 | 7.88834E-01 | 9.99353E-01 |
| 1841.000 | 0.00000E+00 | 5.87585E-04 | 0.00000E+00 |
| 1842.000 | 1.23325E+00 | 1.23404E+00 | 9.99360E-01 |
| 1843.000 | 1.18460E-01 | 1.18915E-01 | 9.96172E-01 |
| 1844.000 | 6.67014E+00 | 6.67093E+00 | 9.99881E-01 |
| 1845.000 | 9.29123E-02 | 9.39450E-02 | 9.89007E-01 |
| 1846.000 | 1.39885E+00 | 1.39970E+00 | 9.99396E-01 |
| 1847.000 | 7.21098E-03 | 8.25521E-03 | 8.73507E-01 |
| 1848.000 | 3.90847E-01 | 3.92222E-01 | 9.96494E-01 |
| 1849.000 | 2.26126E-01 | 2.26844E-01 | 9.96834E-01 |
| 1850.000 | 4.76891E-02 | 4.91543E-02 | 9.70193E-01 |
| 1851.000 | 1.62585E-02 | 1.80364E-02 | 9.01424E-01 |
| 1852.000 | 1.10084E+00 | 1.10184E+00 | 9.99091E-01 |
| 1853.000 | 4.60983E-02 | 4.84383E-02 | 9.51692E-01 |
| 1854.000 | 1.25380E-01 | 1.27749E-01 | 9.81456E-01 |
| 1855.000 | 1.21968E-02 | 1.33667E-02 | 9.12476E-01 |
| 1856.000 | 4.79677E-02 | 5.07227E-02 | 9.45685E-01 |
| 1857.000 | 0.00000E+00 | 4.02937E-03 | 0.00000E+00 |
| 1858.000 | 7.68910E-02 | 7.71865E-02 | 9.96172E-01 |
| 1859.000 | 2.79172E+00 | 2.79398E+00 | 9.99189E-01 |
| 1860.000 | 2.05744E-01 | 2.09901E-01 | 9.80194E-01 |
| 1861.000 | 2.13939E-01 | 2.15827E-01 | 9.91251E-01 |
| 1862.000 | 0.00000E+00 | 4.31009E-03 | 0.00000E+00 |
| 1863.000 | 6.80335E-01 | 6.84718E-01 | 9.93600E-01 |
| 1864.000 | 8.70057E-02 | 8.92750E-02 | 9.74580E-01 |
| 1865.000 | 4.17121E-03 | 8.72517E-03 | 4.78066E-01 |
| 1866.000 | 7.13765E-01 | 7.20161E-01 | 9.91118E-01 |
| 1867.000 | 0.00000E+00 | 2.16940E-03 | 0.00000E+00 |
| 1868.000 | 7.90888E-01 | 7.95463E-01 | 9.94248E-01 |
| 1869.000 | 4.76542E+00 | 4.76997E+00 | 9.99045E-01 |
| 1870.000 | 5.42396E-02 | 5.64285E-02 | 9.61209E-01 |
| 1871.000 | 1.06374E+00 | 1.06805E+00 | 9.95963E-01 |
| 1872.000 | 6.62172E-02 | 7.06409E-02 | 9.37378E-01 |
| 1873.000 | 7.45190E-02 | 7.82577E-02 | 9.52226E-01 |
| 1874.000 | 0.00000E+00 | 3.61718E-03 | 0.00000E+00 |
| 1875.000 | 2.39536E-02 | 2.67025E-02 | 8.97055E-01 |
| 1876.000 | 0.00000E+00 | 2.35569E-03 | 0.00000E+00 |
| 1877.000 | 1.87378E-01 | 1.90303E-01 | 9.84628E-01 |
| 1878.000 | 7.49176E-02 | 7.76534E-02 | 9.64769E-01 |
| 1879.000 | 7.65535E-01 | 7.70855E-01 | 9.93098E-01 |
| 1880.000 | 0.00000E+00 | 6.14137E-02 | 0.00000E+00 |
| 1881.000 | 3.77566E-02 | 4.45209E-02 | 8.48064E-01 |
| 1882.000 | 7.71213E-03 | 1.00610E-02 | 7.66535E-01 |
| 1883.000 | 2.87851E-02 | 3.23074E-02 | 8.90977E-01 |
| 1884.000 | 0.00000E+00 | 4.79106E-03 | 0.00000E+00 |
| 1885.000 | 2.91156E-01 | 2.95994E-01 | 9.83655E-01 |
| 1886.000 | 4.00303E-03 | 1.33467E-02 | 2.99926E-01 |
| 1887.000 | 1.66995E-02 | 2.27782E-02 | 7.33136E-01 |
| 1888.000 | 3.13049E-01 | 3.17243E-01 | 9.86780E-01 |
| 1889.000 | 6.97063E-01 | 7.06259E-01 | 9.86979E-01 |
| 1890.000 | 2.67582E+00 | 2.68658E+00 | 9.95997E-01 |
| 1891.000 | 7.58422E-03 | 1.00386E-02 | 7.55504E-01 |
| 1892.000 | 0.00000E+00 | 1.46486E-02 | 0.00000E+00 |
| 1893.000 | 3.55304E-01 | 3.71928E-01 | 9.55301E-01 |
| 1894.000 | 1.19587E+00 | 1.19824E+00 | 9.98018E-01 |

| | | | |
|---|---|---|---|
| 1895.000 | 4.85214E-01 | 5.07330E-01 | 9.56407E-01 |
| 1896.000 | 6.65682E-01 | 6.94408E-01 | 9.58632E-01 |
| 1897.000 | 2.35876E-01 | 2.45456E-01 | 9.60970E-01 |
| 1898.000 | 7.84364E-01 | 8.17657E-01 | 9.59282E-01 |
| 1899.000 | 1.71847E-02 | 6.19393E-02 | 2.77445E-01 |
| 1900.000 | 0.00000E+00 | 0.00000E+00 | 0.00000E+00 |
| 1901.000 | 0.00000E+00 | 4.19259E-03 | 0.00000E+00 |
| 1902.000 | 1.98486E-01 | 2.75055E-01 | 7.21623E-01 |
| 1903.000 | 1.51216E-01 | 1.57577E-01 | 9.59633E-01 |
| 1904.000 | 1.40304E+00 | 1.47278E+00 | 9.52652E-01 |
| 1905.000 | 1.01847E+00 | 1.10719E+00 | 9.19867E-01 |
| 1906.000 | 0.00000E+00 | 4.84099E-03 | 0.00000E+00 |
| 1907.000 | 1.78280E-01 | 2.69957E-01 | 6.60402E-01 |
| 1908.000 | 3.97881E-01 | 5.08360E-01 | 7.82677E-01 |
| 1909.000 | 4.59625E-03 | 6.57398E-03 | 6.99158E-01 |
| 1910.000 | 2.63918E-01 | 3.71504E-01 | 7.10405E-01 |
| 1911.000 | 9.97430E-03 | 1.30021E-01 | 7.67128E-02 |
| 1912.000 | 2.93227E-02 | 3.02075E-02 | 9.70710E-01 |
| 1913.000 | 5.09998E-01 | 6.31047E-01 | 8.08178E-01 |
| 1914.000 | 5.45852E-01 | 6.67978E-01 | 8.17170E-01 |
| 1915.000 | 0.00000E+00 | 4.78757E-04 | 0.00000E+00 |
| 1916.000 | 1.25404E-02 | 1.32782E-01 | 9.44436E-02 |
| 1917.000 | 0.00000E+00 | 1.37823E-01 | 0.00000E+00 |
| 1918.000 | 1.34279E+00 | 1.37823E+00 | 9.74288E-01 |
| 1919.000 | 1.08428E-01 | 2.59693E-01 | 4.17524E-01 |
| 1920.000 | 0.00000E+00 | 1.24519E-01 | 0.00000E+00 |
| 1921.000 | 2.11765E-01 | 2.12679E-01 | 9.95699E-01 |
| 1922.000 | 2.87305E-01 | 3.93720E-01 | 7.29718E-01 |
| 1923.000 | 2.86905E-01 | 3.81471E-01 | 7.52100E-01 |
| 1924.000 | 2.24905E-03 | 2.64389E-03 | 8.50660E-01 |
| 1925.000 | 5.46755E-02 | 1.32876E-01 | 4.11477E-01 |
| 1926.000 | 0.00000E+00 | 6.26287E-02 | 0.00000E+00 |
| 1927.000 | 6.16489E-02 | 6.18205E-02 | 9.97225E-01 |
| 1928.000 | 1.91880E-02 | 6.15466E-02 | 3.11764E-01 |
| 1929.000 | 5.81495E-02 | 8.23522E-02 | 7.06107E-01 |
| 1930.000 | 1.08739E-02 | 1.10664E-02 | 9.82603E-01 |
| 1931.000 | 2.71200E-01 | 2.78577E-01 | 9.73521E-01 |
| 1932.000 | 0.00000E+00 | 7.02642E-02 | 0.00000E+00 |
| 1933.000 | 1.62961E-01 | 8.91872E-01 | 1.82718E-01 |
| 1934.000 | 8.88682E-03 | 1.63266E-01 | 5.44315E-02 |
| 1935.000 | 5.42173E-02 | 1.09817E-01 | 4.93706E-01 |
| 1936.000 | 1.70400E-03 | 2.83015E-02 | 6.02087E-02 |
| 1937.000 | 6.37189E-02 | 6.57602E-02 | 9.68957E-01 |
| 1938.000 | 0.00000E+00 | 1.47807E-02 | 0.00000E+00 |
| 1939.000 | 6.61570E-02 | 6.70924E-02 | 9.86057E-01 |
| 1940.000 | 0.00000E+00 | 1.03276E-02 | 0.00000E+00 |
| 1941.000 | 2.98582E-01 | 3.05806E-01 | 9.76377E-01 |
| 1942.000 | 1.09882E+00 | 1.09937E+00 | 9.99506E-01 |
| 1943.000 | 1.24203E+00 | 1.24531E+00 | 9.97361E-01 |
| 1944.000 | 2.16834E-01 | 2.18387E-01 | 9.92889E-01 |
| 1945.000 | 1.44388E+00 | 1.44393E+00 | 9.99965E-01 |
| 1946.000 | 0.00000E+00 | 9.35463E-04 | 0.00000E+00 |
| 1947.000 | 0.00000E+00 | 1.52335E-03 | 0.00000E+00 |
| 1948.000 | 2.65565E-02 | 2.69938E-02 | 9.83801E-01 |
| 1949.000 | 7.83953E-03 | 1.19467E-02 | 6.56207E-01 |
| 1950.000 | 0.00000E+00 | 0.00000E+00 | 0.00000E+00 |

MAXIMUM OPTICAL DEPTH FOR THE SPECIES OF INTEREST IS 4.0796E+01 WHICH OCCURS AT WAVENUMBER 1448.000
MINIMUM O.D. (NOT COUNTING 0.0) IS 1.5404E-05 WHICH OCCURS AT WAVENUMBER 1235.000

HISTOGRAM OF THE NUMBER OF OPTICAL DEPTHS FOR THE SPECIES OF INTEREST
WHICH FALL INTO THE RANGE IN OPTICAL DEPTH SHOWN IN THE LAST COLUMN.
HISTOGRAM DOES NOT INCLUDE WAVENUMBERS WHERE THE OPTICAL DEPTH IS ZERO.

| BIN NO. | # O.D. | O.D. RANGE FOR BIN | |
|---|---|---|---|
| 1 | 1 | 1.5404E-05 | 6.7598E-05 |
| 2 | 0 | 6.7598E-05 | 2.9664E-04 |
| 3 | 4 | 2.9664E-04 | 1.3018E-03 |
| 4 | 14 | 1.3018E-03 | 5.7125E-03 |
| 5 | 31 | 5.7125E-03 | 2.5068E-02 |
| 6 | 64 | 2.5068E-02 | 1.1001E-01 |
| 7 | 114 | 1.1001E-01 | 4.8275E-01 |
| 8 | 218 | 4.8275E-01 | 2.1185E+00 |
| 9 | 198 | 2.1185E+00 | 9.2965E+00 |
| 10 | 66 | 9.2965E+00 | 4.0796E+01 |

HISTOGRAM OF THE NUMBER OF WAVENUMBERS WITHIN EACH BIN WHERE THE RATIO OF THE
OPTICAL DEPTHS OF THOSE SPECIES OF INTEREST TO THE TOTAL OPTICAL DEPTH OF ALL
MOLECULES ARE GREATER THAN .5000. ALSO SHOWN IS THE LARGEST RATIO IN EACH BIN,
AND THE RANGE IN OPTICAL DEPTH FOR EACH BIN.
THE WAVENUMBER THAT THE MAXIMUM RATIO OCCURS AT IS GIVEN IN THE NEXT TABLE.
WAVENUMBERS WHERE THE OPTICAL DEPTH FOR THE SPECIES OF INTEREST IS ZERO ARE
IGNORED.

| BIN NO. | # O.D. | MAX O.D./TOT | O.D. RANGE FOR BIN | |
|---|---|---|---|---|
| 1 | 0 | 1.8877E-03 | 1.5404E-05 | 6.7598E-05 |
| 2 | 0 | 0.0000E+00 | 6.7598E-05 | 2.9664E-04 |
| 3 | 0 | 3.8616E-01 | 2.9664E-04 | 1.3018E-03 |
| 4 | 6 | 1.0000E+00 | 1.3018E-03 | 5.7125E-03 |
| 5 | 24 | 1.0000E+00 | 5.7125E-03 | 2.5068E-02 |
| 6 | 60 | 1.0000E+00 | 2.5068E-02 | 1.1001E-01 |
| 7 | 113 | 1.0000E+00 | 1.1001E-01 | 4.8275E-01 |
| 8 | 218 | 1.0000E+00 | 4.8275E-01 | 2.1185E+00 |
| 9 | 198 | 1.0000E+00 | 2.1185E+00 | 9.2965E+00 |
| 10 | 66 | 1.0000E+00 | 9.2965E+00 | 4.0796E+01 |

THE FOLLOWING LISTS THE WAVENUMBER WITHIN EACH BIN WHICH HAS THE
LEAST INTERFERENCE FROM OTHER MOLECULES. IF MORE THAN ONE WAVENUMBER
IS LISTED FOR A PARTICULAR BIN, THAT MEANS THAT ALL WAVENUMBERS LISTED
HAVE THE SAME RATIO.

WAVENUMBER 1214.000 IS BEST FOR BIN NUMBER 3
WAVENUMBER 1235.000 IS BEST FOR BIN NUMBER 1
WAVENUMBER 1271.000 IS BEST FOR BIN NUMBER 7
WAVENUMBER 1272.000 IS BEST FOR BIN NUMBER 10
WAVENUMBER 1273.000 IS BEST FOR BIN NUMBER 9
WAVENUMBER 1274.000 IS BEST FOR BIN NUMBER 9
WAVENUMBER 1275.000 IS BEST FOR BIN NUMBER 7
WAVENUMBER 1276.000 IS BEST FOR BIN NUMBER 9
WAVENUMBER 1278.000 IS BEST FOR BIN NUMBER 8
WAVENUMBER 1279.000 IS BEST FOR BIN NUMBER 8
WAVENUMBER 1280.000 IS BEST FOR BIN NUMBER 9
WAVENUMBER 1281.000 IS BEST FOR BIN NUMBER 9
WAVENUMBER 1282.000 IS BEST FOR BIN NUMBER 9
WAVENUMBER 1283.000 IS BEST FOR BIN NUMBER 7

WAVENUMBER 1284.000 IS BEST FOR BIN NUMBER 8
WAVENUMBER 1286.000 IS BEST FOR BIN NUMBER 9
WAVENUMBER 1287.000 IS BEST FOR BIN NUMBER 9
WAVENUMBER 1288.000 IS BEST FOR BIN NUMBER 10
WAVENUMBER 1289.000 IS BEST FOR BIN NUMBER 9
WAVENUMBER 1290.000 IS BEST FOR BIN NUMBER 8
WAVENUMBER 1291.000 IS BEST FOR BIN NUMBER 9
WAVENUMBER 1294.000 IS BEST FOR BIN NUMBER 8
WAVENUMBER 1295.000 IS BEST FOR BIN NUMBER 8
WAVENUMBER 1296.000 IS BEST FOR BIN NUMBER 10
WAVENUMBER 1297.000 IS BEST FOR BIN NUMBER 8
WAVENUMBER 1298.000 IS BEST FOR BIN NUMBER 8
WAVENUMBER 1299.000 IS BEST FOR BIN NUMBER 9
WAVENUMBER 1301.000 IS BEST FOR BIN NUMBER 9
WAVENUMBER 1302.000 IS BEST FOR BIN NUMBER 9
WAVENUMBER 1303.000 IS BEST FOR BIN NUMBER 8
WAVENUMBER 1304.000 IS BEST FOR BIN NUMBER 8
WAVENUMBER 1305.000 IS BEST FOR BIN NUMBER 9
WAVENUMBER 1306.000 IS BEST FOR BIN NUMBER 10
WAVENUMBER 1307.000 IS BEST FOR BIN NUMBER 9
WAVENUMBER 1308.000 IS BEST FOR BIN NUMBER 9
WAVENUMBER 1309.000 IS BEST FOR BIN NUMBER 8
WAVENUMBER 1310.000 IS BEST FOR BIN NUMBER 8
WAVENUMBER 1311.000 IS BEST FOR BIN NUMBER 9
WAVENUMBER 1312.000 IS BEST FOR BIN NUMBER 8
WAVENUMBER 1313.000 IS BEST FOR BIN NUMBER 8
WAVENUMBER 1314.000 IS BEST FOR BIN NUMBER 7
WAVENUMBER 1315.000 IS BEST FOR BIN NUMBER 8
WAVENUMBER 1316.000 IS BEST FOR BIN NUMBER 8
WAVENUMBER 1317.000 IS BEST FOR BIN NUMBER 10
WAVENUMBER 1318.000 IS BEST FOR BIN NUMBER 9
WAVENUMBER 1319.000 IS BEST FOR BIN NUMBER 9
WAVENUMBER 1320.000 IS BEST FOR BIN NUMBER 10
WAVENUMBER 1321.000 IS BEST FOR BIN NUMBER 9
WAVENUMBER 1322.000 IS BEST FOR BIN NUMBER 9
WAVENUMBER 1323.000 IS BEST FOR BIN NUMBER 9
WAVENUMBER 1324.000 IS BEST FOR BIN NUMBER 9
WAVENUMBER 1325.000 IS BEST FOR BIN NUMBER 8
WAVENUMBER 1326.000 IS BEST FOR BIN NUMBER 9
WAVENUMBER 1327.000 IS BEST FOR BIN NUMBER 9
WAVENUMBER 1328.000 IS BEST FOR BIN NUMBER 8
WAVENUMBER 1329.000 IS BEST FOR BIN NUMBER 9
WAVENUMBER 1330.000 IS BEST FOR BIN NUMBER 8
WAVENUMBER 1331.000 IS BEST FOR BIN NUMBER 8
WAVENUMBER 1332.000 IS BEST FOR BIN NUMBER 10
WAVENUMBER 1333.000 IS BEST FOR BIN NUMBER 10
WAVENUMBER 1334.000 IS BEST FOR BIN NUMBER 9
WAVENUMBER 1335.000 IS BEST FOR BIN NUMBER 9
WAVENUMBER 1336.000 IS BEST FOR BIN NUMBER 9
WAVENUMBER 1337.000 IS BEST FOR BIN NUMBER 9
WAVENUMBER 1338.000 IS BEST FOR BIN NUMBER 9
WAVENUMBER 1339.000 IS BEST FOR BIN NUMBER 10
WAVENUMBER 1340.000 IS BEST FOR BIN NUMBER 10
WAVENUMBER 1341.000 IS BEST FOR BIN NUMBER 9
WAVENUMBER 1342.000 IS BEST FOR BIN NUMBER 8
WAVENUMBER 1343.000 IS BEST FOR BIN NUMBER 8
WAVENUMBER 1344.000 IS BEST FOR BIN NUMBER 7
WAVENUMBER 1345.000 IS BEST FOR BIN NUMBER 8
WAVENUMBER 1346.000 IS BEST FOR BIN NUMBER 8
WAVENUMBER 1347.000 IS BEST FOR BIN NUMBER 8
WAVENUMBER 1348.000 IS BEST FOR BIN NUMBER 8
WAVENUMBER 1349.000 IS BEST FOR BIN NUMBER 10
WAVENUMBER 1350.000 IS BEST FOR BIN NUMBER 8
WAVENUMBER 1351.000 IS BEST FOR BIN NUMBER 9

WAVENUMBER 1352.000 IS BEST FOR BIN NUMBER 9
WAVENUMBER 1353.000 IS BEST FOR BIN NUMBER 9
WAVENUMBER 1354.000 IS BEST FOR BIN NUMBER 8
WAVENUMBER 1355.000 IS BEST FOR BIN NUMBER 9
WAVENUMBER 1356.000 IS BEST FOR BIN NUMBER 9
WAVENUMBER 1357.000 IS BEST FOR BIN NUMBER 9
WAVENUMBER 1358.000 IS BEST FOR BIN NUMBER 10
WAVENUMBER 1359.000 IS BEST FOR BIN NUMBER 9
WAVENUMBER 1360.000 IS BEST FOR BIN NUMBER 8
WAVENUMBER 1361.000 IS BEST FOR BIN NUMBER 8
WAVENUMBER 1362.000 IS BEST FOR BIN NUMBER 8
WAVENUMBER 1363.000 IS BEST FOR BIN NUMBER 9
WAVENUMBER 1364.000 IS BEST FOR BIN NUMBER 8
WAVENUMBER 1365.000 IS BEST FOR BIN NUMBER 8
WAVENUMBER 1366.000 IS BEST FOR BIN NUMBER 9
WAVENUMBER 1367.000 IS BEST FOR BIN NUMBER 8
WAVENUMBER 1368.000 IS BEST FOR BIN NUMBER 9
WAVENUMBER 1369.000 IS BEST FOR BIN NUMBER 9
WAVENUMBER 1370.000 IS BEST FOR BIN NUMBER 10
WAVENUMBER 1371.000 IS BEST FOR BIN NUMBER 8
WAVENUMBER 1372.000 IS BEST FOR BIN NUMBER 8
WAVENUMBER 1373.000 IS BEST FOR BIN NUMBER 9
WAVENUMBER 1374.000 IS BEST FOR BIN NUMBER 10
WAVENUMBER 1375.000 IS BEST FOR BIN NUMBER 9
WAVENUMBER 1376.000 IS BEST FOR BIN NUMBER 9
WAVENUMBER 1377.000 IS BEST FOR BIN NUMBER 8
WAVENUMBER 1378.000 IS BEST FOR BIN NUMBER 10
WAVENUMBER 1379.000 IS BEST FOR BIN NUMBER 9
WAVENUMBER 1380.000 IS BEST FOR BIN NUMBER 9
WAVENUMBER 1381.000 IS BEST FOR BIN NUMBER 9
WAVENUMBER 1382.000 IS BEST FOR BIN NUMBER 8
WAVENUMBER 1383.000 IS BEST FOR BIN NUMBER 9
WAVENUMBER 1384.000 IS BEST FOR BIN NUMBER 8
WAVENUMBER 1385.000 IS BEST FOR BIN NUMBER 8
WAVENUMBER 1386.000 IS BEST FOR BIN NUMBER 9
WAVENUMBER 1387.000 IS BEST FOR BIN NUMBER 8
WAVENUMBER 1388.000 IS BEST FOR BIN NUMBER 10
WAVENUMBER 1389.000 IS BEST FOR BIN NUMBER 8
WAVENUMBER 1390.000 IS BEST FOR BIN NUMBER 7
WAVENUMBER 1391.000 IS BEST FOR BIN NUMBER 7
WAVENUMBER 1392.000 IS BEST FOR BIN NUMBER 8
WAVENUMBER 1393.000 IS BEST FOR BIN NUMBER 9
WAVENUMBER 1394.000 IS BEST FOR BIN NUMBER 10
WAVENUMBER 1395.000 IS BEST FOR BIN NUMBER 7
WAVENUMBER 1396.000 IS BEST FOR BIN NUMBER 10
WAVENUMBER 1397.000 IS BEST FOR BIN NUMBER 9
WAVENUMBER 1398.000 IS BEST FOR BIN NUMBER 9
WAVENUMBER 1399.000 IS BEST FOR BIN NUMBER 9
WAVENUMBER 1401.000 IS BEST FOR BIN NUMBER 8
WAVENUMBER 1402.000 IS BEST FOR BIN NUMBER 9
WAVENUMBER 1403.000 IS BEST FOR BIN NUMBER 10
WAVENUMBER 1404.000 IS BEST FOR BIN NUMBER 8
WAVENUMBER 1405.000 IS BEST FOR BIN NUMBER 9
WAVENUMBER 1406.000 IS BEST FOR BIN NUMBER 8
WAVENUMBER 1407.000 IS BEST FOR BIN NUMBER 8
WAVENUMBER 1408.000 IS BEST FOR BIN NUMBER 9
WAVENUMBER 1409.000 IS BEST FOR BIN NUMBER 7
WAVENUMBER 1410.000 IS BEST FOR BIN NUMBER 8
WAVENUMBER 1411.000 IS BEST FOR BIN NUMBER 9
WAVENUMBER 1412.000 IS BEST FOR BIN NUMBER 9
WAVENUMBER 1413.000 IS BEST FOR BIN NUMBER 9
WAVENUMBER 1414.000 IS BEST FOR BIN NUMBER 9
WAVENUMBER 1415.000 IS BEST FOR BIN NUMBER 10
WAVENUMBER 1416.000 IS BEST FOR BIN NUMBER 9

WAVENUMBER 1417.000 IS BEST FOR BIN NUMBER 9
WAVENUMBER 1418.000 IS BEST FOR BIN NUMBER 9
WAVENUMBER 1419.000 IS BEST FOR BIN NUMBER 9
WAVENUMBER 1421.000 IS BEST FOR BIN NUMBER 9
WAVENUMBER 1422.000 IS BEST FOR BIN NUMBER 10
WAVENUMBER 1423.000 IS BEST FOR BIN NUMBER 8
WAVENUMBER 1424.000 IS BEST FOR BIN NUMBER 10
WAVENUMBER 1425.000 IS BEST FOR BIN NUMBER 8
WAVENUMBER 1426.000 IS BEST FOR BIN NUMBER 9
WAVENUMBER 1427.000 IS BEST FOR BIN NUMBER 9
WAVENUMBER 1428.000 IS BEST FOR BIN NUMBER 10
WAVENUMBER 1429.000 IS BEST FOR BIN NUMBER 8
WAVENUMBER 1430.000 IS BEST FOR BIN NUMBER 9
WAVENUMBER 1431.000 IS BEST FOR BIN NUMBER 9
WAVENUMBER 1432.000 IS BEST FOR BIN NUMBER 9
WAVENUMBER 1434.000 IS BEST FOR BIN NUMBER 8
WAVENUMBER 1435.000 IS BEST FOR BIN NUMBER 8
WAVENUMBER 1436.000 IS BEST FOR BIN NUMBER 9
WAVENUMBER 1437.000 IS BEST FOR BIN NUMBER 8
WAVENUMBER 1438.000 IS BEST FOR BIN NUMBER 7
WAVENUMBER 1439.000 IS BEST FOR BIN NUMBER 4
WAVENUMBER 1440.000 IS BEST FOR BIN NUMBER 6
WAVENUMBER 1441.000 IS BEST FOR BIN NUMBER 8
WAVENUMBER 1442.000 IS BEST FOR BIN NUMBER 8
WAVENUMBER 1443.000 IS BEST FOR BIN NUMBER 8
WAVENUMBER 1444.000 IS BEST FOR BIN NUMBER 9
WAVENUMBER 1445.000 IS BEST FOR BIN NUMBER 10
WAVENUMBER 1446.000 IS BEST FOR BIN NUMBER 10
WAVENUMBER 1447.000 IS BEST FOR BIN NUMBER 8
WAVENUMBER 1448.000 IS BEST FOR BIN NUMBER 10
WAVENUMBER 1449.000 IS BEST FOR BIN NUMBER 9
WAVENUMBER 1450.000 IS BEST FOR BIN NUMBER 9
WAVENUMBER 1451.000 IS BEST FOR BIN NUMBER 9
WAVENUMBER 1452.000 IS BEST FOR BIN NUMBER 9
WAVENUMBER 1453.000 IS BEST FOR BIN NUMBER 8
WAVENUMBER 1454.000 IS BEST FOR BIN NUMBER 10
WAVENUMBER 1455.000 IS BEST FOR BIN NUMBER 8
WAVENUMBER 1456.000 IS BEST FOR BIN NUMBER 9
WAVENUMBER 1457.000 IS BEST FOR BIN NUMBER 10
WAVENUMBER 1458.000 IS BEST FOR BIN NUMBER 9
WAVENUMBER 1459.000 IS BEST FOR BIN NUMBER 8
WAVENUMBER 1460.000 IS BEST FOR BIN NUMBER 6
WAVENUMBER 1461.000 IS BEST FOR BIN NUMBER 7
WAVENUMBER 1462.000 IS BEST FOR BIN NUMBER 7
WAVENUMBER 1463.000 IS BEST FOR BIN NUMBER 9
WAVENUMBER 1464.000 IS BEST FOR BIN NUMBER 7
WAVENUMBER 1465.000 IS BEST FOR BIN NUMBER 10
WAVENUMBER 1466.000 IS BEST FOR BIN NUMBER 9
WAVENUMBER 1467.000 IS BEST FOR BIN NUMBER 9
WAVENUMBER 1468.000 IS BEST FOR BIN NUMBER 9
WAVENUMBER 1469.000 IS BEST FOR BIN NUMBER 5
WAVENUMBER 1470.000 IS BEST FOR BIN NUMBER 8
WAVENUMBER 1471.000 IS BEST FOR BIN NUMBER 8
WAVENUMBER 1472.000 IS BEST FOR BIN NUMBER 10
WAVENUMBER 1473.000 IS BEST FOR BIN NUMBER 8
WAVENUMBER 1474.000 IS BEST FOR BIN NUMBER 8
WAVENUMBER 1475.000 IS BEST FOR BIN NUMBER 8
WAVENUMBER 1476.000 IS BEST FOR BIN NUMBER 10
WAVENUMBER 1477.000 IS BEST FOR BIN NUMBER 9
WAVENUMBER 1478.000 IS BEST FOR BIN NUMBER 9
WAVENUMBER 1479.000 IS BEST FOR BIN NUMBER 9
WAVENUMBER 1480.000 IS BEST FOR BIN NUMBER 9
WAVENUMBER 1481.000 IS BEST FOR BIN NUMBER 9
WAVENUMBER 1482.000 IS BEST FOR BIN NUMBER 10

WAVENUMBER 1483.000 IS EST FOR BIN NUMBER 8
WAVENUMBER 1484.000 IS EEST FOR BIN NUMBER 9
WAVENUMBER 1485.000 IS EEST FOR BIN NUMBER 9
WAVENUMBER 1486.000 IS BEST FOR BIN NUMBER 9
WAVENUMBER 1487.000 IS BEST FOR BIN NUMBER
WAVENUMBER 1488.000 IS BEST FOR BIN NUMBER 8
WAVENUMBER 1489.000 IS BEST FOR BIN NUMBER 10
WAVENUMBER 1490.000 IS BEST FOR BIN NUMBER 9
WAVENUMBER 1491.000 IS BEST FOR BIN NUMBER 10
WAVENUMBER 1492.000 IS BEST FOR BIN NUMBER 7
WAVENUMBER 1493.000 IS BEST FOR BIN NUMBER 7
WAVENUMBER 1494.000 IS BEST FOR BIN NUMBER 7
WAVENUMBER 1495.000 IS BEST FOR BIN NUMBER 8
WAVENUMBER 1496.000 IS BEST FOR BIN NUMBER 9
WAVENUMBER 1497.000 IS BEST FOR BIN NUMBER 5
WAVENUMBER 1498.000 IS BEST FOR BIN NUMBER 9
WAVENUMBER 1499.000 IS BEST FOR BIN NUMBER 9
WAVENUMBER 1501.000 IS BEST FOR BIN NUMBER 8
WAVENUMBER 1502.000 IS BEST FOR BIN NUMBER 10
WAVENUMBER 1503.000 IS BEST FOR BIN NUMBER 10
WAVENUMBER 1504.000 IS BEST FOR BIN NUMBER 7
WAVENUMBER 1505.000 IS BEST FOR BIN NUMBER 9
WAVENUMBER 1506.000 IS BEST FOR BIN NUMBER 10
WAVENUMBER 1507.000 IS BEST FOR BIN NUMBER 8
WAVENUMBER 1508.000 IS BEST FOR BIN NUMBER 9
WAVENUMBER 1509.000 IS BEST FOR BIN NUMBER 9
WAVENUMBER 1510.000 IS BEST FOR BIN NUMBER 9
WAVENUMBER 1512.000 IS BEST FOR BIN NUMBER 10
WAVENUMBER 1513.000 IS BEST FOR BIN NUMBER 8
WAVENUMBER 1514.000 IS BEST FOR BIN NUMBER 8
WAVENUMBER 1515.000 IS BEST FOR BIN NUMBER 10
WAVENUMBER 1516.000 IS BEST FOR BIN NUMBER 8
WAVENUMBER 1517.000 IS BEST FOR BIN NUMBER 8
WAVENUMBER 1519.000 IS BEST FOR BIN NUMBER 7
WAVENUMBER 1520.000 IS BEST FOR BIN NUMBER 9
WAVENUMBER 1521.000 IS BEST FOR BIN NUMBER 10
WAVENUMBER 1522.000 IS BEST FOR BIN NUMBER 8
WAVENUMBER 1523.000 IS BEST FOR BIN NUMBER 9
WAVENUMBER 1524.000 IS BEST FOR BIN NUMBER 10
WAVENUMBER 1525.000 IS BEST FOR BIN NUMBER 9
WAVENUMBER 1526.000 IS BEST FOR BIN NUMBER 9
WAVENUMBER 1527.000 IS BEST FOR BIN NUMBER 8
WAVENUMBER 1528.000 IS BEST FOR BIN NUMBER 10
WAVENUMBER 1529.000 IS BEST FOR BIN NUMBER 8
WAVENUMBER 1530.000 IS BEST FOR BIN NUMBER 8
WAVENUMBER 1531.000 IS BEST FOR BIN NUMBER 8
WAVENUMBER 1532.000 IS BEST FOR BIN NUMBER 9
WAVENUMBER 1533.000 IS BEST FOR BIN NUMBER 8
WAVENUMBER 1534.000 IS BEST FOR BIN NUMBER 9
WAVENUMBER 1535.000 IS BEST FOR BIN NUMBER 10
WAVENUMBER 1536.000 IS BEST FOR BIN NUMBER 9
WAVENUMBER 1537.000 IS BEST FOR BIN NUMBER 8
WAVENUMBER 1538.000 IS BEST FOR BIN NUMBER 9
WAVENUMBER 1539.000 IS BEST FOR BIN NUMBER 9
WAVENUMBER 1540.000 IS BEST FOR BIN NUMBER 9
WAVENUMBER 1541.000 IS BEST FOR BIN NUMBER 9
WAVENUMBER 1542.000 IS BEST FOR BIN NUMBER 9
WAVENUMBER 1543.000 IS BEST FOR BIN NUMBER 10
WAVENUMBER 1544.000 IS BEST FOR BIN NUMBER 8
WAVENUMBER 1545.000 IS BEST FOR BIN NUMBER 6
WAVENUMBER 1546.000 IS BEST FOR BIN NUMBER 9
WAVENUMBER 1547.000 IS BEST FOR BIN NUMBER 8
WAVENUMBER 1548.000 IS BEST FOR BIN NUMBER 9
WAVENUMBER 1549.000 IS BEST FOR BIN NUMBER 6

```
WAVENUMBER   1550.000 IS BEST FOR BIN NUMBER 10
WAVENUMBER   1551.000 IS BEST FOR BIN NUMBER  8
WAVENUMBER   1552.000 IS BEST FOR BIN NUMBER 10
WAVENUMBER   1553.000 IS BEST FOR BIN NUMBER  9
WAVENUMBER   1554.000 IS BEST FOR BIN NUMBER 10
WAVENUMBER   1555.000 IS BEST FOR BIN NUMBER 10
WAVENUMBER   1556.000 IS BEST FOR BIN NUMBER  8
WAVENUMBER   1557.000 IS BEST FOR BIN NUMBER 10
WAVENUMBER   1558.000 IS BEST FOR BIN NUMBER 10
WAVENUMBER   1559.000 IS BEST FOR BIN NUMBER  9
WAVENUMBER   1560.000 IS BEST FOR BIN NUMBER  8
WAVENUMBER   1561.000 IS BEST FOR BIN NUMBER  8
WAVENUMBER   1562.000 IS BEST FOR BIN NUMBER  7
WAVENUMBER   1563.000 IS BEST FOR BIN NUMBER  8
WAVENUMBER   1564.000 IS BEST FOR BIN NUMBER  8
WAVENUMBER   1565.000 IS BEST FOR BIN NUMBER  8
WAVENUMBER   1566.000 IS BEST FOR BIN NUMBER  7
WAVENUMBER   1567.000 IS BEST FOR BIN NUMBER  6
WAVENUMBER   1568.000 IS BEST FOR BIN NUMBER  6
WAVENUMBER   1569.000 IS BEST FOR BIN NUMBER  9
WAVENUMBER   1570.000 IS BEST FOR BIN NUMBER 10
WAVENUMBER   1571.000 IS BEST FOR BIN NUMBER  8
WAVENUMBER   1572.000 IS BEST FOR BIN NUMBER  6
WAVENUMBER   1573.000 IS BEST FOR BIN NUMBER  8
WAVENUMBER   1574.000 IS BEST FOR BIN NUMBER  9
WAVENUMBER   1575.000 IS BEST FOR BIN NUMBER  8
WAVENUMBER   1576.000 IS BEST FOR BIN NUMBER 10
WAVENUMBER   1577.000 IS BEST FOR BIN NUMBER  8
WAVENUMBER   1578.000 IS BEST FOR BIN NUMBER  8
WAVENUMBER   1579.000 IS BEST FOR BIN NUMBER  8
WAVENUMBER   1580.000 IS BEST FOR BIN NUMBER  5
WAVENUMBER   1581.000 IS BEST FOR BIN NUMBER  8
WAVENUMBER   1582.000 IS BEST FOR BIN NUMBER  8
WAVENUMBER   1583.000 IS BEST FOR BIN NUMBER  8
WAVENUMBER   1584.000 IS BEST FOR BIN NUMBER  8
WAVENUMBER   1585.000 IS BEST FOR BIN NUMBER  9
WAVENUMBER   1586.000 IS BEST FOR BIN NUMBER  9
WAVENUMBER   1587.000 IS BEST FOR BIN NUMBER  6
WAVENUMBER   1588.000 IS BEST FOR BIN NUMBER  6
WAVENUMBER   1589.000 IS BEST FOR BIN NUMBER  7
WAVENUMBER   1590.000 IS BEST FOR BIN NUMBER  9
WAVENUMBER   1591.000 IS BEST FOR BIN NUMBER  7
WAVENUMBER   1592.000 IS BEST FOR BIN NUMBER  8
WAVENUMBER   1593.000 IS BEST FOR BIN NUMBER  6
WAVENUMBER   1594.000 IS BEST FOR BIN NUMBER 10
WAVENUMBER   1595.000 IS BEST FOR BIN NUMBER  7
WAVENUMBER   1596.000 IS BEST FOR BIN NUMBER 10
WAVENUMBER   1597.000 IS BEST FOR BIN NUMBER  9
WAVENUMBER   1598.000 IS BEST FOR BIN NUMBER  9
WAVENUMBER   1599.000 IS BEST FOR BIN NUMBER  9
WAVENUMBER   1606.000 IS BEST FOR BIN NUMBER  6
WAVENUMBER   1607.000 IS BEST FOR BIN NUMBER  8
WAVENUMBER   1608.000 IS BEST FOR BIN NUMBER  5
WAVENUMBER   1609.000 IS BEST FOR BIN NUMBER  7
WAVENUMBER   1610.000 IS BEST FOR BIN NUMBER  8
WAVENUMBER   1611.000 IS BEST FOR BIN NUMBER  6
WAVENUMBER   1612.000 IS BEST FOR BIN NUMBER  7
WAVENUMBER   1613.000 IS BEST FOR BIN NUMBER  6
WAVENUMBER   1614.000 IS BEST FOR BIN NUMBER  6
WAVENUMBER   1615.000 IS BEST FOR BIN NUMBER  7
WAVENUMBER   1616.000 IS BEST FOR BIN NUMBER  7
WAVENUMBER   1617.000 IS BEST FOR BIN NUMBER  9
WAVENUMBER   1618.000 IS BEST FOR BIN NUMBER  8
WAVENUMBER   1619.000 IS BEST FOR BIN NUMBER  9
```

WAVENUMBER 1620.000 IS BEST FOR BIN NUMBER 9
WAVENUMBER 1621.000 IS BEST FOR BIN NUMBER 8
WAVENUMBER 1622.000 IS BEST FOR BIN NUMBER 8
WAVENUMBER 1623.000 IS BEST FOR BIN NUMBER 10
WAVENUMBER 1624.000 IS BEST FOR BIN NUMBER 9
WAVENUMBER 1625.000 IS BEST FOR BIN NUMBER 9
WAVENUMBER 1626.000 IS BEST FOR BIN NUMBER 9
WAVENUMBER 1627.000 IS BEST FOR BIN NUMBER 6
WAVENUMBER 1628.000 IS BEST FOR BIN NUMBER 8
WAVENUMBER 1629.000 IS BEST FOR BIN NUMBER 8
WAVENUMBER 1630.000 IS BEST FOR BIN NUMBER 6
WAVENUMBER 1631.000 IS BEST FOR BIN NUMBER 8
WAVENUMBER 1632.000 IS BEST FOR BIN NUMBER 8
WAVENUMBER 1633.000 IS BEST FOR BIN NUMBER 7
WAVENUMBER 1634.000 IS BEST FOR BIN NUMBER 6
WAVENUMBER 1635.000 IS BEST FOR BIN NUMBER 10
WAVENUMBER 1636.000 IS BEST FOR BIN NUMBER 10
WAVENUMBER 1637.000 IS BEST FOR BIN NUMBER 4
WAVENUMBER 1638.000 IS BEST FOR BIN NUMBER 9
WAVENUMBER 1639.000 IS BEST FOR BIN NUMBER 7
WAVENUMBER 1640.000 IS BEST FOR BIN NUMBER 6
WAVENUMBER 1641.000 IS BEST FOR BIN NUMBER 7
WAVENUMBER 1642.000 IS BEST FOR BIN NUMBER 9
WAVENUMBER 1643.000 IS BEST FOR BIN NUMBER 6
WAVENUMBER 1644.000 IS BEST FOR BIN NUMBER 9
WAVENUMBER 1645.000 IS BEST FOR BIN NUMBER 7
WAVENUMBER 1646.000 IS BEST FOR BIN NUMBER 10
WAVENUMBER 1647.000 IS BEST FOR BIN NUMBER 10
WAVENUMBER 1648.000 IS BEST FOR BIN NUMBER 9
WAVENUMBER 1649.000 IS BEST FOR BIN NUMBER 7
WAVENUMBER 1650.000 IS BEST FOR BIN NUMBER 8
WAVENUMBER 1651.000 IS BEST FOR BIN NUMBER 6
WAVENUMBER 1652.000 IS BEST FOR BIN NUMBER 9
WAVENUMBER 1653.000 IS BEST FOR BIN NUMBER 10
WAVENUMBER 1654.000 IS BEST FOR BIN NUMBER 7
WAVENUMBER 1655.000 IS BEST FOR BIN NUMBER 9
WAVENUMBER 1656.000 IS BEST FOR BIN NUMBER 7
WAVENUMBER 1657.000 IS BEST FOR BIN NUMBER 9
WAVENUMBER 1658.000 IS BEST FOR BIN NUMBER 9
WAVENUMBER 1659.000 IS BEST FOR BIN NUMBER 8
WAVENUMBER 1660.000 IS BEST FOR BIN NUMBER 7
WAVENUMBER 1661.000 IS BEST FOR BIN NUMBER 9
WAVENUMBER 1662.000 IS BEST FOR BIN NUMBER 7
WAVENUMBER 1663.000 IS BEST FOR BIN NUMBER 9
WAVENUMBER 1664.000 IS BEST FOR BIN NUMBER 8
WAVENUMBER 1665.000 IS BEST FOR BIN NUMBER 7
WAVENUMBER 1666.000 IS BEST FOR BIN NUMBER 8
WAVENUMBER 1667.000 IS BEST FOR BIN NUMBER 8
WAVENUMBER 1668.000 IS BEST FOR BIN NUMBER 9
WAVENUMBER 1669.000 IS BEST FOR BIN NUMBER 10
WAVENUMBER 1670.000 IS BEST FOR BIN NUMBER 7
WAVENUMBER 1671.000 IS BEST FOR BIN NUMBER 9
WAVENUMBER 1672.000 IS BEST FOR BIN NUMBER 10
WAVENUMBER 1673.000 IS BEST FOR BIN NUMBER 9
WAVENUMBER 1674.000 IS BEST FOR BIN NUMBER 8
WAVENUMBER 1675.000 IS BEST FOR BIN NUMBER 8
WAVENUMBER 1676.000 IS BEST FOR BIN NUMBER 9
WAVENUMBER 1678.000 IS BEST FOR BIN NUMBER 7
WAVENUMBER 1679.000 IS BEST FOR BIN NUMBER 8
WAVENUMBER 1680.000 IS BEST FOR BIN NUMBER 9
WAVENUMBER 1681.000 IS BEST FOR BIN NUMBER 9
WAVENUMBER 1682.000 IS BEST FOR BIN NUMBER 8
WAVENUMBER 1683.000 IS BEST FOR BIN NUMBER 8
WAVENUMBER 1684.000 IS BEST FOR BIN NUMBER 10

```
WAVENUMBER   1685.000 IS BEST FOR BIN NUMBER   8
WAVENUMBER   1686.000 IS BEST FOR BIN NUMBER   8
WAVENUMBER   1687.000 IS BEST FOR BIN NUMBER   7
WAVENUMBER   1688.000 IS BEST FOR BIN NUMBER   8
WAVENUMBER   1689.000 IS BEST FOR BIN NUMBER   8
WAVENUMBER   1690.000 IS BEST FOR BIN NUMBER   9
WAVENUMBER   1691.000 IS BEST FOR BIN NUMBER   7
WAVENUMBER   1692.000 IS BEST FOR BIN NUMBER   9
WAVENUMBER   1693.000 IS BEST FOR BIN NUMBER   7
WAVENUMBER   1694.000 IS BEST FOR BIN NUMBER   8
WAVENUMBER   1695.000 IS BEST FOR BIN NUMBER   8
WAVENUMBER   1696.000 IS BEST FOR BIN NUMBER   8
WAVENUMBER   1697.000 IS BEST FOR BIN NUMBER   6
WAVENUMBER   1698.000 IS BEST FOR BIN NUMBER   8
WAVENUMBER   1699.000 IS BEST FOR BIN NUMBER   8
WAVENUMBER   1700.000 IS BEST FOR BIN NUMBER   8
WAVENUMBER   1701.000 IS BEST FOR BIN NUMBER   9
WAVENUMBER   1702.000 IS BEST FOR BIN NUMBER   9
WAVENUMBER   1703.000 IS BEST FOR BIN NUMBER   7
WAVENUMBER   1704.000 IS BEST FOR BIN NUMBER   9
WAVENUMBER   1705.000 IS BEST FOR BIN NUMBER   7
WAVENUMBER   1706.000 IS BEST FOR BIN NUMBER   8
WAVENUMBER   1707.000 IS BEST FOR BIN NUMBER   9
WAVENUMBER   1708.000 IS BEST FOR BIN NUMBER   8
WAVENUMBER   1709.000 IS BEST FOR BIN NUMBER   6
WAVENUMBER   1710.000 IS BEST FOR BIN NUMBER   9
WAVENUMBER   1711.000 IS BEST FOR BIN NUMBER   8
WAVENUMBER   1712.000 IS BEST FOR BIN NUMBER   8
WAVENUMBER   1713.000 IS BEST FOR BIN NUMBER   8
WAVENUMBER   1714.000 IS BEST FOR BIN NUMBER   9
WAVENUMBER   1715.000 IS BEST FOR BIN NUMBER   9
WAVENUMBER   1716.000 IS BEST FOR BIN NUMBER   8
WAVENUMBER   1717.000 IS BEST FOR BIN NUMBER  10
WAVENUMBER   1718.000 IS BEST FOR BIN NUMBER   8
WAVENUMBER   1719.000 IS BEST FOR BIN NUMBER   8
WAVENUMBER   1720.000 IS BEST FOR BIN NUMBER   8
WAVENUMBER   1721.000 IS BEST FOR BIN NUMBER   5
WAVENUMBER   1722.000 IS BEST FOR BIN NUMBER   6
19.33.36.UCLP, AA, LP2     ,       2.304KLNS.
```

# APPENDIX B - USER INSTRUCTION

INSTRUCTIONS FOR PATH CHARACTERIZATION RETRIEVALS .. **RETRVL**

15 March 1990

```
************************************************************
**    These user instructions for the program RETRVL      **
**   describe the records to include in file: RETVCTL     **
************************************************************
```

RECORD 1

HEADER: 80 characters of user identification (A80)

header for file RADDIF0 if used

RECORD 2

```
IRCASE,  IFSEQ,  IDERIV,  ISIMUL,  IFDIF,  JINVRT,  IATMT5,  IFASC3
   10,      20,      30,      40,      50,      60,      70,      80
 7X,I3,   7X,I3,   7X,I3,   7X,I3,   7X,I3,   7X,I3,   7X,I3,   7X,I3
```

IRCASE (0,1) flag for calculation of Reference Case

= 0 no Reference Case calculation
= 1 Reference Case calculated

Note: IRCASE is set to 1 when IFSEQ = 1

(Requires input files T5REF and TAPE3)

IFSEQ (0,1) flag for creation of file T11SEQ which contains the basis for the derivative calculation

= 0 T11SEQ not created
= 1 T11SEQ created

(Requires input files T5REF and TAPE3)

IDERIV (0,1,2) selects desired derivative calculation which creates the file RADERV0

= 0 no derivatives calculated
= 1 radiance derivatives calculated
= 2 brightness temperatire derivatives calculated

(Requires input file T11SEQ)

RECORD 2 (continued)

ISIMUL (0,1) flag for creation of file T11SIM which contains the basis for the difference calculation when real data is not available

= 0 T11SIM not created
= 1 T11SIM created

(Requires input files T5SIM and TAPE3)

IFDIF (0,1,2) selects desired difference calculation which creates the file RADDIF0

= 0 no difference calculated
= 1 radiance difference calculated
= 2 brightness temperatire difference calculated

(Requires input files T11SEQ and T11SIM)

JINVRT (0,1) flag for Parameter Retrieval

= 0 no parameter retrieval
= 1 parameter retrieval performed

(Requires input files RADERV0, RADDIF0, and optionally PARAMIN and ERCOVCG)

IATMT5 (0,1) flag for creation of file T5ITR which contains the FASCOD3 'TAPE5' for use with the next iteration

= 0 T5ITR not created
= 1 T5ITR created

(Requires input files T5REF and PARAMOT)

IFASC3 (0,1) flag for FASCOD3: input from RETVCTL (Records 5.1 - 5.XX)

= 0 no FASCOD3 run
= 1 FASCOD3 run

(Requires input file TAPE3)

**RECORDS 3.1-3.3 (Required if IFSEQ = 1, otherwise omit)**

| RECORD 3.1 | ICNST, | LAYB, | LAYE, | DELSV |
|---|---|---|---|---|
| | 10, | 20, | 30, | 40 |
| | 7X,I3, | 7X,I3, | 7X,I3, | F10.3 |

**ICNST** is the parameter to be retrieved. ICNST is defined as follows

- 0 or -1 ends read of parameters
- 1-28 corresponds to the molecule as used by FASCOD3 i.e. 1 = H2O, 2 = CO2, 3 = O3, ... etc.
- 29 corresponds to the layer temperature
- 30 corresponds to the surface temperature
- 31 corresponds to the surface emissivity (not currently implemented)
- 32 corresponds to the lowest boundary pressure

**LAYB** is the beginning layer for retrieving this parameter

Note: LAYB and LAYE are used for ICNST = 1-29

**LAYE** is the ending layer for retrieving this parameter

**DELSV** is the change that is applied to the state parameter which is used in calculating the derivatives. For ICNST = 1-28, DELSV is a percentage change in the layer column amount of constituent for a layer. For ICNST = 29 and 30, DELSV is the perturbation (K) added to the temperature value. DELSV is calculated internally for the lowest boundary pressure. Defaults are 3 percent (0.03) for ICNST = 1-28, and 2.0 degrees for ICNST = 29 and 30.

RECORD 3.2 NZFLG

10

7X,I3

NZFLG is the total number of layer boundaries which are to be read in to determine the layers to be used. NZFLG = 0 will default to the NLAYRS on T5REF.

RECORD 3.3 (ZLEVP(N),N=1,NZFLG) (Required if NZFLG > 0, otherwize omit)

(8F10.3)

ZLEVP(I) are the layer boundaries which determine how the atmospheric layers on T5REF are combined in order to form the layers for use by RETRVL. ZLEVP must be a subset of the boundaries which are on T5REF.

RECORDS 4.1 - 4.6.3 *** Required for Retrieval Option (JINVRT = 1), ***
*** otherwise omit. ***

RECORD 4.1

JHEADR: 80 characters of user identification (A80)

used by INVERT

RECORD 4.2

| NUMFIL, | NREF, | NPAR, | NEIG, | NPRT, | IREFD, | NSIM |
|---|---|---|---|---|---|---|
| 10, | 20, | 30, | 50, | 60, | 70, | 80 |
| 7X,I3, | 7X,I3, | 7X,I3, | 10X,7X,I3, | 7X,I3, | 7X,I3, | 7X,I3 |

NUMFIL is the number of different frequency regions (files) required for this retrieval. (maximum = 10)

Note: derivatives are RADERV0 - RADERV9
differences are RADDIF0 - RADDIF9

NREF is the index for Reference Constants

= 0 first guess
> 0 output from previous run is available on PARAMIN

NPAR is the total number of parameters to be retreived.

NEIG is the flag for running the Eigen solution: for informational purposes. (0 = NO, 1 = YES)

NPRT is the total number of parameters to be output per page (maximum = 12)

IREFD flag for reference data input

= 0 from derivative file header
= 1 from file PARAMIN

( option 1 is useful for analysis in case using multiple derivatives )

NSIM is the flag for reading simulation data from file PARAMIN.

RECORD 4.3

(IOUT(I),I=1,NPAR)

(20I4)

IOUT(I) selects the parameters and their order for the retrieval.
i.e. in order to use parameters 1-5 in reverse order, simply set IOUT(1) = 5,
IOUT(2) = 4,
IOUT(3) = 3,
... etc.

RECORD 4.4

| IKMAT, | IHMAT, | IHCOR, | IHINV, | IHICR, | IHHIN, | IYVEC, | IDRDI |
|---|---|---|---|---|---|---|---|
| 10, | 20, | 30, | 40, | 50, | 60, | 70, | 80 |
| 7X,I3, | 7X,I3, | 7X,I3, | 7X,I3, | 7X,I3, | 7X,I3, | 7X,I3, | 7X,I3 |

**IKMAT** selects the printing of the K matrix (derivatives and functions)

- = 0 no output
- = 1 abbreviated output
- = 2 full output for number of measurement values < 100
- =-2 will force full output

**IHMAT** selects the printing of the H matrix

- = 0 no output
- = 1 abbreviated output
- = 2 full output

**IHCOR** selects the printing of the correlation H matrix

- = 0 no output
- = 1 abbreviated output
- = 2 full output

**IHINV** selects the printing of the H inverse matrix

- = 0 no output
- = 1 abbreviated output
- = 2 full output

**IHICR** selects the printing of the correlation H inverse matrix

- = 0 no output
- = 1 abbreviated output
- = 2 full output

**IHHIN** selects the printing of the H matrix times H inverse matrix

- = 0 no output
- = 1 abbreviated output
- = 2 full output

**IYVEC** selects the printing of the Y vector

- = 0 no output
- = 1 abbreviated output
- = 2 full output

RECORD 4.4 (continued)

IDRDI selects the printing of the residuals (RD-Rn), (Rn+1-Rn) and (RD-Rn+1)

where RD - measurement
Rn - reference
Rn+1 - linear prediction

= 0 no output
= 1 abbreviated output
= 2 full output for number of measurement values < 100
=-2 will force full output

RECORD 4.5

IGUESS, MXLKHD, IPEIG

10, 20, 30

7X,I3, 7X,I3, 7X,I3

IGUESS determines whether or not an error covariance matrix is read in and used

= 0 not read in or used
= 1 reads diagonal elements
= 2 reads full matrix

MXLKHD selects retrieval method (for MXLKHD = 1, IGUESS must be > 0)

= 0 ridge regression
= 1 maximum likelihood

IPEIG selects the printing of the eigenvalues and eigenvectors (if NEIG = 1)

= 0 no output
= 1 full output

RECORD 4.6

| GAMMA, | NDAMP, | IWGHT, | NOISE, | DSEED |
|---|---|---|---|---|
| 20, | 30, | 40, | 50, | 70 |
| 10X, E10.3, | 7X,I3, | 7X,I3, | 7X,I3, | 7X,E13.0 |

**GAMMA** damping factor applied to all parameters

**NDAMP** number of individual damping factors

**IWGHT** flag for measurement weights

= 0 all weights unity (= 1)
= 1 non-uniform weighting (see Record 4.6.3)

NOISE flag for noise (requires IWGHT = 1 and Record 4.6.3)

= 0 no noise
= 1 Gaussian noise added to radiance

DSEED seed for inital noise value (random number generator)

RECORD 4.6.1 (Required for NDAMP > 0, otherwise omit)

(IDAMP(I),I=1,NDAMP)

(20I4)

IDAMP(I) damping selected for parameter IDAMP(I)

RECORD 4.6.2 (Required for NDAMP > 0, otherwise omit)

(DAMP(I),I=1,NDAMP)

(20I4)

DAMP(I) damping factor for parameter IDAMP(I)
(ordered by parameter per Record 4.6.1)

RECORD 4.6.3 (Required for NWGHT > 0, otherwise omit)

| IWFLG, | IFWGHT, | IBWGHT, | IEWGHT, | WGTFAC, | FREQ, | CHTMP |
|---|---|---|---|---|---|---|
| 5, | 10, | 20, | 30, | 40, | 60, | 70 |
| I5, | I5, | I10, | I10, | G10.3, | G20.8, | G10.3 |

IWFLG flag to determine how weights are applied

=-1 end of weight input data
= 0 read weight (cannot be used with MXLKHD = 1)
= 1 read weight (W = Sn-1)
weights: diagonal elements of the inverse of the measurement error covariance matrix
= 2 Noise: standard deviation
= 3 Noise: standard deviation in brightness temperature converted to standard deviation in radiance

IFWGHT input file to which weights are applied

=-1 apply weights to all measurement values
= # (0-9) apply weights to measurement values on files # (0-9) == (RADERV0 - RADERV9)

IBWGHT beginning point on file for application of weight values (WGTFAC)

IEWGHT ending point on file for application of weight values (WGTFAC)

WGTFAC weighting factor (applied IBWGHT through IEWGHT)

FREQ wavenumber value (cm-1) used in converting brightness temperature noise (standard deviation) to radiance noise (standard deviation)
(Required for IWFLG = 3)

CHTMP average temperature for spectral interval. Used to convert noise standard deviation in brightness temperature to noise standard deviation in radiance. (In microwave region - set CHTMP = 0.0)

RECORDS 5.1-5.XX (Required for IFASC3 = 1, otherwise omit)

These records correspond exactly to a FASCOD3 TAPE5 input file. See FASCOD3 user instructions for a description.

# APPENDIX C - TEST CASE INPUT

TEST CASE 1

```
THREE LAYER TEST CASE FOR PATH CHARACTERIZATION
RCASE=  1 FSEG =  1 DERIV=  2 SIMUL=  1 FDIFF=  2 INVRT=  1 ATMT5=  1 FSCD3=  00
ICNST= 29 LAYB =  1 LAYE =  3       0.50
ICNST= 30         0         0       0.50
       -1
NZFLG=  0
SCRIBE RUN - THREE LAYER TEST CASE
NFIL =  1 NREF =  0 NPAR =  4             NEIG =  0 NPRT = 12 REFD =  0 NSIM =  1
  3   2   1   4   0   0   0   0   0   0   0   0   0   0   0   0   0   0   0   0
KMAT =  1 HMAT =  2 HCOR =  2 HINV =  2 HICOR=  2 HHINV=  1 YVEC =  1 DRDI =  1
IGSS =  0 MXLK =  0 PEIG =  2
  GAMMA =0.0000E+00 NDMP =  0 IWGHT=  0 NOISE=  0 DSEED= 12345678.D+0
```

THE FOLLOWING 2 FILES ARE REQUIRED FASCODE INPUT FILES FOR USE WITH THIS TEST CASE.

T5REF TEST CASE 1

```
$  TEST CASE FOR RETRIVAL CODE
 HI=1 F4=1 CN=1 AE=0 EM=1 SC=1 FI=0 PL=0 TS=0 AM=0 MG=0 LA=0 MS=0 RD=0     0     0
   720.0    725.0       0.    .0137     .100                    .0002     .001
   295.34     1.
    3    7  1.000000 1  SCRIBE ATMOS H1=    5.10 H2=    1.22 ANG= 180.000 LEN= 0
807.05       288.28           99 1   1.22                    2.80
  1.47E+22  1.06E+21  1.07E+17  1.03E+18  4.48E+17  5.45E+18  6.70E+23  2.52E+24
682.68       281.14           0 1                            4.00
  5.83E+21  6.95E+20  7.43E+16  6.74E+17  2.81E+17  3.58E+18  4.40E+23  1.66E+24
592.45       273.39           2 1                            5.10
  2.98E+21  5.69E+20  6.33E+16  5.52E+17  2.25E+17  2.93E+18  3.60E+23  1.36E+24
     0.053     720.0     725.0    1    3             0.0   12    1    1   11
       -1.
%
```

T5SIM (TEST CASE 1)

```
$  TEST CASE FOR RETRIVAL CODE
 HI=1 F4=1 CN=1 AE=0 EM=1 SC=1 FI=0 PL=0 TS=0 AM=0 MG=0 LA=0 MS=0 RD=0     0     0
   720.0     725.0        0.     .0137      .100                        .0002      .001
   295.34      1.
    3    7  1.000000 1  SCRIBE ATMOS H1=     5.10 H2=     1.22 ANG= 180.000 LEN= 0
807.05        288.28             99 1   1.22                        2.80
  1.47E+22  1.06E+21  1.07E+17  1.03E+18  4.48E+17  5.45E+18  6.70E+23  2.52E+24
682.68        281.64              0 1                           4.00
  5.83E+21  6.95E+20  7.43E+16  6.74E+17  2.81E+17  3.58E+18  4.40E+23  1.66E+24
592.45        273.39              2 1                           5.10
  2.98E+21  5.69E+20  6.33E+16  5.52E+17  2.25E+17  2.93E+18  3.60E+23  1.36E+24
     0.053     720.0      725.0     1     3              0.0    12     1     1    11
       -1.
%
```

PARAMIN (ADDITIONAL INPUT FILE NEEDED BY INVERT FOR TEST CASE 1)

1 SCRIBE RUN - THREE LAYER TEST CASE INVRT 90/03/15 0.00.00
0 AER FASCODE PATH CHARACTERIZATION RETRIEVAL

GAMMA = 0.000E+00

| PAR NUM | LAYER & PARAMETER | C0 SV | DEL C1 | C1 SV | REF DATA | SIM DATA | BOUNDARY ALTITUDES LOWER | UPPER |
|---|---|---|---|---|---|---|---|---|
| 1 | 3 TEMP | 273.390000 | .000000 | .000000 | 273.390000 | 273.390000 | 4.000 | 5.100 |
| 2 | 2 TEMP | 281.140000 | .000000 | .000000 | 281.140000 | 281.640000 | 2.800 | 4.000 |
| 3 | 1 TEMP | 288.280000 | .000000 | .000000 | 288.280000 | 288.280000 | 1.220 | 2.800 |
| 4 | SURF TEMP | 295.340000 | .000000 | .000000 | 295.340000 | 295.340000 | 1.220 | 2.800 |

REGION = 1 V1 = 720.000 V2 = 725.000 DV = 1.325E-02 NLIM = 378

TEST CASE 2

```
TWO LAYER TEST CASE FOR PATH CHARACTERIZATION
RCASE=  1 FSEG =  1 DERIV=  2 SIMUL=  1 FDIFF=  2 INVRT=  1 ATMT5=  1 FSCD3=  0
ICNST= 29 LAYB =  1 LAYE =  2       0.50
ICNST= 30         0         0       0.50
       -1
NZFLG=  0
   1.22       4.00       5.10
SCRIBE RUN - TWO LAYER TEST CASE
NFIL =  1 NREF =  0 NPAR =  3           NEIG =  0 NPRT = 12 REFD =  0 NSIM =  1
  2   1   3   0   0   0   0   0   0   0   0   0   0   0   0   0   0   0   0   0
KMAT =  1 HMAT =  2 HCOR =  2 HINV =  2 HICOR=  2 HHINV=  1 YVEC =  1 DRDI =  1
IGSS =  0 MXLK =  0 PEIG =  2
  GAMMA =0.0000E+00 NDMP =  0 IWGHT=  0 NOISE=  0 DSEED= 12345678.D+0
```

THE FOLLOWING 2 FILES ARE REQUIRED FASCODE INPUT FILES FOR USE WITH THIS TEST CASE.

T5REF (TEST CASE 2)

```
$  TEST CASE FOR RETRIVAL CODE
 HI=1 F4=1 CN=1 AE=0 EM=1 SC=1 FI=0 PL=0 TS=0 AM=0 MG=0 LA=0 MS=0 RD=0     0     0
   720.0     725.0        0.     .0137      .100                        .0002      .001
   295.34       1.
    3    7  1.000000 1  SCRIBE ATMOS H1=     5.10 H2=     1.22 ANG= 180.000 LEN= 0
807.05         288.28             99 1   1.22                      2.80
  1.47E+22  1.06E+21  1.07E+17  1.03E+18  4.48E+17  5.45E+18  6.70E+23  2.52E+24
682.68         281.14             0 1                          4.00
  5.83E+21  6.95E+20  7.43E+16  6.74E+17  2.81E+17  3.58E+18  4.40E+23  1.66E+24
592.45         273.39             2 1                          5.10
  2.98E+21  5.69E+20  6.33E+16  5.52E+17  2.25E+17  2.93E+18  3.60E+23  1.36E+24
     0.053      720.0      725.0     1    3              0.0   12     1    1   11
       -1.
%
```

T5SIM (TEST CASE 2)

```
$  TEST CASE FOR RETRIVAL CODE
 HI=1 F4=1 CN=1 AE=0 EM=1 SC=1 FI=0 PL=0 TS=0 AM=0 MG=0 LA=0 MS=0 RD=0     0     0
   720.0    725.0       0.    .0137     .100                    .0002     .001
   295.34     1.
    3    7  1.000000 1  SCRIBE ATMOS H1=    5.10 H2=    1.22 ANG= 180.000 LEN= 0
807.05        288.78           99 1   1.22                  2.80
  1.47E+22  1.06E+21  1.07E+17  1.03E+18  4.48E+17  5.45E+18  6.70E+23  2.52E+24
682.68        281.64           0 1                          4.00
  5.83E+21  6.95E+20  7.43E+16  6.74E+17  2.81E+17  3.58E+18  4.40E+23  1.66E+24
592.45        273.39           2 1                          5.10
  2.98E+21  5.69E+20  6.33E+16  5.52E+17  2.25E+17  2.93E+18  3.60E+23  1.36E+24
    0.053     720.0     725.0    1    3             0.0   12    1    1   11
      -1.
%
```

PARAMIN (ADDITIONAL INPUT FILE NEEDED BY INVERT FOR TEST CASE 2)

1 SCRIBE RUN - TWO LAYER TEST CASE INVRT 90/03/15 0.00.00
0 AER FASCODE PATH CHARACTERIZATION RETRIEVAL

GAMMA = 0.000E+00

| PAR NUM | LAYER & PARAMETER | C0 SV | DEL C1 | C1 SV | REF DATA | SIM DATA | BOUNDARY ALTITUDES LOWER | UPPER |
|---|---|---|---|---|---|---|---|---|
| 1 | 2 TEMP | 273.390000 | .000000 | .000000 | 273.390000 | 273.390000 | 4.000 | 5.100 |
| 2 | 1 TEMP | 285.440000 | .000000 | .000000 | 285.440000 | 285.940000 | 1.220 | 4.000 |
| 3 | SURF TEMP | 295.340000 | .000000 | .000000 | 295.340000 | 295.340000 | 1.220 | 4.000 |

REGION = 1 V1 = 720.000 V2 = 725.000 DV = 1.325E-02 NLIM = 378

# APPENDIX D - TEST CASE OUTPUT

TEST CASE 1 OUTPUT

SCRIBE RUN - THREE LAYER TEST CASE INVRT 90/03/15 14.34.34

TIME ENTERING INVRT 55.4200

K MATRIX

| | 1 | 2 | 3 | 4 | 5 | 374 | 375 | 376 | 377 | 378 |
|---|---|---|---|---|---|---|---|---|---|---|
| 1 | 1.23E-01 | 1.30E-01 | 1.35E-01 | 1.37E-01 | 1.39E-01 | 5.65E-02 | 5.53E-02 | 5.31E-02 | 5.02E-02 | 4.61E-02 |
| 2 | 1.61E-07 | 1.47E-07 | 1.30E-07 | 1.09E-07 | 8.87E-08 | 9.13E-02 | 8.92E-02 | 8.59E-02 | 8.17E-02 | 7.58E-02 |
| 3 | 0.00E+00 | 0.00E+00 | 0.00E+00 | 0.00E+00 | 0.00E+00 | 1.68E-01 | 1.64E-01 | 1.58E-01 | 1.50E-01 | 1.39E-01 |
| 4 | 0.00E+00 | 0.00E+00 | 0.00E+00 | 0.00E+00 | 0.00E+00 | 5.75E-01 | 5.57E-01 | 5.31E-01 | 5.00E-01 | 4.60E-01 |

TEST CASE 1 OUTPUT

SCRIBE RUN - THREE LAYER TEST CASE INVRT 90/03/15 14.34.34

TIME ENTERING INVRT 55.4200

K MATRIX

| | 1 | 2 | 3 | 4 | 5 | 374 | 375 | 376 | 377 | 378 |
|---|---|---|---|---|---|---|---|---|---|---|
| 1 | 1.23E-01 | 1.30E-01 | 1.35E-01 | 1.37E-01 | 1.39E-01 | 5.65E-02 | 5.53E-02 | 5.31E-02 | 5.02E-02 | 4.61E-02 |
| 2 | 1.61E-07 | 1.47E-07 | 1.30E-07 | 1.09E-07 | 8.87E-08 | 9.13E-02 | 8.92E-02 | 8.59E-02 | 8.17E-02 | 7.58E-02 |
| 3 | 0.00E+00 | 0.00E+00 | 0.00E+00 | 0.00E+00 | 0.00E+00 | 1.68E-01 | 1.64E-01 | 1.58E-01 | 1.50E-01 | 1.39E-01 |
| 4 | 0.00E+00 | 0.00E+00 | 0.00E+00 | 0.00E+00 | 0.00E+00 | 5.75E-01 | 5.57E-01 | 5.31E-01 | 5.00E-01 | 4.60E-01 |

TEST CASE 1 OUTPUT

H MATRIX

| | 1 | 2 | 3 | 4 |
|---|---|---|---|---|
| 1 | 5.86E-02 | 2.79E-02 | 1.68E-02 | 2.76E-02 |
| 2 | 2.79E-02 | 2.21E-02 | 1.78E-02 | 3.59E-02 |
| 3 | 1.68E-02 | 1.78E-02 | 1.88E-02 | 4.21E-02 |
| 4 | 2.76E-02 | 3.59E-02 | 4.21E-02 | 1.24E-01 |

TEST CASE 1 OUTPUT

CORRELATION H MATRIX

| | 1 | 2 | 3 | 4 |
|---|---|---|---|---|
| 1 | 1.00000 | .77608 | .50724 | .32335 |
| 2 | .77608 | 1.00000 | .87608 | .68518 |
| 3 | .50724 | .87608 | 1.00000 | .87098 |
| 4 | .32335 | .68518 | .87098 | 1.00000 |

IER(LGINF) = 0

TEST CASE 1 OUTPUT

H INVERSE MATRIX

| | 1 | 2 | 3 | 4 |
|---|---|---|---|---|
| 1 | 6.34E+01 | -1.46E+02 | 7.87E+01 | 1.49E+00 |
| 2 | -1.46E+02 | 5.56E+02 | -4.55E+02 | 2.63E+01 |
| 3 | 7.87E+01 | -4.55E+02 | 6.61E+02 | -1.10E+02 |
| 4 | 1.49E+00 | 2.63E+01 | -1.10E+02 | 3.74E+01 |

TEST CASE 1 OUTPUT

CORRELATION H INVERSE MATRIX

| | 1 | 2 | 3 | 4 |
|---|---|---|---|---|
| 1 | 1.00000 | -.77893 | .38420 | .03050 |
| 2 | -.77893 | 1.00000 | -.75115 | .18229 |
| 3 | .38420 | -.75115 | 1.00000 | -.69961 |
| 4 | .03050 | .18229 | -.69961 | 1.00000 |

TEST CASE 1 OUTPUT

H MATRIX TIMES H INVERSE MATRIX

| | 1 | 2 | 3 | 4 |
|---|---|---|---|---|
| 1 | 2.13E-14 | -5.22E-14 | -5.33E-14 | -9.77E-14 |
| 2 | -1.78E-14 | 1.63E-13 | 1.63E-13 | 1.71E-13 |
| 3 | 9.95E-14 | -9.95E-14 | -5.68E-14 | -1.14E-13 |
| 4 | -2.13E-14 | 0.00E+00 | 7.11E-15 | 0.00E+00 |

TEST CASE 1 OUTPUT

SCRIBE RUN - THREE LAYER TEST CASE INVRT 90/03/15 14.34.34

AER FASCODE PATH CHARACTERIZATION RETRIEVAL

GAMMA = 0.000E+00

| PAR NUM | LAYER & PARAMETER | C0 SV | DEL C1 | C1 SV | PROBABLE ERROR FOR C1 | PERCENT DEL C1/C0 | DAMPING FACTOR | FIT INDEX |
|---|---|---|---|---|---|---|---|---|
| 1 | 3 TEMP | 273.390000 | .000003 | 273.390003 | .000006 | .000001 | 0.000E+00 | 1.000000 |
| 2 | 2 TEMP | 281.140000 | .499994 | 281.639994 | .000017 | .177845 | 0.000E+00 | 1.000000 |
| 3 | 1 TEMP | 288.280000 | -.000005 | 288.279995 | .000018 | -.000002 | 0.000E+00 | 1.000000 |
| 4 | SURF TEMP | 295.340000 | .000002 | 295.340002 | .000004 | .000001 | 0.000E+00 | 1.000000 |

Y VECTOR

| | 1 | 2 | 3 | 4 |
|---|---|---|---|---|
| 1 | 1.39E-02 | 1.10E-02 | 8.92E-03 | 1.79E-02 |



CHANGE IN RADIANCE (SUM OF K*DELTCN)

| | 1 | 2 | 3 | 4 | 5 | 374 | 375 | 376 | 377 | 378 |
|---|---|---|---|---|---|---|---|---|---|---|
| RD-R0 | 8.05E-08 | 7.36E-08 | 6.51E-08 | 5.46E-08 | 4.43E-08 | 4.56E-02 | 4.46E-02 | 4.30E-02 | 4.08E-02 | 3.79E-02 |
| R1-R0 | 4.04E-07 | 4.14E-07 | 4.17E-07 | 4.14E-07 | 4.09E-07 | 4.56E-02 | 4.46E-02 | 4.30E-02 | 4.08E-02 | 3.79E-02 |
| RD-R1 | -3.23E-07 | -3.40E-07 | -3.52E-07 | -3.60E-07 | -3.65E-07 | -4.00E-06 | 4.80E-07 | -4.48E-06 | 9.35E-08 | 1.53E-06 |

NDAT = 378 EQNP = 4.0000 MEAN(0) = 6.4008E-

SIG2(0) = 5.5133E-03 RMS(0) = 7.4252E-02 AVER(0) = 6.4008E-

SIG2(1) = 1.8998E-10 SIG2DAT = 1.8998E-10 SIG2DMP = 0.0000E+00 RMS(1) = 1.3783E-05 AVER(1) = -8.6250E-

PERR(1) = 7.1272E-07 MEAN(1) = 7.1734E-

TEST CASE 1 OUTPUT

SCRIBE RUN - THREE LAYER TEST CASE INVRT 90/03/15 14.34.34

REFERENCE AND SIMULATION DATA

| PAR NUM | LAYER & PARAMETER | REF DATA | DEL DERIV | DIF C1-REF | PERCENT (C1-REF)/REF | SIM DATA | DIF SIM-REF | DIF SIM-C1 |
|---|---|---|---|---|---|---|---|---|
| 1 | 3 TEMP | 273.390000 | .500000 | .000003 | .000001 | 273.390000 | .000000 | -.000003 |
| 2 | 2 TEMP | 281.140000 | .500000 | .499994 | .177845 | 281.640000 | .500000 | .000006 |
| 3 | 1 TEMP | 288.280000 | .500000 | -.000005 | -.000002 | 288.280000 | .000000 | .000005 |
| 4 | SURF TEMP | 295.340000 | .500000 | .000002 | .000001 | 295.340000 | .000000 | -.000002 |

REGION = 1 V1 = 720.000 V2 = 725.000 DV = 1.325E-02 NLIM = 378

TIMING FOR INVRT

| READ | KMAT | EIGN | INVT | MULT | STAT | OUTP |
|---|---|---|---|---|---|---|
| .304 | .074 | .000 | .006 | .035 | .019 | .057 |

TIME LEAVING INVRT 55.9800 TOTAL .5600

TEST CASE 2 OUTPUT

SCRIBE RUN - TWO LAYER TEST CASE INVRT 90/03/15 15.07.05

TIME ENTERING INVRT 134.3390

K MATRIX

| | 1 | 2 | 3 | 4 | 5 | 374 | 375 | 376 | 377 | 378 |
|---|---|---|---|---|---|---|---|---|---|---|
| 1 | 1.23E-01 | 1.30E-01 | 1.35E-01 | 1.37E-01 | 1.39E-01 | 5.65E-02 | 5.53E-02 | 5.31E-02 | 5.02E-02 | 4.61E-02 |
| 2 | 1.61E-07 | 1.47E-07 | 1.30E-07 | 1.09E-07 | 8.87E-08 | 2.59E-01 | 2.53E-01 | 2.43E-01 | 2.31E-01 | 2.14E-01 |
| 3 | 0.00E+00 | 0.00E+00 | 0.00E+00 | 0.00E+00 | 0.00E+00 | 5.75E-01 | 5.57E-01 | 5.31E-01 | 5.00E-01 | 4.60E-01 |

TEST CASE 2 OUTPUT

H MATRIX

| | 1 | 2 | 3 |
|---|---|---|---|
| 1 | 5.86E-02 | 4.47E-02 | 2.76E-02 |
| 2 | 4.47E-02 | 7.64E-02 | 7.79E-02 |
| 3 | 2.76E-02 | 7.79E-02 | 1.24E-01 |

TEST CASE 2 OUTPUT

CORRELATION H MATRIX

| | 1 | 2 | 3 |
|---|---|---|---|
| 1 | 1.00000 | .66798 | .32335 |
| 2 | .66798 | 1.00000 | .79962 |
| 3 | .32335 | .79962 | 1.00000 |

IER(LGINF) = 0

TEST CASE 2 OUTPUT

H INVERSE MATRIX

| | 1 | 2 | 3 |
|---|---|---|---|
| 1 | 3.96E+01 | -3.94E+01 | 1.59E+01 |
| 2 | -3.94E+01 | 7.55E+01 | -3.86E+01 |
| 3 | 1.59E+01 | -3.86E+01 | 2.87E+01 |

TEST CASE 2 OUTPUT

CORRELATION H INVERSE MATRIX

| | 1 | 2 | 3 |
|---|---|---|---|
| 1 | 1.00000 | -.72050 | .47167 |
| 2 | -.72050 | 1.00000 | -.82878 |
| 3 | .47167 | -.82878 | 1.00000 |

TEST CASE 2 OUTPUT

H MATRIX TIMES H INVERSE MATRIX

| | 1 | 2 | 3 |
|---|---|---|---|
| 1 | -3.55E-14 | -5.68E-14 | -4.26E-14 |
| 2 | -7.11E-15 | 2.84E-14 | 5.68E-14 |
| 3 | 3.55E-15 | -1.42E-14 | -1.42E-14 |

TEST CASE 2 OUTPUT

SCRIBE RUN - TWO LAYER TEST CASE INVRT 90/03/15 15.07.05

AER FASCODE PATH CHARACTERIZATION RETRIEVAL

GAMMA = 0.000E+00

| PAR NUM | LAYER & PARAMETER | C0 SV | DEL C1 | C1 SV | PROBABLE ERROR FOR C1 | PERCENT DEL C1/C0 | DAMPING FACTOR | FIT INDEX |
|---|---|---|---|---|---|---|---|---|
| 1 | 2 TEMP | 273.390000 | .000003 | 273.390003 | .000008 | .000001 | 0.000E+00 | 1.000000 |
| 2 | 1 TEMP | 285.440000 | .500005 | 285.940005 | .000011 | .175170 | 0.000E+00 | 1.000000 |
| 3 | SURF TEMP | 295.340000 | -.000001 | 295.339999 | .000007 | .000000 | 0.000E+00 | 1.000000 |

Y VECTOR

| | 1 | 2 | 3 |
|---|---|---|---|
| 1 | 2.23E-02 | 3.82E-02 | 3.89E-02 |

CHANGE IN RADIANCE (SUM OF K*DELTCN)

| | 1 | 2 | 3 | 4 | 5 | 374 | 375 | 376 | 377 | 378 |
|---|---|---|---|---|---|---|---|---|---|---|
| RD-R0 | 8.05E-08 | 7.36E-08 | 6.51E-08 | 5.46E-08 | 4.43E-08 | 1.29E-01 | 1.26E-01 | 1.22E-01 | 1.16E-01 | 1.07E-01 |
| R1-R0 | 4.06E-07 | 4.16E-07 | 4.20E-07 | 4.17E-07 | 4.12E-07 | 1.29E-01 | 1.26E-01 | 1.22E-01 | 1.16E-01 | 1.07E-01 |
| RD-R1 | -3.25E-07 | -3.43E-07 | -3.55E-07 | -3.62E-07 | -3.67E-07 | 3.38E-07 | 3.09E-05 | 9.37E-06 | 3.02E-05 | -3.88E-05 |

NDAT = 378 EQNP = 3.0000 MEAN(0) = 1.2004E-

SIG2(0) = 1.9092E-02 RMS(0) = 1.3817E-01 AVER(0) = 1.2004E-

SIG2(1) = 5.6875E-10 SIG2DAT = 5.6875E-10 SIG2DMP = 0.0000E+00 RMS(1) = 2.3848E-05 AVER(1) = 1.2341E-

PERR(1) = 1.2315E-06 MEAN(1) = 1.7348E-

TEST CASE 2 OUTPUT

SCRIBE RUN - TWO LAYER TEST CASE INVRT 90/03/15 15.07.05

REFERENCE AND SIMULATION DATA

| PAR NUM | LAYER & PARAMETER | REF DATA | DEL DERIV | DIF C1-REF | PERCENT (C1-REF)/REF | SIM DATA | DIF SIM-REF | DIF SIM-C1 |
|---|---|---|---|---|---|---|---|---|
| 1 | 2 TEMP | 273.390000 | .500000 | .000003 | .000001 | 273.390000 | .000000 | -.000003 |
| 2 | 1 TEMP | 285.440000 | .500000 | .500005 | .175170 | 285.940000 | .500000 | -.000005 |
| 3 | SURF TEMP | 295.340000 | .500000 | -.000001 | .000000 | 295.340000 | .000000 | .000001 |

REGION = 1 V1 = 720.000 V2 = 725.000 DV = 1.325E-02 NLIM = 378

TIMING FOR INVRT

| READ | KMAT | EIGN | INVT | MULT | STAT | OUTP |
|---|---|---|---|---|---|---|
| .277 | .055 | .000 | .004 | .026 | .017 | .051 |

TIME LEAVING INVRT 134.8330 TOTAL .4940

# APPENDIX E - RELATED PUBLICATIONS

# VALIDATION OF FASCODE CALCULATIONS WITH HIS SPECTRAL RADIANCE MEASUREMENTS

*Shepard A. Clough and Robert D. Worsham*
Atmospheric and Environmental Research, Inc.
Cambridge, Massachusetts 02139, USA

*William L. Smith, Henry E. Revercomb, Robert O. Knuteson, and Harold W. Woolf*
Space Science and Engineering Center
University of Wisconsin
Madison, Wisconsin 53706, USA

*Gail P. Anderson, Michael L. Hoke, and Francis X. Kneizys*
Air Force Geophysics Laboratory (OPI)
Hanscom AFB, Massachusetts 01731, USA

ABSTRACT

An extended version of FASCODE (Clough et al., 1986) has been utilized in conjunction with the 1986 AFGL line parameters (Rothman et al., 1987) and the line coupling coefficients for carbon dioxide developed by Hoke et al. (1988), to perform spectral radiance comparisons with data from the High-Resolution Interferometer Sounder (HIS) aircraft instrument (Smith et al., 1983). The HIS instrument is a radiometrically calibrated interferometer with a resolution of 0.5 $cm^{-1}$ from 600 to 1000 $cm^{-1}$ and 1 $cm^{-1}$ from 1100 to 2600 $cm^{-1}$. An absolute spectral radiometric accuracy of 1 K with an RMS reproducibility of 0.1 K has been achieved. The measurements of upwelling radiance for this comparison have been made with the instrument mounted on the NASA high altitude aircraft flying at 20 km. The meteorological conditions for the measurements have been established by simultaneous radiosonde measurements. The agreement between the HIS observations and FASCOD2 calculations is generally within 0.5 K in equivalent brightness temperature. In specific spectral regions, significantly greater differences are observed. These differences are attributable to line coupling effects in the carbon dioxide Q branches and to absorption by the fluorocarbons, CFC11 and CFC12. The extended version of FASCODE provides a significant improvement in the agreement between the calculations and the measurements.

## 1. INTRODUCTION

A detailed comparison between measured and calculated upwelling radiances has been undertaken to validate both the results from the High-resolution Interferometer Sounder, HIS, (Smith et al., 1983) and the atmospheric radiance model, FASCODE (Clough et al., 1986). This constitutes an important step in establishing the extent of the retrieval improvement attainable with the HIS instrument operating in space. Special emphasis has been placed on atmospheric spectroscopic issues associated with line coupling; the 2400 $cm^{-1}$ carbon dioxide band edge; and atmospheric window absorption including effects due to water vapor and chlorofluorocarbons in the 800 to 1200 $cm^{-1}$ region.

## 2. RADIANCE MEASUREMENTS AND FASCOD2 CALCULATIONS

The High-resolution Interferometer Sounder, HIS, (Smith et al., 1983) is an accurately calibrated Fourier Transform spectrometer developed to measure the upwelling infrared emission from earth and to establish the attainable improvement in accuracy and vertical resolution for temperature and humidity retrievals. The important characteristics of the instrument are provided in Table 1 and a schematic optical diagram is shown in Fig. 1. Accurate radiometric calibration has been a central focus of the HIS program. Using two blackbody calibration sources, one at 300 K and the other at 245 K, the responsivity of the instrument and the offset radiance are determined at each wavenumber value. The offset radiance is defined as the equivalent system input radiance that is actually due to internal radiative sources, Revercomb et al. (1987). The calibration has been verified by performing measurements on the ground of a third blackbody. Spectral calibration is achieved by laser measurement of retardation using the nominal laser frequency.

An important aspect of the comparison of the observations with calculations relates to the treatment of the line by line radiance calculations to account for instrumental effects. FASCOD2, an accelerated line by line program (Clough et al., 1986), has been used to obtain a calculated radiance spectrum. This radiance spectrum is then transformed to the Fourier domain at a sampling interval consistent

IRS '88
Lenoble and Geleyn (Eds.)

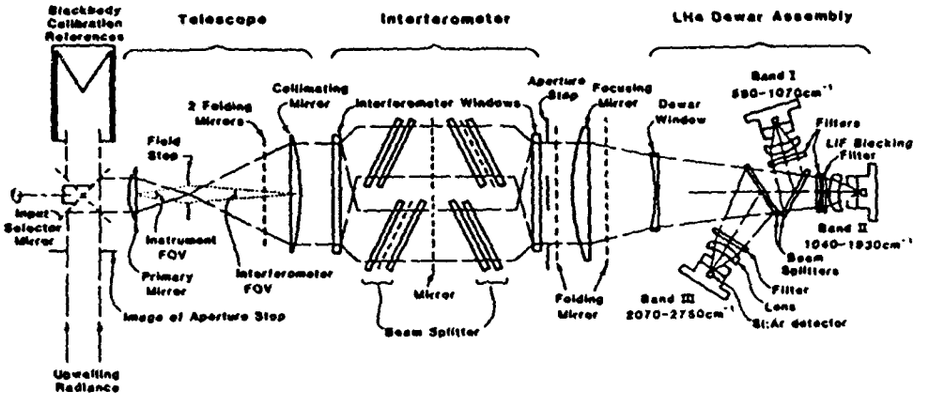


Fig. 1. Functional schematic of HIS optics. Primary, collimating and focusing mirrors are shown as lenses for simplicity.

with the experimental data. A correction is applied to account for the effects of the finite field-of-view, followed by application of the same apodizing function as that used for the experimental interferogram and by truncation to the experimental retardation. Finally, a Fourier transform is performed to obtain the spectrum. The calculated spectral radiances are thus obtained at the identical spectral values as the calibrated experimental spectra, the instrument function having been appropriately taken into account.

Table 1. Characteristics of the HIS Aircraft Instrument

| | |
|---|---|
| Spectra range ($cm^{-1}$)*: | |
| Band I | 590-1070 |
| Band II | 1040-1930 |
| Band III | 2070-2750 |
| Field of view diameter (mr): | |
| Telescope | 100 |
| Interferometer | 10 |
| Blackbody reference sources: | |
| Emissivity | >0.998 |
| Aperture diameter (cm) | 1.5 |
| Temperature stability (K) | ±0.1 |
| Temperatures (K) | 240, 300 |
| Auto-aligned Interferometer: | modified BOMMEM BSDA2.1 |
| Beamsplitter: | |
| Substrate | KCl |
| Coatings (1/4 λ at 3.3 μm | $Ge+Sb_2S_3$ |
| Maximum delay (double sided)-current configuration (cm): | |
| Band I (hardware limit is ±2.0) | ±1.5 |
| Bands II & III (limited by data system) | +1.2,-0.6 |
| Michelson mirror optical scan rate (cm/s): | 0.6-1.0 |
| Aperture stop (at interferometer exit window): | |
| Diameter (cm) | 4.1 |
| Central obscuration area fraction | 0.17 |
| Area ($cm^2$) | 10.8 |
| Area-solid angle product ($cm^2$-sr): | 0.0076 |
| Detectors: | |
| Type | Ar doped Si |
| Diameter (cm) | 0.16 |
| Temperature (K) | 4 |
| Nominal instrument temperature (K): | 260 |

*The ranges shown are de facto ranges. The current bandpass filters were chosen from available stock filters.

The data presented here are from an ER2 flight over the ocean on April 14, 1986 off the California coast. This data set has been chosen primarily because of the greater confidence in the ocean surface properties relative to those for land surface. The atmospheric conditions for this flight represented a relatively dry atmosphere. The calibrated equivalent brightness temperature for a spectral radiance measurement obtained on this flight is shown in Fig. 2. FASCOD2 calculations with 12 atmospheric layers, using available radiosonde measurements of temperature and water vapor and the 1986 HITRAN data base (Rothman et al., 1987), were performed. In Fig. 3 we show the difference between the HIS measurement and the FASCOD2 calculations. The agreement is generally excellent, but a number of spectroscopic issues

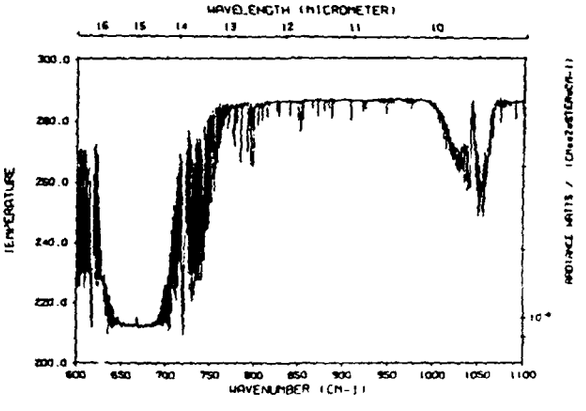


Fig. 2. HIS equivalent brightness spectra: nadir view over ocean from 19.6 km on

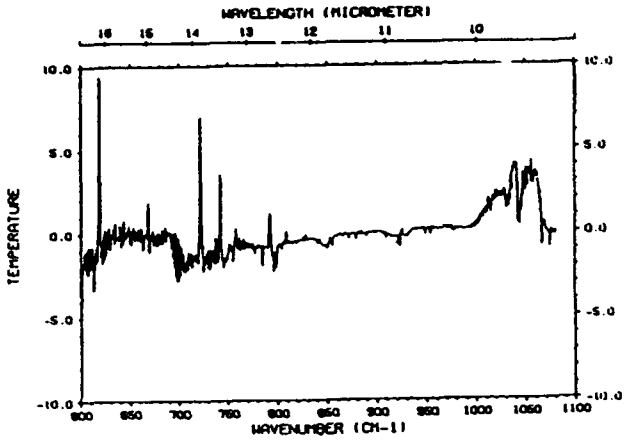


Fig. 3. Difference of equivalent brightness spectra: HIS (April 14, 1986) - FASCOD2.

are clearly evident. The line coupling in the $CO_2$ Q-branches is apparent at 618, 720, 742, and 791 $cm^{-1}$. The spectral feature at 667 $cm^{-1}$ is due to a short path of warmer gas in the instrument pod. The spectral bands due to the chlorofluorocarbons, CFC 11 and CFC 12, are clearly evident centered at 850 $cm^{-1}$ and 920 $cm^{-1}$, respectively. Finally, the deviations of the true ozone profile from that assumed for the calculations, cause the spectral discrepancies from 990 to 1060 $cm^{-1}$.

## 3. EXTENDED FASCODE RADIANCES

An extended version of FASCODE has been developed that treats line mixing effects as a function of temperature and utilizes the cross section data available as part of the HITRAN data base, Massie et al. (1985). The line coupling coefficients for the Q branches of carbon dioxide at 618, 667, 720, 741 and 792 $cm^{-1}$ have been developed by Hoke et al. (1988). The coefficients are provided at four temperatures (200 K, 250 K, 296 K and 340 K) and are incorporated into the FASCODE line file. Linear interpolation is applied in FASCODE to obtain coefficients at the appropriate atmospheric layer temperatures. The cross sections for CFC11 and CFC12 have been utilized in the following manner. The radiances from the extended FASCODE calculations have been attenuated by transmittances, $T(\nu)$, obtained from the relation,

$$T(\nu) = \exp\left(-X_{11}(\nu)\, W_{11} - X_{12}(\nu)\, W_{12}\right)$$

where $X_{11}$ and $X_{12}$ are the wavenumber dependent cross sections for CFC11 and CFC12, and $W_{11}$ and $W_{12}$ are the associated column abundances. This treatment assumes that in the spectral regions affected, that the attenuating species, in this case CFC11 and CFC12, are above the source of radiation and that the attenuating species are cold relative to the radiative source. Further, the temperature dependence of the cross sections is not available and consequently has not been taken into account.

In Fig. 4 the equivalent brightness temperature differences between the extended FASCODE radiance calculation and the FASCOD2 calculation are shown. A sinc function has been used for these calculations with an unappodized resolution of 0.275 $cm^{-1}$ consistent with the HIS retardation for Band I. Comparison of Fig. 4 with Fig. 3 demonstrates that the 618 $cm^{-1}$ Q branch is well modeled by the present treatment supporting the validity of the line coupling coefficients and the treatment of their temperature dependence. The 720 $cm^{-1}$ Q branch is not well modeled which on initial consideration is unexpected since the Q branch is spectroscopically similar to that at 618 $cm^{-1}$. The discrepancy is attributable to incorrect intensities for the weaker carbon dioxide transitions in this spectral region, particularly the isotopic 636 Q branch at 721.5 $cm^{-1}$. The Q branches at 742 $cm^{-1}$ and 791 $cm^{-1}$ may also be affected by a reassessment of the intensities for the weaker carbon dioxide transitions. The spectral feature at 667 $cm^{-1}$ is due to warmer air in the pod area as previously discussed. The spectral features due to CFC11 and CFC12 are well accounted for using values for the column abundances, $W_{11}$ and $W_{12}$, of 3 x $10^5$ (molec/$cm^2$) for both species. The brightness temperature differences on either side of the main 667 $cm^{-1}$ carbon dioxide band and the general trend in the difference from 600 $cm^{-1}$ to 1000 $cm^{-1}$ is not explained. Modification of the temperature profile may be expected to provide some improvement in the comparison.

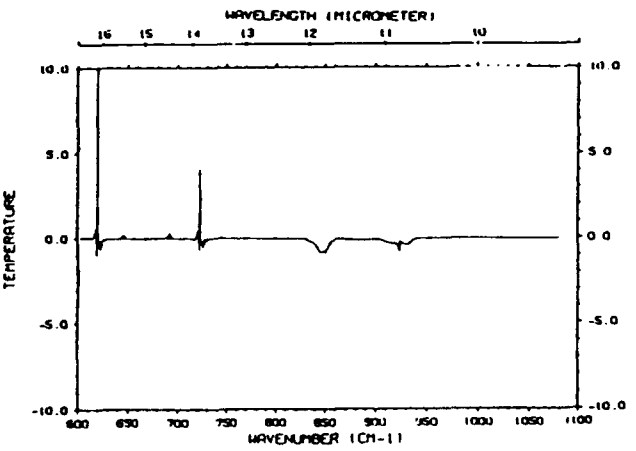


Fig. 4. Difference of equivalent brightness spectra: extended FASCODE (including line coupling and chlorofluorocarbon absorption) - FASCOD2.

Another spectral region of particular interest for remote sensing is the 2385 $cm^{-1}$ region dominated by the high J transitions of carbon dioxide. A comparison of the HIS measurements with FASCOD2 calculations in Fig. 5 indicates reasonable agreement. However, the large increase in the HIS equivalent brightness temperature differences at the higher frequencies is presumably due to scattered sunlight and precludes detailed comparison using radiance calculations for the clear atmosphere.

## 4. CONCLUSIONS

The general agreement between the Band I HIS measurements and the radiance calculations using an extended version of FASCODE is within 2 K between 600 and 1000 $cm^{-1}$. A proper atmospheric profile for ozone would likely extend the agreement to 1100 $cm^{-1}$. Effects of the order of 0.5 K in equivalent brightness temperature such as those attributable to fluorocarbon absorption are unambiguously discernable. A need for improvements in the intensities for the weaker carbon dioxide transitions has been demonstrated.

Evidence indicates that the absolute error in the HIS measured brightness temperatures is better than 1 K and that the relative error in the spectral regions with the highest signal to noise ratio is of the order of 0.1 K. Further improvements in the model will require improved line intensities and further study of the line shape for carbon dioxide to explain the systematic differences of up to 2 K in the 618 $cm^{-1}$ and the 720 $cm^{-1}$ spectral region. No inferences regarding the validity of the water vapor continuum can be drawn from the present comparison.

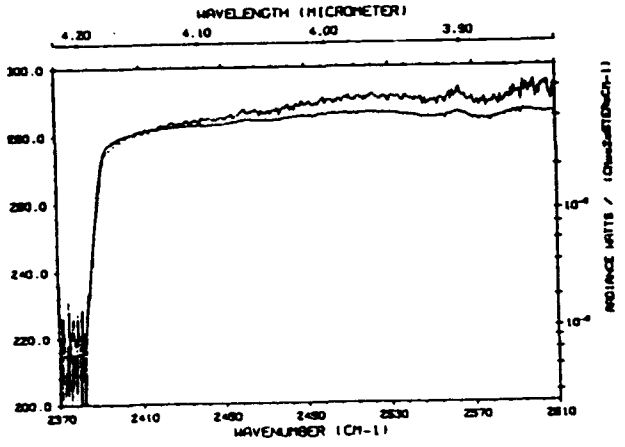


Fig. 5. Equivalent brightness temperature in the 2400 $cm^{-1}$ region: measured (HIS, curve with higher spectral content) and calculated (FASCOD2).

## REFERENCES

Clough, S.A., F.X. Kneizys, E.P. Shettle, and G.P. Anderson, 1986: Atmospheric radiance and transmittance: FASCOD2. Proceedings of the Sixth Conference on Atmospheric Radiance, Williamsburg, VA.

Hoke, M.L., S.A. Clough, W. Lafferty, and B. Olson, 1988: Line coupling in oxygen and carbon dioxide. International Radiation Symposium, Lille, France.

Massie, S.T., A. Goldman, D.G. Murcray and J.C. Gille, 1985: Approximate Absorption Cross Sections of F12, F11, $ClONO_2$, $N_2O_5$, $HNO_3$, $CCl_4$, $CF_4$, F21, F113, F114, $HNO_4$. Appl. Opt., 24, 3426.

Revercomb, H.E., H. Buijs,, H.B. Howell, D.D. LaPorte, W.L. Smith and L.A. Sromovsky, 1988: Radiometric calibration of IR spectrometers: solution to a problem with the High-Resolution Interferometer Sounder. Appl. Opt., 27, 3210-3218.

Rothman, L.S., R.R. Gamache, A. Goldman, L.R. Brown, R.A. Toth, H.M. Pickett, R.L. Poynter, J.-M. Flaud, C. Camy-Peyret, A. Barbe, N. Husson, C.P. Rinsland, and M.A.H. Smith, 1987: The HITRAN Database: 1986 Edition. Appl. Opt., 26, 4058-4097.

Smith, W.L., H.E. Revercomb, H.B. Howell, and H.M. Woolf, 1983: HIS - A Satellite Instrument to Observe Temperature and Moisture Profiles with High Vertical Resolution Fifth Conference on Atmospheric Radiation, American Meteorological Society, Boston, Mass.

*Atmospheric Research*, 23 (1989) 229-241
Elsevier Science Publishers B.V., Amsterdam — Printed in The Netherlands



# Line Shape and the Water Vapor Continuum

S.A. CLOUGH, F.X. KNEIZYS and R.W. DAVIES

*Atmospheric and Environmental Research, Inc., Cambridge, MA 02139 (U.S.A.)*
*Air Force Geophysics Laboratory, Hanscom AFB, MA 01731 (U.S.A.)*
*GTE Laboratories, Waltham, MA 02154 (U.S.A.)*

(Received May 1, 1988; accepted June 1, 1989)

ABSTRACT

Clough, S.A., Kneizys, F.X. and Davies, R.W., 1989. Line shape and the water vapor continuum. Atmos. Res., 23: 229-241.

A formulation is developed in which the contribution of the far wings of collisionally broadened spectral lines to the water vapor continuum absorption is established. The effects of deviations from the impact (Lorentz) line shape due to duration of collision effects are treated semi-empirically to provide agreement with experimental results for the continuum absorption and its temperature-dependence. The continua due to both water-water molecular broadening (self-broadening) and water-air molecular broadening (foreign broadening) are discussed. Several atmospheric validations of the present approach are presented.

RESUME

On développe une formulation dans laquelle on établit la contribution des ailes éloignées des raies élargies par collision au continuum d'absorption de la vapeur d'eau. Les effets des déviations de la forme de raie d'impact (Lorentz) sont traités de façon semi-empirique pour fournir un accord avec les résultats expérimentaux concernant le continuum d'absorption et sa dépendence en température. Les continua dûs à l'effet d'élargissement moléculaire eau-eau (self broadening) et air-eau (foreign broadening) sont discutés. Plusieurs validations atmosphériques de cette approche sont présentées.

## INTRODUCTION

The continuum absorption due to water vapor has posed a complex problem for researchers concerned with atmospheric radiative problems. In fact, a universally accepted definition of continuum absorption has not been established making more difficult the discussion of the effect. The regions of the atmos-

0169-8095/89/$03.50 

pheric spectrum in the microwave and the infrared with the greatest transparency, the windows, are strongly dependent on the water vapor continuum. These spectral regions are at 0 $cm^{-1}$, 800–1200 $cm^{-1}$ and 2000–3000 $cm^{-1}$. Laboratory measurements of the water vapor continuum are made difficult by the long path lengths required with conventional spectroscopic techniques or by the complexities encountered with methods of high sensitivity such as spectrophone detection. Atmospheric measurements are adversely affected by the difficulty in adequately characterizing the path, aerosol attenuation, turbulence, scintillation and instrument calibration. From a theoretical point of view, the continuum has posed a comparably complex problem and still lacks a completely satisfactory explanation. The issue of whether the absorption represents an excess or deficiency is fundamentally dependent on the line shape formulation chosen as reference as well as on the frequency regime of interest. A theoretical understanding of this problem entails a satisfactory description of the line shape and its temperature-dependence from line center to the far line wing requiring a proper treatment of the physical processes occurring in the time associated with the duration of collision. Further, an adequate model must also address the issue of collision-induced spectra as well as the possibility of dimer absorption.

## LINE SHAPE FORMULATION

In our consideration of the continuum, we start with a line shape formulation for the absorption coefficient $k(\nu)$ ($cm^2$/molec.), that is applicable from the microwave to the infrared (Clough et al., 1983):

$$k(\nu) = R(\nu)\langle \phi(\nu) + \phi(-\nu) \rangle \tag{1}$$

with:

$$R(\nu) = \nu \frac{1 - e^{-\beta\nu}}{1 + e^{-\beta\nu}} \tag{2}$$

$$= \nu \tanh(\beta\nu/2) \tag{3}$$

where $\nu$ is the wavenumber value, $R(\nu)$ ($cm^{-1}$) is a radiation field term at temperature $T$ with $\beta = hc/kT$ (cm), and $\langle \phi(\nu) + \phi(-\nu) \rangle$ is the symmetrized power spectral density function (Van Vleck and Huber, 1977). The term $R(\nu)$ includes the effect of stimulated emission. This formulation has a number of attractive properties: its appropriateness to all spectral domains and the fact that the symmetrized power spectral density function satisfies an important intensity sum rule, the Nyquist theorem. For the application of this formalism to the computation of spectra in terms of line transition data, we obtain:

$$k(\nu)=\nu\tanh(\beta\nu/2) \times\sum_i \tilde{S}_i(T)\frac{1}{\pi}\left[\frac{\alpha_i}{(\nu-\nu_i)^2+\alpha_i^2}\chi(\nu_i-\nu)+\frac{\alpha_i}{(\nu+\nu_i)^2+\alpha_i^2}\chi(\nu+\nu_i)\right] \tag{4}$$

where $\tilde{S}_i$ (cm$^2$/molec.) is the intensity of the transition at wavenumber value $\nu_i$ (cm$^{-1}$) and halfwidth $\alpha_i$ (cm$^{-1}$). The Lorentz function, $f(\nu-\nu_i)$ (cm):

$$f(\nu-\nu_i)=\frac{1}{\pi}\frac{\alpha_i}{(\nu-\nu_i)^2+\alpha_i^2} \tag{5}$$

is the line shape function appropriate to the impact approximation for which the collision time is assumed to be instantaneous. The $\chi$ function is a semi-empirical function applied to the impact result to correct for duration of collision effects and to attain agreement between calculated and measured spectra. With $\chi=1$, this line shape reduces to the Lorentz shape in the infrared, since $R(\nu)\to\nu_i$ for $|\nu-\nu_i|\ll\nu$, and to the Van Vleck-Weisskopf shape in the microwave, since $R(\nu)\to\beta\nu^2/2$. We adopt a notation in which a tilde over a quantity indicates that the radiation term, $R(\nu)$, has been excluded from that quantity.

At this stage we define a continuum absorption by excluding from the power spectral density function fast spectral components associated with the line center. The continuum, $\tilde{C}(\nu)$, is given by:

$$\tilde{C}(\nu)=\langle\phi(\nu)+\phi(-\nu)\rangle_c \tag{6}$$

$$=\sum_i \tilde{S}_i[f_c(\nu-\nu_i)\chi(\nu-\nu_i)+f_c(\nu+\nu_i)\chi(\nu+\nu_i)] \tag{7}$$

where $f_c$ is a line shape with the strong central component excluded (Clough et al., 1980). We systematically define $f_c$ $(\nu\mp\nu_i)$ in the following way:

$$f_c(\nu\mp\nu_i)=\begin{cases}\dfrac{1}{\pi}\dfrac{\alpha_i}{25^2+\alpha_i^2} & |\nu\mp\nu_i|\leqslant 25\text{ cm}^{-1}\\[2ex] \dfrac{1}{\pi}\dfrac{\alpha_i}{(\nu\mp\nu_i)^2+\alpha_i^2} & |\nu\mp\nu_i|\geqslant 25\text{ cm}^{-1}\end{cases} \tag{8}$$

The function $f_c$ is indicated schematically in Fig. 1 by the solid curve. Another function that has been used by Burch in some of his work is indicated by the dashed line in Fig. 1. The lack of agreement among researchers on the line shape formulation and on the definition of the function $f_c$ has inhibited the intercomparison and validation of continua. It must be emphasized that the continuum and the details of the line-by-line calculation are inextricably related. The present formulation for the continuum is consistent with the FASCODE line-by-line model (Clough et al., 1986). Similarly, it is important to recognize that band models developed to describe molecular absorption, must also be derived in the context of a consistent treatment of the continuum. To

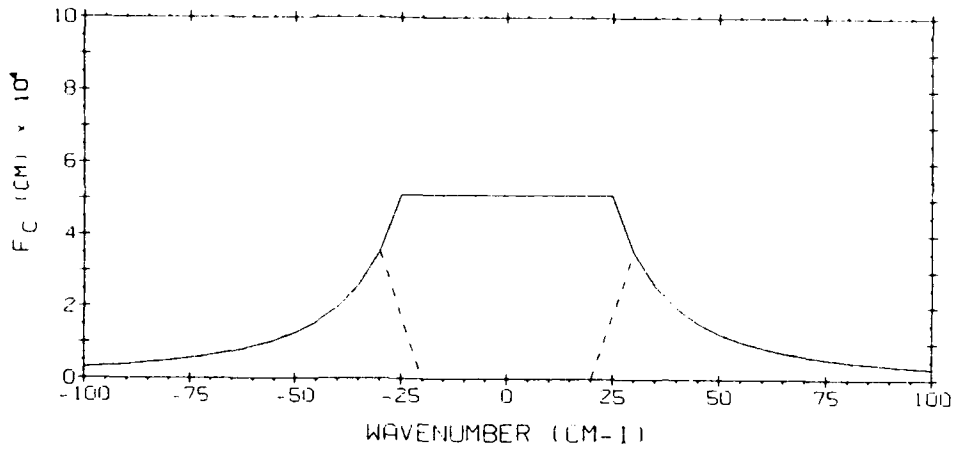


Fig. 1. The line shape function, $f_c(\nu)$, used to develop the continuum (solid curve). The dashed curve represents the function used by Burch.

be more explicit, if a band model is to be used in conjunction with a continuum, then the absorption effects included in the continuum must be excluded from the band model. We should note that the continuum functions have been developed in such a way as to obey Beer's law.

It is an important consideration that the continuum coefficient, $\tilde{C}(\nu)$, is proportional to collider density, $\rho$. Since the collision frequency which is proportional to density determines the broadening, density is more appropriate as the dependent variable than pressure. At constant temperature the distinction is not relevant. The values for the self broadened halfwidths, $\alpha_i^0$, referred to atmospheric density, $\rho_0$, are of the order of 0.1 $cm^{-1}$ (0.5 $cm^{-1}$ for self-broadened water vapor). With the halfwidth density-dependence given by:

$$\alpha_i = \alpha_i^0 (\rho/\rho_0) \tag{9}$$

the $\alpha_i^2$ terms in eq. 8 may be dropped and the continuum shape function becomes:

$$f_c(\nu \mp \nu_i) = \begin{cases} \dfrac{1}{\pi} \dfrac{\alpha_i^0 (\rho/\rho_0)}{25^2} & |\nu \mp \nu_i| \leqslant 25 \text{ cm}^{-1} \\ \dfrac{1}{\pi} \dfrac{\alpha_i^0 (\rho/\rho_0)}{(\nu \mp \nu_i)^2} & |\nu \mp \nu_i| \geqslant 25 \text{ cm}^{-1} \end{cases} \tag{10}$$

The density scaling of the continuum is established as:

$$\tilde{C}(\nu) = \tilde{C}^\circ(\nu)\ (\rho/\rho_0) \tag{11}$$

since $f_c$ is proportional to $(\rho/\rho_0)$ for all values of $\nu$.

The temperature-dependence of the absorption is dependent on the radiation term, $R(\nu)$ in eq. 2, the strength $\tilde{S}_i$, the halfwidth $\alpha_i^0$, and on the line shape factor $\chi$. The dependence is known theoretically for $R(\nu)$ and for $\tilde{S}_i$ and is

satisfactorily described through an empirical exponent, $m$, determined from measurements for $\alpha_i$ where:

$$\alpha_i(\rho,T) = \alpha_i^0 (T/T_0)^m (\rho/\rho_0)$$

For the line shape factor $\chi$ the situation is more complicated. Near line center, $|\nu \pm \nu_i| < 5\ \text{cm}^{-1}$, $\chi$ is essentially unity for all temperatures. However far from line center the temperature-dependence for $\chi$ must be inferred from the temperature of the absorption resulting from many overlapping lines.

## WATER VAPOR

We are now in a position to apply the formulation we have developed to water vapor absorption. Performing a line-by-line calculation using the entire set of water vapor lines from 0 $\text{cm}^{-1}$ to 10,000 $\text{cm}^{-1}$, we obtain the power spectral density function for self-broadened water vapor shown in Fig. 2. The dotted curve is attained by utilizing the continuum line shape function, $f_c$, thus excluding from the power spectral density function the contribution of the line centers, and providing a spectrum of low spectral content designated as the continuum. The well known water vapor bands associated with pure rotation (0 $\text{cm}^{-1}$), $\nu_2$ (1600 $\text{cm}^{-1}$), $\nu_1$ of HDO (2720 $\text{cm}^{-1}$), $2\nu_2$ (3100 $\text{cm}^{-1}$), $\nu_1$ (3660 $\text{cm}^{-1}$) and $\nu_3$ (3760 $\text{cm}^{-1}$) are evident in Fig. 2. In Fig. 3 we indicate two

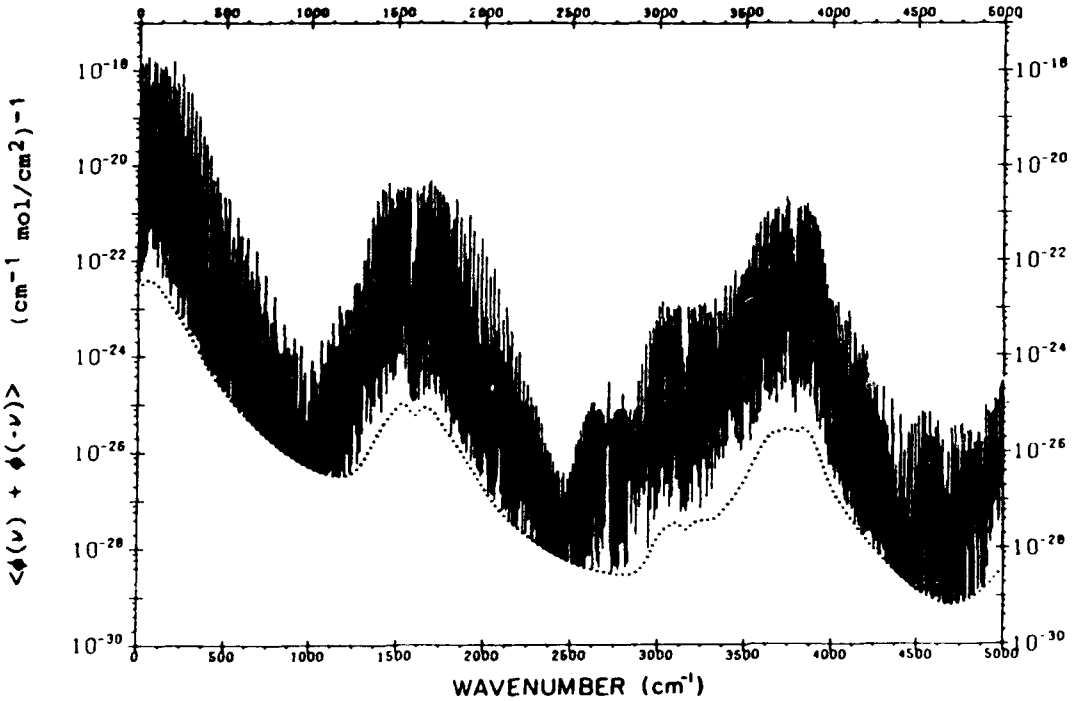


Fig. 2. The symmetrized power spectral density function for self-broadened water vapor at 26.7 mb. and 296 K (solid curve). The continuum is indicated by the dotted curve.

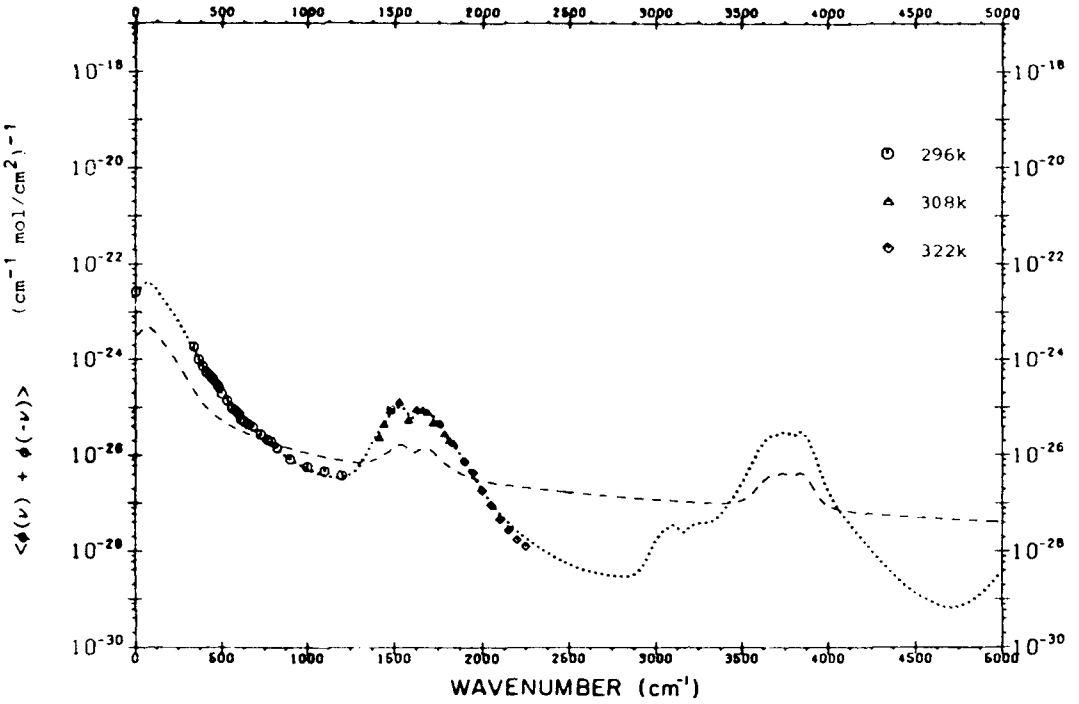


Fig. 3. The continuum for self-broadened water vapor. The dashed line is the impact result and the dotted curve is with the $\chi$ function adjusted to fit the experimental data of Burch, 1981. The broadening pressure is ~~1013~~ 26.7 mb.

continua, one obtained using the impact line shape ($\chi=1$), and the other with a function obtained by adjusting the parameters in an empirical $\chi$-function to attain agreement with the indicated spectral results (Burch, 1981; Burch and Alt, 1984; Burch, 1985).

Note that in Fig. 3 the continuum coefficient for self-broadened water vapor, $\tilde{C}_s^0$, exhibits an excess absorption with respect to the reference impact continuum ($\chi=1$) in the center of the bands at 0–500 $cm^{-1}$ and 1400–1800 $cm^{-1}$ and a deficiency between central band absorption regions, 800–1200 $cm^{-1}$ and 1800–3300 $cm^{-1}$. This result is consistent with theoretical requirements and is a direct consequence of the formulation. The $\chi$ function associated with the line shape for self-broadened water vapor, designated $\chi_s$, is shown by the solid curve in Fig. 4. The functional form of $\chi$ is given by:

$$\chi = \begin{cases} 1-(1-\chi')\dfrac{(\nu \mp \nu_i)^2}{25^2} & |\nu \mp \nu_i| \leqslant 25\ cm^{-1} \\ \chi' & |\nu \mp \nu_i| \geqslant 25\ cm^{-1} \end{cases} \tag{12}$$

where for self-broadening $\chi_s$ is obtained by setting $\chi'=\chi_s'$ with:

$$\chi_s' = 8.63\exp(-z_1^2) + (0.83z_2^2 + 0.033z_2^4)\exp(-|z_2|) \tag{13}$$

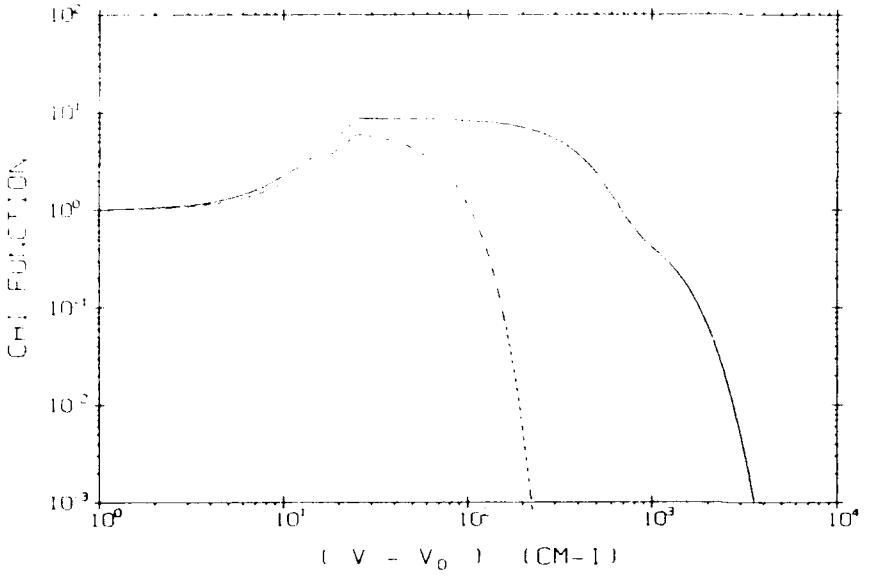


Fig. 4. The $\chi$ function for water at 296 K. The solid curve is for self-broadening; the dashed curve is for foreign-broadening.

where $z_1 = (\nu \mp \nu_i)/400$ and $z_2 = (\nu \pm \nu_i)/250$ at 296 K. From eq. 12 and Fig. 4 we note that $\chi$ is continuous at 25 $cm^{-1}$, but that the first derivative is discontinuous. This is a direct consequence of the choice of $f_c$ (eq. 8) but causes no particular problems in the formulation.

The self-continuum for water vapor demonstrates a rather strong temperature-dependence, particularly in the 1000 $cm^{-1}$ window. It is an important shortcoming of the current state of line shape theory for molecular collisions, that the temperature-dependence of the far wings, or alternatively of the continuum in the window regions, is not explained. Rosenkranz (1985, 1987), in two particularly interesting papers, has proposed an alternative formulation to eqs. 1 and 3, which leads to a strong temperature-dependence consistent with observations in the far-wing regions. This proposed formulation warrants additional scrutiny. The dimer has often been postulated as a source of the continuum absorption primarily as a consequence of its simple and attractive temperature-dependence. However, the absence of spectral structure, difficulties in explaining spectral pressure-dependence and the fact that the absorption in the windows as developed in this paper represents an excess with respect to the impact line shape are in direct contradiction with the dimer theory. On the other hand, dimers should be formed under atmospheric conditions so that the central issue becomes the question of dimer lifetime (Suck et al., 1979).

For pragmatic purposes the temperature-dependence of the continuum has been treated as follows: the parameters in an analytical $\chi$ function are obtained by least-squares fitting the calculated continuum to the data of Burch at 296 K and 338 K. These parameters for 296 K and 338 K are then extrapolated to

260 K and a continuum for that temperature is calculated. This is potentially a source of error; however, validations for atmospheric measurements have provided remarkably good results. Continua for 338 K, 296 K and 260 K are shown in Fig. 5.

An analogous treatment is performed for air-broadening of water vapor, referred to as foreign broadening. Fig. 6 shows the empirical continuum, $\tilde{C}_f^0$, fit to the data of Burch as well as the continuum for the impact approximation. For the foreign-broadened case, the line wings decay much more rapidly as a function of wavenumber difference from line center than for the self-broadened case. This is reflected in the foreign chi-function, $\chi_f$ shown by the dashed curve in Fig. 4. For the foreign continuum $\chi_f$ is obtained by setting $\chi' = \chi'_f$ in eq. 12 with:

$$\chi'_f = 6.65 \exp(-z_1^2) \tag{14}$$

where $z_1 = (\nu \pm \nu_i)/75$. For the window regions of the foreign continuum, 1000 $cm^{-1}$ and 2500 $cm^{-1}$ in Fig. 6, an absorption coefficient has been added to the continuum resulting from the present formalism in order to attain agreement with atmospheric measurements (Roberts et al., 1976). The contribution of the foreign continuum is very small in these spectral regions making the measurements particularly difficult. The observed effect may be due to collision

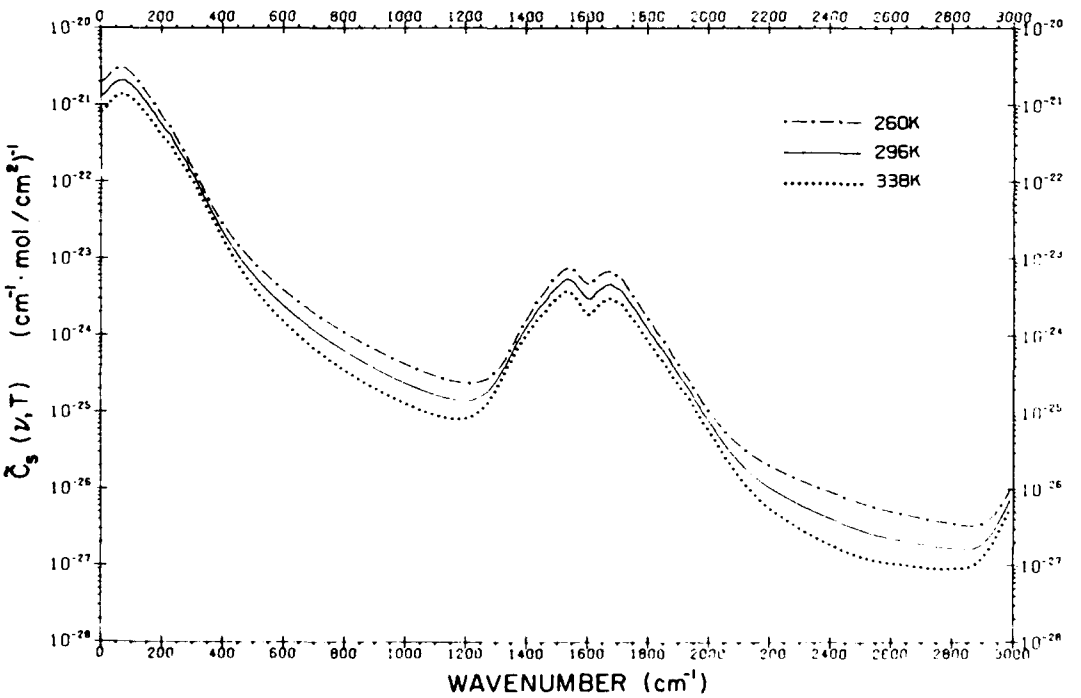


Fig. 5. The self-broadened water vapor continuum at 338 K, 296 K and 260 K. The continua at 338 K and 296 K have been fit to data and the 260 K continua have been extrapolated.

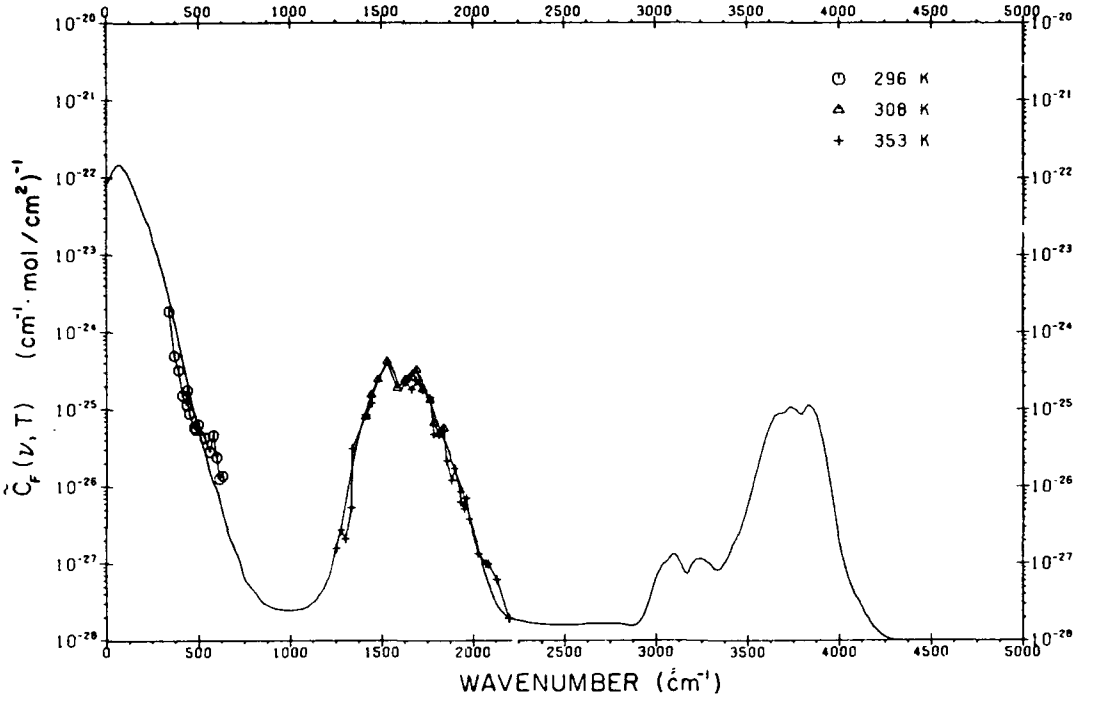


Fig. 6. The continuum for foreign-broadened water vapor. The solid curve is the calculated continuum with the $\chi$ function adjusted to fit the experimental data of Burch, 1981. The broadening pressure is 1013 mb.

induced spectra or humidity-dependent aerosols. No significant temperature-dependence has been observed for the foreign continuum.

The total absorption coefficient due to self- and foreign-water-vapor continuum, $k_c(\nu)$, is given by the relation:

$$k_c(\nu) = \nu \tanh(\beta\nu/2)\ [\tilde{C}_s^0(\rho_s/\rho_0) + \tilde{C}_f^0(\rho_f/\rho_0)] \qquad (15)$$

It is an important point that for atmospheric conditions, the foreign continuum is dominant for in-band absorption and the self continuum is dominant for the out-of-band absorption, the window regions of water vapor spectrum.

## ATMOSPHERIC VALIDATION

The most important element in the development of an atmospheric transmittance/radiance model is validation with atmospheric data. Since the atmospheric window at 1000 $cm^{-1}$ (10 $\mu m$) is of such importance, we consider that spectral region in more detail. The continuum currently being used in FASCOD2 has been adjusted to fit the more recent measurements at 1000 $cm^{-1}$ of Burch and Alt, 1984 (Fig. 7). In Fig. 8 we show a plot of the optical depth for a 1-km path at 990 $cm^{-1}$ as a function of water vapor density from LOWTRAN7 (Kneizys et al., 1988) which incorporates this continuum de-

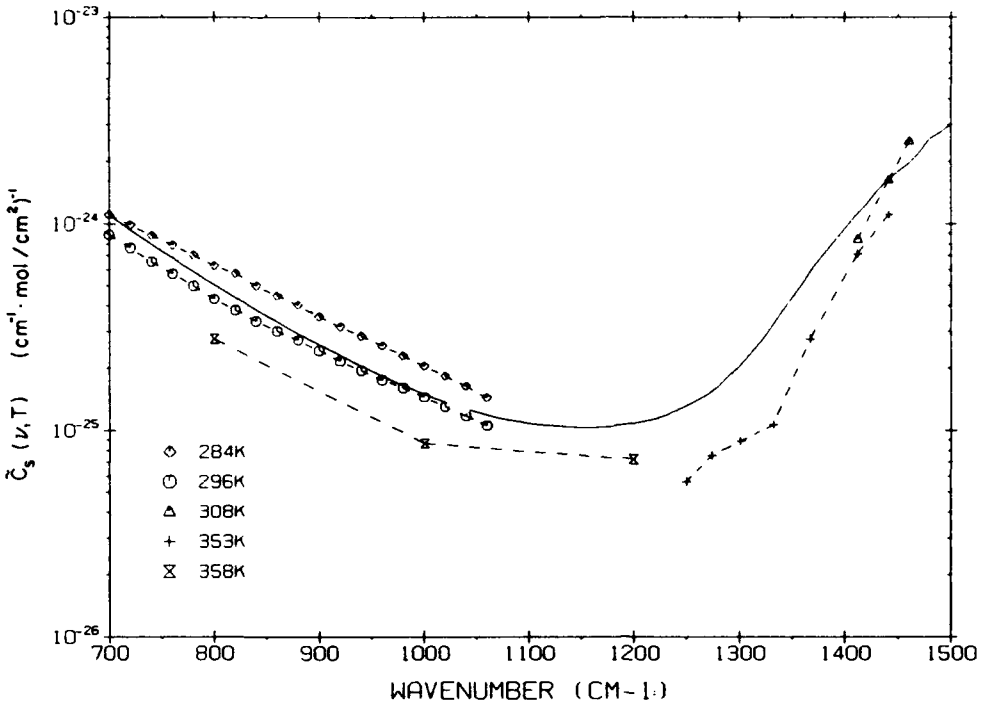


Fig. 7. Details of the self-broadened continuum at 1000 cm$^{-1}$. The solid line is the calculated continuum at 296 K. The data for 284 K and 296 K are from Burch and Alt (1984); the other data are from Burch (1981).

velopment. We consider two sets of atmospheric measurements: one from the Air Force Wright Aeronautical Laboratories (AFWAL) taken over an 8-km path and for a range of visibilities (Kneizys et al., 1984) and the other from the Technion Institute in Israel over an 8.6-km path (Oppenheim and Lipson, 1986). Both of these sets of measurements were taken with circular variable filter (CVF) spectrometers. Since the atmospheric measurements include extinction due to aerosol effects, the calculated optical depths, which do not include aerosol contributions, are less than those for the atmospheric measurements. The calculations do take into effect the contribution from other molecules (intercept) and from the local water vapor lines. Spectral validation of the continuum model with the Technion measurements for the 8–12 micron window is shown in Fig. 9 and for the 3–5 micron window in Fig. 10. Of particular note is the excellent agreement between calculation and observation obtained at 4.75 $\mu$m and 3.2 $\mu$m. These two regions demonstrate the predictive capability of the current formulation since there has been no adjustment with data in these spectral regions. With respect to the continua beyond 5000 cm$^{-1}$, it should be emphasized that the calculations are essentially qualitative and unvalidated. This is particularly the case for the self-broadened continuum, important between the bands.

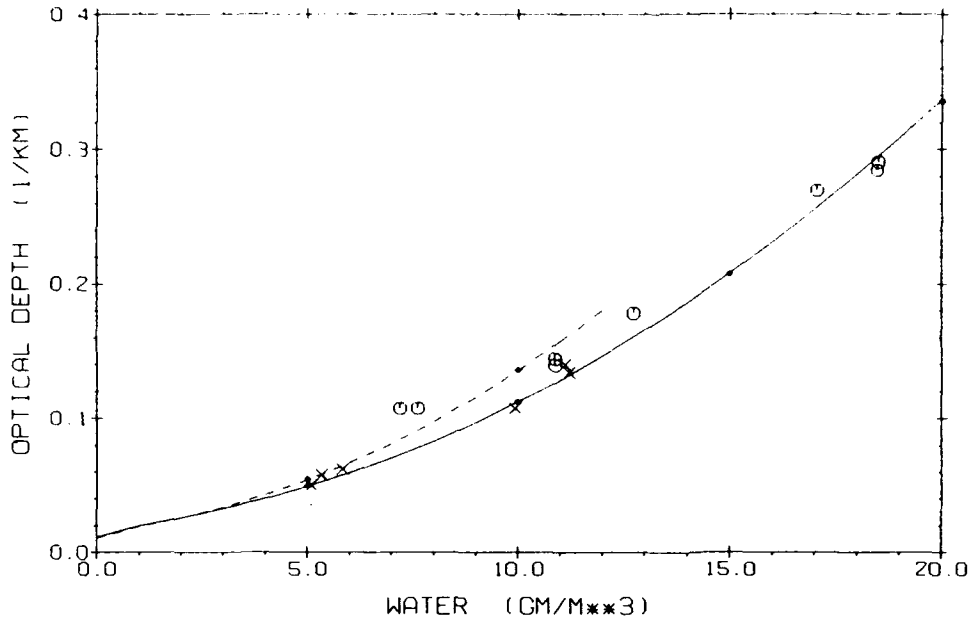


Fig. 8. The optical depth for a 1-km path at 990 $cm^{-1}$ as a function of water vapor density. The calculations are from LOWTRAN with the self-continuum of Fig. 7. The solid curve is for 296 K and the dashed curve is for 284 K. The data are from Kneizys et al., 1984. The $\times$-symbols are for cases with visibilities > 15 km.

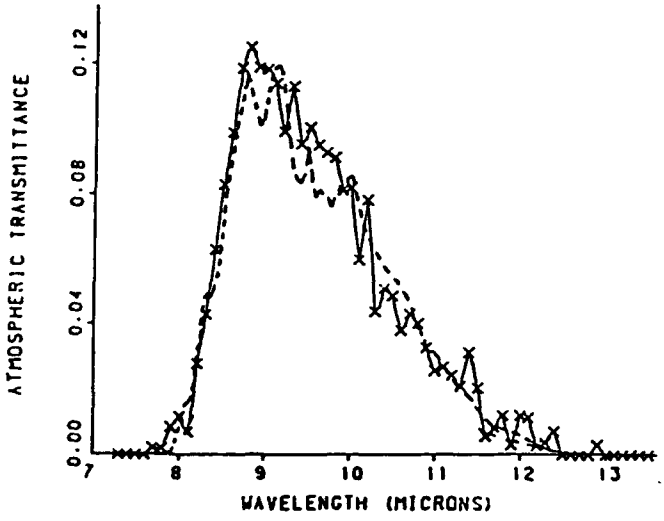


Fig. 9. Spectral comparison between a CVF measurement in the 8-12 micron window over a 8.637-km path by Technion (Oppenheim and Lipson, 1985) and a LOWTRAN calculation with the FASCOD2 continuum (dotted curve). The measurement conditions: $T = 297.5$ K, $P = 1008$ mb., $RH = 85\%$, and visibility = 15 km.

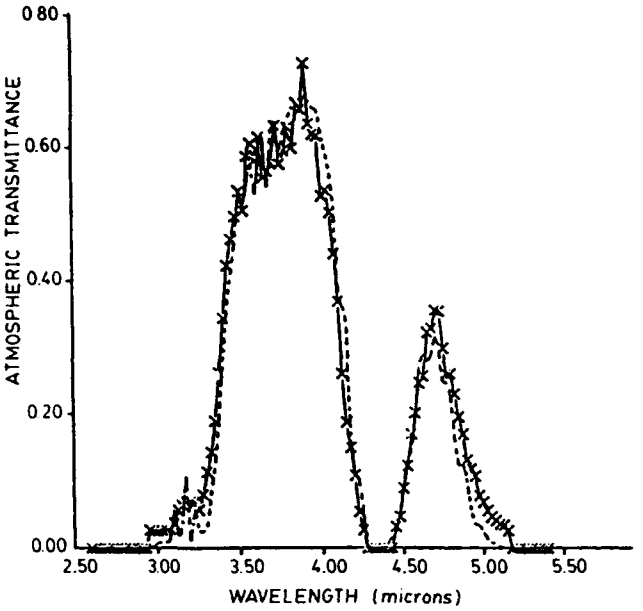


Fig. 10. Spectral comparison between a CVF measurement in the 3-5 micron window over a 10.37-km path by Technion (Oppenheim and Lipson, 1985) and a LOWTRAN6 calculation (dotted curve). The measurement conditions: $T=283$ K, $P=899$ mb., $RH=68\%$ and visibility $=40$ km.

## SUMMARY

The present discussion is not intended as a comprehensive review of the water vapor continuum problem. It is rather a description of a specific approach that is consistent with the physics of the problem and that has been constrained to provide results consistent with experimental measurements. The choice of measurements used for this discussion has been highly selective. This is related to a need for internal consistency of the observations, our estimation of the accuracy of the measurements and a treatment of the data that is in the context of the current development. The present status should be regarded as useful if not definitive. In order to meet current objectives in atmospheric remote sensing and related phenomena, more observations of high accuracy both in the laboratory and in the atmosphere are required, and significant advances in the theoretical treatment of the effects of collision on molecular line shape need to be achieved. A floppy disk containing a program to calculate continuum absorption coefficients as described here and consistent with FASCOD2 and LOWTRAN7 is available from the authors.

## ACKNOWLEDGEMENTS

One of us, S.A.C., would like to acknowledge the invaluable support received while at AFGL during which time most of the work was performed. In particular we wish to recognize the contribution of James Chetwynd for the extensive

calculations leading to the current results. We would also like to thank our many colleagues, experimentalists and theoreticians, for the discussions that have clarified our understanding of a very difficult problem. The discussion and experimental results due to Darrel Burch have been invaluable in reaching the present state of understanding. To our other colleagues not mentioned here, we hope to do greater justice in a more extensive paper in preparation.

REFERENCES

Burch, D.E., 1981. Continuum Absorption by $H_2O$. AFGL-TR-81-0300.

Burch, D.E., 1985. Absorption by $H_2O$ in Narrow Windows Between 3000-4200 $cm^{-1}$. AFGL-TR-85-0036.

Burch, D.E. and Alt, R.L., 1984. Continuum Absorption in the 700-1200 $cm^{-1}$ and 2400-2800 $cm^{-1}$ Windows. AFGL-TR-84-0128.

Clough, S.A., Kneizys, F.X., Davies, R.W., Gamache, R. and Tipping, R.H., 1980. Theoretical line shape for $H_2O$ vapor: application to the continuum. In: A. Deepak, T.D. Wilkerson and L.H. Ruhnke (Editors), Atmospheric Water Vapor. Academic Press, London, pp. 25-46.

Clough, S.A., Davies, R.W. and Tipping, R.H., 1983. The line shape for collisionally broadened molecular transitions: a quantum theory satisfying the fluctuation dissipation theorem. Proc. 6th Conf. Spectral Line Shapes. Walter de Gruyter, New York, N.Y., pp. 553-568.

Clough, S.A., Kneizys, F.X., Shettle, E.P. and Anderson, G.P., 1986. Atmospheric radiance and transmittance: FASCOD2. Proc. 6th Conf. Atmospheric Radiance. AMS, Williamsburg, VA, pp. 141-144.

Kneizys, F.X., Gruenzel, R.R., Martin, W.C., Schuwerk, M.J., Gallery, W.O., Clough, S.A., Chetwynd, J.H. and Shettle, E.P., 1984. Comparison of 8 to 12 Micrometer and 3 to 5 Micrometer CVF Transmissometer Data with LOWTRAN Calculations. AFGL-TR-84-0171.

Kneizys, F.X., Shettle, E.P., Abrev, L.W., Chetwynd, J.H., Anderson, G.P., Gallery, W.O., Selby, J.E.A. and Clough, S.A., 1988. User's Guide to LOWTRAN7, AFGL-TR-88-0177.

Oppenheim, U.P. and Lipson, S.G., 1986. Private Communication. See also A. Ben-Shalom, A.D. Devir, S.G. Lipson, U.P. Oppenheim and E. Ribak, 1985. Absorption of IR radiation by atmospheric water vapor in the regions 4.3-5.5 micron and 8-13 micron. Proc. Topical Meeting on Remote Sensing of the Atmosphere, OSA.

Roberts, R.E., Selby, J.E.A. and Biberman, L.M., 1976. Infrared continuum absorption by atmospheric water vapor in the 8-12 $\mu$m window. Appl. Opt., 15: 2085.

Rosenkranz, P.W., 1985. Pressure broadening in rotational bands, I. A statistical theory. J. Chem. Phys., 83: 6139.

Rosenkranz, P.W., 1987. Pressure broadening in rotational bands, II. Water vapor from 300 to 1100 $cm^{-1}$. J. Chem. Phys., 87: 163.

Suck, S.H., Kassner, J.L., Jr. and Yamagushi, Y., 1979. Water cluster interpretation of IR absorption spectra in the 8-14 $\mu$m wavelength region. Appl. Opt., 18: 2609.

Van Vleck, J.H. and Huber, D.L., 1977. Absorption, emission and linebreadths: a semihistorical perspective. Rev. Mod. Phys., 49: 939.

**Application of the Optimal Probability Method to the Retrieval of Temperature, Water Vapor and Ozone Profiles**

S.A. Clough, R.G. Isaacs, R.D. Worsham and J.L. Moncet
Atmospheric and Environmental Research, Inc.
840 Memorial Drive
Cambridge, MA 02139

A code has been developed to perform the retrieval of atmospheric state parameters using the method of nonlinear least squares in conjunction with a program to compute the forward problem (Isaacs, 1988). In the present study, FASCODE (Clough et al., 1986) has been utilized for the forward problem; other algorithms including rapid algorithms may readily be accommodated. The method has been applied to retrievals of temperature profiles, surface temperature and pressure, water vapor profiles and other constituent distributions using both real and simulated data. The method is applicable to both sequential and simultaneous retrievals. Either of two approaches may be selected for performing retrievals: the method of ridge regression or the maximum likelihood method. Our implementation of the latter approach is similar to that discussed by Rodgers (1976, 1987) and more recently by Eyre (1989).

The problem of retrieving atmospheric state parameters, x, is posed in terms of minimizing the square of the differences between the observations and the forward model F(x) such that the variance, $\sigma^2$, given by

$$\sigma^2 = \sum_i W_i \, [R_i - F_i(x)]^2 \tag{1}$$

is a minimum. $W_i$ is the weight for the i'th observed radiance, $R_i$. This approach has two attractive attributes: (1) an extensive body of work exists on methods for solving the problem formulated in this way and (2) the final solution is in the linear regime enabling the implementation of a comprehensive error analysis. We follow the customary approach to the solution of this problem by adding a penalty function, $x^T \Gamma x$, to $\sigma^2$ obtaining

$$\sigma^2 = [R - F(x)]^T \, W \, [R - F(x)] + x^T \Gamma \, x \tag{2}$$

For the maximum likelihood method we have

$$\Gamma = S_x^{-1} \tag{3}$$

with $S_x$ the error covariance of the first guess and

$$W = S_R^{-1} \tag{4}$$

with $S_R$ the error covariance of the measurements. For the ridge regression approach, $\Gamma$ is given by

$$\Gamma_{ij} = S_{ij} \gamma_j \tag{5}$$

where $\gamma_j$ is a stability (damping) parameter. In this approach $\Gamma$ is viewed as constraining the direction and length of the step for the nonlinear problem (Levenberg-Marquardt) as well as providing a procedure to treat the ill-posedness.

The retrieval is obtained by iterative implementation of the relation

$$x^{n+1} = x^n + (K^T W K + \Gamma)^{-1} K^T W r^n \quad . \tag{6}$$

The radiance residuals, $r^n$, are given by

$$r^n = R - F(x^n) \tag{7}$$

with $x^0$ the first guess. The matrix K represents the Jacobian of the forward model with respect to the state parameters, obtained in our case from finite forward differences,

$$K = \frac{F(x^0 + \delta x) - F(x^0)}{\delta x} \tag{8}$$

The derivatives are updated as infrequently as possible as a consequence of the high cost of the forward calculation. In the cases we have studied, convergence has been achieved in two or three iterations without derivative updates.

For the analysis of the error we follow Rodgers (1987),

$$E\left[(x - x^r)\,(x - x^n)^T\right] = S_N + S_M + S_b \tag{9}$$

where $S_N$ represents null space error, $S_M$ measurement error and $S_b$ model error. In the present analysis, we have not considered the important problem of model error. For the general case we obtain the error covariance for the state parameters from

$$S_N = H^{-1}\,[\Gamma S_x \Gamma]\,H^{-1} \tag{10}$$

and

$$S_M = H^{-1}[K^T W\, S_R\, W K]\, H^{-1} \tag{11}$$

where

$$H = (K^T W\, K + \Gamma) \quad . \tag{12}$$

For the maximum likelihood method we obtain the important result, applying Eq. 3 to Eq. 10 and Eq. 4 to Eq. 11,

$$E[(x - x^n)(x - x^n) = H^{-1} \quad . \tag{13}$$

We have applied this method to the retrieval of an ozone profile from data taken with the University of Wisconsin High Resolution Interferometer Sounder (HIS; Smith et al., 1983). The data were taken with the NASA ER2 at 19.6 km with a nadir view. The measured unappodized radiance spectrum in equivalent brightness temperature is shown in Fig. 1A. The initial guess is obtained from the U.S. Standard ozone profile, with resulting residuals $r^o$ given in Fig. 1B. The retrieval converges after two iterations providing the radiance residuals in Fig. 1C and the retrieved profile given in Table 1.

A second application to be discussed is a temperature retrieval using simulated radiances for an extended set of AMSU channels. The simulated data correspond to temperatures associated with the tropical atmosphere and the initial guess is taken as the U.S. Standard Atmosphere. Convergence is achieved in two iterations for this near linear call. As an example of the response of the method to a temperature impulse, we have added a 3° temperature increase in the second layer, and studied the response of the retrieval procedure to the impulse. A noise analysis using the maximum likelihood approach has been performed.

This research has been supported by the Geophysics Laboratory (AFSC) under contract F19628-87-C-0129.

Clough, S.A., F.X. Kneizys, E.P. Shettle and G.P. Anderson, 1986: Atmospheric Radiance and Transmittance: FASCOD2, Proc. of the Sixth Conference on Atmospheric Radiation, Williamsburg, VA, 141-144.

Eyre, J.R., 1989: Inversion of Cloudy Satellite Radiances by Nonlinear Optimal Estimation. I. Theory and Simulation for TOVS.

Isaacs, R.G., 1988: Modeling of the Atmosphere, Proc. of SPIE 928, 136-164.

Rodgers, C.D., 1976: Retrieval of Atmospheric Temperature and Composition from Remote Measurements of Thermal Radiation, Rev. Geophys. Space Physics, 14, 609-624.

Rodgers, C.D., 1987: A General Error Analysis for Profile Retrieval, Advances in Remote Sensing Methods, edited by A. Deepak, H.E. Fleming and J.S. Theon, A. Deepak Publishing (1989), 285-297.

Smith, W.L, H.E. Revercomb, H.B. Howell, and H.M. Woolf, 1983: HIS - A Satellite Instrument to Observe Temperature and Moisture Profiles with High Vertical Resolution, Proc. of the Sixth Conference on Atmospheric Radiation, AMS, Boston, MA.

Table 1

| layer pressure (mb) | $x^0$ mixing ratio (PPMV) | retrieved change (%) | error ($1\sigma$) mixing ratio (%) |
|---|---|---|---|
| 64.5 | 1.97 | -5.6 | 2.5 |
| 101.1 | 1.17 | -20.7 | 1.5 |
| 182.0 | 0.348 | -19.7 | 2.5 |
| 256.0 | 0.188 | -1.8 | 8 |
| 299.9 | 0.121 | 0.2 | 8 |

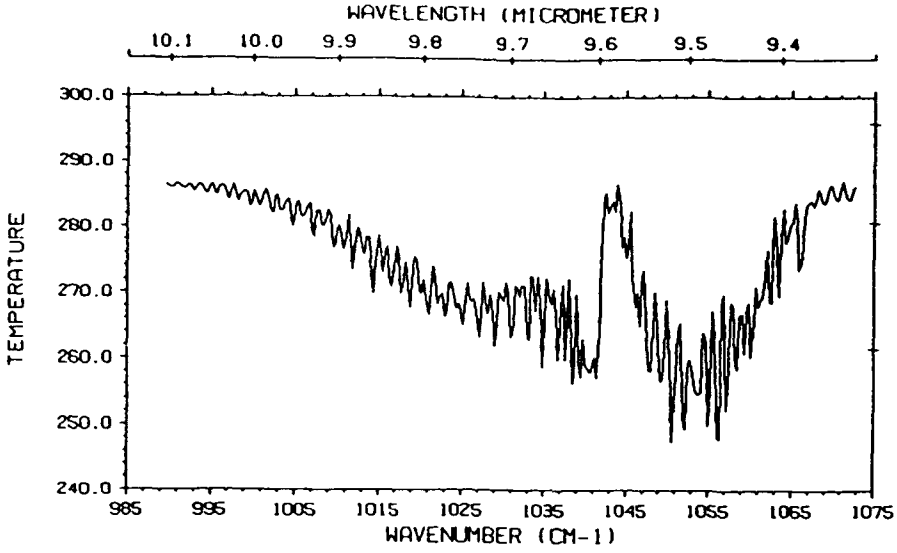


Fig. 1A. Brightness temperature spectrum from HIS (19.6 km alt., nadir view).

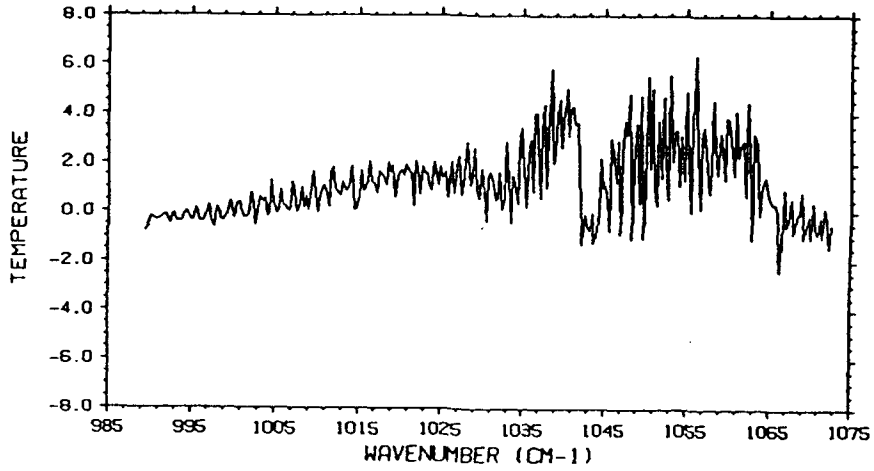


Fig. 1B. Brightness temperature residuals from FASCODE with U.S. Standard ozone profile (radiosonde temperature profile).

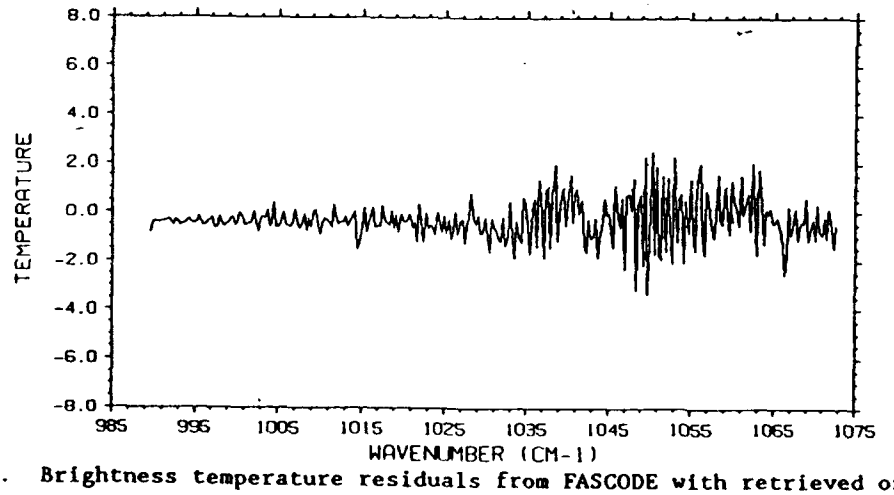


Fig. 1C. Brightness temperature residuals from FASCODE with retrieved ozone profile.

# LINE BY LINE COMPARISON WITH HIS AND SCRIBE RADIANCE MEASUREMENTS

S.A. Clough, R. D. Worsham
Atmospheric and Environmental Research, Inc. (AER), Cambridge, MA, USA

M.L. Hoke, L.S. Rothman
Air Force Geophysics Laboratory, Hanscom Air Force Base, MA, USA

R.O. Knuteson
Space and Engineering Center, University of Wisconsin, Madison, WI, USA

We describe the comparison of radiance calculations using the accelerated line by line code FASCODE, with spectral radiance data obtained from the High-Resolution Interferometer Sounder (HIS) (Smith et al., 1983) and from the Stratospheric Cryogenic Interferometer Balloon Experiment (SCRIBE) (Murcray et al., 1984). Evaluation of measurements from both instruments established the necessity for proper treatment of line coupling in carbon dioxide and an improvement in the intensities for the carbon dioxide transitions relative to the 1986 AFGL data base values. Some HIS ground based measurements will be presented stressing implications for the water vapor continuum.

References:

Murcray, F.H., F.J. Murcray, D.G. Murcray, J. Pritchard, G. Vanasse, and H. Sakai, 1984: Liquid nitrogen-cooled Fourier transform spectrometer system for measuring atmospheric emission at high altitudes. J. Atmos. Ocean. Technology, 1, 351-357.

Smith, W.L., H.E. Revercomb, H.B. Howell, and H.M. Woolf, 1983: HIS - A Satellite Instrument to Observe Temperature and Moisture Profiles with High Vertical Resolution Fifth Conference on Atmospheric Radiation, American Meteorological Society, Boston, Mass.

Presented as paper TR.1 at the Fifth Scientific Assembly of the International Association of Meteorology and Physics (IAMAP), University of Reading, UK, 7 August 1989.

* U. S. GOVERNMENT PRINTING OFFICE: 1990--500-000/20027